UNIVERSITY OF BIRMINGHAM

FUNCTIONAL AND MOLECULAR RESPONSES OF HUMAN NEUTROPHILS TO *FUSOBACTERIUM NUCLEATUM* SUBSPECIES

by

Mária Muchová

A thesis submitted to
The University of Birmingham
for the degree of
DOCTOR OF PHILOSOPHY

Institute of Clinical Sciences
School of Dentistry
College of Medical & Dental Sciences
University of Birmingham
July 2024

UNIVERSITY OF
BIRMINGHAM

University of Birmingham Research Archive

e-theses repository

This unpublished thesis/dissertation is copyright of the author and/or third parties. The intellectual property rights of the author or third parties in respect of this work are as defined by The Copyright Designs and Patents Act 1988 or as modified by any successor legislation.

Any use made of information contained in this thesis/dissertation must be in accordance with that legislation and must be properly acknowledged. Further distribution or reproduction in any format is prohibited without the permission of the copyright holder.

Abstract

Fusobacterium nucleatum is a Gram-negative, commensal oral anaerobe, which is a key structural member of dental plaque biofilms. It is also considered an opportunistic pathogen due to its association with periodontitis and systemic extraoral diseases, such as cardiovascular disease and colorectal cancer. Five subspecies are currently recognised: *animalis*, *fusiforme*, *nucleatum*, *polymorphum* and *vincentii*. These subspecies, found in the oral cavity and in the extraoral tissues, interact with host innate immune cells, such as neutrophils, which form the first line of defence against microbes. Neutrophils possess a powerful antimicrobial arsenal to remove the invaders, however, excessive responses can cause collateral tissue damage and lead to chronic inflammation. Subspecies-specific neutrophil responses toward *F. nucleatum* have been reported in the neutrophil-like cell line HL-60, however responses of primary human neutrophils are largely unexplored. Additionally, *F. nucleatum* typically resides in biofilms, yet, the immunogenicity of biofilm-grown *F. nucleatum* subspecies has not been addressed to date. Therefore, this doctoral thesis systematically characterised biofilm formation by all subspecies. Subsequently, functional and molecular responses of primary human neutrophils were evaluated when stimulated with planktonic and biofilm-grown *F. nucleatum* subspecies.

Characterisation of single-subspecies biofilm formation included biomass quantification using crystal violet (CV) staining, evaluation of biofilm architecture by scanning electron microscopy (SEM) and assessment of biofilm thickness and stability using confocal laser scanning microscopy (CLSM). Adhesion proteins (adhesins) involved in *F. nucleatum* biofilm formation were analysed *in silico* bioinformatically. Formalin-inactivated (planktonic) and live *F. nucleatum* subspecies (planktonic and biofilm-grown) were used as stimuli to evaluate functional and molecular responses of primary neutrophils isolated from human peripheral blood. Responses of HL-60 cells were evaluated alongside primary neutrophils for comparison.

Generation of reactive oxygen species (ROS) was quantified using enhanced chemiluminescent assay and NETosis was quantified fluorometrically. Release of neutrophil cytokines (TNF-α, IL-1β, IL-6 and IL-8) and antimicrobial enzymes (matrix metalloproteinase 9 and human neutrophil elastase) was analysed using enzyme-linked immunosorbent assay (ELISA).

F. nucleatum biofilm formation was found to be subspecies-specific, with ssp. *polymorphum* being unable to form stable biofilms. Subspecies-specific differences in conservation of adhesin orthologues were identified *in silico*, with the lowest percentage identity values in ssp. *polymorphum*. FN23 adhesin mutants ΔFadA and ΔFap2 formed significantly higher amounts of biofilm. No differences were found in ROS generation and NET formation by primary neutrophils stimulated with formalin-fixed subspecies. When live subspecies were employed as stimuli, biofilm-grown bacteria stimulated higher and faster ROS response and lower IL-1β release. Following a more detailed analysis, notable differences were found in extracellular superoxide release, with FNA and FNP stimulating the highest generation, while FNV stimulated the lowest superoxide generation. When compared to the parental strain FN23, ΔFap2 stimulated lower and slower ROS release while ΔFadA stimulated higher and faster ROS release and this was statistically significant in superoxide generation. Mutant strains stimulated similar levels of superoxide release when compared to FNV. Evaluation of cytokine production also revealed subspecies-specific statistically significant differences, which were inversely correlated with the superoxide release. Release of neutrophil antimicrobial enzymes did not seem to be subspecies-specific. No differences were found in NET-DNA release.

The data presented in this thesis showed significant subspecies-specific differences as well as differences between planktonic and biofilm-grown *F. nucleatum* with regard to their ability to activate neutrophils. These results indicate that individual subspecies may differ in virulence and that biofilms may be more immunogenic than planktonic bacteria, thus highlighting the fact

that it is essential to study *F. nucleatum* subspecies separately. Better understanding of the subspecies' immunogenicity and virulence in biofilms may help reveal potential therapeutic targets in *F. nucleatum*-associated diseases.

Dedication

I dedicate this thesis to my younger self, who dreamt big and moved to a completely foreign country to pursue her dream to become a microbiologist. Her love for microbes and microscopes pushed her forward and despite the challenges of studying in a foreign language, living away from her family and very often a terrible home-sickness, she did not give up and worked incredibly hard to reach her goals. Without her bravery and ambitions, this thesis would not have been written.

Acknowledgements

I would like to wholeheartedly thank my supervisors Dr Josefine Hirschfeld, Dr Sarah Kuehne, Dr Melissa Grant and Prof Iain Chapple for giving me the opportunity to work on this amazing project. I am so grateful for all your support, both academic and mental, especially when I was struggling with the project and writing. You have dedicated so much of your time to me and I would not have done this without your help.

I would also like to thank the research technicians at the Dental hospital labs, especially Dr Helen Wright for teaching me how to tame neutrophils and for her comfort candy stash when the experiments did not go well. I am also grateful to Dr Jianguo Liu for all his help with the SEM.

I would like to acknowledge the help of Pooja Sridhar from the School of Biosciences, University of Birmingham, who assisted with the extraction of membrane proteins from *F. nucleatum*.

Special thanks to Peter Smith for all his help with blood drawing and to Dr Ajoy Bardhan for sharing his blood samples for neutrophils.

I cannot begin to express my thanks to the fantastic researchers from the student office, who helped me survive this often turbulent journey and became my very dear friends in the process, namely Dr Benjamin Hewitt, Dr Dario Balacco, Lisa Shriane, Dr Olga Yevlashevskaya, Dr Sandeep Shirgill, Rachel Martin, Dr Lauter Eston Pelepenko, Dr Luciana Solera Sales, Dr Onalenna Neo and Alex Robinson. In spite of the academic challenges of the project, you made my PhD years unforgettable.

I am deeply indebted to my friends outside of lab, especially Dr Veronika Toth and Dr Dominika Boldovjakova, who kept cheering me on and believing in me. Thank you for always checking on me and giving me a chance to have a break with a long phone call.

Most of all, my academic success would not have been possible without the support of my husband Dr Stefano Calabrò, who was always there to prevent a meltdown during the data analysis and writing, and my mum Oľga, dad Alojz and my brother Alojz, who sacrificed so much for me to be able to study and never stopped supporting my ambitions. Mamina, ocino, ďakujem vám za všetku vašu podporu a za to, že ste mi umožnili študovať, aj keď to znamenalo, že som odišla do zahraničia. Viem, že ste kvôli mne veľa obetovali a naozaj si veľmi cením, že ste mi pomohli dosiahnuť vysokoškolské vzdelanie a splniť si sen stať sa mikrobiologičkou.

Table of Contents

List of figures

List of tables

Abbreviations

aGCF	Artificial gingival crevicular fluid
AS	Artificial saliva
ATCC	American Type Culture Collection
AUC	Area under the curve
BCA	Bicinchoninic acid (Protein assay)
BSA	Bovine serum albumin
CFU	Colony forming units
CHAPS	3-[(3-Cholamidopropyl)dimethylammonio]-1-propanesulfonate
CLSM	Confocal laser scanning microscopy
CR	Complement receptor
CRC	Colorectal cancer
CT	Cycle threshold
CV	Crystal violet
dHL-60	Differentiated human leukaemia cell line
DMSO	Dimethyl sulfoxide
DTT	Dithiothreitol
EDTA	Ethylenediaminetetraacetic acid
ELISA	Enzyme-linked immunosorbent assay
EPS	Extracellular polymeric substances
FACS	Fluorescence-activated cell sorting
FadA	Fusobacterium adhesin A
Fap2	Fibroblast activation protein-2
FBS	Fetal bovine serum
fMLP	N-Formylmethionyl-leucyl-phenylalanine
FN23	*Fusobacterium nucleatum* ssp. *nucleatum* ATCC 23726
FN25	*Fusobacterium nucleatum* ssp. *nucleatum* ATCC 25586
FNA	*Fusobacterium nucleatum* ssp. *animalis*
FNF	*Fusobacterium nucleatum* ssp. *fusiforme*
FNP	*Fusobacterium nucleatum* ssp. *polymorphum*
FNV	*Fusobacterium nucleatum* ssp. *vincentii*
Gal-GalNAc	D-galactose-β(1-3)-N-acetyl-D-galactosamine
GCF	Gingival crevicular fluid
gDNA	Genomic DNA
GFP	Green fluorescent protein
GI tract	Gastrointestinal tract
GPBS	Glucose-supplemented phosphate buffered saline
H_2O_2	Hydrogen peroxide
HA	Hydroxyapatite
HCT	Hoechst stain
HEPES	4-(2-hydroxyethyl)-1-piperazineethanesulfonic acid
HL-60	Human leukaemia cell line
HMDS	Hexamethyldisilazane
HNE	Human neutrophil elastase
HOCl	Hypochlorous acid
HRP	Horseradish peroxidase
IEF	Isoelectric focusing

IL	Interleukin
IQR	Interquartile range
LL-37	Cathelicidin
LPS	Lipopolysaccharide
MMP-9	Matrix metalloproteinase 9
MOI	Multiplicity of infection
MPO	Myeloperoxidase
mRNA	Messenger ribonucleic acid
NADPH	Nicotinamide adenine dinucleotide phosphate-oxidase
NC	Negative control
NETs	Neutrophil extracellular traps
NK cell	Natural killer cells
ns	not significant
$O_2 \cdot -$	Superoxide anion
OD	Optical density
OH-	Hydroxyl radical
OpSA	Opsonised *Staphylococcus aureus*
PBS	Phosphate buffered saline
PCR	Polymerase chain reaction
PFA	Paraformaldehyde
pI	Isoelectric point
PKC	Protein kinase C
PMA	Phorbol myristate acetate
PMN	Polymorphonuclear
PRR	Pattern recognition receptor
qRT-PCR	Quantitative reverse transcription polymerase chain reaction
RFU	Relative fluorescence units
RLU	Relative light units
ROS	Reactive oxygen species
RPMI	Roswell Park Memorial Institute (Medium)
rRNA	Ribosomal RNA
SAA	Schaedler anaerobe agar
SAB	Schaedler anaerobe broth
SD	Standard deviation
SDS-PAGE	Sodium dodecyl sulphate polyacrylamide gel electrophoresis
SEM	Scanning electron microscopy
SOD	Superoxide dismutase
SRB	Sample rehydration buffer
sRPMI	Supplemented Roswell Park Memorial Institute (Medium)
TEAB	Triethylammonium bicarbonate
TIGIT	T cell immunoglobulin and ITIM domain
TLR	Toll-like receptor
TNF-α	Tumor necrosis factor alpha

CHAPTER 1: INTRODUCTION

Fusobacterium nucleatum is a Gram-negative, anaerobic commensal found in the oral cavity (Han, 2015). However, it is also considered to be an opportunistic pathogen (Brennan and Garrett, 2019) due to its involvement in periodontal disease as well as in extraoral diseases, like cardiovascular disease, inflammatory bowel disease, various types of cancers (Fan et al., 2023) and likely endometriosis (Muraoka et al., 2023). Five subspecies are currently recognised: *animalis*, *fusiforme*, *nucleatum*, *polymorphum* and *vincentii* (Han, 2015). Whether in the oral cavity or in extraoral tissues, *F. nucleatum* subspecies interact with leukocytes responding to the presence of bacteria, amongst which neutrophils are the first responders as part of the innate immune system (Rosales, 2018). Neutrophils perform antimicrobial activities to remove microbial invaders, yet, they may also cause collateral tissue damage, especially if their functional response is abnormal (Filep, 2022). Considering the involvement of *F. nucleatum* in a number of diseases and the importance of neutrophils in clearing microorganisms as well as in causing tissue damage, responses of human neutrophils to individual *F. nucleatum* subspecies warrant more detailed exploration.

This introductory section will focus on *F. nucleatum* and its involvement in health and disease, as well as its virulence factors, including biofilm formation. Neutrophils and their antimicrobial strategies will also be described, together with the collateral damage they may cause and their contribution to disease.

1.1. Fusobacterium nucleatum

F. nucleatum is a spindle-shaped, long, non-spore forming bacterium, which is not motile (Brennan and Garrett, 2019). This microbe belongs to a group of the most numerous bacterial species present in the oral environment (Huang et al., 2011). Additionally, it clusters in the

orange complex of subgingival plaque species as classified by Socransky et al. (1998)[1]. It is a key member of oral biofilms, polymicrobial communities growing in a self-produced extracellular polymeric substance, attached predominantly on tooth surfaces. Here it acts as an intermediate coloniser and a bridging organism: thanks to its adhesins RadD and FadA, among others, *F. nucleatum* binds to the early colonisers of teeth, such as *Streptococcus* species (Manson McGuire et al., 2014), which represent commensals belonging to the green and yellow Socransky's complex associated with oral health. The presence of *F. nucleatum* facilitates attachment of late colonisers, such as *Porphyromonas gingivalis, Tannerella forsythia* and *Treponema denticola*, Socransky's red complex pathogens, which thrive especially during dysbiosis, when the equilibrium between the oral microbiota and the host's immune system is disturbed (Lima et al., 2017). Thus, *F. nucleatum* facilitates co-aggregation of the above-mentioned periopathogens and health-related microbiota, two groups of microbes that would not directly attach to each other (Park et al., 2016). This results in accumulation of disease-associated dental plaque leading to different levels of periodontal disease, which can have far-reaching effects beyond the oral cavity, as will be explained in the following.

1.1.1. *F. nucleatum* and periodontal disease

Pathogen-harbouring biofilms on the surface of the tooth can initiate gingivitis, inflammation of the gingival (gum) tissue. This condition is usually reversible upon removal of these biofilms (Chapple et al., 2018). However, if not treated, gingivitis can progress into periodontitis, a

[1] Socransky complexes (Socransky et al., 1998) – five major bacterial complexes identified in subgingival plaque samples from healthy subjects and patients with periodontitis, which exhibited a significant clustering and strong relationship with periodontal health and disease. For the arguments discussed in this section, three complexes are important: yellow complex comprising of early colonisers *Streptococcus oralis, S. mitis, S. gordonii* and *S. intermedius* strongly associating with oral health; red complex containing *Porphyromonas gingivalis, Tannerella forsythia* and *Treponema denticola*, late colonisers strongly associating with increasing periodontal pocket depth and periodontitis; and orange complex, comprising *Fusobacterium* spp., *Prevotella intermedia* and *Parvimonas micra,* also associated with increasing pocket depth.

chronic inflammation of periodontal tissues including alveolar bone. Persistent inflammation then leads to irreversible damage and loss of the tooth supporting tissues, culminating in tooth loss (Erchick et al., 2019). It was shown that *F. nucleatum* residing in periodontitis-related plaque leads to damage of the tissues surrounding teeth, promotes immunoglobulin A (IgA) degradation and acquires nutrients by release of serine proteases (de Andrade et al., 2019). Thus, *F. nucleatum* plays an active role in this debilitating periodontal disease affecting more than 1 billion people worldwide (Wu et al., 2022). Severe periodontitis has become a major public health concern due to its adverse effect on nutrition and quality of life of affected individuals, as well as due to placing an immense financial burden on the health services around the globe (Tonetti et al., 2017).

Apart from periodontitis, *F. nucleatum* has also been frequently isolated among the most abundant species from inflamed peri-implant lesions (Hashimoto et al., 2022, Carvalho et al., 2023). Peri-implantitis is an inflammation of the soft and hard tissues surrounding a dental implant, characterised by progressive bone loss and in many cases resulting in implant failure (Renvert et al., 2018). It is at present unclear how and whether *F. nucleatum* as an individual species contributes to the development and progression of peri-implantitis, however, its strong ability to co-aggregate with other periopathogens and to support biofilm formation might play an important role (Chen et al., 2022b).

It has been proposed that biofilms related to periodontal disease may serve as a reservoir of opportunistic as well as true pathogens, which can actively disseminate into different parts of the body and initiate systemic diseases (Vieira Colombo et al., 2016). *F. nucleatum* has also been identified in a number of systemic diseases and extraoral tissues, with this bacterium likely originating from the oral cavity.

1.1.2. *F. nucleatum* in systemic diseases

This primarily oral bacterium has been isolated from a number of extraoral sites. *F. nucleatum* was implicated in adverse pregnancy outcomes, such as preterm labour, miscarriage, stillbirth or neonatal sepsis (Han, 2015). Han et al. (2010) demonstrated that *F. nucleatum* isolated from mothers' subgingival plaque was genetically identical with *F. nucleatum* isolated from the placenta and the infant in a case of stillbirth. This confirmed the oral origin of *F. nucleatum*, as neither rectal nor vaginal microflora contained *F. nucleatum*.

A recent publication by Muraoka et al. (2023) revealed that *F. nucleatum* might be involved in the development of endometriosis. During this disease, quiescent uterine fibroblasts are stimulated to transform to myofibroblasts, which are motile and migratory. Cell transformation is provoked by chronic inflammation. The authors of the study showed that mice infected with *F. nucleatum* developed endometriotic lesions. When cells from these lesions were transferred to recipient mice, further endometriotic lesions formed in the recipient mice, indicating that *F. nucleatum* infection resulted in stimulation of differentiation of fibroblasts into myofibroblasts (Muraoka et al., 2023).

F. nucleatum has also been shown to be involved in disorders of the gastrointestinal (GI) tract. It has gained a lot of research attention due to its active role in colorectal cancer (CRC). This bacterium was found to be enriched in tumours when compared to non-cancerous adjacent tissue. Additionally, *F. nucleatum* was found to have a direct ability to modulate inflammation in CRC and to promote tumour growth and metastases (Wu et al., 2019). Inflammation modulation by *F. nucleatum* was observed not only in CRC, but also in ulcerative colitis, a type of inflammatory bowel disease, where presence of this microbe exacerbated the damage of the intestinal tissue (Liu et al., 2019b).

Apart from the GI tract, *F. nucleatum* was associated with inflammation in the central nervous system presenting as brain abscess (Kai et al., 2008) as well as with cardiovascular disease (Han, 2015). Moreover, it was reported to work in concert with *Fusobacterium necrophorum* when causing a poorly understood upper respiratory tract infection known as Lemierre's syndrome, which affects healthy young adults and may have fatal consequences (Han, 2015). Considering the implication of *F. nucleatum* infection in these extraoral conditions as well as the fact that in many cases the bacterium likely originated in the oral cavity, it is clear that periodontal disease-related plaque containing *F. nucleatum* should not be underestimated. A deeper understanding of its virulence and interaction with the immune system in the oral cavity is required. Furthermore, due to the polymorphic nature of *F. nucleatum* species, which provoked further division into the five subspecies (Dzink et al., 1990, Gharbia and Shah, 1990, Gharbia and Shah, 1992), it is imperative that *F. nucleatum* is studied in more detail, as some subspecies have been related to health, while others have been linked with disease (Han, 2015).

1.1.3. *F. nucleatum* subspecies

To date, five subspecies are included in the *F. nucleatum* species: *animalis, fusiforme, nucleatum, polymorphum* and *vincentii* (Figure 1.1) (Dzink et al., 1990, Gharbia and Shah, 1990, Gharbia and Shah, 1992). *F. nucleatum* ssp. *nucleatum* further involves two frequently used strains deposited in the American Tissue Culture Collection (ATCC): a type strain ATCC 25586, which is largely resistant to genetic modifications, and the genetically tractable strain ATCC 23726 (Brennan and Garrett, 2019).

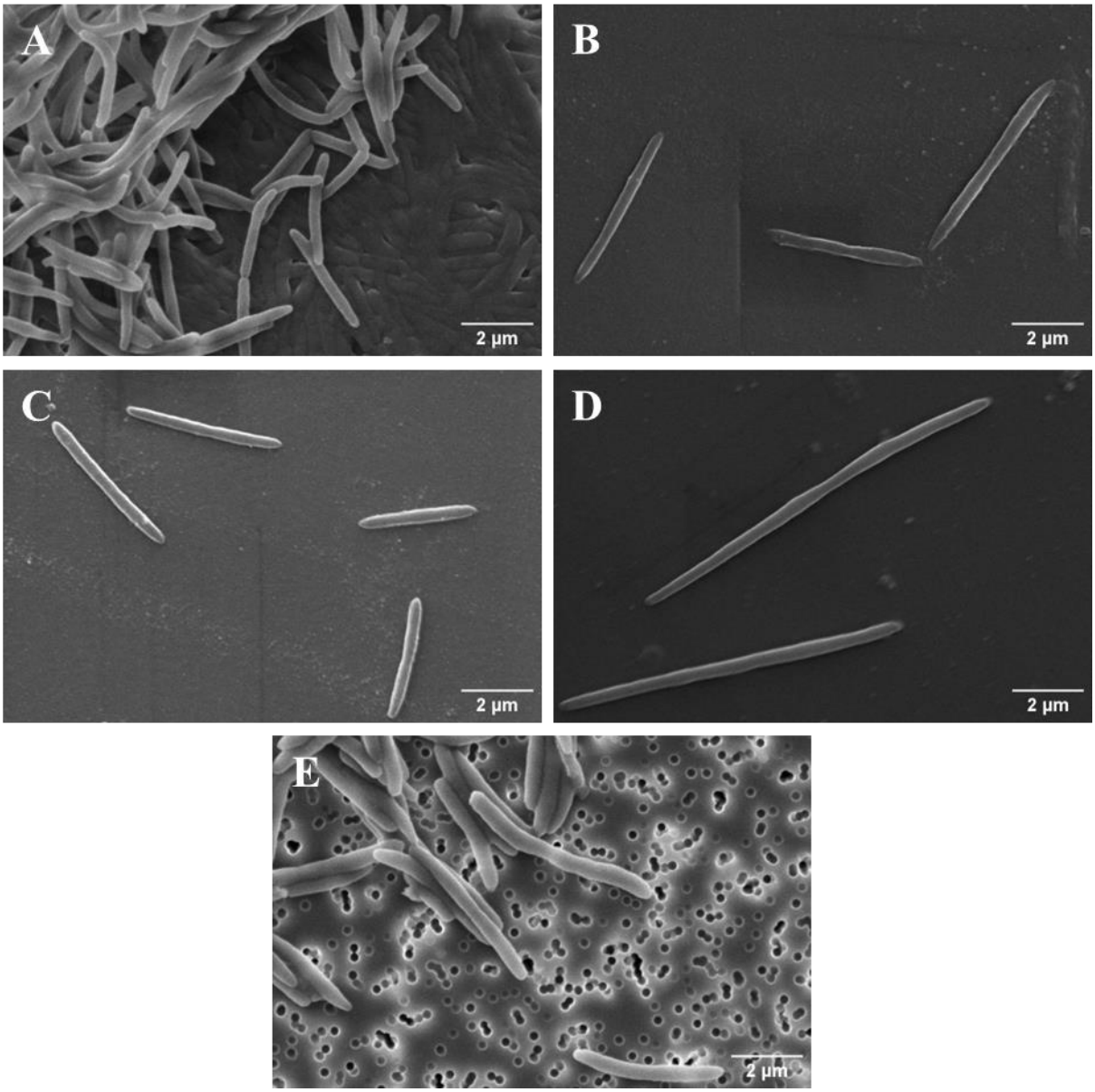

Figure 1.1. Scanning electron micrographs showing the morphology of *F. nucleatum* subspecies. A - *F. nucleatum* ssp. *animalis*; B - *F. nucleatum* ssp. *fusiforme* ; C - *F. nucleatum* ssp. *nucleatum*; D - *F. nucleatum* ssp. *polymorphum*; E - *F. nucleatum* ssp. *vincentii*. Bacteria in A-D were fixed on transparent, plastic Thermanox™ coverslips. Bacteria in E were fixed on Isopore™ membranes containing track-etched pores. Micrographs were obtained from the author's master's thesis (Muchova, 2020).

Gharbia and colleagues were among the first to suggest a subspecies-specific involvement of *F. nucleatum* in health and disease. Their analysis of oral isolates from health-associated dental plaque samples, necrotic root canal infections and periodontal pockets showed that *F.*

nucleatum ssp. *nucleatum* was mostly isolated from diseased oral sites while *F. nucleatum* ssp. *polymorphum* and *fusiforme* were cultivated from healthy individuals' plaque (Gharbia et al., 1990). Furthermore, recent research revealed that *F. nucleatum* ssp. *animalis* is a subspecies most frequently identified in intrauterine infections (Han, 2015). In terms of CRC, subspecies *animalis* has been recently identified as the dominant subspecies closely associated with tumours. Interestingly, this subspecies was found to be further divided into 2 specific clades, denoted as FNA C1 and FNA C2, and only FNA C2 was prevalent in CRC tumours (Zepeda-Rivera et al., 2024).

Yet, literature describing subspecies in specific conditions is still limited. In general, authors performing high-throughput, culture-independent genomic analyses to determine the involvement of specific bacteria in diseases usually report their results at the genus or species level and identification and reporting of bacteria at the subspecies level is often absent. In *in vitro* studies investigating *F. nucleatum* pathogenicity, authors either failed to report the subspecies used in their study or they did not use ATCC subspecies (type strains) as a reference to their non-type strains. In some cases, researchers only used clinical isolates obtained at their institution, which makes it difficult to compare the results across *in vitro* studies. This clearly highlights gaps in our understanding of the involvement of individual *F. nucleatum* subspecies in health and diseases. Differential representation of specific subspecies in healthy or diseased conditions could be attributed to likely differences in their virulence mechanisms. Indeed, a small number of authors have appreciated the need to study *F. nucleatum* subspecies separately and some of their findings will be summarised next.

1.1.4. Virulence of *F. nucleatum* subspecies

A number of virulence properties have been identified in *F. nucleatum*. The subspecies were shown to adhere to host cells and invade them. They were also found to modulate immune responses. Additionally, being a bridging organism in dental biofilms, *F. nucleatum* has a strong ability to form biofilms by adhering to other bacteria.

The invasive potential of *F. nucleatum* and other oral pathogens was studied by Han et al. (2000). They observed that *F. nucleatum* strain 12230, which is reported as non-type ssp. *polymorphum*, was highly invasive into human gingival epithelial cells. Additionally, ssp. *polymorphum* (ATCC 10953) and ssp. *nucleatum* (ATCC 25586) were even more invasive into KB cells, oral epithelial carcinoma cells, when compared to strain 12230. This was evaluated by quantification of intracellular bacteria after lysis of KB cells infected with *F. nucleatum*. While data were obtained from ssp. *polymorphum* and *nucleatum*, the information on other *F. nucleatum* subspecies was missing. Ji et al. (2010) later confirmed that *F. nucleatum* ssp. *nucleatum* (ATCC 25586) is highly invasive when cultured with gingival epithelial cells (immortalised oral keratinocyte cell line HOK-16B), yet the study only investigated this subspecies comparing it to other oral non-pathogenic and pathogenic species.

In terms of immune modulation, *F. nucleatum* elicited subspecies-specific responses in differentiated neutrophil-like human leukaemia cell line (HL-60) (Kurgan et al., 2017). Subspecies *nucleatum* (ATCC 25586), *polymorphum* (ATCC 10953) and *vincentii* (ATCC 49256) were shown to prevent superoxide generation induced by N-Formylmethionyl-leucyl-phenylalanine (fMLP) in HL-60 cells in a subspecies-specific manner. Subspecies *polymorphum* significantly increased the rate of apoptosis in HL-60 cells when compared to the other subspecies. Additionally, it was suggested that the subspecies differentially stimulate neutrophil-like cell function via toll-like receptors 2 and 4 (TLR-2 and TLR-4), with ssp.

polymorphum stimulating higher expression of only TLR-2 mRNA and ssp. *vincentii* inducing higher expression of both TLR-2 and TLR-4 mRNA when compared to ssp. *nucleatum*. While modulation of immune responses by individual subspecies was studied in this cell line, responses by primary human neutrophils have not been studied to date.

Biofilm formation of *F. nucleatum* subspecies in complex multi-species oral biofilm models was evaluated *in vitro* by Thurnheer et al. (2019). The group studied differences in the ability of *F. nucleatum* ssp. *fusiforme, nucleatum, polymorphum* and *vincentii* to aggregate with early and late colonisers of tooth surfaces and their effect on maturation of biofilms. Incorporation of individual subspecies was analysed in supragingival and subgingival biofilms by confocal laser scanning microscopy and by culture on selective and non-selective media and subsequent colony-forming unit (CFU) enumeration. In both biofilm models, the incorporation of ssp. *fusiforme, polymorphum* and *vincentii* was significantly lower compared to control ssp. *nucleatum*. Interestingly, in the subgingival model, the numbers of *P. gingivalis, Streptococcus oralis, Prevotella intermedia* and *Campylobacter rectus* were significantly decreased in the presence of ssp. *fusiforme, polymorphum* and *vincentii* compared to the ssp. *nucleatum* control group. These results showed that interactions with other oral bacteria and biofilm formation might be subspecies-specific. To the best of the author's knowledge, single-subspecies biofilm formation has not been systematically studied to date.

Taken together, the above-mentioned findings demonstrate that *F. nucleatum* subspecies need to be investigated separately, especially when it comes to virulence properties such as biofilm formation and possible suppression of the immune responses as seen in the HL-60 cell line. A specific group of *F. nucleatum* virulence factors, known as adhesins, has been studied in the context of biofilm formation and aggregation with other oral species, as well as cell invasion and carcinogenesis.

1.1.5. Adhesins in *F. nucleatum*

Adhesins are a specific group of proteins present on the surface of a bacterial cell, generally aiding adhesion to host cells, other bacterial cells or abiotic surfaces (Lipke and Ragonis-Bachar, 2023).

A number of adhesion proteins mediating coaggregation and biofilm formation with other oral species as well as proteins from saliva, have been identified in *F. nucleatum*: adhesin FadA (Meng et al., 2021), outer membrane protein RadD with an accessory protein Aid1, autotransporter Fap2, porin FomA and outer membrane protein CmpA (Diaz and Valm, 2020). Homologous adhesion proteins found in other non-oral bacterial species have also been recognised in *F. nucleatum in silico*, such as the YadA-like adhesin previously identified in *Yersinia* species (Umaña et al., 2019) (overview of adhesins in Figure 1.2.).

The adhesin FadA, which has also been characterised as an invasin (Manson McGuire et al., 2014), is utilised by *F. nucleatum* to perform active invasion into host cells, which may aid extra-oral translocation. Additionally, FadA binds to cell junction molecules known as vascular endothelial cadherins, loosening the tight junctions in the layer of endothelial cells. This way, *F. nucleatum* disseminates via the hematogenous route by increasing vascular permeability and entering the blood stream, then exiting the blood stream elsewhere. This process enables *F. nucleatum*, and likely other pathogenic residents of the dental biofilm, to escape the oral environment and establish infection in various body sites, such as heart and placenta (Shammas et al., 1993, Vander Haar et al., 2018). FadA was also found to promote auto-aggregation and formation of biofilms in *F. nucleatum* 12230 (non-type ssp. *polymorphum*) (Meng et al., 2021). The most studied virulence aspect of FadA is its direct involvement in progression of CRC. FadA of *F. nucleatum* binds malignant CRC cells via Annexin A1 present on actively proliferating CRC cells, stimulating cell Wnt/β-catenin signalling and promoting CRC cell

growth (Rubinstein et al., 2019). Studies utilising FadA deletion mutants showed that bacterial binding to oral epithelial KB cells and Chinese hamster ovary (CHO) cells was significantly reduced (70% to 80%) (Han et al., 2005). Moreover, the mutant strain was severely defective in adhesion and invasion into CHO cells and human oral keratinocytes OKF6/Tert and in colonisation of mouse placenta *in vivo* (Ikegami et al., 2009).

Adhesin RadD is involved in coaggregation with early colonisers, such as *Streptococcus* species, and in supporting formation of multispecies oral biofilms (Kaplan et al., 2009). Deletion mutants showed significantly lower coaggregation with Gram-positive bacteria *Streptococcus sanguinis*, *S. oralis*, *S. gordonii* and *S. mutans* (Kaplan et al., 2009, Guo et al., 2017) and significantly decreased biofilm formation with *S. sanguinis* (Kaplan et al., 2009). This membrane protein also plays a role in *F. nucleatum* invasion into host cells (Manson McGuire et al., 2014). Interestingly, RadD is also involved in inducing apoptosis in human lymphocytes, as shown by studies using RadD-deficient strain, which lead to decreased apoptosis compared to the wild type strain (Kaplan et al., 2010).

Fap2 (Fibroblast activation protein 2) is an adhesin and an autotransporter, which facilitates co-aggregation with *P. gingivalis* and mammalian cells, as confirmed by studies including mutant strains (Coppenhagen-Glazer et al., 2015). Together with FadA, it is another adhesin involved in CRC: it binds CRC cell surface factor D-galactose-β(1-3)-N-acetyl-D-galactosamine (Gal-GalNAc), aiding CRC tumour colonisation by *F. nucleatum* (Abed et al., 2016). Mutant Fap2 strain was shown to have a decreased ability to attach to human colon adenocarcinoma tissue (Abed et al., 2016). Fap2 further interacts with natural killer (NK) cells via TIGIT (T cell immunoglobulin and ITIM domain) on the surface of NK cells, preventing tumour cell killing by NK cells, as established by mutant studies (Gur et al., 2015).

FomA is a major outer membrane porin (Toussi et al., 2012) involved in biofilm formation with *P. gingivalis* (Chen et al., 2022b) and its expression was confirmed to be significantly higher in biofilm-grown *F. nucleatum* (Chew et al., 2012). It also assists *F. nucleatum* binding to host cells and stimulates immune responses via Toll-like receptor 2 (TLR-2) (Toussi et al., 2012). There is a lack of studies utilising FomA mutant strains, however, this membrane protein was characterised using either purified recombinant FomA expressed in *Escherichia coli* (Toussi et al., 2012) or via serum neutralisation of the protein (Liu et al., 2010).

CmpA (Coaggregation-mediating Protein A) was characterised as an adhesin co-aggregating with *S. gordonii*, which forms part of the early colonisers in oral biofilms. CmpA mutant strain showed significantly reduced coaggregation as well as biofilm formation with *S. gordonii* (Lima et al., 2017).

The YadA-like protein, which was originally reported as an adhesin and virulence factor in *Yersinia* species and was later identified by liquid chromatography-tandem mass spectrometry (LC/MS/MS) in outer membrane vesicles *F. nucleatum* (Liu et al., 2019a), adheres to fibronectin and collagen present in the salivary pellicle and extracellular matrix of human cells (Umaña et al., 2019). Currently, there are no available mutant strains deficient of YadA-like protein.

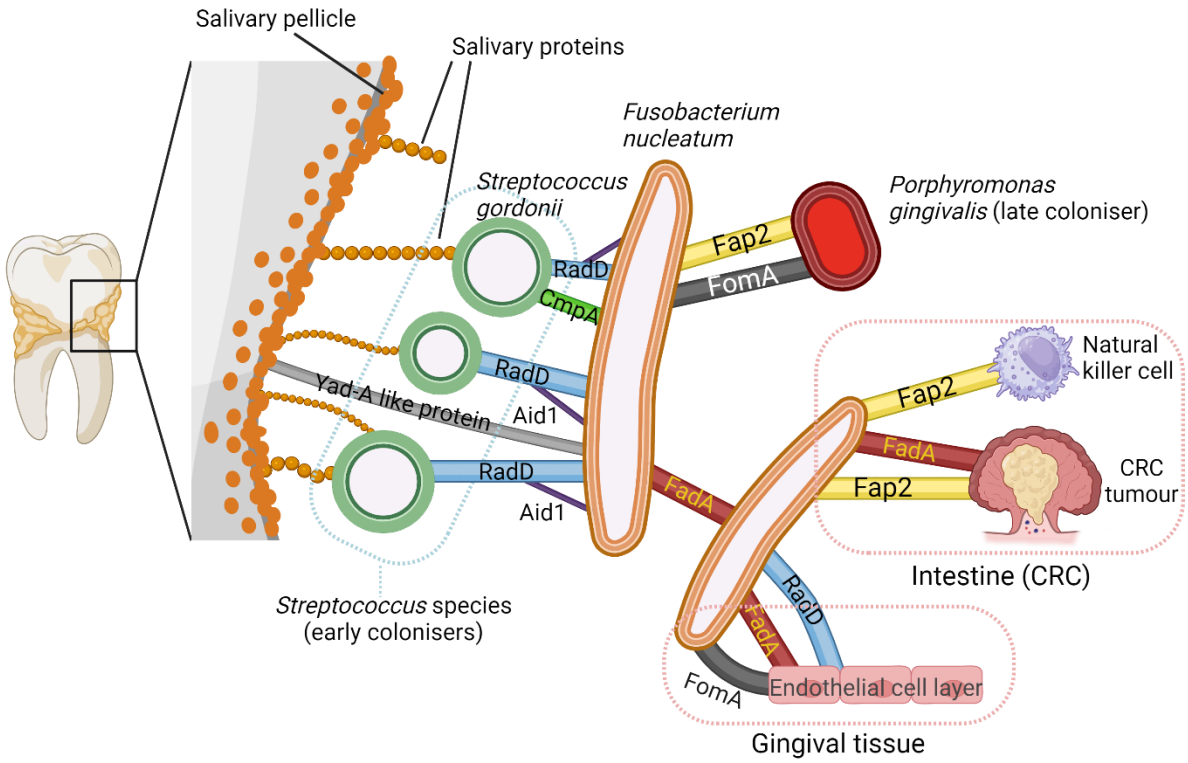

Figure 1.2. Schematic representation of *F. nucleatum* adhesins and binding partners. *F. nucleatum* bridges early colonisers (health-related green complex bacteria) and late colonisers (red complex pathogens, such as *P. gingivalis*) in the dental plaque. Its adhesins also interact with CRC tumour cells, natural killer cells and other host cells (endothelial cells of gingival vasculature and epithelial cells). Adapted from Chen et al., 2022, created with BioRender.com.

Co-aggregation with other bacterial species aided by *F. nucleatum* adhesins has been investigated, nevertheless, the involvement of the adhesins in auto-aggregation and single-subspecies biofilm formation has not been evaluated. While it is true that *F. nucleatum* mostly resides in and structurally supports multispecies biofilms, it is important to explore auto-aggregation, as understanding the involvement of adhesins in these processes could help identify therapeutic targets in *F. nucleatum*-dominated diseases. Additionally, the findings described above show that *F. nucleatum* with its virulence factors has been studied either in the context of epithelial cell invasion or carcinogenesis, but the interaction of subspecies with innate immune cells, such as neutrophils, is poorly understood.

1.2. Neutrophils

Neutrophils, also called polymorphonuclear (PMN) leukocytes, form the first line of defence in human tissues. Bone marrow produces around 10^{11} neutrophils per day and these terminally-differentiated, non-dividing leukocytes form the most abundant portion of white blood cells in human blood. Morphologically, they can be distinguished by their multi-lobed nucleus (Manley et al., 2018) and the presence of granules in the cytoplasm (Sheshachalam et al., 2014). Neutrophils have the ability to leave the circulation and enter tissues, where they act as innate immune system effectors. They constantly patrol bodily tissues, searching for the presence of pathogens (Rosales, 2018). Neutrophils utilise a number of interconnected antimicrobial strategies to fight pathogens (Figure 1.3):

1) Ingestion of the intruders by active phagocytosis involving the employment of the antimicrobial enzymes stored in the intracellular granules (intracellular degranulation) (Rosales, 2018).
2) Generation of intracellular as well as extracellular reactive oxygen species (Batot et al., 1995, Matthews et al., 2007a, Matthews et al., 2007b).
3) Release of neutrophil extracellular traps (NETs) (Brinkmann et al., 2004).
4) Extracellular degranulation of antimicrobial proteins to kill non-phagocytosed microorganisms (Lacy, 2006).
5) Secretion of proinflammatory cytokines in order to recruit additional immune cells to the site of infection (Cassatella, 1995).

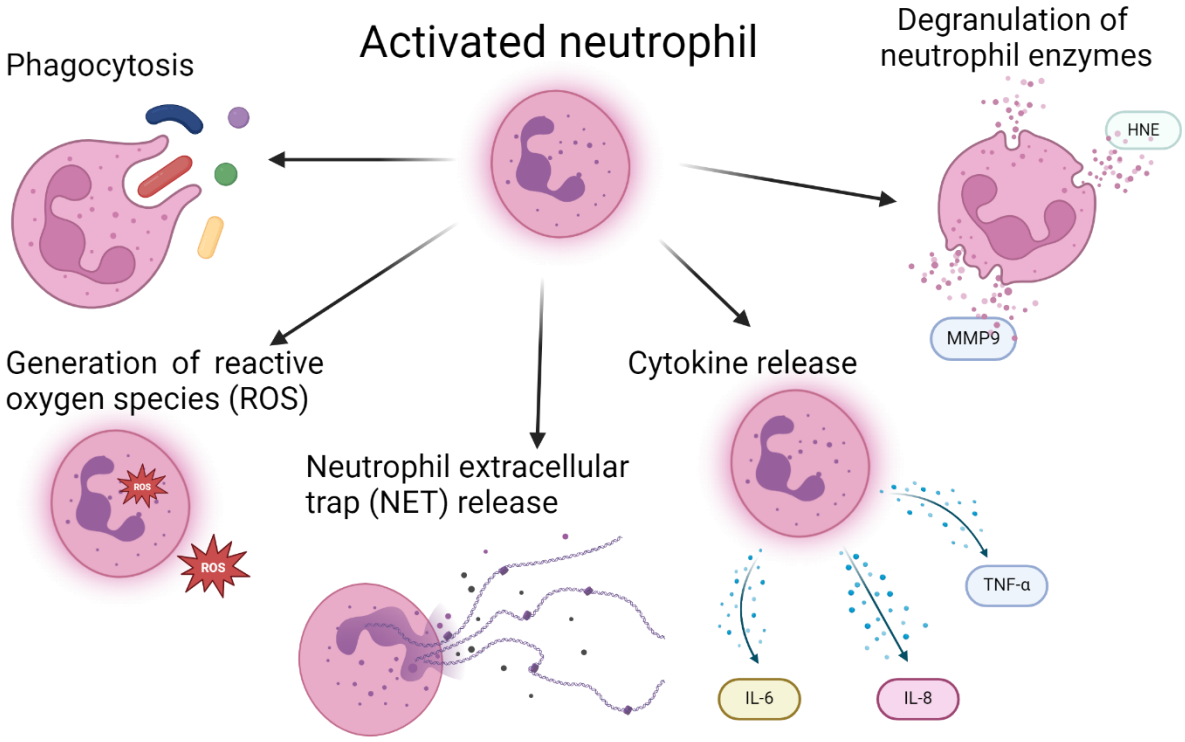

Figure 1.3. Antimicrobial strategies of activated neutrophils. Neutrophils activated by bacteria or bacterial products remove pathogens by phagocytosis, generation of bactericidal reactive oxygen species (ROS), NETosis or release of antimicrobial enzymes. Neutrophils also release cytokines to communicate with other immune cells. HNE – Human neutrophil elastase; MMP9 – Matrix metalloproteinase 9; IL-6 – Interleukin 6; IL-8 – Interleukin 8; TNF-α – Tumour necrosis factor α. Created with BioRender.com.

1.2.1. Antimicrobial strategies of neutrophils and selected methods to quantify them

A combination of rapid antimicrobial strategies makes neutrophils powerful first responders to the presence of pathogens and infection. In order to study, quantify and understand neutrophil responses, various approaches have been developed and these will be described together with the specific antimicrobial strategies next.

1.2.1.1. Phagocytosis

Neutrophils belong to a group of professional phagocytic cells due to their ability to engulf microorganisms (van Kessel et al., 2014). Microorganisms or other particles can be phagocytosed especially when opsonised by immunoglobulins and complement particles. Upon engagement of specific cell surface receptors described in more detail in section 1.2.2, neutrophils actively modify the cell membrane by actin cytoskeleton rearrangement, surrounding the microorganism by pseudopods. Microorganisms are then completely engulfed and enclosed in a vacuole called phagosome, which undergoes membrane structure as well as content modifications. Phagosomes ultimately become phagolysosomes by fusion with lysosomes, which are vacuoles filled with a variety of lytic enzymes facilitating killing and digestion of the ingested microorganisms (Uribe-Querol and Rosales, 2020).

Evaluation of phagocytosis can be performed by counting viable colony-forming units collected after the bacterial stimulation and subsequent neutrophil lysis, however this approach is laborious (Boero et al., 2021) and could generate false negative results as bacterial killing could take place before the quantification. A more accurate measurement of phagocytosis is flow cytometry, which can quantify neutrophils in a buffered liquid medium. This method uses lasers to obtain scattered signals dividing cells based on the cell size and granularity, as well as fluorescent signals based on the detection of fluorescent proteins, dyes or antibodies (McKinnon, 2018). GFP-expressing bacteria or bacteria stained with nucleic acid dyes are usually used as stimuli in phagocytosis assays as their fluorescent signal provides direct quantification of engulfed bacteria (McKinnon, 2018).

1.2.1.2. Generation of reactive oxygen species (ROS)

Microorganisms in phagosomes are also eliminated with the help of ROS produced in a process known as oxidative burst. Following phagocytosis, the multi-protein nicotinamide adenine dinucleotide phosphate-oxidase (NADPH) complex is assembled in the membrane of a developing phagolysosome (Nguyen et al., 2017). NADPH oxidase transfers electrons through the complex, reducing molecular oxygen to superoxide anions (O_2·-) intracellularly. This species can further be converted to hydrogen peroxide (H_2O_2) by superoxide dismutase (SOD). H_2O_2 can be acted upon by myeloperoxidase (MPO) to generate hypochlorous acid (HOCl), which has strong bactericidal activity (Winterbourn et al., 2016, Nguyen et al., 2017). Superoxide ions can also be generated extracellularly if the NADPH oxidase complex is assembled on the cell membrane.

Quantification of ROS by neutrophils can be carried out employing a commonly used and highly sensitive enhanced chemiluminescent assay (Matthews et al., 2007a, Hirschfeld et al., 2017, Sharma et al., 2019). Luminol, isoluminol and lucigenin are chemiluminescent reagents which emit light in the presence of ROS (Jancinová et al., 2006, Sharma et al., 2019). Luminol is used to quantify total ROS, including intracellular and extracellular (O_2·-, H_2O_2, ·OH-) because its uncharged state allows the passage of the molecule through the cell membrane (Sharma et al., 2019). Isoluminol differs from luminol in the molecular structure, it is hydrophilic and cannot cross the cell membrane, therefore it only measures extracellular ROS (Jancinová et al., 2006). Lucigenin, due to its positive charge, is not membrane-permeable and specifically measures extracellular superoxide ions (O_2·-) and hydroxyl radicals (·OH-) (Sharma et al., 2019).

1.2.1.3. Formation of neutrophil extracellular traps (NETs)

Activated neutrophils fight pathogens also by the release of NETs, in a process sometimes termed NETosis. This process can be activated by bacteria, bacterial products, fungi, immune complexes and factors produced by the host, usually in quantities and sizes that cannot be eliminated by phagocytosis, such as fungal hyphae (Urban et al., 2006) or large bacteria (Branzk et al., 2014). The role of NETs is to immobilise microbes and possibly kill them (Hirschfeld et al., 2017). NETs comprise nuclear material – decondensed chromatin with DNA, histones, antimicrobial peptides and additional antimicrobial proteins (Hirschfeld et al., 2015, Moonen et al., 2019). When bacterial challenge triggers NETosis, the nuclear membrane disintegrates and the content of cytoplasmic granules combines with nuclear material. This is followed by rupture of the cell membrane and release of NETs. This type of NETosis was termed suicidal due to the death of the neutrophil (Fuchs et al., 2007). Interestingly, vital NETosis has also been characterised, when neutrophils did not undergo cell death and maintained some level of cell activity (Pilsczek et al., 2010). Release of mitochondrial DNA as NETs has also been noted and this was shown not to affect neutrophil viability (Yousefi et al., 2009).

NET formation can be studied by observing extruded NET-DNA structures using fluorescent microscopy. NETs released upon stimulation can be stained with cell impermeable DNA stains, such as SYTOX green (de Buhr and von Köckritz-Blickwede, 2016). Fluorescent staining of released NETs can also be utilised in fluorometric quantification of NETs. Stained NET-DNA structures can be digested using a nuclease enzyme and after the elimination of the cellular debris by centrifuging, fluorescence of the resulting supernatant can be quantified using a fluorometer (White et al., 2016, Hirschfeld et al., 2017). Additionally, NETosis can be quantified by enzyme-linked immunosorbent assay (ELISA), using specific antibodies

targeting DNA-bound proteins in NETs, such as neutrophils elastase, myeloperoxidase or cathepsin G (Matta et al., 2022) as well as citrullinated histone H3 (Thålin et al., 2020).

1.2.1.4. Degranulation

Apart from oxidative killing, neutrophils also employ non-oxidative bacterial killing by proteases stored in intracellular granules. This process is tightly regulated, and neutrophils can kill microorganisms either intracellularly by delivery of these enzymes to the phagosome after phagocytosis, or extracellularly by releasing proteases into the extracellular milieu (Eichelberger and Goldman, 2020). Granules are divided into 4 distinct classes: primary (azurophilic), secondary (specific), tertiary granules and secretory vesicles. Contents of the primary granules are the most toxic antimicrobials, such as neutrophil elastase and myeloperoxidase. Neutrophil elastase targets bacterial outer membrane proteins, destabilising the cell membrane and thus causing bacterial cell death. Additionally, it cleaves and activates host antimicrobial peptides (Stapels et al., 2015). Myeloperoxidase kills microorganisms indirectly by generating bactericidal hypochlorous acid HOCl from H_2O_2 during the oxidative burst (Klebanoff et al., 2013). Secondary granules enclose proteins such as lactoferrin and lysozyme, and tertiary granules contain matrix metalloproteinase 9 (MMP-9) (Lacy, 2006), an enzyme degrading component of the extracellular matrix and playing a role in neutrophil transit through tissues and tissue remodelling (Wang, 2018, Velasquez et al., 2023). Secretory vesicles serve to restore neutrophil surface receptors such as complement or Fc receptors and are released constantly during the neutrophil life cycle (Lacy, 2006). Importantly, granules can only be released when the corresponding signalling pathway is activated by the engagement of a membrane receptor due to their highly tissue-destructive potential (Lacy, 2006).

Release of antimicrobial enzymes during degranulation is often quantified using ELISA (Özçaka et al., 2011, Lee et al., 2021, Huang et al., 2022). Detection of released enzymes is performed from supernatants collected after bacterial or drug stimulation. Additionally, expression of antimicrobial enzyme genes can be investigated by quantitative real-time reverse transcription polymerase chain reaction (qRT-PCR) (Sng et al., 2017), however this approach alone does not provide direct quantification of enzyme release into the extracellular environment.

1.2.1.5. Release of pro- and anti-inflammatory cytokines

A considerable amount of research has been conducted in the last five years to identify cytokines released by neutrophils and define their biological functions (Cassatella et al., 2019). Neutrophils produce both anti- and proinflammatory cytokines to communicate with other neutrophils as well as other cells of innate immunity, such as macrophages (Bouchery and Harris, 2019). Additionally, they were shown to play a role in the acquired immune system responses by regulating T and B cell activity (Li et al., 2019).

Production of most cytokines is transcriptionally regulated and is induced in response to specific stimuli, such as binding of ligands to Toll-like receptors (TLRs), and therefore their release is slower compared to degranulation. Interestingly, some cytokines were found to be stored in resting neutrophils, such as IL-16 and IL-18 (Cassatella et al., 2019), indicating that these can be released more rapidly.

Similarly to the detection of antimicrobial enzymes, ELISA is frequently utilised also for the quantification of extracellular neutrophil cytokine release by analysing supernatant obtained from neutrophils stimulated with bacteria (Ling et al., 2015, Tamassia et al., 2018). Pro-

inflammatory cytokines previously studied by our group included IL-1β, TNF-α, IL-6 and IL-8 (Ling et al., 2015). Moreover, the expression of cytokine genes can be analysed by qRT-PCR, as performed by Wright et al. (2011), who studied, among other proteins, expression of the cytokines CXCL-1, CXCL-2 and CXCL-3 in human neutrophils in response to stimulation with *F. nucleatum* ssp. *polymorphum*.

In order for neutrophils to initiate these antimicrobial processes, invading microbes have to be recognised by specific receptors present on the surface of neutrophils.

1.2.2. Neutrophil receptors for detection of microbes and activation of antimicrobial pathways

Neutrophil surface receptors detecting the presence of microbes, also known as pattern-recognition receptors (PRRs), can be broadly divided into phagocytic and non-phagocytic PRRs.

Phagocytic receptors are essential for internalisation of microbes and other particles. Rapid formation of pseudopods around the microbe and a complete entrapment occur thanks to Fc receptors stimulated by immunoglobulins opsonising the intruder (Lee et al., 2003). Despite being considered as phagocytic PRRs, Fc receptors were also found to be involved in NET formation (Alemán et al., 2016) as well as ROS generation (Nguyen et al., 2017). If the microbe is opsonised by complement particles, these engage complement receptors, such as CR1 and CR3, and the process is said to be slower compared to Fc receptor-mediated responses (van Kessel et al., 2014). Non-opsonised fungal pathogens can be recognised by receptors such as C-type lectins (Dectin-1, Dectin-2), which are lectin-like recognition molecules, as well as scavenger receptors (Uribe-Querol and Rosales, 2020).

The main type of non-phagocytic receptors is the TLR. TLRs detect a wide variety of microbial molecules, such as DNA, RNA, lipids, lipoproteins and proteins (Mayadas et al., 2014). For the purposes of this study, TLR2 and TLR4 are the most important receptors. TLR2 detects predominantly Gram-positive bacteria (such as oral commensal *Streptococcus* species) by binding cell wall components such as lipoteichoic acid. TLR4 can recognise Gram-negative bacteria (such as *F. nucleatum*) by interacting with lipopolysaccharide (LPS) in the outer bacterial membrane (Branger et al., 2004). Stimulation of both TLR2 and TLR4 leads to NETosis (Singh et al., 2016) and ROS generation (Prince et al., 2011), as well as upregulation of cytokine gene transcription (Futosi et al., 2013).

Receptors involved in mobilisation of granule-containing vesicles include G protein-coupled receptors, integrins and TLRs on the neutrophil surface (Eichelberger and Goldman, 2020). Vesicle trafficking can be directed both intracellularly to the bacteria-containing phagosome or extracellularly. Stimulation of these receptors activates signalling pathways leading to a multi-step modification process in the neutrophil and resulting in fusion of the granule-containing vesicle with the target membrane (Lacy, 2006, Eichelberger and Goldman, 2020).

Interestingly, NETosis and ROS generation were found to be activated also without receptor involvement by phorbol myristate acetate (PMA) (Gray et al., 2013). PMA enters the cell and directly activates protein kinase C (PKC) which in turn activates the NADPH oxidase system and NET extrusion. Additionally, hypochlorous acid (HOCl), a product of myeloperoxidase activity, was found to trigger NET release (Palmer et al., 2012).

Knowledge of neutrophil antimicrobial responses and the receptors involved has been acquired using not only peripheral blood neutrophils, but also an established cell line mentioned above, the human promyelocytic leukaemia cell line (HL-60).

1.2.3. Neutrophil-like human promyelocytic leukaemia cell line (HL-60)

HL-60 cells were first obtained from an adult female diagnosed with acute promyelocytic leukaemia. Upon isolation, the majority of cells were described to be either myeloblasts or promyelocytes, precursors of neutrophils (Collins et al., 1977). After the initial discovery that these cells can be cultured for extended periods of time and that they terminally differentiate towards neutrophil-like cells either spontaneously (Collins et al., 1977) or when stimulated with various compounds (butyrate, dimethyl sulfoxide [DMSO], retinoic acid) (Breitman et al., 1980), HL-60 became a very popular model to study differentiation of bone marrow-derived myeloid cells (Birnie, 1988) as well as development and progression of leukaemia (Basu et al., 2023). Additionally, a number of more recent studies used HL-60 cells to elucidate neutrophil functional responses.

As described in section 1.1.4, HL-60 cells were studied in the context of *F. nucleatum* infection and ROS generation, cytokine release and cell survival (Kurgan et al., 2017). HL-60 cells have also been utilised in the investigation of NETosis. Yasuda et al. (2020) demonstrated that NETosis was epigenetically regulated, as DNA demethylation increased the level of NETosis. Yet, it is important to mention that HL-60 cells were reported to have a limited ability to produce NETs, and optimisation of differentiation conditions was deemed necessary for more effective NETosis (Guo et al., 2021). The use of serum-free medium facilitated a successful differentiation, however NETosis in this study was not compared to that of primary neutrophils. Release of antimicrobial proteins by HL-60 was studied by Bhakta et al. (2024), who showed that differentiated HL-60 cells had the ability to undergo degranulation and released primary granules containing MPO.

Advantages of undifferentiated HL-60 cells include the immortal nature of this cell line. Thanks to the possibility of maintaining HL-60 cells in continuous culture as well as freezing cells for

long-term storage without affecting their activity, the need for freshly isolated neutrophils from donors is removed. This also eliminates inter-donor variation in assays. Moreover, HL-60 cell doubling time is considerably short (between 20 and 45 hours) and genetic modifications, such as electroporation or lentiviral transduction, can be successfully performed (Blanter et al., 2021).

On the other hand, a major limitation of HL-60 cells is the fact that immortalised, cancer-derived cell lines might not reflect cell processes in physiological conditions (Basu et al., 2023). A study comparing transcriptomic profiles of undifferentiated HL-60 cells and healthy neutrophil progenitor cells showed differences in gene expression, indicating a significantly lower level of complexity of HL-60 cell differentiation compared to the primary cells. While information on HL-60 differentiation by various compounds is available, studies comparing this process to primary progenitor cell differentiation are absent (Basu et al., 2023). Therefore, results obtained from HL-60 cells should be carefully evaluated and potentially supported by data from primary human neutrophils to be able to validate the results obtained from a cell line. This is especially important if HL-60 cells are utilised in studies investigating the responses of neutrophils in various diseases. Drawing conclusions from data obtained from HL-60 cells alone may underestimate the infection-resolving neutrophil capacity as well as the destructive potential of neutrophils, which is exemplified by excessive activation of neutrophils leading to collateral tissue damage and unresolved chronic inflammation along with autoimmune diseases (Fu et al., 2021).

1.2.4. Neutrophils contributing to disease

The antimicrobial activity of neutrophils can be a double-edged sword – on the one hand efficiently eliminating intruders, on the other causing tissue damage and contributing to

inflammation. Inappropriate neutrophil function has gained significant attention in recent years due to its direct destructive effect in various diseases, such as periodontitis, rheumatoid arthritis and cancer (Amulic et al., 2012, Uriarte et al., 2016).

The presence of complex dental biofilms on tooth surfaces and more specifically in the gingival sulcus, where the gingival tissue is in close contact with the tooth surface, constantly attracts circulating neutrophils (Uriarte et al., 2016). It is no surprise that neutrophils are found in the gingival epithelium and the sulcus in large numbers, creating a protective wall between the microbial community and the epithelium (Cortés-Vieyra et al., 2016), to ensure that oral homeostasis is maintained. Neutrophil interaction with healthy, commensal microbes is considered to be symbiotic (Hirschfeld et al., 2015, Moonen et al., 2019). However, in periodontitis, pathogens such as *P. gingivalis* residing in biofilms are able to evade neutrophil killing mechanisms, thus creating a vicious circle of pathogenic presence and increase of neutrophil numbers and bactericidal activity. Neutrophils in periodontitis have been found to be hyperactive (excessive ROS production without stimulation) and hyper-reactive (excessive ROS production when stimulated) (Matthews et al., 2007a, Matthews et al., 2007b, Roberts et al., 2015), damaging the surrounding tissue by increased release of ROS, antimicrobial peptides as well as enzymes, which worsen the progression of periodontitis (Uriarte et al., 2016). Hyper-reactivity in neutrophils from periodontitis patients was also reported in terms of cytokine release (Ling et al., 2015).

Neutrophil antimicrobial enzymes were found to have tissue-damaging effects in periodontitis: Hiyoshi et al. (2022) demonstrated that human neutrophil elastase (HNE) exacerbates periodontitis by breaking the gingival epithelial barrier and contributing to periodontal bone loss. Another neutrophil enzyme, MMP-9, which can cause pathological connective tissue destruction, is detected in higher amounts in periodontitis (Bildt et al., 2008, Luchian et al.,

2022), including in saliva and gingival crevicular fluid (GCF) of patients (Gursoy et al., 2013, Luchian et al., 2022).

Of note is a process of "frustrated phagocytosis", where neutrophils attempt to eliminate the dental biofilm by engulfing it. As this biomass cannot be internalised, neutrophils release their intracellular antimicrobial arsenal instead, having the same detrimental effect as hyperactivity and hyper-reactivity (Scott and Krauss, 2012). Additionally, neutrophil chemotaxis, cell movement along a chemical gradient, was shown to be impaired in periodontitis patients by Roberts et al. (2015). Neutrophils had a significantly lower speed and velocity, and impaired accuracy of directional movement when compared to healthy controls. This might prolong the transit time in the tissues, thus impacting on the clearance of microbes and affecting periodontitis prognosis. Overall, poor oral health is known to have direct connections with diseases affecting other areas of the organism, making periodontitis a complex disease.

One of the extraoral diseases, which has been associated with periodontitis as a risk factor, is CRC (Idrissi Janati et al., 2022). As mentioned, *F. nucleatum* as an oral species has been directly related to carcinogenesis in CRC. Neutrophils were also reported to be involved in CRC with *F. nucleatum*-colonised tumours. Kong et al. (2023) detected higher neutrophil infiltration in tumour tissues with *F. nucleatum* present compared to adjacent healthy tissues. Moreover, *F. nucleatum*-infected CRC tissues contained significantly greater amounts of NETs. Further *in vitro* investigations using *F. nucleatum* ssp. *nucleatum* showed that *F. nucleatum*-induced NETs stimulated angiopoiesis and tumour metastasis (Kong et al., 2023).

CRC progression is negatively affected also by neutrophil enzymes. HNE from NETs was found to significantly increase the migratory activity of CRC cells *in vitro* and inhibition of HNE activity in mice decreased migration of tumour cells to liver tissue, suggesting that HNE plays a role in the formation of liver metastases in CRC (Okamoto et al., 2023). Analysis of CRC

tumour tissues also showed that the expression of MMP-9 was significantly higher compared to adjacent healthy tissue. Moreover, there was a strong correlation between high MMP-9 expression and pathological parameters such as lymph node and distant metastasis as well as poorer patient survival (Wang et al., 2019). MMP-9 produced by tumours was reported to promote breast cancer progression, metastasis and angiogenesis (Mehner et al., 2014, Guo et al., 2024).

Neutrophils were also studied in the context of women's health and were shown to play an important role in endometriosis (Xu et al., 2020). A positive correlation was found between the number of neutrophils in the ovarian endometrioma and the severity of the disease. Moreover, neutrophils were found to exhibit an immunosuppressive phenotype towards T cells.

Regarding complications in pregnancy, involvement of neutrophils was reported in pre-eclampsia, a pregnancy disorder with possible severe features characterized by maternal new-onset high blood pressure and high levels of protein in urine. This disorder increases the risk of placental abruption and preterm birth and in severe cases can lead to maternal death. In pre-eclampsia, a higher level of neutrophil activation was observed together with significantly higher level of NETosis in the placenta (Bert et al., 2021). Additionally, NETs in uterine endothelium were shown to cause apoptosis and tissue damage in pre-eclampsia (Liu et al., 2022).

To recapitulate, oral bacteria form dental biofilms with *F. nucleatum,* one of the most important structural residents of oral biofilms, allowing integration of pathogens such as *P. gingivalis*, which can establish infection. Neutrophils, as the first line of defence, mount an inflammatory response aiming to eliminate the pathogens, which in turn resist the clearance and neutrophil

antimicrobial activities are deflected. This leads to pathological and progressive tissue destruction rather than inflammation- and healing-associated physiological remodelling. While neutrophil interaction with a major culprit in periodontitis, *P. gingivalis,* has been studied extensively (How et al., 2016), little is known about the immunogenicity of *F. nucleatum* on a species level and even less on a subspecies level. Therefore, this doctoral thesis focuses on functional and molecular responses of neutrophils to planktonic as well as biofilm-grown *F. nucleatum* subspecies. Understanding *F. nucleatum* involvement in periodontitis in greater detail, and possible differences in the immunogenicity of the subspecies when interacting with neutrophils, may provide novel insights into prevention and treatment of periodontitis and associated *F. nucleatum*-related systemic diseases.

1.3. Research aims and objectives

Research focusing on interactions between the subspecies of an important biofilm-supportive bacterium *F. nucleatum* and the human innate immune cells is currently limited. Thus, the main research aim of this doctoral thesis was to investigate responses of primary human neutrophils to individual *F. nucleatum* subspecies and validate potential differences in the subspecies immunogenicity as previously shown in a neutrophil-like cell line. The secondary aim was to assess the immunogenicity of subspecies grown planktonically and in biofilms. In order to fulfil the aims, the following objectives were set:

1) To grow single-subspecies *F. nucleatum* biofilms to be used as stimuli for neutrophil functional and molecular assays and to systematically characterise *F. nucleatum* biofilm formation on different surfaces and surface treatments in terms of quantity, stability and structure.

2) To evaluate functional responses of human neutrophils to formalin-fixed *F. nucleatum* subspecies grown planktonically.
3) To analyse functional and molecular responses of human neutrophils to live *F. nucleatum* subspecies as clinically more relevant assay stimuli.
4) To determine whether biofilm-grown live *F. nucleatum* subspecies, likely expressing biofilm-specific virulence factors, stimulate more potent neutrophil responses.

CHAPTER 2: MATERIALS AND METHODS

2.1. Bacterial strains and culture conditions

Fusobacterium nucleatum type strains (Table 2.1) used in this project were obtained from the Oral Microbiology Research Group culture collection (research laboratories of the Dental Hospital, University of Birmingham). Acronyms in brackets stated in Table 2.1 are used to indicate the subspecies in the Results section. Mutant FN23 strains lacking adhesion proteins Fap2 and FadA (ΔFap2 and ΔFadA, respectively) were kindly provided by Dr Daniel Slade (Virginia Polytechnic Institute and State University, Blacksburg VA, USA). All strains used were grown for 48 hours at 37°C in an anaerobic chamber (80% N_2, 10% CO_2 and 10% H_2; Don Whitley DG250 Anaerobic Workstation, Don Whitley Scientific, Bingley, UK) on agar plates (Schaedler anaerobe agar, SAA; 91019, Sigma-Aldrich, Darmstadt, Germany).

Liquid bacterial cultures were grown overnight in an anaerobic chamber at 37°C in Schaedler anaerobe broth (SAB; CM0497, Oxoid, Oxoid, Basingstoke, UK). The identity of all subspecies was confirmed previously by PCR and 16S rRNA sequencing during the author's master's project (Muchova, 2020).

Table 2.1. Bacterial strains used in this study.

Bacterial species	Strain
Fusobacterium nucleatum ssp. *animalis* (FNA)	ATCC 51191
Fusobacterium nucleatum ssp. *fusiforme* (FNF)	ATCC 51190
Fusobacterium nucleatum ssp. *nucleatum* (FN23)	ATCC 23726
Fusobacterium nucleatum ssp. *nucleatum* ΔFap2 (ΔFap2)	ATCC 23726
Fusobacterium nucleatum ssp. *nucleatum* ΔFadA (ΔFadA)	ATCC 23726
Fusobacterium nucleatum ssp. *nucleatum* (FN25)	ATCC 25586
Fusobacterium nucleatum ssp. *polymorphum* (FNP)	ATCC 10593
Fusobacterium nucleatum ssp. *vincentii* (FNV)	ATCC 49256

Methodology related to chapter 3

2.2. Dynamic single-subspecies biofilm setup using flow cell

To establish the methodology, biofilms were grown both in aerobic as well as anaerobic conditions. Planktonic cultures were grown in 10 ml SAB anaerobically overnight at 37°C. Cultures were centrifuged at 2,600 x g for 10 minutes (IEC Centra-CL2 Centrifuge) and pellets washed once with 5 ml PBS. Bacteria were resuspended in 7 ml PBS, OD measured at 600 nm (Jenway 7315 Spectrophotometer) and adjusted to OD600=1 in SAB. Flow cell system (FC 270-AL, BioSurface Technologies, Bozeman, Montana, USA) was assembled and 500 µl of each bacterial suspension was introduced into the flow cell using the injection ports (see Figure 2.1). Bacteria were left to attach to borosilicate glass coupons overnight and the peristaltic pump (ISM834, Reglo Digital, Ismatec, Switzerland) was turned on the next day to ensure a constant flow of SAB through the flow cell (speed: 2 rpm/min, which corresponds to approximately 100 µl/min).

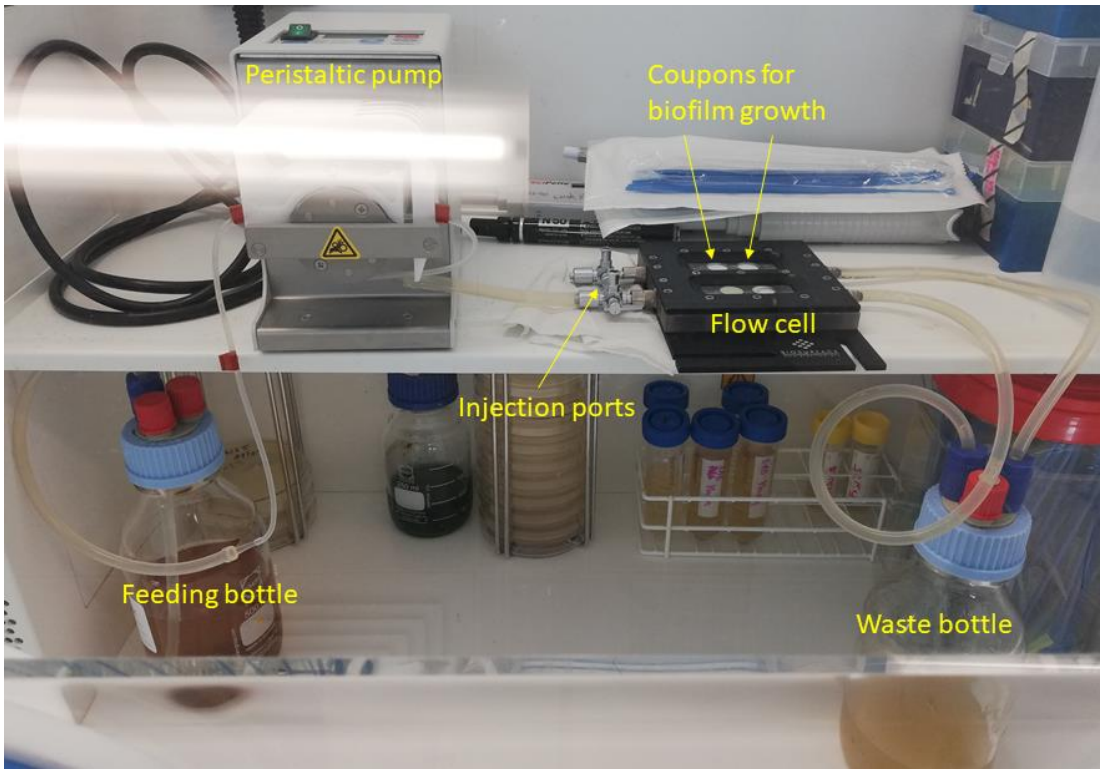

Figure 2.1. Flow cell system assembled in an anaerobic chamber. Sterile medium is continuously supplied at a very low speed from the feeding bottle by a peristaltic pump. Biofilms can be examined visually in the flow cell during the growth period.

2.3. Static single-subspecies biofilm setup

2.3.1. Initial evaluation of biofilm formation on selected surfaces

The method described in this section is related to results presented in sections 3.2.2 and 3.3. Planktonic cultures were grown in SAB overnight at 37°C anaerobically. Cultures were centrifuged at 2,600 x g for 10 minutes (IEC Centra-CL2 Centrifuge), pellets were resuspended in 5 ml PBS and centrifuged again. Bacteria were then resuspended in 7 ml PBS and the optical density (OD) was measured at either 550 nm or 600 nm (Jenway 7315 Spectrophotometer) depending on the source of methodology.

a) **Biofilms grown in multiwell plates** (for specifications see Table 2.2)**:**

   i. ***Lower bacterial starting concentration***: OD of bacterial cultures was adjusted to OD_{550}=0.2 corresponding to 1 x 10^8 CFU/ml (Millhouse et al., 2014) and 500

µl of the bacterial suspension in SAB was added into each well containing unmodified glass coverslips, while 200 µl of bacterial culture were added to 96-well plates. Media were changed every 24 hours and biofilms in 24-well plates were evaluated visually on day 3, whereas biofilms in 96-well plates were quantified using crystal violet staining (section 2.5).

ii. ***Higher bacterial starting concentration***: OD was adjusted to OD_{600}=1 (information provided by Forsyth Institute) in the corresponding medium (SAB or artificial gingival crevicular fluid (aGCF: 60% RPMI 1640 medium [SH30605.01, Cytiva, USA], 40% horse serum [Thermo Fisher Scientific, Loughborough, UK], 0.5 µg/ml menadione, 5 µg/ml haemin)) and 1 ml of suspension was added into each well containing either hydroxyapatite (HA) discs, sandblasted glass coverslips or collagen coating. Sandblasting was completed using a Basic quattro sandblasting unit (Renfert, Hilzingen, Germany), in which each coverslip was treated for 5 seconds with aluminium oxide (25 µm grit size, 1.2 mm nozzle). Collagen coating was performed by diluting according to the manufacturer's instructions and adding 50 µl, 25 µl, 12 µl or 6 µl of collagen to the wells of the 24-well plate (Figure 3.3) and letting it bind overnight at 4°C.

Media were changed every 24 hours and biofilms were evaluated visually on day 3, 5 or 7. For biofilms in collagen coated plates, biofilms were evaluated on day 4.

All biofilms were tested for contamination daily by streaking biofilm supernatant on SAA plates and observing colony morphology in addition to Gram staining confirmation of *F. nucleatum* morphology.

b) **Biofilms grown in tissue culture flasks** (for specifications see Table 2.2)**:** OD was adjusted to OD_{600}=0.15 in 10 ml SAB. Each bacterial suspension was transferred into 25 cm^2 tissue culture flask and incubated for 96 hours anaerobically without media change.

Table 2.2. Surfaces, surface treatments and media used for single-species static biofilms. SAB – Schaedler anaerobe broth, aGCF – artificial gingival crevicular fluid.

Surface used	Surface treatment	Growth medium used	Manufacturer
Glass coverslips (diameter 9 mm and 12 mm)	None	SAB	Coverslips: Marienfeld Superior, Lauda-Königshofen, Germany
	Sandblasting (grit size 25µm)		
	Artificial saliva (AS) composition Table 2.3		
	Fibronectin (from human plasma, Sigma-Aldrich/Merck)		
	Gelatin (from porcine skin, Sigma-Aldrich/Merck)		
	Poly-L-lysine (Sigma-Aldrich/Merck)		
96-well plate (Thermo Scientific™ Nunc™ MicroWell™, Nunclon Delta-Treated)	None	SAB	Multiwell plates: Thermo Fisher Scientific, Loughborough, UK
24-well plate (Thermo Scientific™ Nunc™ MicroWell™, Nunclon Delta-Treated)	Collagen (Collagen I, Rat, 50µg/ml, Corning™, Fisher Scientific; diluted according to the manufacturer's instructions)	SAB	
Tissue culture flasks (Nunc™ EasYFlask™ Nunclon™ Delta Surface, 25 cm^2)	None	SAB	Thermo Fisher Scientific, Loughborough, UK
Plastic coverslips	None	SAB	Coverslips: Thermo Fisher Scientific,
	Artificial saliva (AS) composition Table 2.3		

(diameter 13 mm, Thermo Scientific™ Nunc™ Thermanox™)	Fibronectin (from human plasma, Sigma-Aldrich/Merck)		Loughborough, UK
	Gelatin (from porcine skin, Sigma-Aldrich/Merck)		
	Poly-L-lysine (Sigma-Aldrich/Merck)		
Hydroxyapatite discs (diameter 12 mm)	None	SAB	Biosurface Technologies, USA
	None	aGCF	

2.3.2. Modifications of surfaces used for biofilm formation evaluation

After the initial evaluation of biofilm formation, glass (12 mm diameter; Table 2.2) and plastic (13 mm diameter; Table 2.2, referred to as "Thermanox" hereafter) coverslips were chosen for further biofilm characterisation.

Both glass and Thermanox coverslips were placed in a 24-well plate with sterile forceps and additionally disinfected with 70% ethanol for 10 minutes at room temperature. After the removal of ethanol, coverslips were washed once with sterile PBS and left to dry.

Artificial saliva (AS) was used as a coating agent to mimic human saliva and formation of salivary pellicle to promote bacterial adhesion (Vyas et al., 2020). AS was prepared according to Millhouse et al. (2014) by dissolving the reagents specified in Table 2.3 in ultrapure water; urea was added after autoclaving. Additionally, substrates were coated using agents promoting cell attachment to culture surfaces: fibronectin (from human plasma) (Kalaskar et al., 2013), gelatin (from porcine skin; 250 µl/well) (Bello et al., 2020), and poly-L-lysine (250 µl/well) (Park et al., 2014) (all from Sigma-Aldrich/Merck). Coating agents are also summarised in Table 2.2.

Substrate coating was performed as follows: AS (250 µl/well) was added to coverslips and incubated at 37°C for 1 hour (Ismail et al., 2020). Next, AS was removed and bacterial cultures were added immediately without substrate washing or drying to simulate *in vivo* conditions. Fibronectin diluted in PBS (270 µl/well; 5 µg/cm^2) was applied and incubated for 45 minutes at room temperature. Gelatin solution (250 µl/well; 0.1% in PBS) was incubated for 20 minutes at 37°C. Poly-L-lysine coating (250 µl/well) was performed for 10 minutes at room temperature. These surface coatings were left to dry in a flow hood as per the manufacturers' instructions without washing. Additionally, a set of glass coverslips was sandblasted to create a roughened surface. Sandblasting was completed using a Basic quattro sandblasting unit (Renfert, Hilzingen, Germany), in which each coverslip was treated for 5 seconds with aluminium oxide (25 µm grit size, 1.2 mm nozzle).

Table 2.3. Reagents used for preparation of AS.

Reagent	Concentration	Supplier
Porcine stomach mucins	0.25% w/v	Sigma-Aldrich/Merck, Darmstadt, Germany
Potassium chloride	0.02% w/v	
Calcium chloride dihydrate	0.02% w/v	
Yeast extract	0.2% w/v	
Proteose peptone	0.5% w/v	
Sodium chloride	0.35% w/v	Thermo Fisher Scientific, Loughborough, UK
Lab-Lemco powder	0.1% w/v	Oxoid, Basingstoke, UK
Urea (added after autoclaving)	0.05% v/v	Sigma-Aldrich/Merck, Darmstadt, Germany

2.4. Biofilm setup for systematic evaluation of biofilm formation by all *F. nucleatum* subspecies

The following method is related to the results presented in sections 3.4, 3.5 and 3.6. To initiate biofilm growth, planktonic *F. nucleatum* overnight cultures were washed once with PBS and the optical density of each culture was adjusted to OD_{600}=1 in SAB, corresponding to 1.62 x 10^9 CFU/ml for each subspecies. For each single-subspecies biofilm, 400 µl of bacterial suspension was added to each well containing studied substrates and biofilms were incubated statically for 72 hours under anaerobic conditions. SAB was replaced after 24 and 48 hours and biofilms were monitored for contamination daily by streaking biofilm supernatant on SAA plates and observing colony morphology in addition to Gram staining confirmation of *F. nucleatum* morphology.

2.5. Biofilm biomass quantification

Biofilm biomass was quantified by crystal violet (CV) staining. After 72 hours of incubation, biofilms were carefully washed once with 100 µl PBS and air-dried for 2 hours at 37°C, then stained with a CV solution (200 µl, 0.05 % w/v; Sigma-Aldrich/Merck, Darmstadt, Germany) at RT for 30 minutes. After staining, biofilms were gently washed with 200 µl PBS and air dried at 37°C for 2 hours. Ethanol (100%, 200 µl) was used to destain the biofilms for 1 hour on a plate shaker. Ethanol solution from each well was diluted in Milli-Q water 1:10 in a 96-well plate and the absorbance was measured at 600 nm (Microplate reader Spark®, Tecan; software SparkControl, v. 2.3, Tecan). To account for differences between glass and plastic coverslip surface area, absorbance readings per cm^2 were calculated using the formula below. The surface area of a glass coverslip was 113.04 mm^2, the area of a Thermanox coverslip was 132.67 mm^2.

$$average\ CV\ absorbance\ corrected\ for\ blank\ x\ \frac{100\ mm^2}{area\ of\ the\ coverslip\ (mm^2)}$$

2.6. Fluorescent biofilm staining and confocal laser scanning microscopy (CLSM)

Biofilms for CLSM analysis were grown in 24-well black plates with clear base (polystyrene, thickness 190 μm, Vision Plate™, 4titude, Surrey, UK) either with no surface treatment, or coated with fibronectin, gelatin, poly-L-lysine or AS as stated in Table 2.2. In order to avoid excessive detachment, biofilms were first fixed with 4% paraformaldehyde for 10 min, then washed in PBS once and stained using green fluorescent, cell permeant nucleic acid stain SYTO™ 9 (FilmTracer™ LIVE/DEAD® Biofilm Viability Kit, Invitrogen, Renfrew, UK) according to the manufacturer's instructions. Briefly, 3 μl of SYTO™ 9 were added to 1 ml of sterile PBS and biofilms were stained with 200 μl of the diluted stain for 20 min at room temperature in the dark.

Diluted stain was removed and biofilms were not washed to avoid biofilm removal. Samples were imaged immediately after staining using CLSM (LSM 700, Zeiss, Germany), with a 40X oil immersion objective at 488/500 nm. Maximum thickness of the biofilms was estimated by obtaining z-stack horizontal images at 1.3 μm intervals. Biofilms were grown once in technical triplicates and images were acquired in the centre of each well using Zeiss Zen 2011 software.

2.7. Preparation of biofilms and scanning electron microscopy (SEM)

In order to examine single-subspecies biofilm architecture using SEM, biofilms were grown on poly-L-lysine coated plastic (Thermanox™) coverslips in 24-well plates. Biofilms were fixed

using 2.5% glutaraldehyde (Agar Scientific, Stansted, United Kingdom) in 0.1 M sodium cacodylate buffer (pH 7.4, BioWorld, Dublin, Ireland) for 10 min at room temperature. Following fixation, biofilms were dehydrated with increasing ethanol concentrations (20%, 30%, 40%, 50%, 60%, 70%, 90%, two times 95%, two times 100%) and incubated for 10 min at each step.

Finally, drying agent hexamethyldisilizane (HMDS; Sigma-Aldrich/Merck, Darmstadt, Germany) was applied and left to evaporate overnight. Coverslips with biofilms were mounted onto aluminium specimen stubs (Agar Scientific, Stansted, United Kingdom), sputter coated with two layers of gold and visualised using a scanning electron microscope (Zeiss EVO MA10). A visible layer of biofilm was chosen after visual evaluation of each specimen under low magnification (50X) and recorded at 1,000X and 5,000X magnification.

2.8. Bioinformatics and phylogenetic analysis

Bacterial genomes of *F. nucleatum* ssp. *animalis* ATCC 51191 (GCA_000220825), *F. nucleatum* ssp. *nucleatum* ATCC 23726 (GCA_000178895), *F. nucleatum* ssp. *nucleatum* ATCC 25586 (GCA_000007325), *F. nucleatum* ssp. *polymorphum* ATCC 10953 (GCA_000153625), *F. nucleatum* ssp. *vincentii* ATCC 49256 (GCA_000182945) were retrieved from EnsemblBacteria (Release 52) (Howe et al., 2020). *F. nucleatum* ssp. *fusiforme* data were not available on this portal, possibly due to their close genetic relatedness with *F. nucleatum* ssp. *vincentii*.

Orthologues were identified using blastp (v. 2.12.0) (States and Gish, 1994) with default parameters and *F. nucleatum* ssp. *nucleatum* ATCC 25586 proteins as queries, with a cutoff e-value of 1e-10. Protein domains were annotated using InterPro (Blum et al., 2021) with a cutoff

e-value of 1e-5. Multisequence alignment of CmpA and Fap2 proteins was performed using MAFFT (v. 6) (Katoh et al., 2019) with the "– auto" option. The phylogenetic tree was constructed using the Neighbour-Joining method (Saitou and Nei, 1987), JTT substitution model and bootstrap 1000.

2.9. Isolation of membrane proteins from planktonic and biofilm-grown *F. nucleatum* subspecies

Planktonic bacteria were obtained by inoculating each subspecies into 100 ml of SAB and incubating the cultures overnight anaerobically at 37°C. Overnight cultures were centrifuged and pellets resuspended in 30 ml of 0.1M triethylammonium bicarbonate (TEAB) buffer (90114, Thermo Fisher Scientific, Loughborough, UK) and stored at -20°C until processing. Biofilms were grown for 3 days on poly-L-lysine coated (section 0) 6-well plates (2 plates per subspecies to ensure sufficient amounts of biofilm, 3 ml per well) as described in section 2.4. Supernatants were carefully removed and biofilms were harvested from each well by vigorous pipetting of 0.1M TEAB buffer (2 ml/well). Resuspended biofilms were collected and volumes adjusted with 0.1M TEAB buffer to give final volume of 30 ml. Bacterial lysis and membrane harvesting were performed at the School of Biosciences, University of Birmingham. Bacterial cells were lysed two times under 15,000 psi using C3 Emulsiflex Cell Disruptor (Avestin, Canada). Lysates were collected and centrifuged to collect unbroken cells at 10,000 x g for 30 minutes (Avanti JXN-26, Beckman Coulter). Membrane-containing supernatants were transferred to ultracentrifuge tubes and centrifuged at 100,000 x g (Type 70 Ti Fixed-Angle Titanium Rotor, Beckman Coulter, Germany) for 1 hour at 4°C. The pellet of membrane proteins was resuspended in 500 µl of TEAB buffer and stored at -20°C until further processing.

2.10. Membrane protein quantification using Bicinchoninic acid (BCA) protein assay

Membrane proteins isolated from planktonic and biofilm-grown *F. nucleatum* subspecies were quantified using the Pierce™ BCA Protein Assay Kit (23227, Thermo Fisher Scientific, Loughborough, UK.) according to the manufacturer's instructions. Bovine serum albumin (BSA) standards were prepared in 0.1M TEAB buffer and 25 µl were added to wells of a 96-well plate in triplicate. Membrane proteins were further diluted 1:2 in 0.1M TEAB buffer and 25 µl were added in triplicate to the 96-well plate. Standards and samples were combined with 200 µl of Working Reagent (50 parts of Reagent A, 1 part of Reagent B) and the plate was briefly mixed for 30 seconds on a plate shaker (R100/TW Rotatest Shaker, Luckham Ltd.; speed level 3). Samples were incubated at 37°C for 30 minutes and a microplate reader (Spark, Tecan, Switzerland) was used to read absorbance at 562 nm. Concentrations of proteins were calculated from a 9-point standard curve obtained from the BSA standards.

2.11. One-dimensional sodium dodecyl sulphate polyacrylamide gel electrophoresis (1D SDS-PAGE)

All reagents and protein gels were purchased from Thermo Fisher Scientific, Loughborough, UK. Membrane proteins were prepared for 1D SDS-PAGE by mixing 5 µg of each protein sample with 2.5 µl of NuPAGE® LDS Sample Buffer 4X (NP0007), 1 µl of NuPAGE® Reducing agent (NP0009) and adjusted with molecular grade water to the final volume of 10 µl. Samples were incubated at 70°C for 10 minutes. During incubation, protein gels (NuPAGE® Bis-Tris Gels 12%, NP0342BOX) were placed in the mini-gel tank and the tank was filled with 400 ml of 1X Running buffer (NuPAGE® MOPS SDS Running buffer, NP0001) combined

with 1 ml of NuPAGE® Antioxidant (NP0005). Protein ladder (Mark12™ Unstained Standard, LC5677) and the protein samples were then loaded into the well of the gel and electrophoresis was run for 50 minutes at 180V. Gels were then silver-stained as detailed in section 2.13.

2.12. Two-dimensional sodium dodecyl sulphate polyacrylamide gel electrophoresis (2D SDS-PAGE)

2D SDS-PAGE was performed according to the manufacturer's instructions for ZOOM® IPGRunner™ System. All ZOOM® branded reagents and protein gels were purchased from Thermo Fisher Scientific, Loughborough, UK. Similarly to 1D SDS-PAGE, 5 µg of protein per sample were used in this method. Samples for the first dimension were prepared in 1X Sample Rehydration Buffer (SRB; containing 8M Urea, 2% w/v 3-[(3-Cholamidopropyl)dimethylammonio]-1-propanesulfonate [CHAPS], 0.5% v/v ZOOM Carrier Ampholytes pH 3-10 [ZM0021] and 0.002% w/v of bromophenol blue). Prior to use, dithiothreitol (DTT) was added to the SRB to a final concentration of 20mM. 10 µl of protein sample were combined with 140 µl of SRB and loaded to ZOOM® IPGRunner™ Cassette (ZM0003) with ZOOM® Strips (pH 3-10 non-linear; ZM0011). The ZOOM® Strips were rehydrated at room temperature for 1 hour. The cassette with the strips was loaded to ZOOM® IPGRunner™ Core and the isoelectric focusing (IEF) was performed with the following settings: 200 V for 20 minutes, 450 V for 15 minutes, 750 V for 15 minutes and 2,000 V for 1 hour. After IEF, the cassette was disassembled and the strips were equilibrated for 15 minutes at room temperature in 10 ml of Equilibration Buffer (9 ml of 1X NuPage® LDS Sample buffer [4X buffer diluted in deionised water] and 1 ml of 10X NuPage® Sample Reducing Agent). Following equilibration, strips were alkylated for 15 minutes at room temperature in 125 mM

alkylating solution (232 mg of iodoacetamide in 10 ml of 1X NuPage® LDS Sample buffer). One strip per gel was applied to the IPG well of NuPAGE® Bis-Tris Gel (4-12%, NP0326BOX) and overlayed with 400 µl of 0.5% w/v agarose. Second dimension SDS-PAGE was performed for 45 minutes at 200V. Protein gels were silver-stained as described in section 2.13.

2.13. Silver staining of proteins in polyacrylamide gels

Protein gels were stained using SilverQuest™ Silver Staining Kit (LC6070, Thermo Fisher Scientific, Loughborough, UK) following the manufacturer's instructions. All incubation steps were performed with gentle rotation on a plate shaker. Briefly, each gel was rinsed with ultrapure water and fixed for 20 minutes in 100 ml of Fixative (40% v/v ethanol, 10% v/v acetic acid, made in MilliQ® ultrapure water). Gels were then washed in 100 ml of 30% v/v ethanol for 10 minutes, followed by incubation for 10 minutes in 100 ml of Sensitising solution (30 ml ethanol, 10 ml Sensitiser, 60 ml ultrapure water). Gels were then washed again in 100 ml of 30% v/v ethanol for 10 minutes, followed by 100 ml of ultrapure water for 10 minutes. Staining was performed by incubating the gels for 15 minutes in the Staining solution (1 ml Stainer, 99 ml ultrapure water) and then washed in 100 ml of ultrapure water for 40 seconds. Gels were then developed in 100 ml of Developing solution (10 ml of Developer, 1 drop of Developer enhancer, 90 ml of ultrapure water) for 5 minutes and 10 ml of Stopper solution was used to stop further gel development. Gels were washed in 100 ml of ultrapure water for 10 minutes. Pictures of gels were taken immediately after staining on a light box.

Methodology related to chapter 4

2.14. Stimuli used for neutrophil assays

Stimuli used in assays with peripheral blood neutrophils were phorbol 12-myristate 13-acetate (PMA; Sigma-Aldrich/Merck), opsonised *Staphylococcus aureus* and formalin-inactivated *Fusobacterium nucleatum* (FN) subspecies. Stimuli are also detailed in Table 2.4, MOI values used as stated in Wright et al. (2011). Opsonised *S. aureus* was kindly provided by Dr Helen Wright. *F. nucleatum* subspecies were formalin-inactivated as follows: cultures were grown in 10 ml SAB in anaerobic conditions at 37°C overnight. Cultures were centrifuged for 10 minutes at 2,600 x g (IEC Centra-CL2 Centrifuge) and pellets washed once with 10 ml PBS. Bacteria were then resuspended in 5 ml PBS and the OD of each culture was adjusted to OD_{600} = 1 in final volume of 1 ml in a sterile Eppendorf tube, corresponding to 1.62 x 10^9 CFU/ml. Bacteria were centrifuged for 10 minutes, 2,000 x g (Eppendorf, 5415 D). Pellets were resuspended in 1 ml 10% buffered formalin and incubated at room temperature for 10 minutes. Samples were centrifuged for 10 minutes, 2,000 x g and the resulting pellets washed twice more with 1 ml PBS. The final OD of each culture was re-adjusted to OD_{600} =1 due to loss of bacteria during washing steps. Cultures were spot-plated on SAA plates and incubated at 37°C in anaerobic conditions for 48 hours to confirm inactivation.

Table 2.4. Stimuli used to challenge neutrophils in the initial experiments.

Stimulus	ROS assay	NET-DNA assay
Phorbol 12-myristate 13-acetate (PMA), Sigma-Aldrich/Merck	25 nM	50 nM
Opsonised *Staphylococcus aureus* (OpSA)	MOI 300	MOI 300

Formalin-inactivated *Fusobacterium nucleatum* (FN) subspecies	MOI 100	MOI 100

2.15. Isolation of human neutrophils from peripheral blood

Peripheral blood was collected from healthy volunteers by venepuncture (ethical approval 18/ES/0092, 19/SW/0198 and BCHCDent024.2024) in 6 ml lithium heparin vacutainers (Greiner Bio-One, Germany). Blood was layered on the discontinuous Percoll density gradients (1.079 g/ml on top of 1.098g/ml gradient; Percoll, 17089101, Cytiva, USA) and centrifuged for 8 minutes at 150 x g followed by 10 minutes at 1,200 x g (Hettich Rotina 380 R). Layers of plasma, monocytes, lymphocytes and Percoll material was removed from the gradients (Figure 2.2) and neutrophils were transferred into 30 ml of lysis buffer (Matthews et al., 2007a) and incubated at room temperature for 5-10 minutes to lyse erythrocytes. Cells were then centrifuged for 6 minutes at 350 x g. Supernatant was removed and lysis was repeated using 3 ml lysis buffer and incubating the cells for 5 minutes, followed by centrifugation at 350 x g for 6 minutes. Cell pellets were washed with 3 ml PBS and centrifuged at 350 x g for 6 minutes. Cells were resuspended in 3 ml PBS, counted using a haemocytometer and trypan blue, and the cell number was adjusted in the corresponding medium used in the assays.

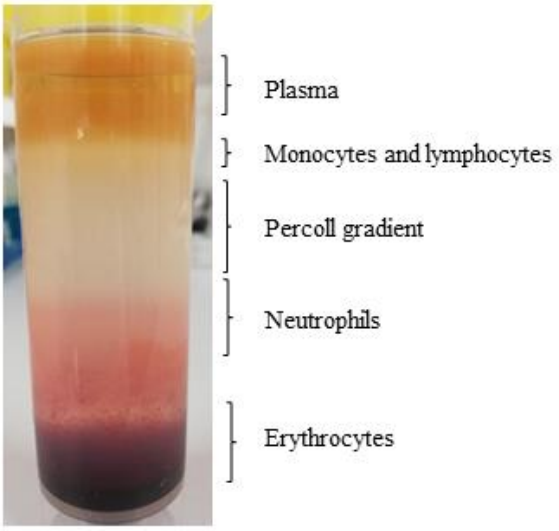

Figure 2.2. Separation of cellular components of blood using Percoll gradients. Neutrophils can be isolated from a distinct layer above erythrocytes.

2.16. Enhanced chemiluminescent assay for ROS quantification using formalin-fixed *F. nucleatum* subspecies

Wells of an untreated white 96-well plate (611F96WT, Sterilin Microplate White) were blocked with 1% bovine serum albumin (BSA) in PBS overnight at 4°C. On the day of the assay, blocking buffer was removed from the 96-well plate. Neutrophils isolated from peripheral blood were adjusted to 1 x 10^6 cells/ml in glucose supplemented PBS (GPBS: Dulbecco's phosphate buffered saline no calcium, no magnesium, Gibco™, Thermo Fisher Scientific, Loughborough, UK; 10mM glucose; 1.35 mM $CaCl_2$; 1.5 mM $MgCl_2$) and 100 µl of the suspension was added in the wells of the 96-well plate. To quantify total ROS, 30 µl of membrane-permeable luminol (3 mmol/l; pH 7.3; 123072, Sigma-Aldrich/Merck, Darmstadt, Germany) was added to each well. 45 µl of GPBS was added to obtain a total volume of 175 µl in each well. To quantify extracellular ROS, 60 µl of membrane-impermeable isoluminol (4-aminophthalhydrazide, 3 mmol/l; A8264, Sigma-Aldrich/Merck, Darmstadt, Germany) was added together with 15 µl

horseradish peroxidase (HRP, Type XII, 7.5 U/ml to each well; Sigma-Aldrich/Merck, Darmstadt, Germany) to enhance the chemiluminescent signal. The plate was placed into a luminometer (Berthold Microplate Luminometer LB 96V) and incubated at 37°C for 30 minutes to record the baseline light output. Cells were then stimulated with 25 µl of stimuli: PMA (25 mM), OpSA (MOI 300) or formalin-fixed FN subspecies (MOI 100) (see Table 2.4). Light output was measured for a further 150 minutes. Results were expressed as peak relative light units (RLU).

2.17. Quantification of neutrophil extracellular traps (NETs)

Wells of a transparent 96-well plate were blocked with 1% bovine serum albumin (BSA) in PBS overnight at 4°C. On the day of the assay, blocking buffer was removed from the 96-well plate. Neutrophils isolated from peripheral blood were adjusted to 1 x 10^6 cells/ml in RPMI 1640 medium (SH30605.01, Cytiva, USA) and 100 µl of the suspension was added in the wells of the 96-well plate. The volume in each well was made up to 175 µl with RPMI 1640 and the plate was incubated at 37°C, 5% CO_2 for 30 minutes in order for the neutrophils to settle to the well bottoms. Cells were then stimulated with 25 µl of PMA (50 mM), OpSA (MOI 300) or FN subspecies (MOI 100) (see Table 2.4) and further incubated for 120 minutes. Next, 15 µl of Micrococcal nuclease (14.3 units/ml, LS004797, Worthington, USA) was added to each well for 10 minutes at 37°C. The microplate was centrifuged for 10 minutes at 1,800 x g (Universal 320 R, Hettich), and 150 µl of the supernatant was carefully removed and mixed with 15 µl of SYTOX green (S7020, Invitrogen, Thermo Fisher Scientific, Loughborough, UK) diluted in PBS (1:500) in a black 96-well plate (611F96BK, Thermo Scientific™ Sterilin™ Microtiter™ Plates, Thermo Fisher Scientific, Loughborough, UK). DNA-derived fluorescence was read

using a microplate reader (Spark®, Tecan, Switzerland) with excitation at 485 nm and emission at 525 nm. Readings were expressed as relative fluorescence units (RFU).

2.18. Fluorescent labelling of bacteria for flow cytometry

In order to quantify neutrophil phagocytosis using flow cytometry, fluorescently stained bacteria were utilised, as their fluorescent signal can be detected when phagocytosed. Overnight bacterial cultures of *Staphylococcus aureus* and *F. nucleatum* subspecies were adjusted to OD_{600}=1 and washed in PBS 2 times, then resuspended in 1 ml of PBS with 3 µl Syto 9 (Syto 9, Invitrogen, Thermo Fisher Scientific, Loughborough, UK). The samples were incubated for 15 minutes protected from light, followed by washing with PBS 2 times. Bacterial suspensions were inactivated: *S. aureus* was heat-killed for 10 minutes at 90°C and *F. nucleatum* subspecies were formalin-inactivated (section 2.14). After inactivation, OD of cultures was adjusted to OD_{600}=1 and stimuli were stored at -20°C.

2.19. Neutrophil phagocytosis analysed by flow cytometry

Neutrophils isolated from peripheral blood were adjusted to 1 x 10^6 cells/ml in FACS buffer (1% foetal bovine serum in GPBS). For each analysed sample, 100 µl of the cell suspension was mixed with fluorescently labelled bacteria (see section 2.18) - *S. aureus* (MOI 5) or *F. nucleatum* subspecies (MOI 100) and incubated in a shaking incubator at 37°C (100 rpm; NB-205, N-BIOTEK) for 30 minutes, protected from light. Samples were filled up to 1 ml with FACS buffer and 5 µl of 4% Trypan blue was added to quench possible fluorescence signals due to extracellular binding of bacteria to neutrophils. Samples were then analysed using flow cytometer (BD Accuri C6 Flow cytometer; 50,000 events per sample, 488 nm laser and 533/30 filter) and the corresponding BD Accuri C6 software. Gating was performed around populations

of cells corresponding to neutrophils and the percentage of fluorescent neutrophils was assessed using Accuri C6 software.

2.20. Culture of HL-60 cells

Human leukaemia (HL-60) cell line, which can be differentiated into neutrophil-like cells, was seeded at 1 x 10^5 cells/ml in RPMI 1640 medium supplemented with 10% foetal bovine serum (FBS), L-glutamine (300 mg/l) and HEPES (25 mM, Thermo Fisher Scientific, Loughborough, UK). Cells were incubated at 37°C, 5% CO_2 for 2 days. Cells were adjusted to 8 x 10^5 cells/ml in supplemented RPMI containing 1.25% dimethyl sulfoxide (DMSO) in order to stimulate differentiation and incubated for three, four or six days (Palmer, 2010, Kurgan et al., 2017). To perform chemiluminescence assay and quantification of NET-DNA, cells were centrifuged for 7 minutes as 130 x g (Universal 320 R, Hettich). The pellet was resuspended in PBS, cells enumerated and adjusted to 1 x 10^6 cells/ml in the appropriate medium.

Methodology related to chapter 5

2.21. DNA extraction from *F. nucleatum* subspecies

Optimisation of DNA extraction from *F. nucleatum* subspecies was performed using a silica-based column system as well as in-solution DNA extraction.

2.21.1. GenElute Bacterial genomic DNA extraction

Silica-based column system GenElute Bacterial genomic kit (NA2110, Sigma-Aldrich, Darmstadt, Germany) was used for this DNA extraction. Bacterial overnight cultures were

adjusted to 1 x 10^8 CFU/ml or 1 x 10^9 CFU/ml and 1 ml of cultures was centrifuged for 2 minutes at 12,000 x g (Fisherbrand accuSpin Micro 17R, Fisher Scientific). Supernatant was removed and the bacterial pellet was resuspended in 180 µl of Lysis Solution T. 20 µl of the supplied Proteinase K solution was added and incubated for 30 minutes at 55°C. Bacterial cells were then lysed by adding 200 µl of Lysis Solution C and incubated at 55°C either for 10 minutes (standard procedure) or 30 minutes (extended lysis). Columns were prepared for binding by adding 500 µl of Colum Preparation Solution and centrifuging at 12,000 x g for 1 minute. Bacterial lysate was mixed with 200 µl of molecular grade ethanol, mixed thoroughly and transferred onto the column. Samples were centrifuged at 6,500 x g for 1 minute and eluate was discarded. Columns were washed with 500 µl of Wash Solution 1, centrifuged at 6,500 x g for 1 minute and the eluate was discarded. Columns were washed again with 500 µl ethanol-diluted Wash Concentrate (Wash Solution), centrifuged for 3 minutes at 12,000 x g and the eluate was discarded. DNA was then eluted from the columns by adding 200 µl of molecular grade water, incubated for 5 minutes at room temperature and centrifuged. Experiments were performed at least 2 times in duplicate.

2.21.2. Wizard Genomic DNA extraction and purification

Wizard Genomic DNA purification kit (A1120, Promega, Chilworth Southampton, UK) was utilised for in-solution DNA extraction. For evaluation of lysis efficiency and comparison with *F. nucleatum*, *Escherichia coli* was chosen as another Gram-negative bacterium, which is well characterised and most DNA extraction protocols are optimised for this bacterium. *F. nucleatum* and *E. coli* bacterial overnight cultures were adjusted to 1 x 10^9 CFU/ml and 1 ml of cultures was centrifuged at 16,000 x g for 2 minutes. Supernatant was discarded and the bacterial pellet was resuspended in 600 µl of Nuclei Lysis Solution. Samples were incubated at 80°C for 5

minutes and 3 µl of RNase Solution were added to the lysate and mixed thoroughly by tube inversion. Samples were further incubated at 37°C for 30 minutes. Samples were mixed with 200 µl of Protein Precipitation Solution, vortexed vigorously and incubated on ice for 5 minutes. Following centrifugation at 16,000 x g for 3 minutes, supernatant was mixed with 600 µl of molecular grade isopropanol in a clean Eppendorf tube. Solution was mixed gently by inversion and centrifuged at 16,000 x g for 2 minutes. The pellet was gently washed with 600 µl of molecular grade 70% ethanol and samples were centrifuged at 16,000 x g for 2 minutes. Ethanol was completely removed and pellets were air-dried for 10 minutes. DNA pellets were rehydrated using 100 µl of Rehydration Solution at 65°C for 1 hour. Experiments were performed at least 2 times in duplicate.

2.21.3. Chemical and mechanical disruption of bacteria combined with Wizard Genomic DNA Purification

The original protocol for disruption of bacteria was developed for DNA and RNA extraction from *Brucella* sp. and was kindly provided by Dr Daniel Slade (Virginia Tech, Virginia, USA). This protocol was also modified for use with *F. nucleatum* (Muchova, 2020, Master's thesis). Bacterial overnight cultures were adjusted to 1 x 10^9 CFU/ml and centrifuged at 16,000 x g for 15 minutes to obtain a more compact pellet to avoid loss of bacteria during supernatant removal. A solution of ice cold molecular grade ethanol:acetone (ratio 1:1) was used to resuspend the pellet (1 ml) and the bacterial suspension was stored at -80°C overnight. The sample was centrifuged at 16,000 x g for 3 minutes and the pellet was resuspended in 500 µl Tris-EDTA (TE) Buffer (1 mM EDTA [E5134, Sigma-Aldrich, Darmstadt, Germany], 10 mM Tris-HCl [Trizma hydrochloride, T6666, Sigma-Aldrich, Darmstadt, Germany], pH 7.5) and centrifuged

for 3 minutes at 16,000 x g. 200 µl 0.04 M sodium acetate, pH 5.2 (71196, Sigma-Aldrich, Darmstadt, Germany) was used to resuspend the bacterial pellet and 200 µl 1% zwittergent (693017, Millipore, Darmstadt, Germany) was added to the mixture, followed by vortexing for 15 seconds. The suspension was centrifuged at 8,000 x g for 3 minutes and the pellet was resuspended in nuclease-free water, followed by another centrifuging step at 8,000 x g for 3 minutes. Pellet was resuspended in 200 µl 0.04 M sodium acetate, 160 µl nuclease-free water and 40 µl 10% sodium dodecyl sulphate (SDS; L4390, Sigma-Aldrich, Darmstadt, Germany). The suspension was thoroughly vortexed for 15 seconds and incubated for 7 minutes at 90°C. From this point, the Wizard Genomic DNA Purification kit was used. The lysate was combined with 3 µl of RNase Solution, mixed thoroughly by tube inversion and incubated at 37°C for 30 minutes. The remaining steps of the method described in section 2.21.2 were performed without changes. Experiments were performed at least 2 times in triplicate.

2.22. Standard curves for quantification of *F. nucleatum* subspecies

Bacterial standard curves were generated by plotting colony-forming unit (CFU/ml) values against bacterial optical density (OD). Overnight bacterial cultures were centrifuged at 2,600 x g for 10 minutes (Universal 320 R, Hettich) and pellets were washed once with 5 ml PBS. Cultures were adjusted to OD_{600}=1 in PBS and serially diluted 6 times 1:2 in PBS. OD values of each dilution were re-measured and related to the CFU/ml values. CFU/ml of each dilution were obtained by viable colony counting as described by Miles and Misra (1938). Briefly, each analysed dilution was further diluted 7 times 1:10 in PBS, 20 µl were plated on SAA in technical triplicates and plates were incubated anaerobically at 37°C for at least 48 hours. Colonies were then counted and the CFU/ml calculated. Experiments were performed in technical and biological triplicates.

2.23. Evaluation of viability of live bacterial stocks stored at -20°C and -80°C

Viability of bacterial stocks was assessed in order to confirm that freezing storage conditions do not negatively affect live *F. nucleatum* stimuli. The Miles and Misra method was used as described in section 2.22 and viable CFU/ml were calculated from each aliquot quantified. Defrosted aliquots were either discarded after use (samples defrosted once) or they were frozen again (thawing-freezing cycles).

2.24. Live planktonic and biofilm-grown bacterial stimuli used for neutrophil assays

To prepare live planktonic *F. nucleatum* subspecies for the assays, 10 ml of SAB were inoculated with each subspecies and incubated at 37°C for 18 hours anaerobically. Cultures were centrifuged for 10 minutes at 2,600 x g and pellets washed once with PBS, then adjusted in PBS to OD_{600}=1, which corresponded to the CFU/ml values calculated in section 2.22. Each adjusted subspecies was mixed with glycerol (15% v/v final concentration) and aliquots were stored at -80°C as this temperature provided better long-term storage.

Single-subspecies biofilms were grown in 6-well plates (Nunclon™ Delta Surface, Thermo Scientific, Loughborough, UK). Overnight planktonic cultures were washed once with PBS, then adjusted in SAB to OD_{600}=1, which corresponded to CFU/ml values calculated in section 2.22. Three ml of the adjusted culture was added to wells of 6-well polystyrene plates without additional surface coating and biofilms were grown for 72 hours anaerobically. Growth medium was changed after 24 and 48 hours of incubation and contamination monitoring was performed daily. After 72 hours of incubation, supernatant was carefully removed and single-subspecies

biofilms were resuspended by vigorous pipetting in PBS. Bacterial concentration was adjusted to OD_{600}=1 and bacterial numbers were calculated for each subspecies. Subspecies were then mixed with glycerol (15% v/v final concentration) and aliquots stored at -80°C.

2.25. Enhanced chemiluminescent assay for ROS quantification using live *F. nucleatum* subspecies

Wells of an untreated white 96-well plate (611F96WT, Sterilin Microplate White) were blocked with 1% bovine serum albumin (BSA) in PBS overnight at 4°C. On the day of the assay, blocking buffer was removed from the 96-well plate. Neutrophils isolated from peripheral blood were adjusted to 1 x 10^6 cells/ml in GPBS and 100 µl of the suspension was added to the wells of the 96-well plate.

a) **To quantify total ROS (intracellular and extracellular)**: 30 µl of luminol (3 mmol/l, pH 7.3; Sigma-Aldrich/Merck, Darmstadt, Germany) with 15 µl horseradish peroxidase (HRP, Type XII, 7.5 U/ml in the well; Sigma-Aldrich/Merck, Darmstadt, Germany) was used.

b) **To quantify intracellular ROS**: 30 µl of luminol (3 mmol/l) was combined with 3 µl superoxide dismutase (SOD, bovine, 50 U/ml in the well; Sigma-Aldrich/Merck, Darmstadt, Germany), 17.5 µl catalase (from bovine liver, 20 U/ml in the well; Sigma-Aldrich/Merck, Darmstadt, Germany) and 15 µl horseradish peroxidase (HRP, Type XII, 7.5 U/ml in the well; Sigma-Aldrich/Merck, Darmstadt, Germany). SOD and catalase were used to neutralise extracellular ROS in order to specifically measure intracellular ROS.

c) **To measure extracellular superoxide generation:** Lucigenin (30 µl, 0.33 mg/ml) was used without the addition of the reagents which were used in combination with luminol above.

Cells were then stimulated with 35 µl of *F. nucleatum* subspecies (MOI 100). Light output was measured for a further 150 minutes. Results were expressed as peak relative light units (RLU).

2.26. Quantification of neutrophil extracellular traps (NETs)

Quantification of NETs was performed as described in section 2.17, with the following changes: after the addition of neutrophils, the volume in each well was made up to 165 µl with RPMI 1640 and the plate was incubated at 37°C, 5% CO_2 for 30 minutes. Cells were stimulated with 35 µl of live planktonic and biofilm-grown *F. nucleatum* subspecies (MOI 100).

2.27. Microscopic visualisation of NETs

NETs were stained and microscopically visualised as described by Hirschfeld et al. (2023). Neutrophils were isolated as described in section 2.15 and the NET assay was set up as described in section 2.17. Stimulated neutrophils were incubated for 120 minutes and centrifuged at 1,800 x g for 10 minutes. Supernatant was removed and cells were fixed with 50 µl of paraformaldehyde (PFA) for 10 minutes at room temperature. PFA was removed and cells were washed two times with PBS. 180 µl of PBS was added to each well and combined with 20 µl of 10µM SYTOX Green and 20 µl of Hoechst 33258 solution (20 µg/ml). NETs were visualised using an epifluorescent microscope (Nikon Eclipse TE300 with a coolLED PE-100 LED excitation system). The excitation wavelengths used for SYTOX Green and Hoechst were 488 and 405 nm, respectively.

2.28. Quantification of neutrophil cytokine and enzyme release using enzyme-linked immunosorbent assay (ELISA)

Isolated neutrophils were incubated as described in Ling et al. (2015). Cells were diluted to 2.5 x 10^6 cells/ml in supplemented RPMI (sRPMI: RPMI 1640, without L-glutamine and phenol red, Cytiva, USA; 10% heat-inactivated FBS, 25 mM HEPES, Sigma-Aldrich/Merck, Darmstadt, Germany; 2 mM glutamine). Neutrophils were then stimulated with *F. nucleatum* subspecies diluted in sRPMI (MOI 100) and incubated at 37°C, 5% CO_2 for up to 18 hours. Culture supernatants were collected either after 18 hours for endpoint quantification or after 1, 2, 4, 6 and 18 hours of incubation for time-course quantification. Commercial ELISA kits (R&D Systems, Abingdon, UK) were used to quantify human cytokines IL-1β, IL-6, TNF-α, IL-8 and neutrophil enzymes matrix metalloproteinase 9 (MMP-9) and human neutrophil elastase (HNE/ELA2). All ELISA measurements were performed in technical duplicate and according to the manufacturer's instructions.

2.29. Quantification of apoptosis and necrosis

Viability of neutrophils stimulated with *F. nucleatum* subspecies was assessed by measuring apoptosis and necrosis following the manufacturer's instructions (RealTime-Glo™ Annexin V Apoptosis and Necrosis Assay, Promega, UK). Briefly, isolated neutrophils diluted in sRPMI (1 x 10^5 cells in 100µl) were stimulated either with positive controls (100 ng/ml Fas ligand for apoptosis, 50 µg/ml LL-37 for necrosis; 50 µl each) or with *F. nucleatum* subspecies (MOI 100; 50 µl). 100 µl of 2X detection reagent was added and the cells were incubated for 18 h at 37°C (Infinite 200 PRO, Tecan, Switzerland) and luminescence (apoptosis) as well as fluorescence (necrosis) were recorded automatically every 15 minutes.

The rate of apoptosis and necrosis were determined from the highest peak of the first derivative of the apoptosis and necrosis curve, respectively. Start of apoptosis and necrosis were calculated from the highest peak of the second derivative of the apoptosis and necrosis curve, respectively. First and second derivatives were calculated using GraphPad Prism (version 10.1.1 for Windows, Boston, Massachusetts USA). Data was minimally smoothed with the following GraphPad settings: 6^{th} order of the smoothing polynomial and 4 neighbours to average on each size.

2.30. Statistical analysis

GraphPad Prism (version 10.1.1 for Windows, Boston, Massachusetts USA) was used to perform statistical analysis and to generate graphs. Normality of the data was first analysed using Shapiro-Wilk test. If the data were shown to conform to normal distribution, one-way ANOVA with Tukey's multiple comparison test was performed. If the data were not normally distributed, either Mann-Whitney U-test or Kruskal-Wallis test was performed followed by Dunn's post hoc test, unless stated otherwise in the figure legends. The results were statistically significant if $p < 0.05$.

CHAPTER 3: CHARACTERISATION OF *FUSOBACTERIUM NUCLEATUM* SINGLE-SUBSPECIES BIOFILMS

This chapter is based to a large degree on our published article:

Muchova M, Balacco DL, Grant MM, Chapple ILC, Kuehne SA and Hirschfeld J (2022) *Fusobacterium nucleatum* Subspecies Differ in Biofilm Forming Ability *in vitro*. *Frontiers in Oral Health*, 3:853618. doi: 10.3389/froh.2022.853618

3.1. Introduction

In order to fulfil the aims of this project, biofilm formation by all *F. nucleatum* subspecies was investigated. Results from the author's previous work (master's thesis, Muchova (2020)) showed that subspecies differ in their ability to form single-subspecies biofilms, which could potentially suggest differences in their immunogenicity, as biofilm formation is one of the virulence determinants of oral bacteria. Thus, it was necessary to further characterise subspecies-specific biofilm formation, expanding the selection of substrates to plastic, glass and hydroxyapatite. A number of substrate treatments promoting cell attachment to culture surfaces were tested by coating with artificial saliva (AS), collagen, gelatin, fibronectin and poly-L-lysine. Sandblasted glass was used to assess the effect of a roughened surface on *F. nucleatum* subspecies biofilm formation. Compared to the author's previous work, which used AS as a biofilm growth medium, this work utilised more nutritious Schaedler anaerobe broth (SAB) to encourage biofilm formation and artificial gingival crevicular fluid (aGCF) to mimic the physiological conditions of the gingival crevice and thus serve as a more suitable medium supporting biofilm growth. Additionally, dynamic and static biofilm models were compared in order to evaluate *F. nucleatum* biofilm formation with and without shear stress, since shear stress can promote biofilm formation and is reported to promote formation of stable and uniform biofilms (Park et al., 2011).

3.2. Comparison of dynamic and static biofilm model

Apart from static conditions with finite amounts of nutrients and buffering capacity, biofilms can be grown dynamically, with a constant flow of fresh medium and nutrients. To evaluate whether growing *F. nucleatum* biofilms in dynamic conditions with a constant supply of

nutrients and shear stress improves biofilm formation, a comparison of dynamic and static models was undertaken.

3.2.1. Dynamic biofilm model

Biofilm formation of FN23, FN25 and FNP was evaluated in aerobic and anaerobic conditions on borosilicate glass coupons. We previously demonstrated that *F. nucleatum* survives in the presence of oxygen for at least 8 hours (Muchova 2020, master's thesis), therefore aerobic incubation was not considered detrimental to bacterial adhesion and initiation of biofilm formation. To evaluate the amount of biomass, coupons were assessed visually for the presence of a biofilm layer as well as vortexed in PBS with visual assessment of turbidity. No biofilm was formed by any of the three subspecies when grown for three days, regardless of the conditions. Even when the initial bacterial concentration was increased from OD_{550}=0.2 to OD_{600}=1 (note difference in wavelength used for OD measurement due to differences in available literature) and the time of the incubation was increased to five days, no biofilm was isolated from the discs when vortexed to detach the biomass.

3.2.2. Static biofilm model

Biofilms were set up as outlined in section 2.3.1 in 24-well plates with glass coverslips and in 96-well plates (wells only) for three days in anaerobic conditions. 500 µl of the bacterial suspension were added to wells of the 24-well plates, while 200 µl were added to 96-well plates. Quantification of biomass using CV showed that among the subspecies FNP formed the lowest amount of biofilm, while FNA and FNF formed the highest amount of biomass (Figure 3.1).

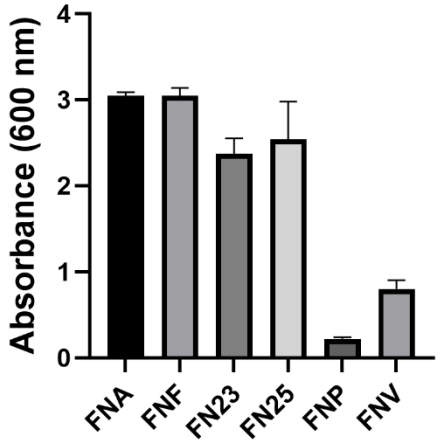

Figure 3.1. Quantification of biomass formed by individual *F. nucleatum* subspecies in a 96-well plate. The graph shows means of one experiment performed in five technical replicates. Error bars represent standard deviations. All values were corrected for blank (wells with medium without bacteria).

To establish a reproducible protocol, biofilms grown on glass coverslips in 24-well plates were evaluated only visually. All biofilms formed were observed to be very fragile and to detach easily upon handling the plates and changing media. The most fragile biofilm was observed in wells with ssp. *polymorphum*, which is in agreement with the results of biomass quantification using CV (see figure 3.1).

Results showed that the dynamic biofilm model is unsuitable for *F. nucleatum* biofilms, therefore the static model was chosen for further biofilm characterisation. Based on the results of the static biofilm incubation, FNP was the weakest biofilm former, thus additional experiments were undertaken focusing on this subspecies in order to determine whether changing the type of substrate and medium and increasing the seeding density of bacteria improves biofilm formation.

3.3. Qualitative evaluation of FNP biofilm formation

FNP may form unstable biofilms due to the low number of bacteria adhering to the substrate during the initial stages of biofilm formation, hence it was decided to increase the initial concentration of bacteria and standardise the bacterial cultures in the following experiments to an OD_{600}=1 (1.62 x 10^9 CFU/ml) and use 1 ml of each culture in 24-well plates (See section 2.3.1). Two subspecies were chosen to perform subsequent experiments: FNP as the weakest biofilm former and FN25, which is commonly used in standard multispecies biofilm models (Thurnheer et al., 2019). A different surface (hydroxyapatite [HA] discs mimicking the tooth enamel surface), glass surface treatment (collagen coating or roughening by sandblasting) and a longer incubation time were chosen to determine whether FNP biofilm formation could be improved. Moreover, a different medium – aGCF – was added (overview of surfaces and media in Table 2.2).

Interestingly, none of the modifications improved FNP attachment to substrates and biofilm formation. When compared to FN25, which formed a visible and considerably thicker layer of biofilm on all surfaces when grown in SAB, even when the incubation time varied, FNP either formed a very fragile layer, which detached upon plate agitation, or there was no layer at all and only planktonic cultures were observed, regardless of the incubation time (Figure 3.2). Artificial GCF did not improve FNP attachment and worsened attachment of FN25 when the subspecies were grown on HA discs for seven days, as no biofilm was isolated when HA discs were vortexed to detach any biomass present (data not shown).

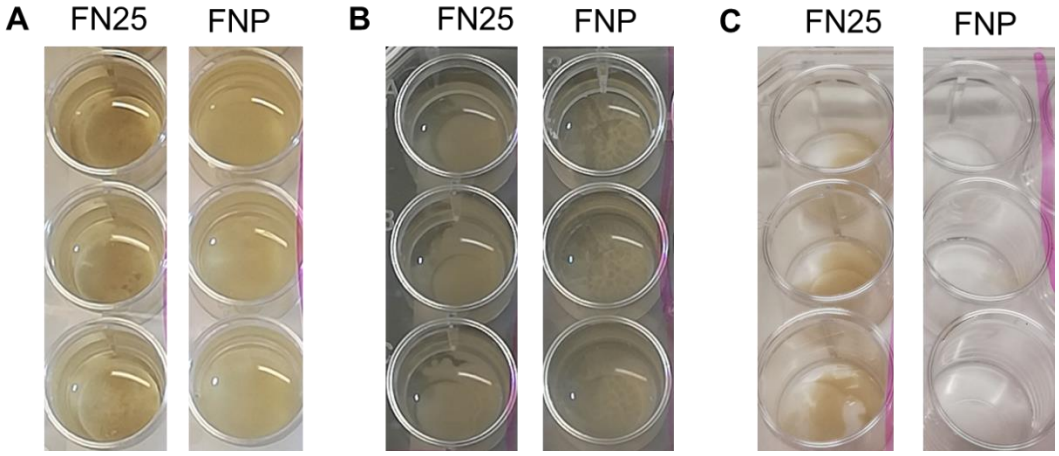

Figure 3.2. Visual evaluation of biofilm formation on HA and sandblasted glass coverslips. **A:** FN25 forms visible biofilms when grown on HA in SAB, while FNP does not appear to adhere, picture taken after seven days of incubation. **B:** FN25 forms a thick layer of biofilm on sandblasted glass coverslips, while FNP forms a very fragile biofilm, picture taken after four days of incubation before media removal. **C:** Biofilms from panel B after seven days of incubation after final media removal.

Collagen coating did not promote biofilm formation in FNP, while FN25 formed a visible stable layer of biofilm (Figure 3.3). Biofilms were assessed only visually as it was not possible to stain them due to the presence of a layer of collagen which would also take up the stain, obscuring the real amount of biofilm.

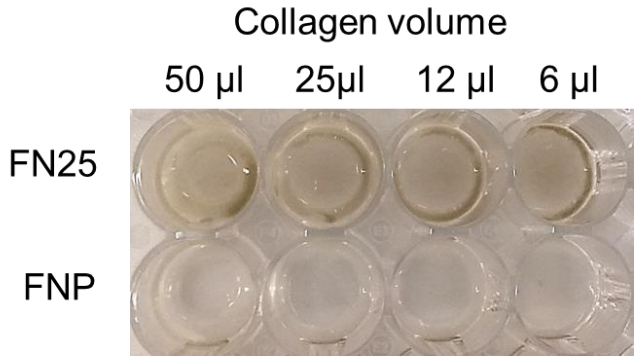

Figure 3.3. Visual evaluation of biofilm formation by FN25 and FNP on a collagen-coated plate after 4 days of incubation. Only FN25 formed a visible layer of biofilm. Collagen concentration was 50µg/ml.

Due to the fact that FNP had a very limited ability to form biofilms on all substrates assessed, biofilms were additionally set up in 25cm^2 tissue culture flasks (as detailed in section 2.3.1.),

using a higher volume of the medium, which was not changed during the biofilm incubation. Similarly to previous results, FN25 formed a visible, considerably thicker layer of biofilm, seen as a light-brown layer in the flask, while FNP did not, and no layer was observed in the flask (Figure 3.4). This subspecies was only observed to grow planktonically during incubation.

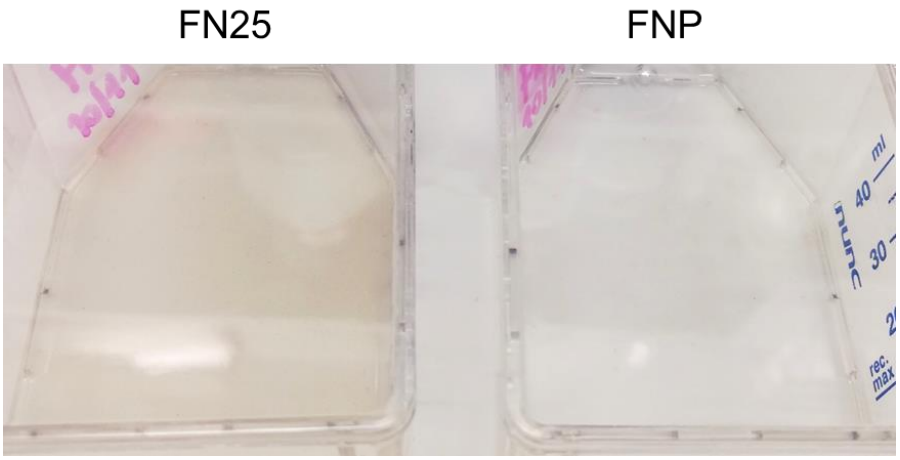

Figure 3.4. Visual evaluation of biofilms grown in tissue culture flasks after 4 days of incubation. Biofilm formed can be observed in FN25 flask as a light-brown layer formed on the bottom of the flask, while the flask with FNP is clear.

These initial results showed that FNP did not form stable biofilms on tested surfaces and surface treatments, therefore additional culture surface treatments routinely used to improve cell adhesion during culture were investigated. A more systematic approach was selected to compare and quantify biofilm formation of all subspecies, including FNP, on glass and plastic surfaces with a number of surface modifications described next.

3.4. Systematic evaluation of biofilm formation by all *F. nucleatum* subspecies

In order to quantify and compare biofilm formation among the subspecies, biofilms grown for three days (section 2.4) were stained using CV (section 2.5). This technique allows direct

quantification as the amount of biomass is directly proportional to the amount of stain taken up by the biofilms.

3.4.1. Biofilm formation by all subspecies on modified surfaces

All subspecies formed biofilms detectable with CV, except for FNP, which did not form a continuous layer of biofilm on any of the surfaces tested (Figure 3.5). None of the surface modifications improved substrate adhesion and biofilm formation by FNP. When examined visually during the incubation period, this subspecies was found to remain planktonic in the biofilm supernatant.

Differences in biofilm mass were seen amongst the different subspecies and on the different surfaces (Figure 3.5A, B): Generally, sandblasted glass surfaces supported biofilm formation best with significantly higher biofilm mass in most subspecies compared to untreated glass (Figure 3.5A). The second most effective surface coating was AS, supporting significantly higher biofilm formation by FN25 and FNP on glass surfaces (Figure 3.5A), and FN25, FNP and FNV on plastic surfaces (Figure 3.5B). However, even though absorbance values of FNP biofilms were significantly higher on both glass and plastic coated with AS compared to untreated surfaces ($p=0.04$ and $p=0.02$, respectively), the amount of biofilm quantified was consistently low and close to the detection limit (mean absorbance values of 0.017 and 0.029, respectively). FNA and FNF were the best biofilm formers on plastic surfaces.

When the surfaces were compared (Figure 3.5C), FNF adhered significantly better to uncoated as well as fibronectin-coated Thermanox coverslips, and FNA formed significantly higher amounts of biofilm on AS-coated Thermanox coverslips, however the other subspecies showed no statistically significant difference in biofilm formation between glass and plastic surfaces.

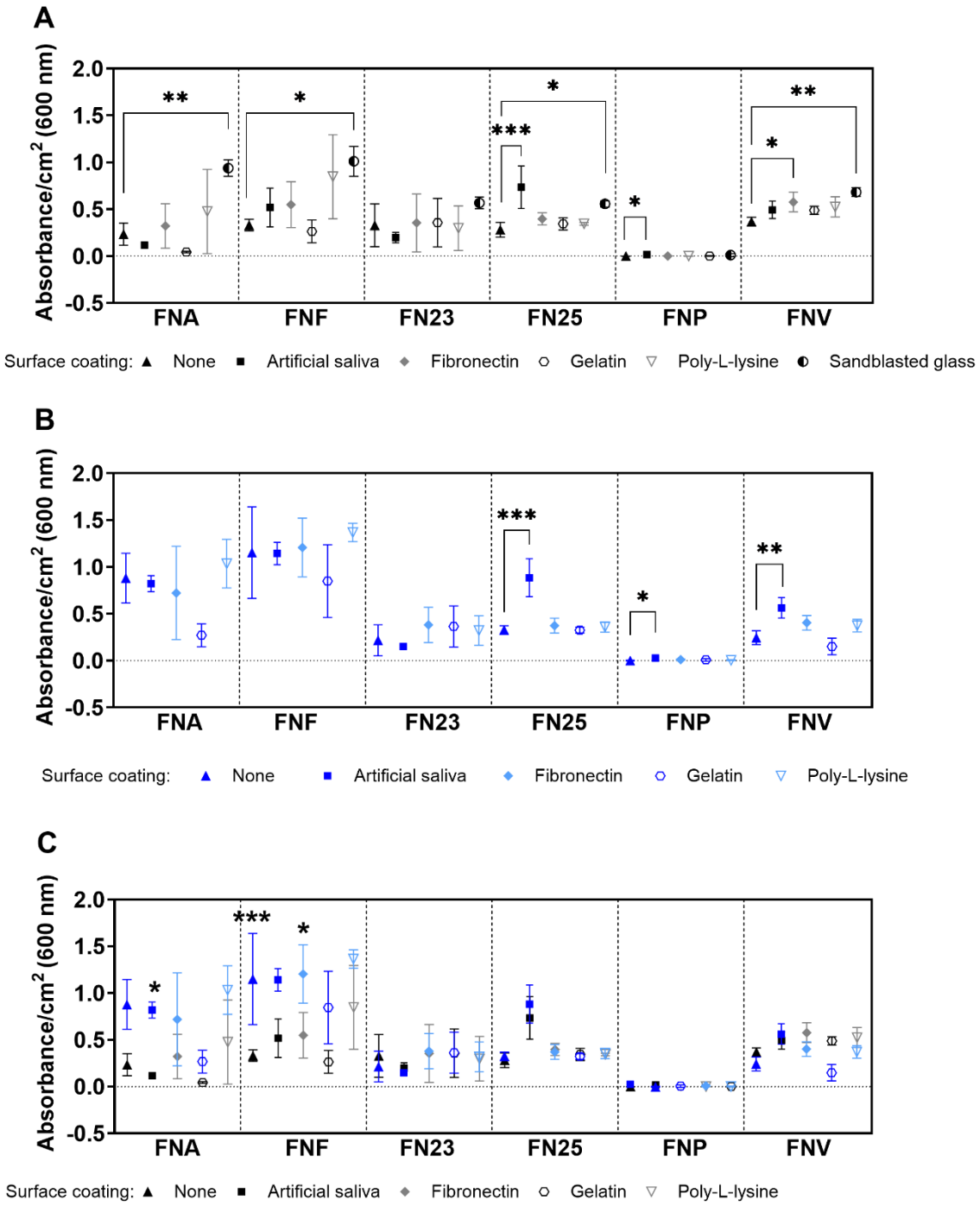

Figure 3.5. Single-subspecies biofilms quantified using CV. A: Quantification on glass coverslips with or without (control) surface coatings. No significant differences were found for FN23. **B**: Quantification on Thermanox coverslips with or without (control) surface coatings. No significant differences were found for FNA, FNF and FN23. **C**: Overlayed graphs of values from glass and plastic surfaces to show differences between the surfaces and surface treatments. Sandblasted glass was omitted from the analysis due to the absence of sandblasted plastic surface. Symbols in blue shades show values from plastic surfaces, symbols in grey shades values from glass surfaces. Assays were carried out as three independent experiments in triplicate. Mean values with standard deviations are shown. One-way ANOVA was performed

followed by Dunnett's post hoc test for within subspecies differences between control (uncoated glass/uncoated Thermanox) and test samples in A and B. One-way ANOVA with Tukey's post hoc test was performed in C. *p<0.05; **p<0.01; ***p<0.001.

As all *F. nucleatum* subspecies formed detectable biofilms under the conditions investigated except FNP, we considered whether spontaneous mutations may have occurred in this subspecies. This phenomenon has been reported in bacterial type strains commonly used in laboratories, such as *E. coli,* during long-term storage and propagation in growth media (Dorman and Thomson, 2020). Therefore, we proceeded to compare its biofilm formation to a newly purchased FNP type strain, ATCC 10593. The strain number was identical to the strain from our culture collection.

3.4.2. Comparison of biofilm forming ability of two FNP strains

Biofilms were set up as described in section 2.4. and biomass was quantified using CV staining (section 2.5). The FNP strain from the PRG culture collection was labelled as "old" strain (oFNP), while the newly purchased FNP strain was labelled as "new" strain (nFNP).

Interestingly, only nFNP grown on glass coated with fibronectin (Figure 3.6) formed a significantly higher amount of biomass when compared to oFNP (p=0.0125), however mean absorbance values were consistently low and nFNP did not form a stable, detectable layer of biofilm under any conditions tested.

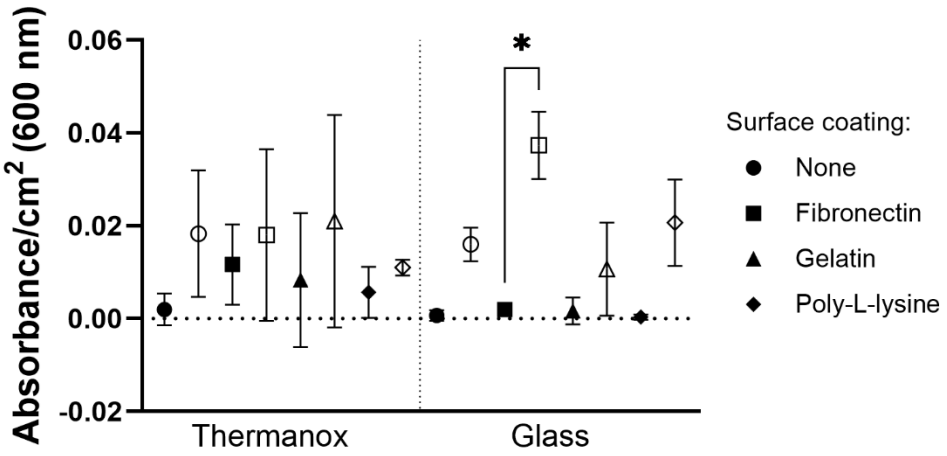

Figure 3.6. Comparison of two FNP strains. Strain oFNP is shown as filled symbols, nFNP strain is shown as empty symbols. In each type of surface coating, nFNP was compared with oFNP and the only statistically significant difference was found in fibronectin-coated glass as indicated. Assays were carried out as three independent experiments in triplicate. One-way ANOVA was performed followed by Tukey's post hoc test (*p=0.0125).

3.4.3. Biofilm formation by FN23 strains lacking adhesion proteins

In addition to the characterisation of biofilm formation by all *F. nucleatum* subspecies, the role of adhesion proteins in single-subspecies biofilm formation was examined. Single gene knockout FN23 strains ΔFadA and ΔFap2 were grown on uncoated Thermanox coverslips since no difference was found among surface modifications in the case of FN23 (Figure 3.5B).

Both ΔFadA and ΔFap2 formed significantly higher amounts of biofilm when compared to the parental strain FN23 (WT; Figure 3.7). The mean amount of biomass formed by ΔFadA was almost five times higher, while the mean amount of biomass formed by ΔFap2 was four times higher than the parental FN23 strain.

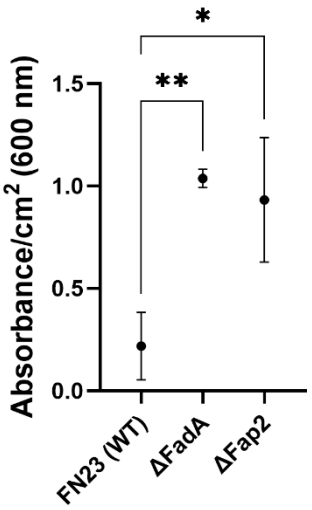

Figure 3.7. Biofilm formation by FN23 mutant strains lacking adhesion proteins FadA and Fap2. Assays were carried out as three independent experiments in triplicate. One-way ANOVA was performed followed by Tukey's post hoc test (*p=0.012; **p=0.006). Data shown as means with standard deviations.

3.5. Estimation of biofilm stability and thickness of *F. nucleatum* subspecies using CLSM

Biofilm thickness was examined using CLSM and mean values obtained from three-dimensional biofilm images (Figure 3.9A). Similar to the results obtained by CV staining, all subspecies except FNP formed a continuous layer of biofilm.

Only single bacterial cells of FNP were observed on untreated and coated surfaces (Figure 3.8, Figure 3.9B). A small area of biofilm formation by FNP was detected in the centre of poly-L-lysine coated wells, for which the thickness was determined (Figure 3.9B; 9.1 µm ±1.3 µm, mean +/- SD).

Large standard deviations were associated with some subspecies-surface combinations seen in CLSM experiments. Ssp. FNA and FNF on poly-L-lysine coated plastic exhibited a high standard deviation when biofilm thickness was evaluated (Figure 3.9A). Additionally, a high standard deviation was observed in ssp. FN23 on all surface treatments apart from poly-L-lysine

coated plastic (Figure 3.9A). These reflect a high degree of visually observed biofilm detachment during handling, indicating low adhesive strength of these biofilms.

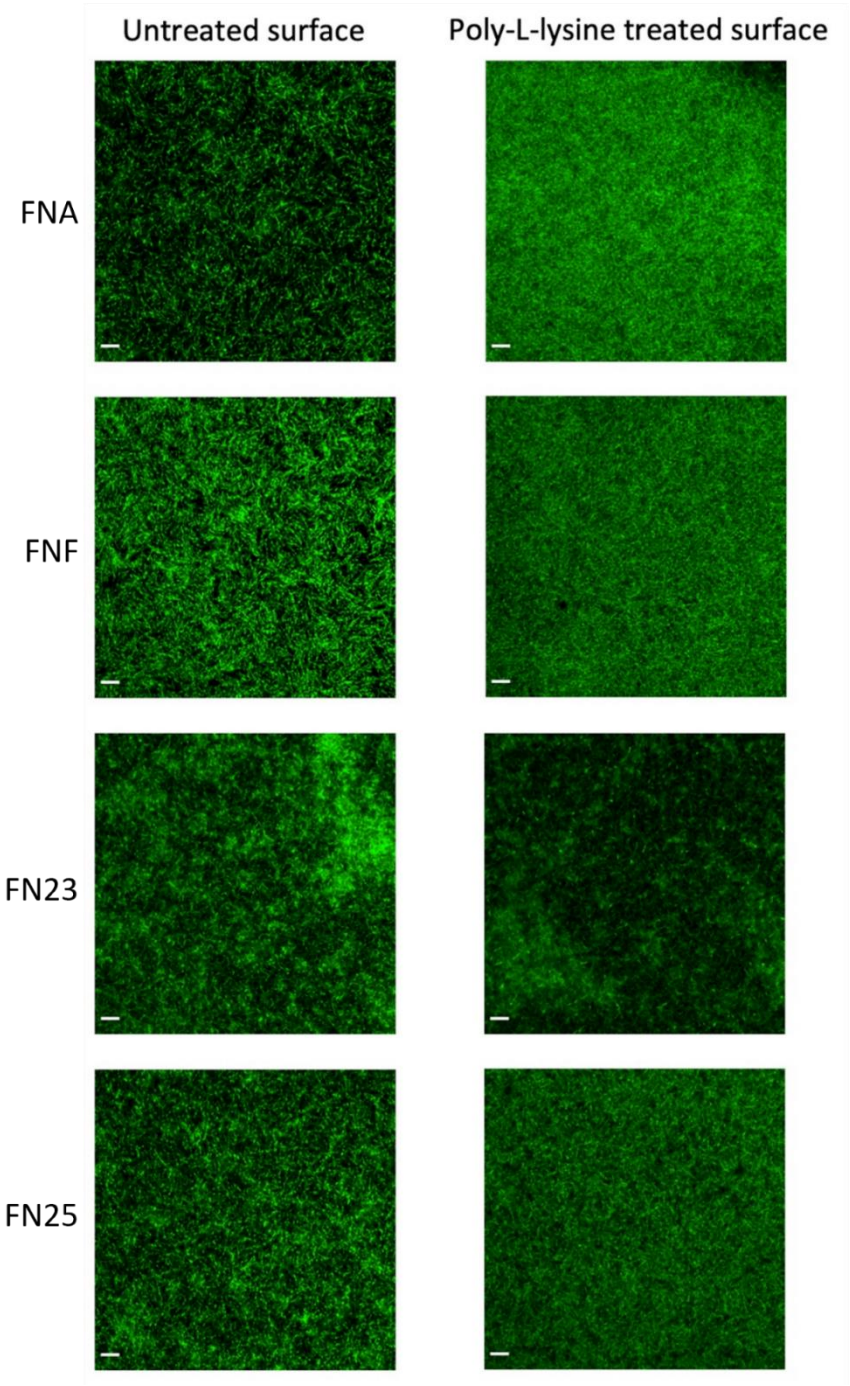

Figure 3.8. Representative 2D images of single-subspecies *F. nucleatum* biofilms imaged by CLSM. Figure legend continued on the next page.

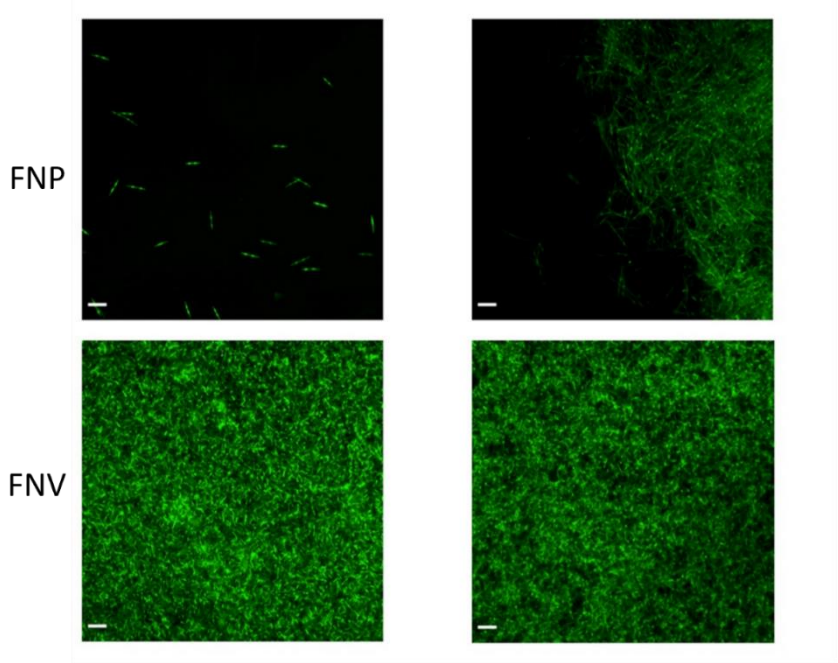

Figure 3.8. Representative 2D images of single-subspecies *F. nucleatum* biofilms imaged by CLSM. Biofilms were grown on untreated and poly-L-lysine coated plastic surfaces. Note the absence of a continuous biofilm layer in FNP: only single cells were observed on the untreated surface while a bacterial aggregate was observed on the poly-L-lysine treated surface. Scale bar: 10 μm.

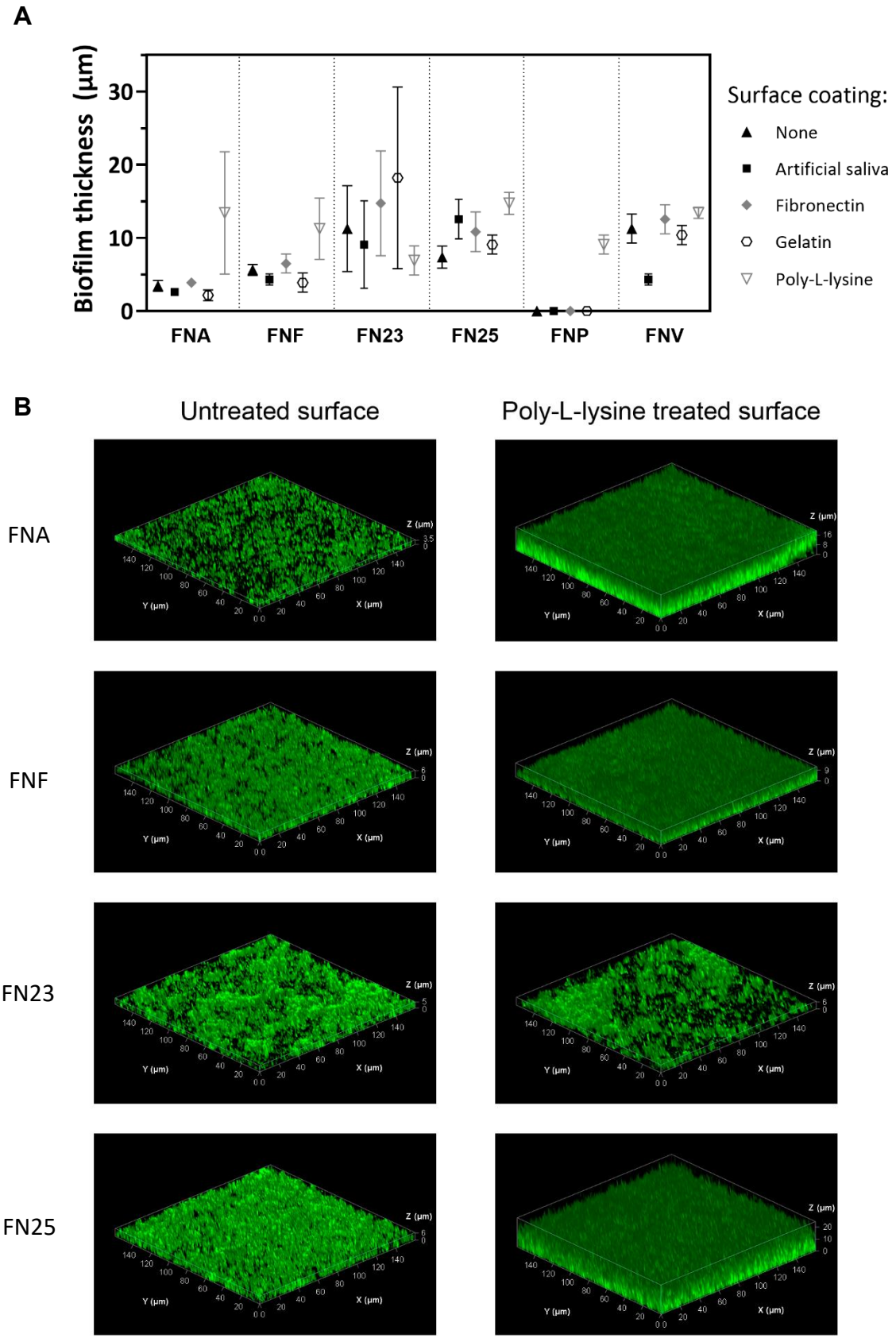

Figure 3.9. Biofilm thickness of *F. nucleatum* subspecies determined by CLSM. Figure legend continued on the next page.

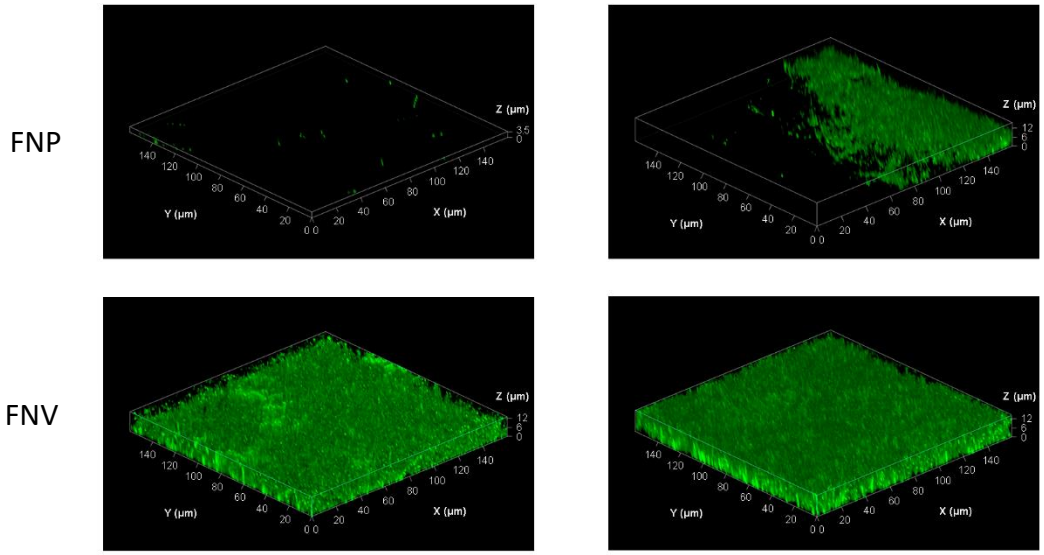

Figure 3.9. Biofilm thickness of *F. nucleatum* subspecies determined by CLSM. A: Biofilm thickness estimated from z-stacks. Experiment was performed once with biofilms grown in triplicates. Mean values with standard deviations are shown. **B**: Representative Z-stack 3D images of single-subspecies biofilms grown on untreated and poly-L-lysine coated plastic surface. Biofilms are enclosed in a bounding box with scaled coordinates; x, y, and z axes show the dimensions indicated in µm.

3.6. Biofilm architecture analysed by SEM

Thermanox coverslips coated with poly-L-lysine were chosen as the surface for biofilm analysis by SEM based on CLSM results, which exhibited greater biofilm thickness on this type of surface. Biofilms were grown for 3 days as described in section 2.4. Overall, high magnification (1,000X, Figure 3.10A) revealed uneven layers of biofilm with raised areas, especially in FNA, FN23 and FN25 (raised areas indicated with white arrows). FNA, FNF and FN25 formed continuous, multi-layered biofilms with visible aggregates, whilst FN23 formed thinner biofilms, mostly observed as monolayers with smaller aggregates. Biofilms formed by FNV appeared as flat, continuous monolayers. Again, FNP did not form a continuous layer of biofilm, but individual bacteria and small pre-biofilm aggregates were observed.

Cell-to-cell cohesion was examined in more detail under 5,000X magnification (Figure 3.10B). In all biofilms, bacterial cells were found to cohere with neighbouring cells either in a parallel fashion, or cells were intertwined. All biofilms analysed seemed to be lacking extracellular matrix (ECM). Taken together, biofilm architecture visibly differed among *F. nucleatum* subspecies with regard to thickness and formation of aggregates and voids. Cell-to-cell cohesion did not seem to differ among subspecies.

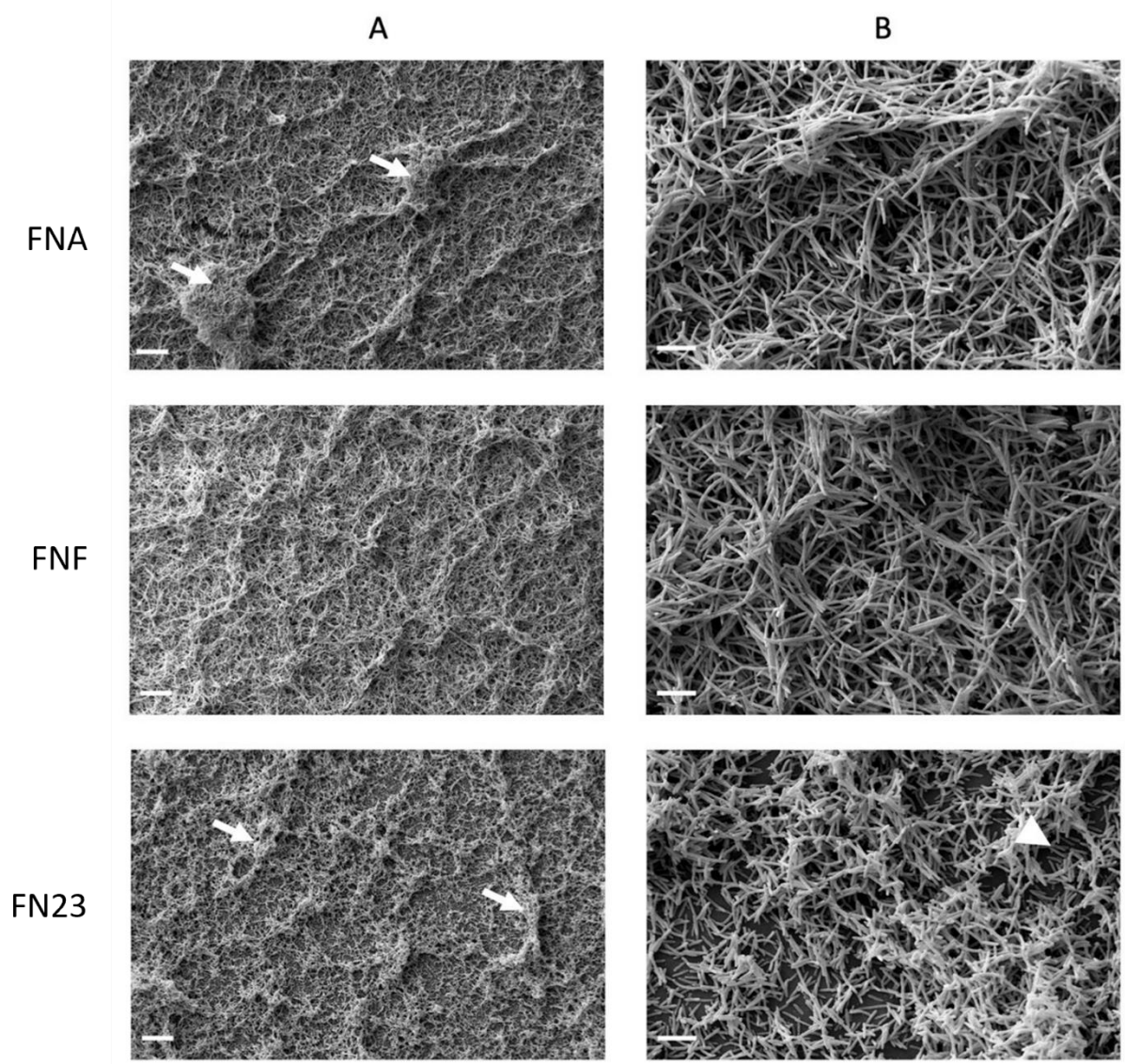

Figure 3.10. Micrographs of single-subspecies *F. nucleatum* biofilms grown on poly-L-lysine coated Thermanox coverslips. Figure legend continued on the next page.

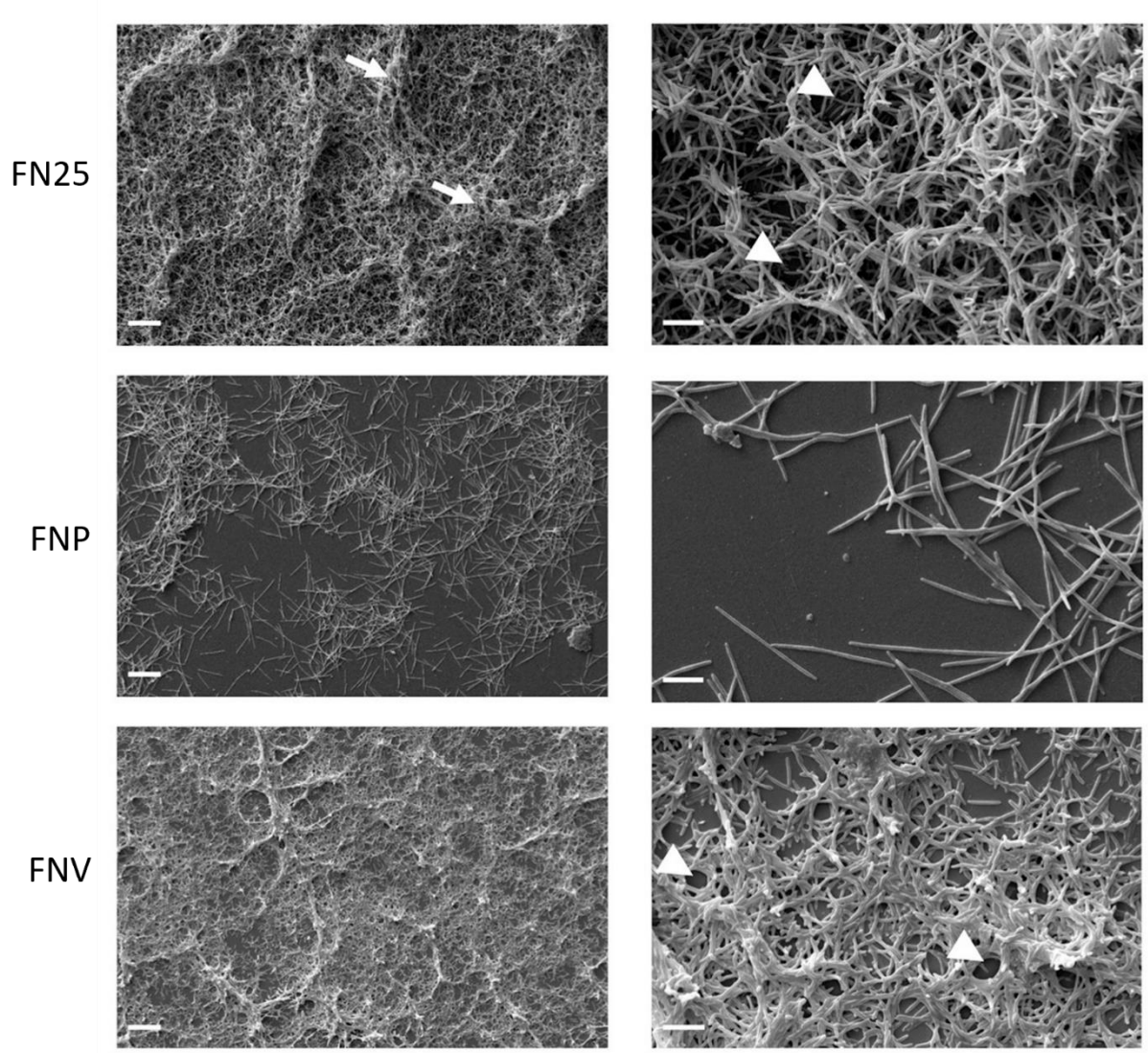

Figure 3.10. Micrographs of single-subspecies *F. nucleatum* biofilms grown on poly-L-lysine coated Thermanox coverslips. A: Micrographs showing differences in biofilm architecture. White arrows indicate bacterial aggregates within the biofilm. 1,000X magnification, scale bar 20µm. **B:** Micrographs showing cell-to-cell cohesion. White arrow heads indicate voids in the biofilm. 5,000X magnification, scale bar 5µm. Biofilms from two independent experiments grown in duplicates were imaged and representative micrographs are shown.

3.7. Bioinformatic analysis of *F. nucleatum* adhesins

To investigate possible differences in adhesion proteins amongst the subspecies, which may explain the observed lack of biofilm formation in FNP, analysis of the bacterial genomes was

undertaken. This bioinformatic analysis was carried out by Dr Dario L. Balacco as part of the publication detailed at the beginning of this chapter.

Sequence alignments of Aid1, CmpA, FadA, Fap2, FomA, RadD, and YadA from FN25 identified orthologous proteins in the *F. nucleatum* ATCC subspecies genomes publicly available on EnsemblBacteria (Release 52) (Howe et al., 2020). As expected, adhesin orthologs in FN23 were highly conserved, as shown in the heat map by percentage identity values equal or higher than 90% (Figure 3.11A left, light creamy colour). In contrast, our approach did not identify any Aid1, FomA, and RadD orthologs in FNV or any FadA and YadA orthologs in FNA, as indicated by black boxes in the heat map (Figure 3.11A left). The genome of FNF was not available on this database, therefore it could not be included in the analysis.

Orthologs of all the considered proteins were found in FNP. Interestingly, CmpA and Fap2 orthologs were identified in all subspecies analysed; however, FNP orthologs were less conserved with the lowest percentage identity among the four analysed subspecies, as shown by the red boxes in the heat map, with 61% identity for Fap2 and 52% identity for CmpA (Figure 3.11A, left). Availability of the gene and protein sequence data allowed prediction of structures and the presence of specific protein domains in the analysed adhesins. Annotation of these protein domains highlighted their variability as well as differences in the length of proteins (Figure 3.11A, right). Interestingly, both CmpA and Fap2 presented an Autotransporter domain in FN25 (Figure 3.11A, right). Thanks to this shared domain, CmpA and Fap2 were chosen for further analysis, as this indicated a common origin and possibly function and allowed alignment of the amino acid sequences (Figure 3.11B) A phylogenetic tree of CmpA and Fap2 shows that the respective orthologs in all the subspecies are highly conserved, which is indicated by the closeness of the subspecies branching out from the same node, except for the FNP proteins,

which are more distantly related (Figure 3.11B), as shown by an earlier separation from the nodes of the phylogenetic tree.

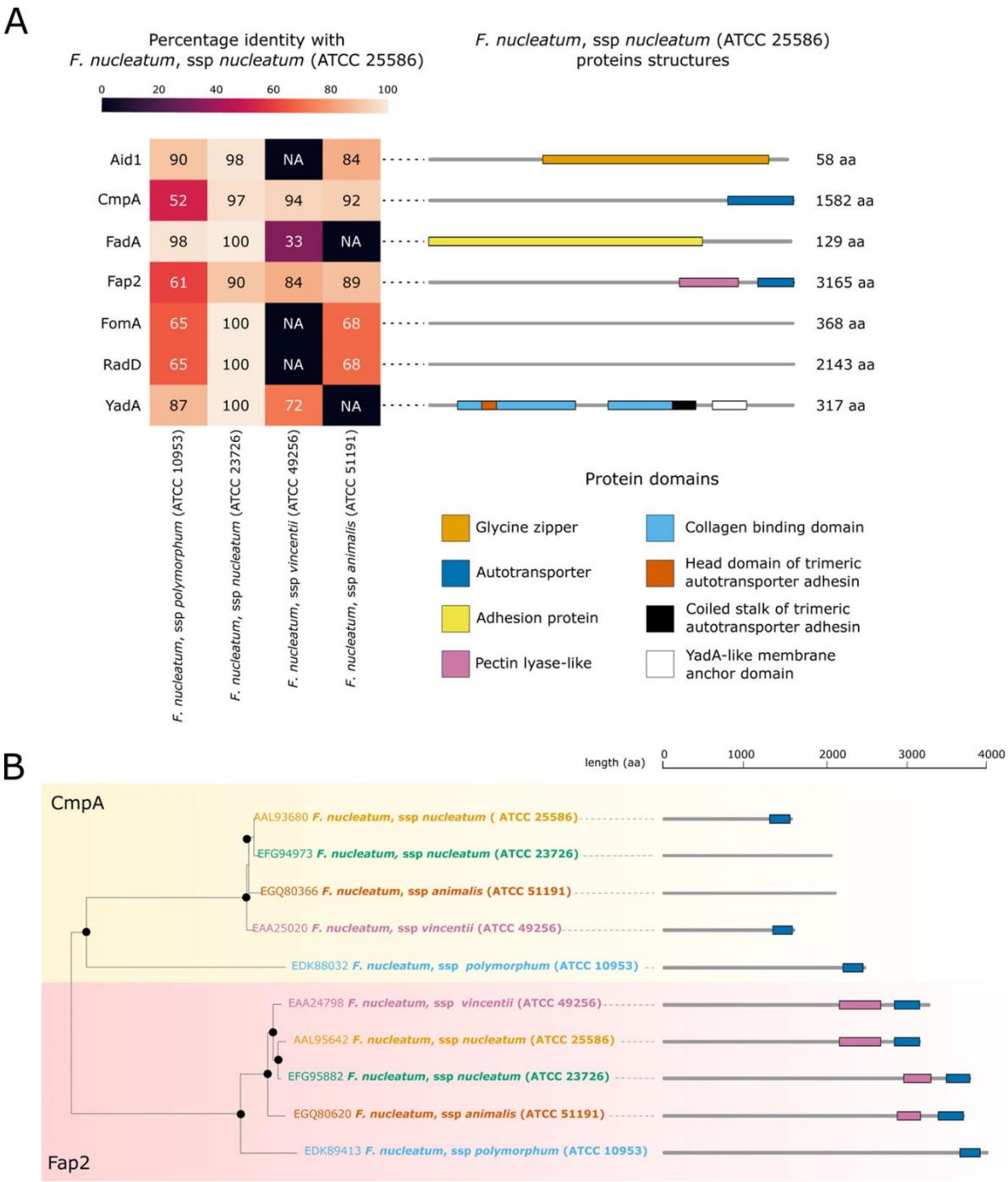

Figure 3.11. Bioinformatic analysis of adhesion proteins in *F. nucleatum* subspecies. A: Conservation of adhesion proteins in ATCC strains of *F. nucleatum*. The heatmap shows the percentage of identity with the FN25 adhesion proteins Aid1, CmpA, FadA, Fap2, FomA, RadD, YadA. Protein length and domain organisation are indicated on the right for each of

FN25 proteins. The domains are indicated and coloured differently: glycine zipper (orange); autotransporter (dark blue); adhesion protein (yellow); pectin lyase-like (pink); collagen binding domain (light blue); head domain of trimeric autotransporter adhesin (dark orange); coiled stalk of trimeric autotransporter adhesin (black); YadA-like membrane anchor domain (white). **B**: CmpA and Fap2 phylogenetic tree. The CmpA branch is highlighted in yellow, the Fap2 branch is highlighted in pink. Black circles represent bootstrap values > 95. FN25 proteins are coloured in orange; FN23 proteins in green; FNA proteins in dark orange; FNV in pink; FNP in light blue. Protein structures and lengths are outlined on the right of the tree. Autotransporter domains are coloured in blue, pectin lyase-like domains in pink. Figures were drawn with seaborn (version 0.11.2; (Waskom, 2021)) and R statistical software (version 4.1.2).

Based on the results of this *in silico* analysis of adhesins, it seemed appropriate to investigate the presence or absence of adhesins in *F. nucleatum* subspecies employed in this work. This would be investigated using protein gel electrophoresis.

3.8. Membrane protein profile analysis of *F. nucleatum* subspecies

Membrane proteins isolated from planktonic and biofilm-grown subspecies were analysed using one- and two-dimensional gel electrophoresis of membrane proteins in order to obtain membrane protein profiles and compare the subspecies-specific expression of the adhesins studied.

3.8.1. One-dimensional sodium dodecyl-sulphate (SDS) polyacrylamide gel electrophoresis (PAGE)

Firstly, membrane proteins were separated based on their molecular weight by 1D SDS-PAGE. The quantity of proteins loaded on the gels was standardised for each sample. Considering that only the membrane protein fraction was resolved on the gels, all subspecies exhibited highly complex protein profiles (Figure 3.12). Differences among planktonic as well as biofilm-grown

subspecies were observed, especially in the abundance of various proteins based on the relative intensity of the bands. Of note, a strong protein band was observed in P1 (FNP new strain) at ~40 kDa, which was absent in P2 (FNP old strain). However, due to the complexity of the profiles and high abundance of proteins, it was not possible to isolate individual proteins exhibiting differences.

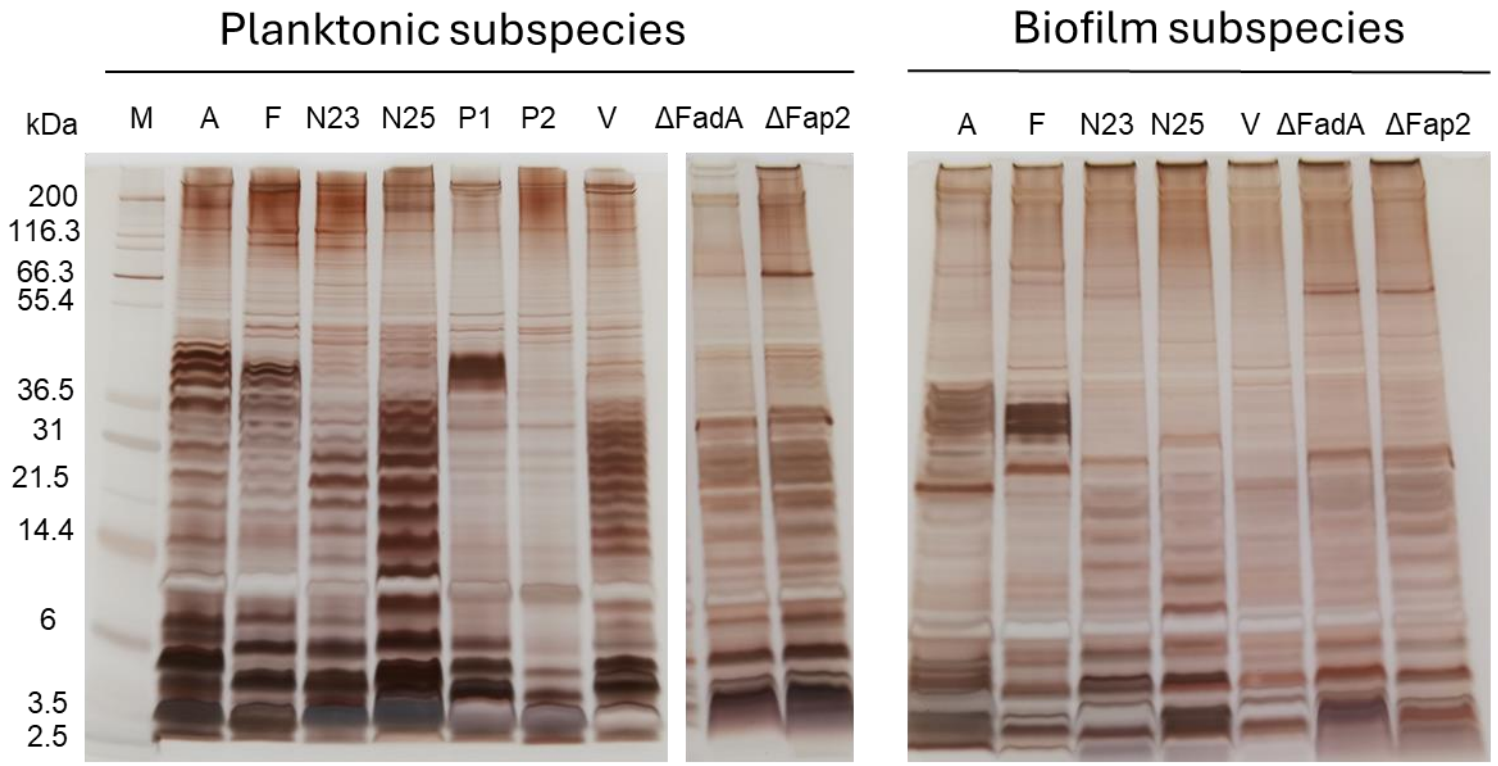

Figure 3.12. Membrane protein profiles of planktonic and biofilm *F. nucleatum* subspecies on 1D SDS-PAGE. A silver-stained 1D SDS-PAGE shows complex mixtures of membrane proteins in each subspecies, including the mutant strains FadA and Fap2. Lane 1 (M) contains the molecular weight marker ranging from 200 kDa to 2.5 kDa. A – FNA; F – FNF; N23 – FN23; N25 – FN25; P1 - new FNP strain; P2 – old FNP strain; V – FNV.

Additionally, some of the proteins of interest, such as Fap2 and RadD, were not resolved in the gel due to their molecular weights being higher than the largest fragment of the molecular weight marker. Only molecular weight of FadA was within the range of the marker with the weight of 14.4 kDa (information retrieved from the UniProt database: https://www.uniprot.org/uniprotkb/Q5I6B0/entry), however no clear gap was visible in the mutant strain. Thus, it was decided to perform two-dimensional SDS-PAGE, to provide a better resolution of the complex protein mixtures.

3.8.2. Two-dimensional sodium dodecyl-sulphate (SDS) polyacrylamide gel electrophoresis (PAGE)

2D SDS-PAGE resolves proteins in a mixture in the first dimension based on their isoelectric point (pI; acidic or basic proteins) and in the second dimension based on their molecular weight. In order to optimise the methodology and to focus on subspecies-specific differences, FN25 as a strong biofilm former and FNP (old strain) as a weak biofilm former were chosen.

While the electrophoresis of the samples studied based on size in the second dimension resulted in a spread of membrane proteins across the size range of the gel, separation in the first dimension based on the isoelectric point was unsuccessful and did not lead to the expected discrete protein spots (Figure 3.13). Despite insufficient resolution of the protein mixtures, some differences were observed between the subspecies: certain more abundantly expressed proteins were observed in FNP (enclosed in circles in the gel on the right; Figure 3.13) compared to FN25. Additionally, two bands of proteins (size approximately 50 kDa) were observed on the FNP gel (highlighted with two black arrows) compared to the FN25 gel, where

only one band was observed. In both gels, the majority of membrane proteins migrated towards the acidic part of the gel (left).

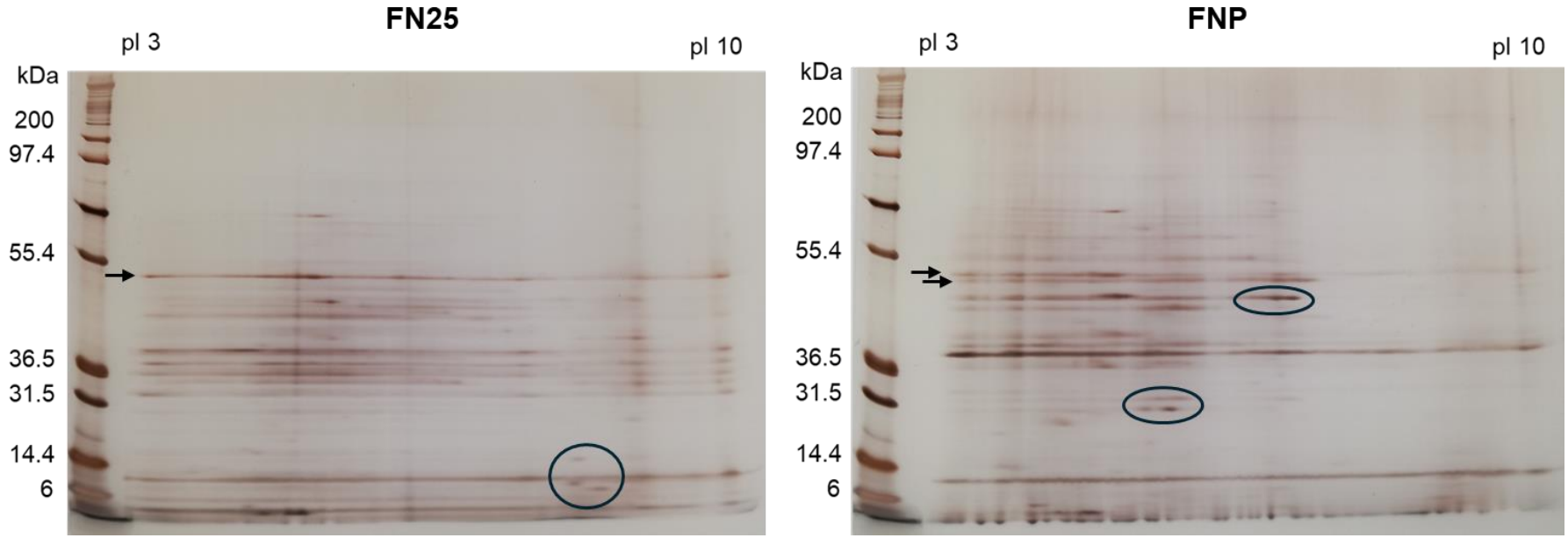

Figure 3.13. Membrane protein profiles of FN25 and FNP (old strain) on 2D SDS-PAGE. Gels were stained with silver. Fragments of the molecular weight marker on the left of each gel range from 200 kDa to 6 kDa. Acidic proteins are separated on the left half of each gel (pI 3), basic proteins on the right half (pI 10). Some of the differences are highlighted in the gels: circles enclose exemplary proteins with differing abundance, arrows point at differing protein bands.

3.9. Chapter discussion

Initial biofilm analysis in this chapter comparing static and dynamic biofilm models showed that dynamic biofilm incubation is unsuitable for *F. nucleatum* alone since no biofilm was formed in the conditions studied. This may be due to an abundance of fresh nutrients, as it was shown that nutrient deficiency promotes adhesion and biofilm formation in another anaerobic microorganism *Listeria monocytogenes* (Wang et al., 2022). Alternatively, bacteria may be washed away by the flow of medium, which in our conditions is significantly higher (100 µl/min) compared to the flow conditions used by Park et al. (2011) (0.1 µl/min), which were reported to promote biofilm formation. The present investigations were limited by the settings of the peristaltic pump and therefore such a low flow rate of medium could not be selected. Considerably lower flow velocity and potentially a different setup would need to be used if the dynamic model is revisited in the future.

Furthermore, growing biofilms in a dynamic setup with a flow cell proved to be challenging due to frequent occurrence of contamination. If the system is not handled with caution, contaminants can easily be introduced during assembly of the flow cell, via addition of the media into the feeding bottle, via the injection ports or retrogradely via tubing leading to the waste bottle.

Further systematic qualitative as well as quantitative analysis of biofilm formation by all subspecies confirmed that *F. nucleatum* subspecies differ in biofilm forming ability and that not all subspecies have the ability to form stable biofilms. FNP did not form biofilms but only small bacterial aggregates. In support of this finding, similar results were obtained by Karched et al., (2015) who showed poor single-subspecies biofilm formation by FNP, whilst a strong auto-aggregating ability was shown in this subspecies.

Considerable biomass variation was observed, likely due to unstable biofilm formation. In physiological conditions in the oral cavity, *F. nucleatum* aggregates with other bacterial species. Periasamy et al. showed that the subspecies *polymorphum* formed stable biofilms with the early coloniser *Actinomyces naeslundii*, however, it did not form single-subspecies biofilms in saliva (Periasamy et al., 2009). This further supports our observation that FNP does not form stable biofilms on its own. Another factor, which was not considered in the present study, is pH: its manipulation and increase to 8.2 was found to induce biofilm growth in the subspecies *polymorphum* (Zilm and Rogers, 2007, Chew et al., 2012). Investigating the impact of pH on biofilm formation by all subspecies may be an important parameter to include in future experiments.

Comparison of two FNP strains showed that nFNP did not exhibit an improved biofilm forming ability. Significantly higher biomass on fibronectin-coated glass could be explained by a combination of adhesion to fibronectin-coated substrates (Babu et al., 1995) and a strong ability of FNP to autoaggregate (Karched et al., 2015). Absence of a biofilm layer indicated that our laboratory strain is unlikely to have mutated, however, whole genome sequencing of the FNP strain could provide a definite proof. If no mutations are confirmed, the inability of FNP to form stable biofilms needs to be investigated further.

Biofilm formation by the remaining subspecies was substrate-specific. Firstly, AS mimicking the salivary pellicle on teeth significantly supported biofilm formation only in the case of FN25 on glass and plastic, and of FNV on plastic surfaces. *F. nucleatum* single-species biofilm formation on AS coated surfaces has not previously been reported, however Tavares et al. showed stable biofilm formation by FNF on plastic surfaces coated with human saliva (Tavares et al., 2018).

Secondly, fibronectin, a glycoprotein present in physiological fluids such as plasma and saliva (Babu et al., 1995), supported intermediate amounts of biofilm formation by all subspecies except FNP. Similarly, in a previous study, subspecies *polymorphum* (ATCC 10953) was found to adhere to fibronectin-coated gingival epithelial cells and fibronectin-coated coverslips as single cells. However, biofilm formation was not investigated (Babu et al., 1995).

Thirdly, gelatin, a derivative of collagen found in the extracellular matrix of tissues, is a commonly used polymer for coating tissue culture vessels (Bello et al., 2020). Benn et al. reported that adhesion of *E. coli* was improved by gelatin, but was dependent on specific buffering conditions and bacterial strains (Benn et al., 2019). In our study, however, gelatin supported only low levels of biofilm formation and is therefore not recommended as a coating agent for *F. nucleatum* biofilms.

Additionally, surfaces coated with poly-L-lysine, a cationic coating agent promoting bacterial adhesion by electrostatic interactions as mostly shown in *E. coli* studies (Cowan et al., 2001, Benn et al., 2019), led to higher amounts of biofilm seen microscopically in the present study, but this was not significant in CV assays. Nevertheless, due to the ease of coating with poly-L-lysine, this agent appears to be suitable for *F. nucleatum* biofilm studies.

In addition to surface coatings, surface roughness was also found to improve biofilm formation by providing a larger surface area for adhesion of bacteria and also protecting adherent bacteria from detachment by shear forces (Zheng et al., 2021). In our study, the highest mean amount of biomass on glass surfaces was measured on sandblasted glass coverslips. However, sandblasting makes glass surfaces opaque, leading to imaging challenges when conventional CLSM is used.

Significantly higher amounts of biofilm mass were observed in the case of mutant strains ΔFap2 and ΔFadA. The results suggest that the lack of FadA and Fap2 adhesion proteins does not

negatively affect biomass quantification, instead, biofilm forming ability was improved in these FN23 mutant strains. This indicates that the adhesins may not play a key biofilm-forming role in isolation. Additionally, their absence might be compensated for by a number of other adhesins with overlapping functions leading to thicker biofilms, as suggested in *Actinobacillus suis* biofilms (Bujold et al., 2016). Further transcriptomic investigations could shed more light on the expression of studied adhesins.

Assessment of biofilm architecture revealed differences among the subspecies. Similar observations were made in a previous study investigating *Staphylococcus aureus* and *Pseudomonas aeruginosa*, showing strain-specific differences such as large mushroom-like structures, aggregates and differences in thickness (Bridier et al., 2010). Possible underlying reasons for differences in the architecture of *F. nucleatum* biofilms may reflect differences in utilisation of available nutrients by subspecies, affecting biofilm maturation or subspecies-specific combination of outer membrane proteins influencing coaggregation.

Based on the *in silico* adhesin analysis addressing the inability of FNP to form biofilms, all proteins were found in the FNP genome, however four of these (CmpA, Fap2, FomA, and RadD) were not well-conserved. Only two proteins, CmpA and Fap2 were detected in all subspecies and were found to share a common autotransporter domain when protein structures were predicted based on the FN25 genome data. In addition, the analysis found the autotransporter domain in Fap2 in all subspecies. Hence, one may speculate that these adhesion proteins and perhaps the autotransporter domain are important for cell-cell adhesion in single-subspecies biofilms. CmpA and Fap2 had a very low percentage identity in FNP indicating these adhesins were not highly conserved, and this subspecies was the most distant in the phylogenetic tree. This might indicate an inability to form stable single-subspecies biofilms. It is, however, important to note that these bioinformatic results have to be interpreted with

caution and no definitive conclusions can be drawn due to the small scale of the analysis. Only a selected set of adhesion proteins reported in the literature were analysed and it is likely that other putative adhesion proteins involved in biofilm formation remain to be discovered.

With the methods employed here, no autotransporter domains for CmpA were detected in subspecies FNA and FN23. Additionally, despite a high identity of the YadA-like protein in FNP, a general lack of enhanced adhesion of FNP to fibronectin and gelatin in our study might suggest that YadA in FNP does not play a key role in adhesion to these proteins.

Membrane protein profiles studied utilising 1D SDS-PAGE showed potential differences in protein composition among the subspecies. Moreover, a strong band was observed in the "new" FNP strain when compared to the "old" FNP strain. This could be further analysed by isolation of the band and identifying the protein using mass spectrometry. Despite the composition differences observed, the protein mixtures were too complex to be resolved on the gel using this approach. Employing 2D SDS-PAGE can provide much more powerful resolution of protein mixtures (Zhan et al., 2019), nevertheless, it did not yield conclusive results in this study due to under-focusing of the first dimension of separation. This led to streaks of proteins observed on the gels instead of separate protein spots. This will have to be optimised in the future by extending each step of the isoelectric focusing (IEF) as reported by Basic et al. (2017), who performed the final IEF step for 20 hours, compared to only 1 hour performed in this study. Once this method is optimised, further work should involve identification of protein spots with differing abundance, excision of these spots and submitting them to mass spectrometry for protein identification. Additionally, a more sophisticated approach could be chosen in the future, such as analysing the adhesins using quantitative labelled mass spectrometry (Chen et al., 2021). This method could shed more light on the differences in the adhesin content among the subspecies.

An important point to consider when analysing membrane proteins is confirmation of successful isolation of the membrane protein fraction without the presence of contaminating cytoplasmic proteins (Molloy, 2008). As mentioned above, mass spectrometry analysis could reveal the identity of proteins in these complex mixtures, thus confirming purity of the membrane protein extracts. Simpler options would involve targeting known cytoplasmic and membrane proteins using western blotting to confirm whether the correct fraction is being studied. Alternatively, 1D and 2D protein profiles of both cytoplasmic and membrane protein fraction analysed by SDS-PAGE could be compared to rule out membrane protein contamination by cytoplasmic proteins.

Overall, the work presented in this chapter demonstrated that biofilm formation in *F. nucleatum* is subspecies-specific and subspecies *polymorphum* does not form biofilms under the conditions tested. Biofilms differ in stability as well as architecture. Differences in the ability to form biofilms may be caused by differences in conservation and expression of surface adhesins.

CHAPTER 4: RESPONSES OF NEUTROPHILS TO FORMALIN-FIXED *FUSOBACTERIUM NUCLEATUM* SUBSPECIES GROWN PLANKTONICALLY

4.1. Introduction

Work on functional and molecular responses of human neutrophils from peripheral blood are presented in this chapter. Previous work performed in our group focused either on neutrophil responses to a panel of periodontal bacteria including selected *F. nucleatum* subspecies (Hirschfeld et al., 2017), or only FNP was used in assays (Wright et al., 2011, Ling et al., 2015), however human neutrophil responses to all subspecies have not been systematically studied to date. Furthermore, the studies so far used heat-killed *F. nucleatum* stimuli, however it was shown that heat-killed bacteria stimulated significantly lower immune responses (Strunk et al., 2011), likely due to heat-denatured proteins (Wang et al., 2021), including surface proteins. If working with inactivated bacteria is required, fixation with formalin is an alternative, since it cross-links proteins, maintaining their structure (Dassanayake et al., 2020). Thus, all *F. nucleatum* subspecies grown planktonically were fixed with formalin and used as stimuli to evaluate neutrophil responses and potential differences in immunogenicity among the subspecies.

Apart from primary neutrophils isolated from blood of donors, the human promyelocytic leukaemia cell line (HL-60) is often used as a neutrophil-like substitute for *in vitro* studies. The use of these cells can help eliminate inter-individual differences in neutrophil functions. When cell lines like HL-60 are used, the need for human donors is eliminated (Kurgan et al., 2017). Furthermore, as discussed in more detail in the main thesis introduction (1.1.4), Kurgan et al. (2017) had previously shown that there were differences in immunogenic effects among *F. nucleatum* subspecies in the HL-60 cell line. Thus, in addition to neutrophil studies, HL-60 cells were differentiated into neutrophil-like cells and their responses to *F. nucleatum* subspecies were analysed.

4.2. Responses of human neutrophils to planktonic *F. nucleatum* subspecies

Neutrophils isolated from peripheral blood of healthy donors were used for functional assays studying ROS production and NETosis in response to all *F. nucleatum* subspecies. In addition, neutrophil ability to phagocytose the subspecies was evaluated.

4.2.1. ROS generation

Generation of total ROS was analysed using luminol, a substance widely used to detect ROS due to its ability to emit blue light when oxidised (Bedouhène et al., 2017). Luminol can diffuse into cells, therefore this technique detects not only extracellular, but also intracellular ROS generation. Generation of extracellular ROS was quantified utilising isoluminol, a substance that does not cross cell membranes (Jancinová et al., 2006). Neutrophils were stimulated using three types of stimuli, representing three different stimulation pathways: Phorbol 12-myristate 13-acetate (PMA; stimulation of ROS and NET release directly, without a receptor), opsonised *S. aureus* (OpSA; stimulation of Fc receptors) and individual *F. nucleatum* subspecies (stimulation of TLRs).

4.2.1.1. Total ROS generation

Firstly, total ROS generation was analysed. All test samples had a significantly higher light output when compared to the negative control stimulated with GPBS (Figure 4.1A). There was no significant difference between the positive controls PMA, OpSA and *F. nucleatum*-stimulated cells. Additionally, no differences were found among the samples stimulated with *F. nucleatum* subspecies (Figure 4.1A). Inter-donor variation was observed in neutrophil function, demonstrated by relatively large standard deviations.

When time to peak total ROS was measured, only the subspecies FNA was significantly different compared to the positive control OpSA (Figure 4.1B). This subspecies also had a significantly longer time to peak compared to FNF. No statistical differences were found between the remaining subspecies and the positive controls PMA and OpSA and within the test samples.

Overall total ROS released over the duration of the assay was also assessed and positive controls as well as all subspecies stimulated significantly higher amounts of overall ROS when compared to the negative control GPBS (Figure 4.1C). No differences were found among the subspecies.

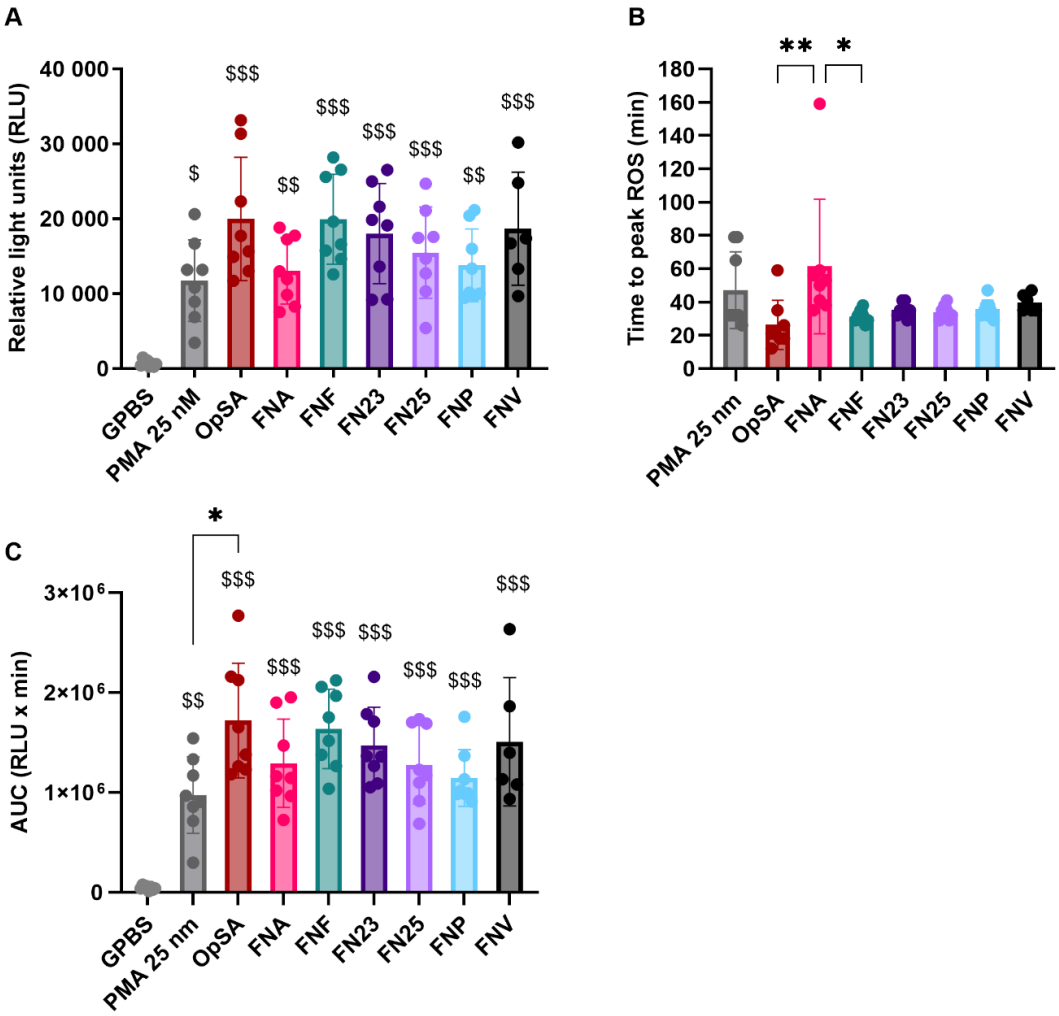

Figure 4.1. Generation of total ROS by neutrophils stimulated with formalin-fixed *F. nucleatum* subspecies. A: Quantification of peak total ROS. Test samples stimulated

significantly higher peak ROS release when compared to the negative control GPBS ($$ - p<0.01; $$$ - p<0.001). **B:** Time to peak total ROS released. Negative control was omitted due to the absence of peak ROS. **C:** Overall total ROS released expressed as area under the curve (AUC). Positive controls as well as test samples were significantly higher compared to the negative control GPBS ($$ - p<0.01; $$$ - p<0.001). Data was normally distributed. Statistical test: ANOVA with Tukey's post hoc test * - p<0.05; ** - p<0.01. N=8, except for FNV where N=6, data are expressed as means with SD.

4.2.1.2. Extracellular ROS generation

Next, generation of extracellular ROS was analysed. With regards to peak extracellular ROS (Figure 4.2A), all test samples led to significantly lower ROS release compared to the positive control PMA, while only PMA was significantly higher compared to the negative control GPBS. Assessment of time to peak release of ROS showed only FNA stimulated significantly slower ROS release compared to the positive control OpSA (Figure 4.2B). Additionally, all subspecies stimulated significantly lower overall extracellular ROS release compared to PMA, but not OpSA (Figure 4.2C). Overall, no statistical differences were detected among the subspecies.

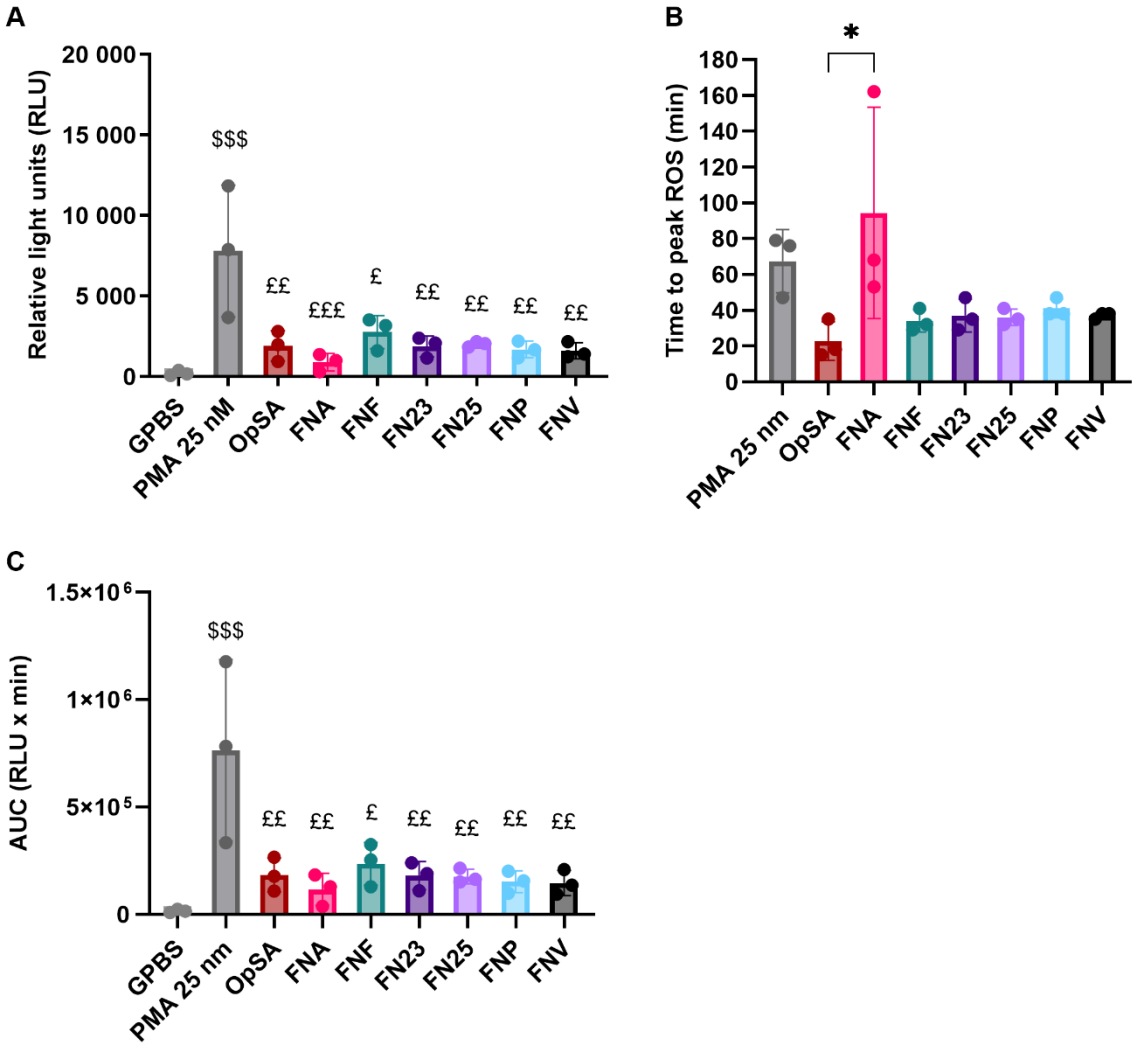

Figure 4.2. Generation of extracellular ROS by neutrophils stimulated with formalin-fixed *F. nucleatum* subspecies. A: Quantification of peak extracellular ROS. Only PMA was significantly higher than GPBS ($$$ - p=0.0002). "£" symbols indicate differences between PMA and the test samples. **B:** Time to peak extracellular ROS released. Negative control was omitted due to the absence of peak ROS. **C:** Overall extracellular ROS released expressed as area under the curve (AUC). Only PMA was significantly higher than GPBS ($$$ - p=0.0003). "£" symbols indicate differences between PMA and the test samples. Data was normally distributed. Statistical test: ANOVA with Tukey's post hoc test. */£ - p<0.05; ££ - p<0.01; £££ - p<0.001. N=3, data are expressed as means with SD.

4.2.2. Quantification of NET release

Next, NET release by neutrophils was assessed. Extracellular DNA released by neutrophils was detected upon stimulation with three different types of stimuli, including all *F. nucleatum*

subspecies. However, no statistically significant differences were found among test samples when compared to the negative control stimulated with RPMI (Figure 4.3). An inter-donor variation, similar to that seen in ROS generation assays, was observed, particularly in PMA-stimulated cells.

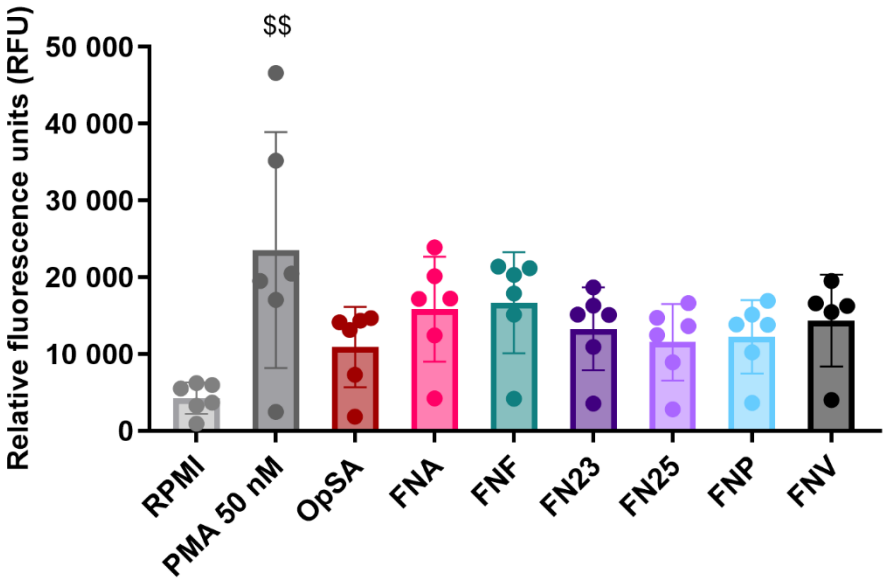

Figure 4.3. Quantification of extracellular NET-derived DNA from neutrophils stimulated with formalin-fixed *F. nucleatum* subspecies. No significant difference was detected among the samples when One-way ANOVA test was performed followed by Tukey's multiple comparison test (data was normally distributed). Cells stimulated with PMA released significantly higher amounts of NET-DNA compared to the negative control RPMI ($$ - p=0.001). Data are presented as means with SD, n=6.

4.2.3. Evaluation of phagocytosis

PBN belong to the group of professional phagocytes, therefore, their ability to phagocytose individual *F. nucleatum* subspecies was analysed. Fluorescently labelled non-opsonised *S. aureus* was used as a well-characterised positive control and the phagocytic ability of PBN was assessed by flow cytometry.

Results showed that each studied neutrophil population (n=5) successfully phagocytosed *S. aureus* as well as all *F. nucleatum* subspecies (Figure 4.4). At this point, phagocytosis was

evaluated only qualitatively, based on the position of the histogram obtained, thus all neutrophils were confirmed to be positive for *F. nucleatum* phagocytosis. All peaks shifted to the right as shown previously (White-Owen et al., 1992, Boero et al., 2021), indicating ingestion of fluorescently labelled bacteria by neutrophils.

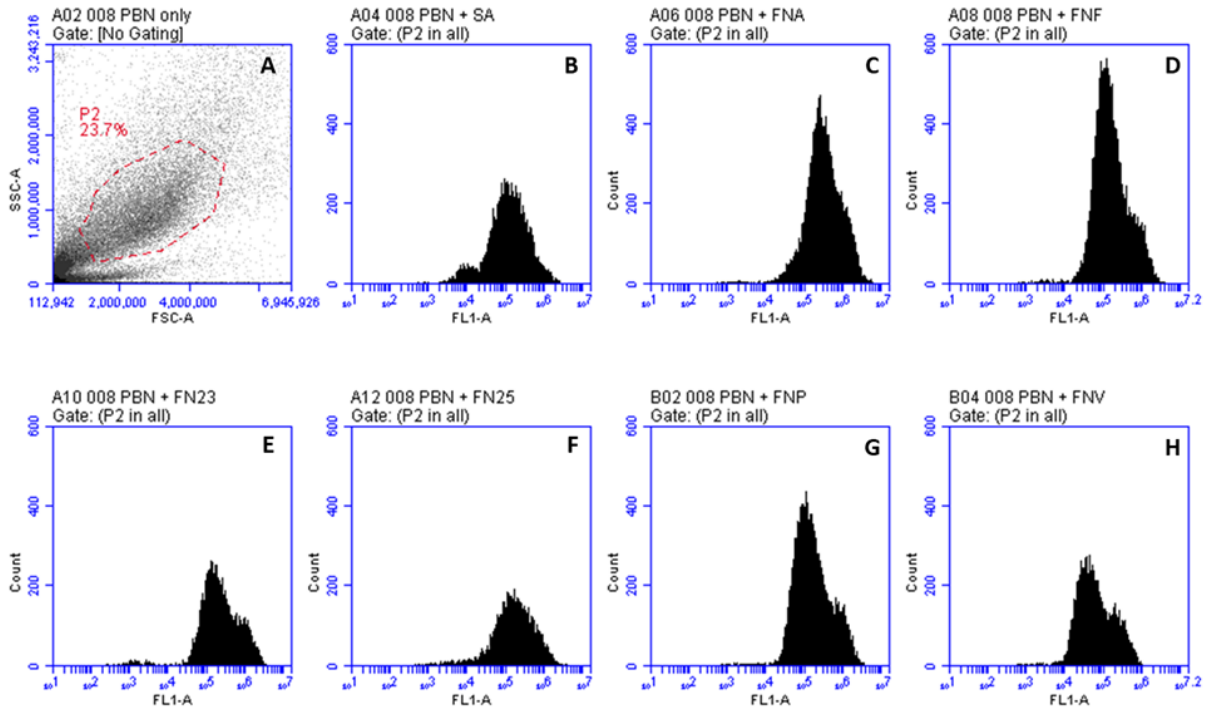

Figure 4.4. *F. nucleatum* phagocytosis by neutrophils from a representative donor. A: a scatter plot of neutrophils isolated from peripheral blood. Neutrophil population was gated to exclude cell debris and erythrocytes. **B**: histogram showing phagocytosis of *S. aureus*. **C – H**: histograms showing phagocytosis of all tested *F. nucleatum* subspecies. Trypan blue was used to quench possible fluorescence signals derived from extracellular binding of bacteria to PBN.

4.3. Responses of differentiated HL-60 cells to planktonic *F. nucleatum* subspecies

In order to compare the responses of human primary neutrophils to the HL-60 neutrophil-like cell line, HL-60 cells were utilised for functional neutrophil assays next. Additionally, previous work by Kurgan et al. (2017) used only subspecies *nucleatum*, *polymorphum* and *vincentii* as

stimuli in assays, therefore all *F. nucleatum* subspecies were employed in this study. After the evaluation of HL-60 differentiation, ROS generation as well as NETosis by stimulated HL-60 cells were analysed.

4.3.1. Confirmation of HL-60 differentiation

Cells were differentiated in complete medium containing 1.25% DMSO for four and six days. Cell differentiation can be confirmed examining morphological changes in HL-60 cells, which resemble primary human neutrophils (Baxter et al., 2009). Thus, HL-60 cells, as well as peripheral blood neutrophils, were smeared on a microscope slide and stained using haematoxylin & eosin, which stains nuclei in a dark purple/blue colour, while cytoplasm appears light pink.

When differentiated HL-60 (dHL-60) cells were compared to non-differentiated cells (Figure 4.5A, B), some differences in morphology were observed. dHL-60 cells were smaller in size, and the nuclei appeared more condensed (Figure 4.5B, C). Differences were also found between dHL-60 differentiated for four days (Figure 4.5B) and six days (Figure 4.5C). Cells with a longer differentiation period (Figure 4.5C) exhibited lobulated nuclei, characteristic for neutrophils. However, when dHL-60 were compared to primary neutrophils, they were morphologically distinct from them (Figure 4.5D), without the presence of cytoplasmic granules, which can be observed in primary neutrophils.

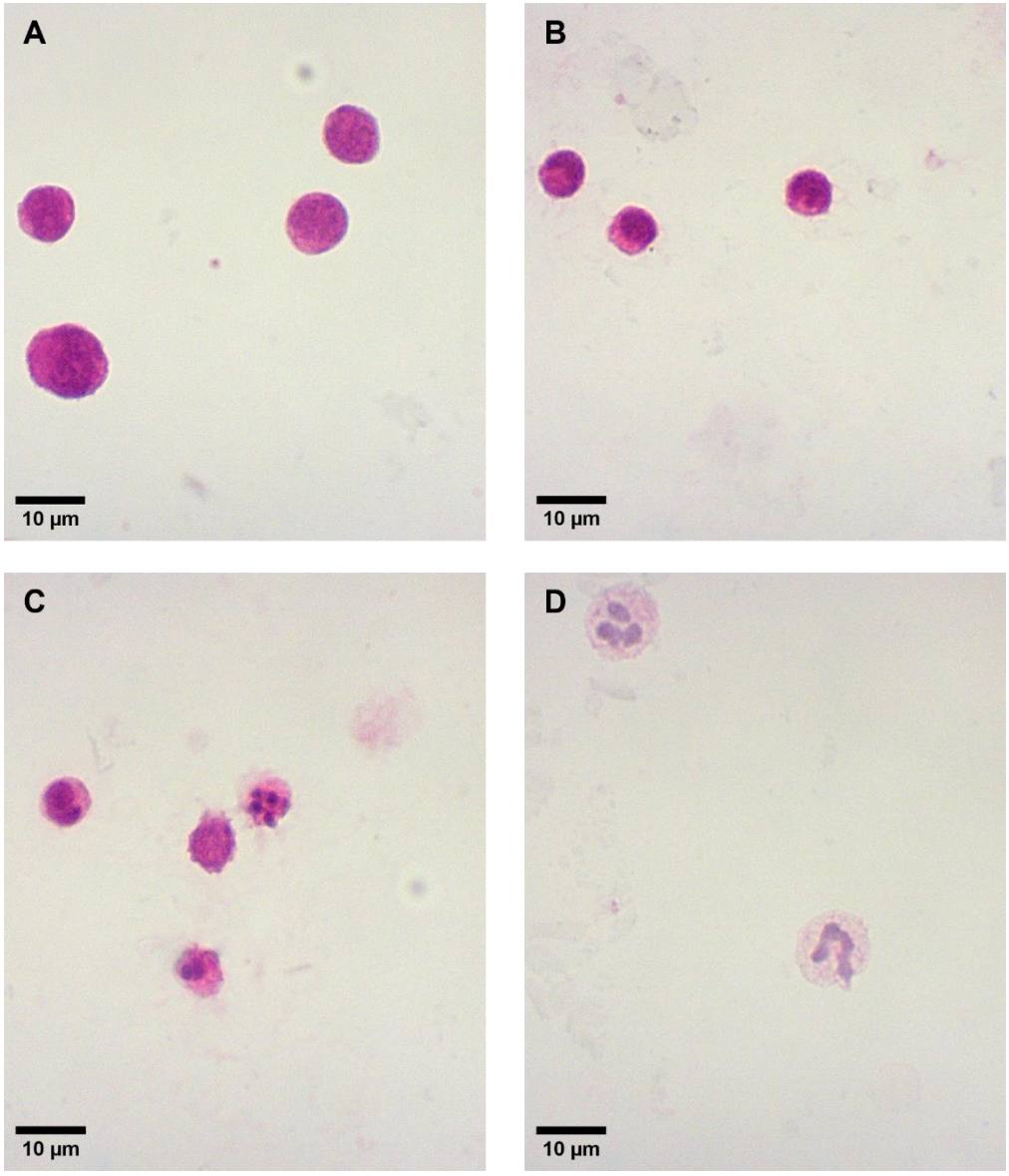

Figure 4.5. Morphological differences between dHL-60 cells and human neutrophils from peripheral blood. Cells were visualised using a light microscope (100 X objective lens with oil) **A:** undifferentiated HL-60 cells; **B:** dHL-60 (4 days); **C:** dHL-60 (6 days); **D:** peripheral blood neutrophils. Scale bar – 10 µm.

4.3.2. Total ROS generation by dHL-60 cells

An enhanced chemiluminescent assay was performed as detailed in section 2.16. The amount of total ROS generated was analysed in HL-60 cells differentiated for four and six days in two separate assays. The assays showed that dHL-60 cells only responded to 50 nM PMA, being

twice as high as the concentration used in chemiluminescent assays with primary neutrophils. The amount of ROS produced in response to OpSA and *F. nucleatum* subspecies was similar to the negative PBS control (Figure 4.6). Additionally, the response of dHL-60 cells was not consistent, as the first assay showed a higher response to 50 nM PMA in cells differentiated for four days (indicated by an empty square), while the second assay showed a higher response in cells differentiated for six days (indicated by a filled triangle). A high standard deviation was observed due to this inconsistency.

Interestingly, the peak RLU detected in dHL-60 stimulated with 50 nM PMA (positive control) was within the range of that detected in primary neutrophils exposed to GPBS only (negative control). Due to the fact that no responses to *F. nucleatum* and a very limited response to PMA by dHL-60 cells were observed, the assays were performed only two times and then terminated.

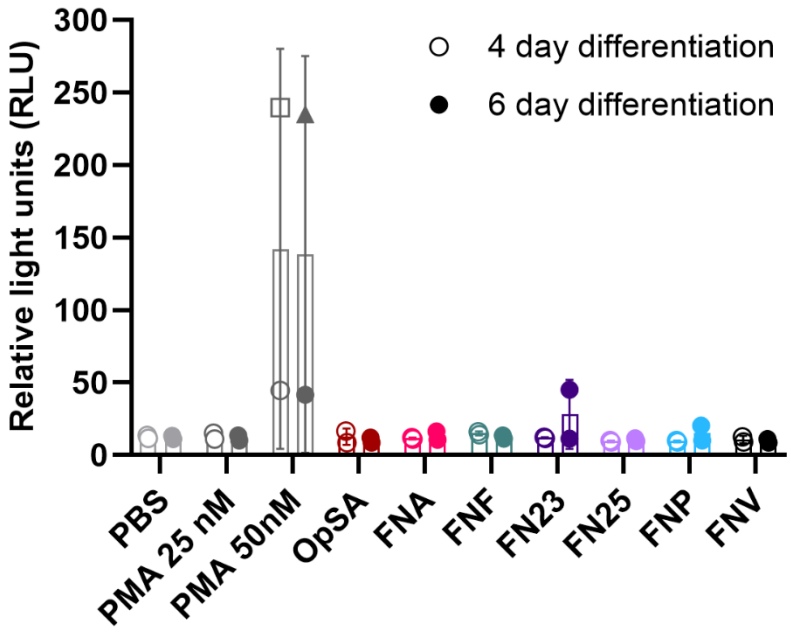

Figure 4.6. ROS generation by dHL-60 cells stimulated with formalin-fixed *F. nucleatum* subspecies. No differences in ROS generation were found between 4 days and 6 days long differentiation. Empty square shows a higher response from the first experiment, a filled

triangle shows a higher response from the second experiment. The bars show means of two independent experiments with standard deviations.

4.3.3. Quantification of NET release by dHL-60 cells

NET-DNA release was quantified in dHL-60 cells differentiated for three days, as this was the length of differentiation that was used in assays performed by other researchers from our group (PhD thesis by Palmer, 2010). NET-DNA quantification revealed that there was a uniformly high response with no difference between the negative control (RPMI) and the test samples (Figure 4.7). Interestingly, the amount of NET-DNA detected in the negative control (RPMI) was significantly higher compared to the equivalent number of primary neutrophils exposed to RPMI. Repeats in FN25 and FNV are missing due to issues with bacterial stimuli stocks.

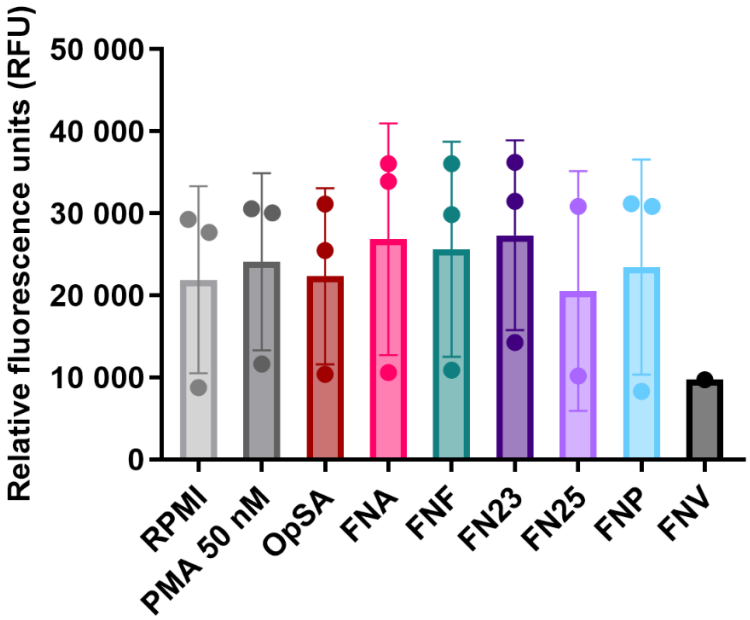

Figure 4.7. Quantification of NET-DNA release by dHL-60 cells. No difference was found between the negative control and the positive controls, as well as the test samples, however statistical testing was not performed due to the absence of more repeats in FN25 and FNV. N=3 for all samples except FN25, where n=2 and FNV, where n=1. Each sample was tested in technical triplicate.

4.4. Chapter discussion

Neutrophil responses upon challenge with formalin-inactivated *F. nucleatum* subspecies were investigated in this chapter. Generation of total as well as extracellular ROS by neutrophils was assessed and no statistical difference was found among the subspecies. A high degree of inter-donor variability, which was reported elsewhere (Hirschfeld et al., 2015), was observed in our experiments, which likely affected statistical significance. In order to address this problem, more assays will have to be performed to increase statistical power in the future. Additionally, bacterial numbers for all subspecies used for standardisation of stimuli were based on a value calculated for FN25 (value provided by The Forsyth Institute). Bacterial OD is, however, affected by bacterial size (Mira et al., 2022) and previous work identified size differences among the subspecies (master's thesis, Muchova (2020)). Therefore standard curves of bacterial numbers against OD may need to be established for each subspecies in order to use uniform MOI values in future assays.

Regarding NETosis in response to individual subspecies, no differences were found among the subspecies and again, high inter-donor variation was observed, as reported previously (Yang et al., 2003, Hirschfeld et al., 2015, Hoffmann et al., 2016). Similar to ROS assays, performing more biological repeats in future studies might help reveal whether there is a true difference observed among the subspecies. In addition to quantification of NETs by SYTOX stain, NETosis should be analysed also by fluorescent microscopy. A limitation of the quantification assay used here is that SYTOX Green stains all extracellular DNA and is not specific to NET-associated DNA. Therefore DNA released by bacteria or by neutrophils undergoing other forms of cell death may be quantified in this assay also (Rostami et al., 2020). Fluorescent microscopy including immunofluorescence using specific NET markers such as triple-citrullinated histone (Thålin et al., 2020) can help confirm whether NETosis occurs in these neutrophils.

Results of phagocytosis assays showed that *F. nucleatum* can be phagocytosed by human neutrophils. It is important to note, however, that after the analysis of the data, the flow cytometry instrument was found to be faulty due to a valve blockage, discovered sometime after the experiments were performed, and the obtained results may have been inaccurate. This could also explain a relatively low number of neutrophils in the gated population, along with a high background signal. Nevertheless, a methodology for neutrophil phagocytosis of *F. nucleatum* was developed during this process and the experiments will have to be repeated in the future to obtain more conclusive results. Additionally, survival of phagocytosed *F. nucleatum* in neutrophils should be analysed. Interestingly, *P. gingivalis* was found to be able to avoid intracellular neutrophil killing when internalised (Olsen and Hajishengallis, 2016), and it is possible that *F. nucleatum* subspecies share this ability with *P. gingivalis.*

Differentiated HL-60 cells were found not to generate ROS in response to bacterial stimuli in our assays, but only to PMA which activates ROS generation bypassing receptor pathways. These results together with morphological differences observed by H & E staining suggest HL-60 might either not be successfully differentiated, or do not share sufficient morphological and functional properties with primary neutrophils, even when fully differentiated. Kurgan et al. (2017) showed subspecies-specific induction of superoxide production in HL-60 cells, supporting the theory that cells in our experiments may not have been fully differentiated. Successful differentiation may be achievable by using an alternative inducer, such as all-trans-retinoic acid (Babatunde et al., 2021). Also, a more accurate approach to confirm that the cells were successfully differentiated could be the detection of neutrophil surface markers, such as CD11b, CD16 and CD66b, as performed by Guo et al. (2021).

Concerning NETosis studied in dHL-60, our results further support incomplete differentiation of this cell line into neutrophil-like cells. As shown by Guo et al. (2021) flow cytometrically as

well as spectrofluorometrically, a clear difference can be observed between unstimulated control cells and stimulated dHL-60 cells. Thus, the fact that the negative control and the test samples in our experiments yielded the same results suggests that no response was mounted. Additionally, considering the fact that SYTOX Green fluorescent dye stains all extracellular DNA, high values of fluorescence might indicate cell death by apoptosis or necrosis in addition to or instead of NETosis (Zhang and Xu, 2000, Rostami et al., 2020). NET release is connected to intracellular ROS generation, therefore, it is plausible that no NETs were released from dHL-60 cells in our assays. It is, however, important to mention that functions of HL-60 cells were reported to be impaired in comparison with primary neutrophils in the context of bacterial infection represented by *S. aureus* (Yaseen et al., 2017). The antimicrobial activity of dHL-60 measured by bacterial survival was significantly lower than that of the primary neutrophils. The generation of ROS was also significantly reduced in comparison with neutrophils while there was no difference in phagocytic activity. dHL-60 also extruded significantly less NETs when stimulated with *S. aureus*. These results suggested that dHL-60 should not be used as an alternative to primary neutrophils in studies analysing pathogen interaction with the host immune system (Yaseen et al., 2017).

In summary, primary neutrophil assays showed that human neutrophils can be successfully stimulated with formalin-fixed *F. nucleatum* subspecies to generate ROS both intracellularly and extracellularly and to release NETs. HL-60 cells on the other hand were possibly not successfully differentiated into neutrophil-like cells and did not react to stimulation with *F. nucleatum* stimuli.

CHAPTER 5: RESPONSES OF HUMAN NEUTROPHILS TO LIVE *FUSOBACTERIUM NUCLEATUM* SUBSPECIES GROWN PLANKTONICALLY AND IN BIOFILMS

5.1. Introduction

In this chapter, neutrophil functional and molecular responses to live *F. nucleatum* subspecies were analysed. In the previous chapter of this thesis, formalin-fixed *F. nucleatum* subspecies were used as stimuli. Fixed bacteria are, however, not found *in vivo*, thus live bacteria were utilised in order to better mimic physiological conditions and obtain more physiologically relevant results.

Additionally, planktonic and biofilm-grown subspecies were employed in order to evaluate possible differences in their immunogenicity. Considering that the expression of virulence genes in biofilms is significantly higher than in planktonic cultures (Becker et al., 2001, Resch et al., 2005) and *F. nucleatum*-containing oral biofilms are crucial in the development of periodontal disease (Vieira Colombo et al., 2016), utilising biofilm stimulation in *F. nucleatum* pathogenicity studies may provide more clinically relevant results. While other studies have utilised intact biofilms adhered to a substrate (Millhouse et al., 2014, Ramage et al., 2017), resuspended biofilms were used in this work to improve standardisation of bacteria and subsequent comparison with the planktonic stimuli in terms of immunogenicity.

Live biofilm-grown and planktonic stimuli were first quantified and their viability post-freezing (-20°C/-80°C) was assessed. The following neutrophil antimicrobial responses were subsequently analysed: generation of ROS, release of NETs and production of neutrophil cytokines and enzymes. Differences between planktonic and biofilm-grown stimuli as well as differences among individual subspecies were evaluated.

5.2. Quantification of bacteria grown in biofilm

In order to obtain accurate and reliable results from neutrophil response assays, it is necessary to work with standardised numbers of bacteria and multiplicities of infection (MOI). Standardisation of planktonic cultures is relatively easy, performed using optical density (OD) values corresponding to a known number of viable bacteria represented by colony forming units (CFU). Standardisation of resuspended biofilms is more challenging due to the presence of extracellular matrix (ECM), which could confound the OD, and the potential presence of dead bacteria. Therefore, to accurately quantify all bacteria from biofilms, quantitative PCR (qPCR) was performed in order to calculate bacterial numbers from standard curves of known bacterial numbers (known DNA concentrations) against cycle threshold (CT) values, which indicate the cycle numbers at which the target DNA is detected (Bonacorsi et al., 2021). The first step in this process involved successful DNA extraction from a range of serially diluted *F. nucleatum* cultures and preparation of standard curves.

5.2.1. Quantification using extracted bacterial DNA for subsequent qPCR quantification

In order to establish the method for this study, DNA extraction was carried out from a 10-fold serially-diluted FN23 overnight culture, between 1 x 10^8 and 1 x 10^3 CFUs (Table 5.1), following the protocol by Millhouse (2015). This initial experiment was performed once. Concentrations of the extracted DNA were low across the samples, leading to very small differences between the concentrations from 1 x 10^8 and 1 x 10^3 CFUs. The quality of the extracted samples was also low overall, as indicated by 260nm/280nm ratio. Only DNA extracted from 1 x 10^6 CFUs had DNA purity close to 1.8, the recommended value (Lucena-

Aguilar et al., 2016). These results showed that the DNA extraction protocol was inefficient, resulting in a low DNA yield in addition to the presence of contaminants. Thus, it was necessary to optimise the extraction process using only higher bacterial concentrations.

Table 5.1. Quantification of DNA extracted from different concentrations of planktonic FN23 using GenElute Bacterial Genomic DNA kit.

Number of bacteria (CFU)	**1 x 10^8**	**1 x 10^7**	**1 x 10^6**	**1 x 10^5**	**1 x 10^4**	**1 x 10^3**
DNA concentration (µg/ml)	8.30	0.00	2.46	1.22	0.00	7.59
Purity ratio 260nm/280nm	1.325	N/A	1.77	1.194	N/A	0.577

Optimisation of DNA extraction was performed using two different commercially available extraction kits – GenElute Bacterial Genomic DNA kit (GenElute kit hereafter) and Wizard Genomic DNA purification kit (Wizard DNA kit hereafter). In order to increase DNA yield, 1 x 10^9 FN23 was used for the extraction using the GenElute kit and compared to 1 x 10^8 FN23, however a ten-fold increase in the number of bacteria did not markedly increase DNA concentration (Table 5.2). Next, it was hypothesised that bacterial lysis may be insufficient, therefore the lysis time was extended from 10 minutes to 30 minutes. Extending the lysis time did not seem to positively affect the DNA yield. Even if the concentration of DNA extracted from 1 x 10^9 FN23 was almost 10 times higher than the DNA extracted from 1 x 10^8 FN23, the amounts extracted were consistently low. Next, a Wizard DNA kit was used to compare DNA yield from FNA and a Gram-negative control *Escherichia coli* to assess whether the kits are suitable for efficient bacterial lysis. Interestingly, *E. coli* DNA yield (925.72 µg/ml) was significantly higher compared to FNA DNA yield (15.64 µg/ml), suggesting that *F. nucleatum*

may be a difficult to lyse bacterium. For that reason, insufficient chemical lysis with the lysis buffer from the Wizard DNA kit was replaced with a combined mechanical and chemical lysis originally developed for *Brucella* RNA and DNA extraction (protocol provided by Dr Daniel Slade; see Materials and Methods, section 2.21.3). This combined approach resulted in a higher DNA yield from FNA, yet the DNA concentrations obtained from multiple extraction repeats were not consistent and considerable differences were observed. The differences could be partially explained by progressively losing bacteria after centrifuging, as neither of the subspecies formed compact pellets and bacteria were visibly removed during supernatant removal.

Table 5.2. Optimisation of DNA extraction from planktonic *F. nucleatum* subspecies and *E. coli*, with representative experiments shown here.

Protocol used	**GenElute Bacterial genomic DNA kit, manufacturer's instructions**		**GenElute Bacterial genomic DNA kit, lysis time extended**		**Wizard Genomic DNA purification kit, manufacturer's instructions**		**Chemical and mechanical disruption of bacteria combined with Wizard Genomic DNA Purification kit**
Subspecies, number of bacteria	FN23, 1×10^9	FN23, 1×10^8	FN23, 1×10^9	FN23, 1×10^8	FNA, 1×10^9	*E. coli*, 1×10^9	FN23, 1×10^9
Mean DNA concentration in µg/ml (SD)	36.71 (8.7)	8.60 (2.62)	18.39 (1.67)	1.40 (1.01)	11.62 (3.48)	835.89 (80.75)	112.66 (4.81)

Of note, bead beating was also tested as a type of mechanical cell disruption, however this approach proved unsuitable as most of the bacterial suspension was soaked into the bead mixture and it was not possible to recover the sample. Sonication was also considered, but the lysis buffer used was prone to frothing when sonicated, thus hindering efficient cell lysis. Additionally, sonication may shear the DNA to smaller fragments (Sun et al., 2022), decreasing its quality for subsequent qPCR analysis (Golenberg et al., 1996).

Due to the observed issues and inaccuracies in the DNA extraction process, it was decided that bacteria grown in biofilms would be quantified using the more established method of correlating OD measurements and CFU counting, accepting the potential limitations of dead bacterial cells not being accounted for.

5.2.2. Preparation of bacterial standard curves and quantification of viable bacteria by colony counting

Quantification of *F. nucleatum* subspecies by colony counting was performed for both planktonic (grown overnight) and biofilm-grown bacteria (grown in biofilm for three days) to ensure subsequent standardisation for neutrophil assays. Standard curves were constructed for planktonic bacteria plotting measured OD of the cultures against the number of microorganisms counted (CFU/ml) (Figure 5.1). Interestingly, CFU/ml corresponding to OD of 1 was different for each subspecies (Table 5.3) and none of our lab subspecies had CFU/ml value identical with the previously reported value of 1.62×10^9 (Forsyth Institute).

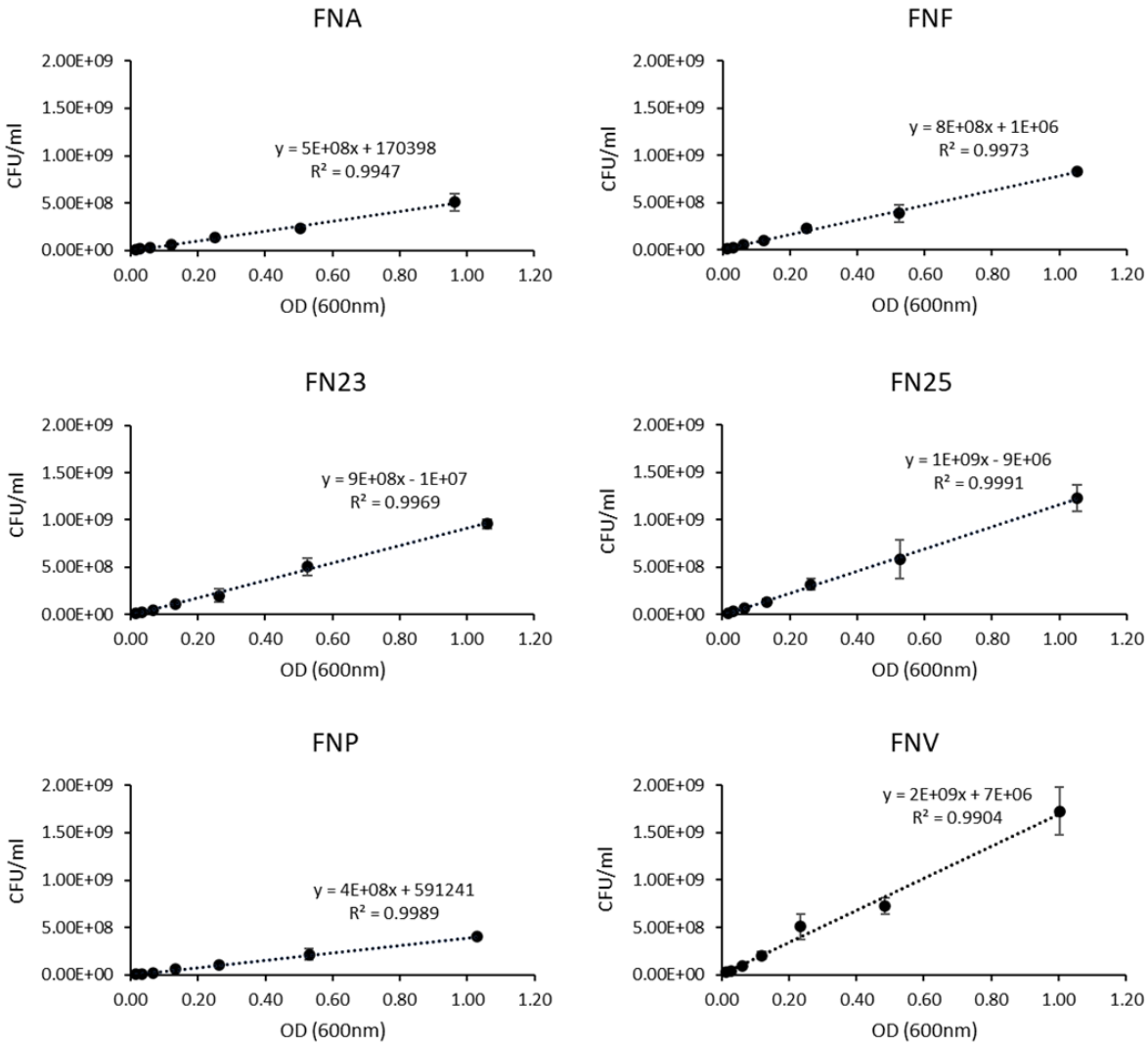

Figure 5.1. Standard curves of planktonic *F. nucleatum* subspecies. Standard curves were repeated three times in technical replicate. Dotted line shows the trend line of the curves. Data presented as means with standard deviation.

Table 5.3. Planktonic *F. nucleatum* numbers represented as mean colony-forming units (CFU) corresponding to OD=1 calculated from formulas obtained from correlation curves in Fig. 5.1.

Subspecies	FNA	FNF	FN23	FN25	FNP	FNV
Mean CFU/ml	5.00×10^8	8.01×10^8	8.90×10^8	9.91×10^8	4.01×10^8	2.01×10^9

Next, biofilm-grown viable *F. nucleatum* subspecies were quantified. Harvested biofilms were diluted to OD=1 and bacterial suspensions were plated. Bacterial concentrations in biofilms

ranged from 4.78 x 10^8 CFU/ml in FN23 to 1.43 x 10^9 CFU/ml in FNV (Table 5.4). Numbers of viable bacteria quantified in biofilms were also compared with bacterial numbers from planktonic cultures and a significant difference was found only in FN23 (Figure 5.2).

Table 5.4. Biofilm *F. nucleatum* numbers represented as mean colony-forming units (CFU) corresponding to OD=1.

Subspecies	FNA	FNF	FN23	FN25	FNV
Mean CFU/ml	4.99 x 10^8	6.78 x 10^8	4.78 x 10^8	8.11 x 10^8	1.43 x 10^9

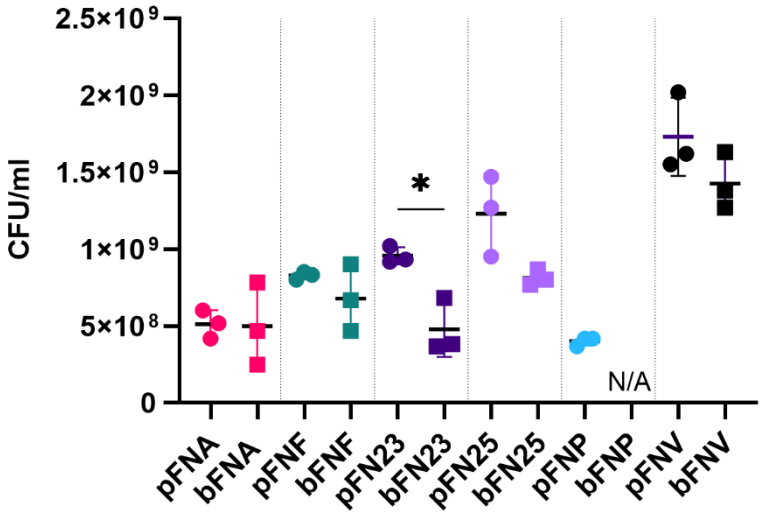

Figure 5.2. Comparison of bacterial numbers from planktonic (p) and biofilm (b) cultures corresponding to OD=1. Data shown as mean ±SD. For each subspecies, planktonic and biofilm-grown *F. nucleatum* was compared. Statistical analysis was performed using unpaired t-test (* - p=0.011). Statistical significance was identified only in FN23.

5.3. Viability of live bacterial stocks stored at -20°C and -80°C

Live *F. nucleatum* subspecies prepared as stimuli for subsequent neutrophil assays were stored frozen for ease of use. Inter-batch variability may be avoided by using bacterial stimuli from the same batch. Viability of the subspecies stored at -20°C and -80°C was therefore tested to assess whether storage conditions affect survival of the live bacteria.

5.3.1. Viability of live bacterial stocks stored at -20°C

Planktonic samples stored at -20°C for up to 8 weeks were either defrosted once only or they were subjected to weekly freeze-thaw cycles (Figure 5.3).

Viability of bacteria stored in aliquots defrosted only once every week and then discarded (Figure 5.3A) remained considerably stable for the duration of the viability testing in the case of FNA and FNF. The most prominent decrease in viability over the 8-week period was observed in FNP. Missing data points were due to no growth of FN25 and excessive growth (thus uncountable bacterial growth) of FNA.

Viability of bacterial stimuli that were regularly thawed and frozen again (Figure 5.3B) decreased markedly following the second freeze-thaw cycle at week 3. At this time point, only FNA, FNF and FNV grew. At the end of the testing period, after 7 freeze-thaw cycles, none of the subspecies were found to be viable.

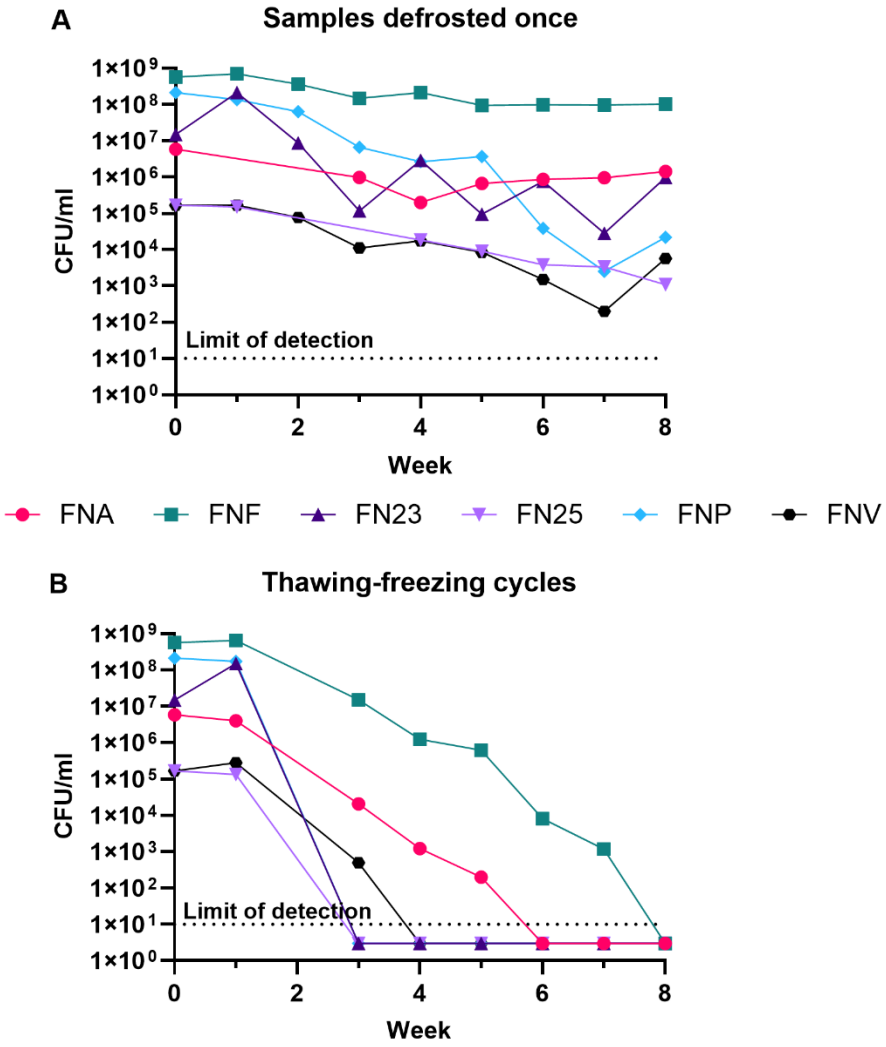

Figure 5.3. Quantification of viable planktonic bacteria in bacterial stocks stored at -20°C for 8 weeks. A – Quantification of bacteria when stocks were defrosted only once for the experiment. **B** – Quantification of bacteria when stocks were thawed for the experiment, then frozen again. Limit of detection was 10 bacterial cells. Week 2 values were not recorded for this experiment due to COVID-19-related restricted access to the laboratories.

5.3.2. Viability of live bacterial stocks stored at -80°C

Considering the viability of most *F. nucleatum* subspecies stored at -20°C was stable only for a short period of time (2 weeks) and not for the entire duration of the testing period, storage of stimuli at -80°C was investigated (Figure 5.4), as lower temperatures improve long term viability (De Paoli, 2005).

Planktonic cultures were stored frozen for 1 and 2 months and viable bacteria then quantified (Figure 5.4A). When compared to numbers of live bacteria recovered after 1 month's storage at -20°C, storage at -80°C improved viability of all subspecies, as the numbers of bacteria remained between 1 x 10^8 and 1 x 10^9 CFU/ml. Viability after 2 months was also largely unaffected among the subspecies, except for FNF, which showed reduced viability. Values for FNP at month 2 could not be recorded due to no growth after plating.

Next, the long-term viability of biofilms stored at -80°C was assessed (Figure 5.4B). With regard to short-term preservation of frozen stimuli (up to 2 months), it was assumed that resuspended biofilms were identical to planktonic cultures when the effect of freezing on live bacterial stimuli was investigated, therefore biofilms were not included in the short-term analyses. Quantification after 5 months showed that the viability of biofilms did not markedly decrease with longer storage times. Data on FNP biofilms were not available due to the inability of FNP to form biofilms (see Chapter 3).

Successful bacterial quantification as well as confirmation of bacterial viability allowed accurate standardisation of bacteria and neutrophil assays were performed subsequently, using stimuli stored at -80°C.

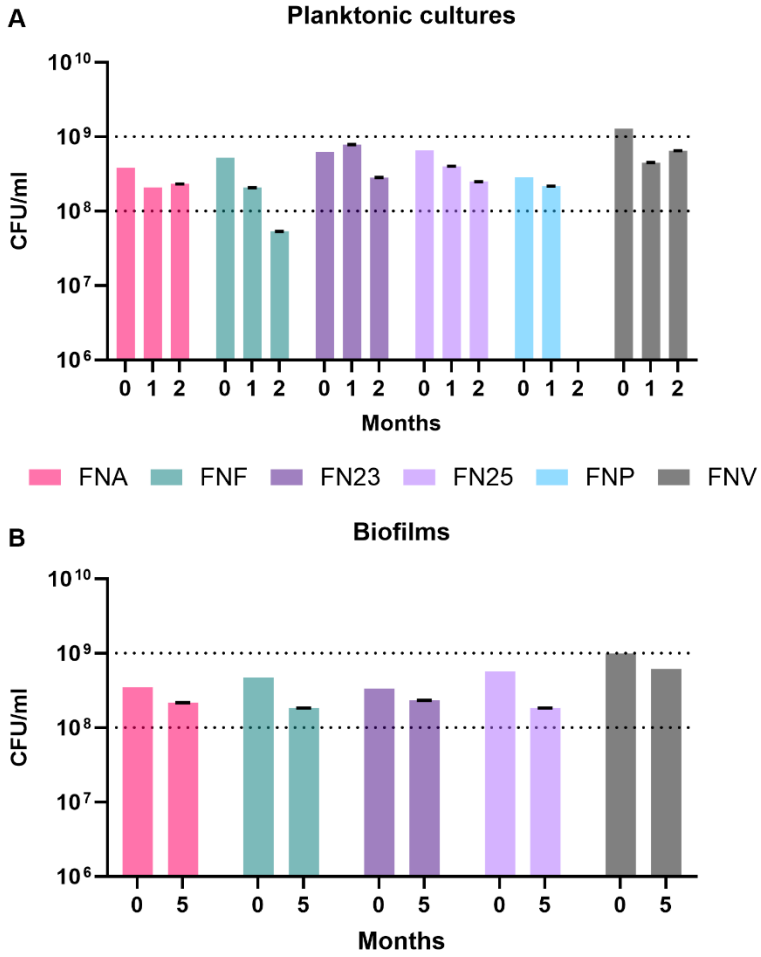

Figure 5.4. Viability of *F. nucleatum* subspecies stored at -80°C. A – Viability of planktonic cultures after 1 and 2 months at -80°C. Values at month 0 were calculated from standard curves (Figure 5.1). At months 1 and 2, the quantification was performed once in technical triplicates, data shown as mean values ±SD (short black lines). **B – Viability of biofilm-grown cultures after 5 months at -80°C.** Values at month 0 were calculated by plating resuspended biofilms grown for 3 days and subsequent colony counting (Table 5.4). At month 5, the quantification was performed once in technical triplicates, data shown as mean values ±SD (short black lines). SD of planktonic FNA 1 month (panel A) and biofilm FNV5 months (panel B) was too small to be plotted.

5.4. Comparison of neutrophil responses to planktonic and biofilm-grown *F. nucleatum* at a species level

To test the hypothesis that there is a difference in immunogenicity between planktonic and biofilm-grown *F. nucleatum*, an *a priori* decision was made to combine data from neutrophil

stimulations following exposure to individual *F. nucleatum* subspecies grown planktonically and in single-subspecies biofilms into two groups: planktonic (p) and biofilm-grown (b). One set of experimental data was analysed using two different approaches: analysis in this chapter (5.4.) was performed on a species level to allow the comparison of planktonic and biofilm-grown *F. nucleatum*, whereas the same dataset was analysed in more detail on a subspecies level in chapter 5.5 to reveal differences among the subspecies. The analysis was performed including all subspecies except FNP due to its inability to form biofilms *in vitro*, as described earlier (Chapter 3).

The data for the analysis in this chapter were combined as follows: each assay was performed with a minimum of 6 donors and the cells from each donor were stimulated with 5 separate planktonic or biofilm-grown subspecies (excluding FNP). Next, 5 mean values per donor were calculated (assays were performed in technical duplicate) and then combined to create a new dataset of at least 30 mean values for planktonic or biofilm-grown stimuli. These values were further analysed as planktonic or biofilm datasets, allowing comparison at a species level. More detailed information on the number of donors is stated in figure legends of the corresponding neutrophil assays below.

5.4.1. Comparison of ROS release

An enhanced chemiluminescent assay (section 2.25) was performed to quantify the generation of total, intracellular and extracellular ROS, as well as superoxide by human neutrophils. Neutrophils were stimulated for 150 minutes, multiplicity of infection (MOI) was 100.

5.4.1.1. Bacterial luminescence

In order to accurately quantify ROS released by neutrophils when stimulated with *F. nucleatum* and to be able to assess the true signal of the assay, the non-specific luminescence of the bacterial stimuli was quantified first. Luminescence of bacteria combined only with luminol and bacteria combined with luminol, superoxide dismutase (SOD) and catalase was measured (Figure 5.5.). The results showed that bacterial luminescence in both cases was negligible in comparison with the neutrophil-derived ROS signal. The highest value recorded in this assay was 444 RLU for pFNP (Figure 5.5.), while ROS signals derived from neutrophils stimulated with this subspecies were in the range between 35,952.5 and 61,374.5 RLU (Figure 5.13).

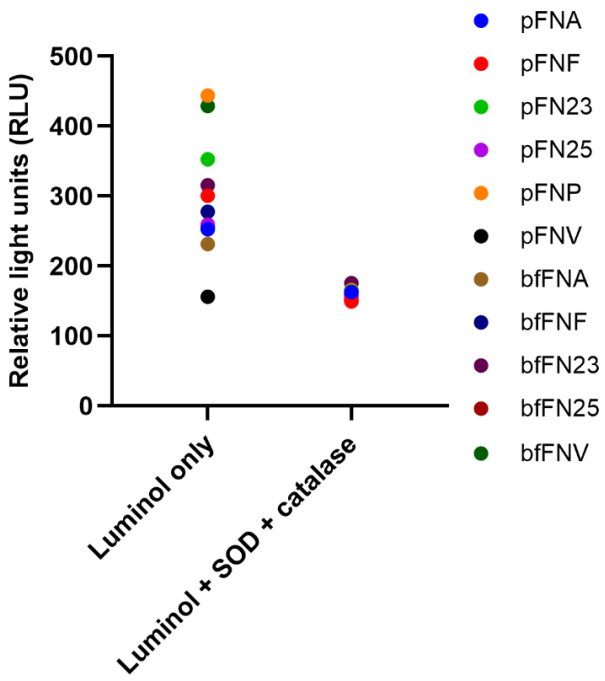

Figure 5.5. Quantification of bacterial luminescence of planktonic (p) and biofilm-grown (b) *F. nucleatum* subspecies. Luminol was used to measure total ROS released, Luminol combined with superoxide dismutase (SOD) and catalase was used for quantification of intracellular ROS. Experiment was performed in technical duplicates, N=1.

5.4.1.2. Total ROS release

Total ROS release, including both intracellular and extracellular ROS, was assessed and it was shown that biofilm-grown *F. nucleatum* stimulated significantly higher total peak ROS release (p=0.0001; Figure 5.6A) as well as total overall ROS release (p=0.0005; Figure 5.6C). Biofilm-grown *F. nucleatum* elicited a significantly faster neutrophil response (p=0.044; Figure 5.6B) when time to total peak ROS was measured.

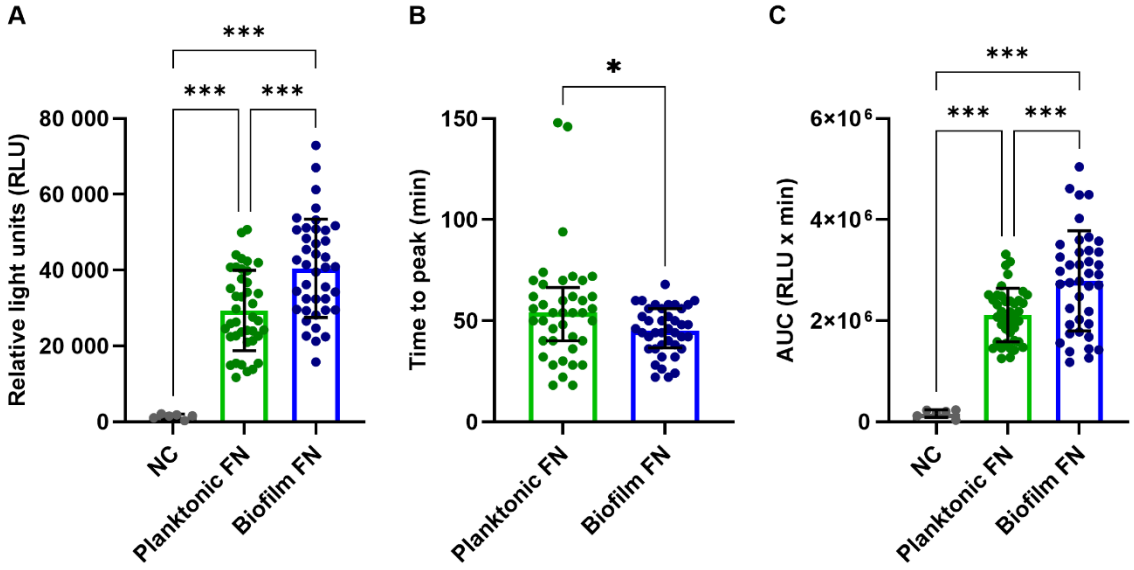

Figure 5.6. Comparison of total ROS generation triggered by planktonic and biofilm-grown *F. nucleatum* (subspecies combined). Neutrophils were stimulated for 150 minutes. **A** – Quantification of total peak ROS. **B** – Time measured to total peak ROS. No peak occurred in the NC, thus only pFN and bFN were compared. **C** – Quantification of overall total ROS release expressed as area under the curve (AUC). Values in A and C are shown as mean (± standard deviation, SD), and in B as median (interquartile range; IQR). Datasets in A and C analysed using One-way ANOVA with Tukey's post hoc test, in B Mann Whitney U test. * - $p<0.05$; *** - $p<0.001$. NC – negative control (GPBS). N(NC)=6; N(test samples)=40 (8 healthy donors multiplied by 5 bacterial stimuli). Multiplicity of infection (MOI) = 100. The source dataset used for this species level analysis is the same dataset that is used for the subspecies level analysis in chapter 5.5.

5.4.1.3. Intracellular ROS release

Specific intracellular ROS generation was quantified utilising superoxide dismutase (SOD) and catalase enzymes, which eliminate extracellular ROS in the chemiluminescent assay. Biofilm-

grown *F. nucleatum* triggered significantly higher intracellular peak ROS release (p=0.0005; Figure 5.7A) as well as overall intracellular ROS release (p=0.012; Figure 5.7C). No significant difference was found between planktonic and biofilm-grown *F. nucleatum* when time to peak intracellular ROS was measured (p=0.052; Figure 5.7B).

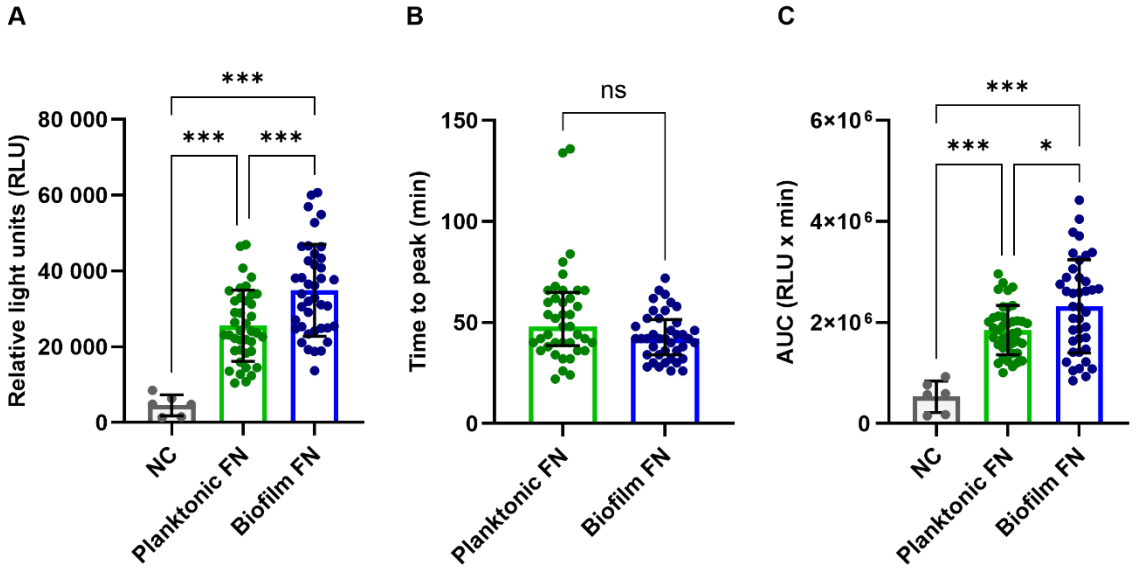

Figure 5.7. Comparison of intracellular ROS generation triggered by planktonic and biofilm-grown *F. nucleatum* (subspecies combined). A – Quantification of intracellular peak ROS. **B –** Time to peak intracellular ROS. No peak occurred in the NC, thus only pFN and bFN were compared. **C –** Quantification of overall intracellular ROS release expressed as area under the curve (AUC). Values in A and C shown as mean (± standard deviation), in B as median (interquartile range; IQR). Datasets in A and C analysed using One-way ANOVA with Tukey's post hoc test, in B Mann Whitney U test. Ns – not significant; * - p<0.05; *** - p<0.001. NC – negative control (GPBS). N(NC)=6; N(test samples)=40 (8 healthy donors multiplied by 5 bacterial stimuli). MOI = 100. The source dataset used for this species level analysis is the same dataset that is used for the subspecies level analysis in chapter 5.5.

5.4.1.4. Extracellular ROS release

Extracellular ROS values in this experiment were obtained by subtracting intracellular ROS from total ROS values, as extracellular ROS was not directly quantified by the chemiluminescent assay. This method was chosen due to the fact that isoluminol, which is normally used to quantify extracellular ROS, does not yield results comparable to luminol, as shown by work performed by our group (unpublished results). It is important to note that

negative ROS values resulting from the subtraction were replaced with 0, as negative light values cannot be obtained from the assay. In terms of peak ROS release (Figure 5.8), there was no difference between the planktonic and biofilm *F. nucleatum* stimuli. Results for time to peak ROS release and overall extracellular ROS release were not calculated due to the presence of multiple 0 values which would have resulted in inaccurate results.

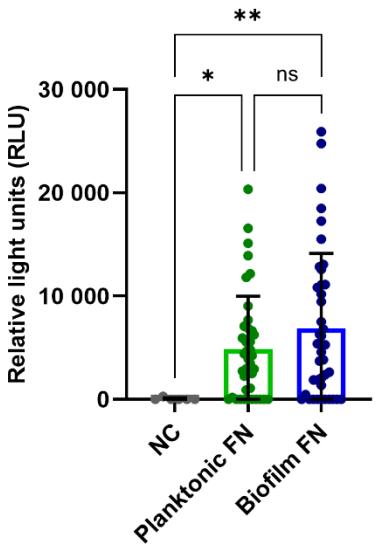

Figure 5.8. Comparison of peak extracellular ROS released upon stimulation with planktonic and biofilm-grown *F. nucleatum* (subspecies combined). Data were not normally distributed, therefore a Kruskal-Wallis statistical test was performed followed by Dunn's post hoc test. Values shown as median (interquartile range; IQR). ns – not significant; * - $p<0.05$; ** - $p<0.001$. NC – negative control (GPBS). N(NC)=6; N(test samples)=40 (8 healthy donors multiplied by 5 bacterial stimuli). MOI = 100. The source dataset used for this species level analysis is the same dataset that is used for the subspecies level analysis in chapter 5.5.

5.4.1.5. Superoxide release

Superoxide generation was also evaluated as the primary upstream ROS produced by NADPH-oxidase activation. While planktonic and biofilm-grown stimuli stimulated significantly higher responses when compared to the negative control (NC) in the quantification of peak superoxide release and overall superoxide release (Figure 5.9A and C), no significant differences were found between the planktonic and biofilm-grown *F. nucleatum* (peak superoxide release p=0.9999; time to peak release p=0.1074; overall superoxide release p=0.9985).

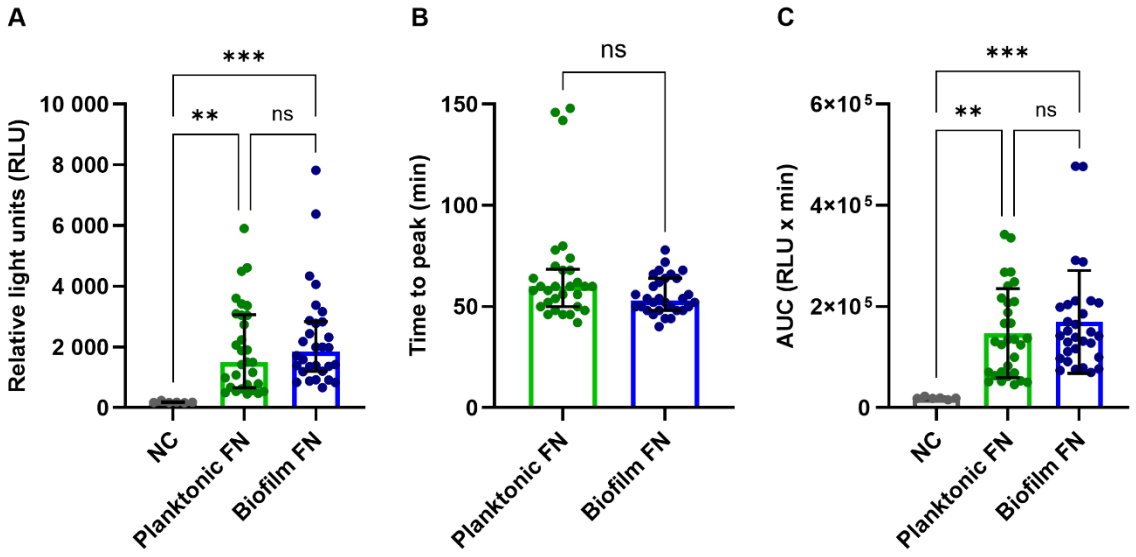

Figure 5.9. Comparison of superoxide release stimulated by planktonic and biofilm-grown *F. nucleatum* (subspecies combined). A – Quantification of peak superoxide release. **B –** Time to peak superoxide. No peak occurred in the NC, thus only pFN and bFN were compared. **C –** Quantification of overall superoxide release expressed as area under the curve (AUC). All values shown as median (IQR). Datasets in A and C analysed using Kruskal-Wallis test with Dunn's post hoc test, in B Mann Whitney U test. ns – not significant; ** - $p<0.01$; *** - $p<0.001$. NC – negative control (GPBS). N(NC)=6; N(test samples)=30 (6 healthy donors multiplied by 5 bacterial stimuli).. MOI = 100. The source dataset used for this species level analysis is the same dataset that is used for the subspecies level analysis in chapter 5.5.

5.4.2. Comparison of NET release

Quantification of NET-DNA released by stimulated neutrophils was performed fluorometrically as described in Materials and Methods (section 2.26). Neutrophils were stimulated for 120 minutes, multiplicity of infection (MOI) was 100. No significant differences were found between planktonic and biofilm stimuli (Figure 5.10). Additionally, there was no difference between the NC and the test samples.

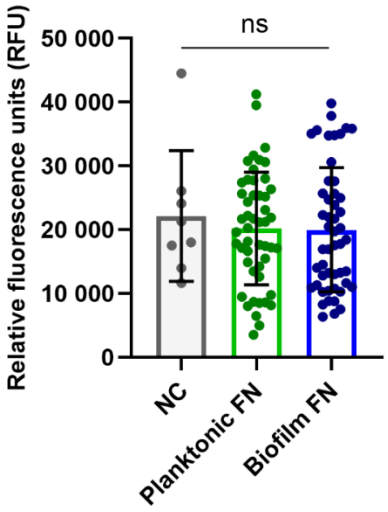

Figure 5.10. Comparison of DNA-NET release stimulated by planktonic and biofilm-grown *F. nucleatum* (subspecies combined). Neutrophils were stimulated for 120 minutes. Values shown as mean (± SD). Statistical test: One-way ANOVA with Tukey's post hoc test. ns – not significant. NC – negative control (RPMI). N(NC)=8 healthy donors; N(test samples)=50 (10 healthy donors multiplied by 5 bacterial stimuli). MOI = 100. The source dataset used for this species level analysis is the same dataset that is used for the subspecies level analysis in chapter 5.5.

5.4.3. Comparison of cytokine and neutrophil enzyme release

Cytokine and lysosomal enzyme release upon stimulation with *F. nucleatum* was analysed by enzyme-linked immunosorbent assay (ELISA). Neutrophils were incubated with *F. nucleatum* for 18 hours, multiplicity of infection (MOI) was 100.

5.4.3.1. Comparison of cytokine release

Four different cytokines were quantified in this study: IL-1β, TNF-α, IL-6 and IL-8 (Fig. 5.11 A-D). Interestingly, significant differences were found only in the case of IL-1β, in which biofilm-grown *F. nucleatum* led to significantly reduced cytokine release in comparison with the planktonic bacteria. In the remaining cytokines analysed, differences were found only between the NC and the test samples.

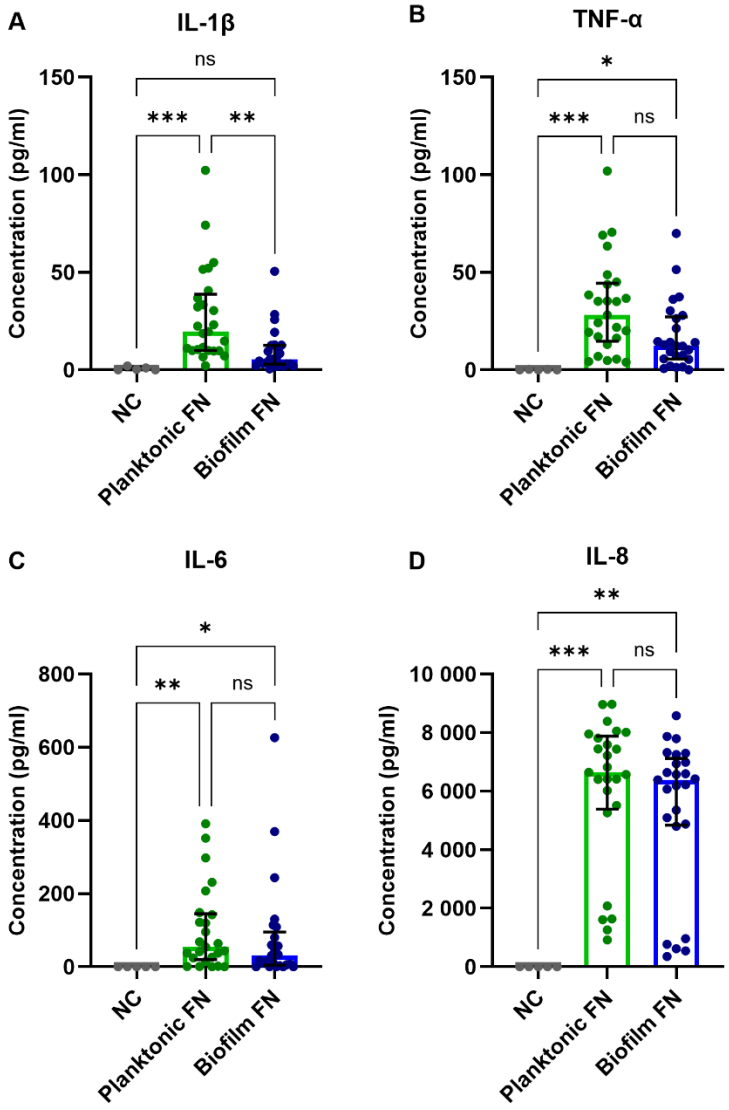

Figure 5.11. Comparison of cytokine release from neutrophils stimulated by planktonic and biofilm-grown *F. nucleatum* (subspecies combined). Neutrophils were incubated with *F. nucleatum* for 18 hours **A** – Quantification of IL-1β. **B** – Quantification of TNF-α. **C** – Quantification of IL-6. **D** – Quantification of IL-8. All values shown as median (IQR). Datasets were analysed using Kruskal-Wallis test with Dunn's post hoc test. N=5 in NC, N=25 in test samples (5 healthy donors multiplied by 5 bacterial stimuli). NC – negative control (RPMI); ns – not significant; * - $p<0.05$; ** - $p<0.01$; *** - $p<0.001$. MOI = 100. The source dataset used for this species level analysis is the same dataset that is used for the subspecies level analysis in chapter 5.5.

5.4.3.2. Comparison of neutrophil enzyme release

Neutrophil enzymes analysed in this study were matrix metalloproteinase 9 (MMP-9) and human neutrophil elastase (HNE). Overall, no differences were found between planktonic and

biofilm stimuli in both MMP-9 and HNE (Figure 5.12). Test samples in both cases were significantly higher when compared to the NC.

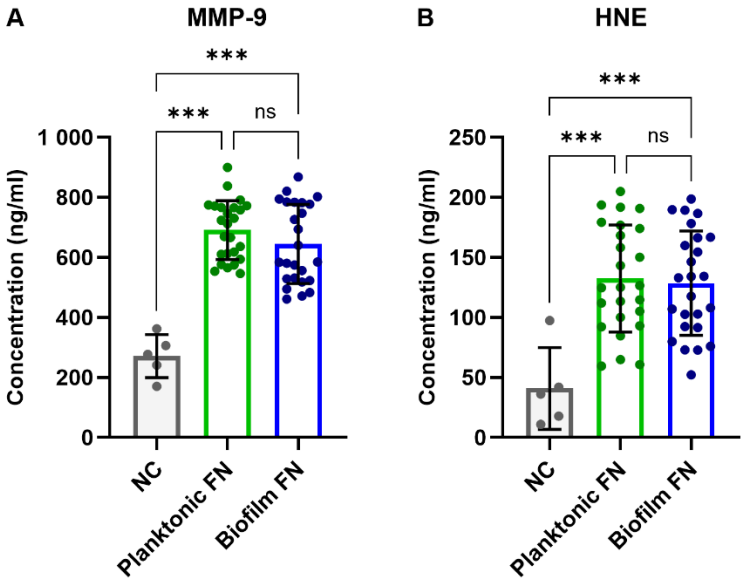

Figure 5.12. Comparison of neutrophil enzyme release stimulated by planktonic and biofilm-grown *F. nucleatum* (subspecies combined). Neutrophils were incubated with *F. nucleatum* for 18 hours. Values shown as mean ± standard deviation. Data were normally distributed and analysed using a one-way ANOVA followed by Tukey's post hoc test. N=5 in NC, N=25 in test samples (5 healthy donors multiplied by 5 bacterial stimuli). ns – not significant; *** - $p<0.001$. MOI = 100. The source dataset used for this species level analysis is the same dataset that is used for the subspecies level analysis in chapter 5.5.

It is noteworthy that a high degree of variation was observed in the analysed neutrophil responses, suggesting that subspecies-specific differences may exist in these combined datasets. Therefore more detailed analyses of individual neutrophil responses was undertaken.

5.5. Evaluation of neutrophil responses to planktonic and biofilm-grown *F. nucleatum* at a subspecies level

In order to identify whether there are significant differences among *F. nucleatum* subspecies and where exactly these differences are, we next analysed ROS generation, NET formation and

cytokine and enzyme release by human neutrophils when triggered by individual *F. nucleatum* subspecies. As explained above (section 5.4.), the same dataset was analysed in sections 5.4. and 5.5. While in section 5.4. the dataset was evaluated at a species level, in this section 5.5., the dataset was analysed in more detail at a subspecies level, investigating differences among individual subspecies.

5.5.1. Quantification of ROS

Generation of total ROS, intracellular and extracellular ROS, as well as superoxide by neutrophils in response to individual *F. nucleatum* subspecies grown planktonically and in biofilms was quantified.

5.5.1.1. Total ROS

In terms of total ROS generation (which comprises both intracellular and extracellular ROS), significant differences were identified among planktonic as well as biofilm-grown subspecies. The highest peak ROS release was stimulated by pFNP, bFNF and bFN25 (Figure 5.13A). Furthermore, bFN25 and bFNV elicited significantly higher peak ROS when compared to their planktonic counterparts. The fastest response was evoked by pFNP, while pFNV led to the slowest response on average (Figure 5.13B; Appendix 1). The highest overall total ROS generation followed stimulation by bFN25 and bFNV and the amount of ROS generated was significantly higher when compared to their planktonic counterparts (Figure 5.13C).

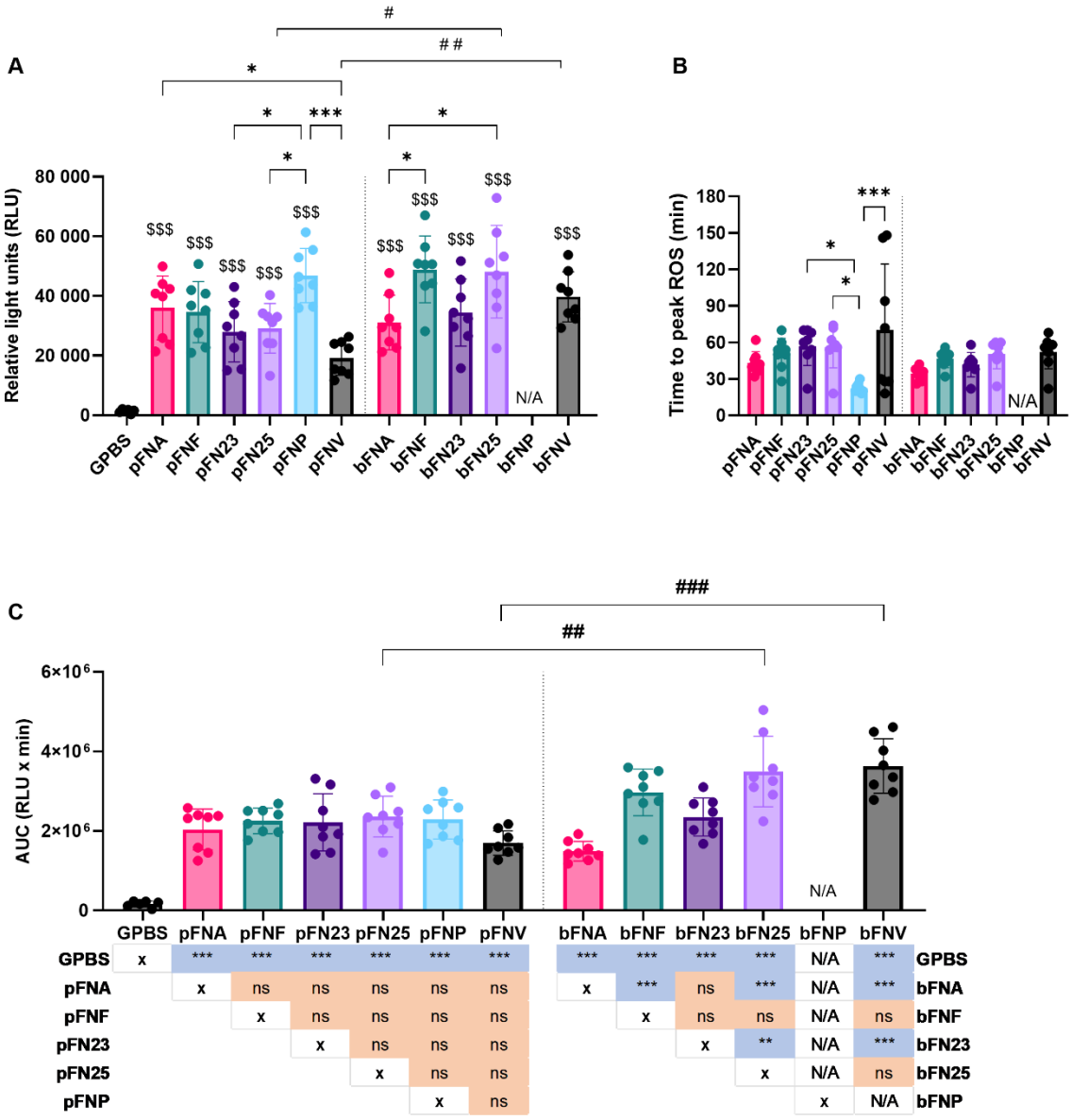

Figure 5.13. Analysis of total ROS release by neutrophils stimulated with *F. nucleatum* subspecies. Biofilm-grown FNP (bFNP) was unavailable due to the absence of biofilm formation. **A –** Quantification of total peak ROS release. All subspecies except pFNV are significantly higher than the negative control (GPBS), differences are shown by "$" symbols. **B –** Time to total peak ROS release. No differences between planktonic and biofilm subspecies were identified. No peak occurred in the negative control (GPBS), therefore it was excluded from the analysis. **C –** Quantification of overall total ROS release. Statistical significance detailed in a p-value matrix. Significant differences between planktonic and biofilm-grown subspecies are indicated by "#" symbols. All data are shown as mean values ±SD. Datasets were analysed using one-way ANOVA with Tukey's post hoc test. ns – not significant; */#/$ - $p<0.05$; **/##/$$ - $p<0.01$; ***/###/$$$ - $p<0.001$. N= 8 healthy adult volunteers. MOI = 100.

5.5.1.2. Intracellular ROS

When intracellular ROS were analysed, only bFNF led to significantly higher neutrophilic peak ROS generation compared to other subspecies, and the only difference between planktonic and biofilm stimuli was seen in FNV (Figure 5.14A). The fastest and slowest responses were elicited by pFNP and pFN25, respectively (Figure 5.14B; Appendix 1). No differences were found among the planktonic subspecies in terms of overall ROS release, while significant differences were found in bFNA and bFN23 when compared to the remaining subspecies. Biofilm-grown FN25 and FNV triggered significantly higher overall ROS generation compared to the planktonic stimuli (Figure 5.14C).

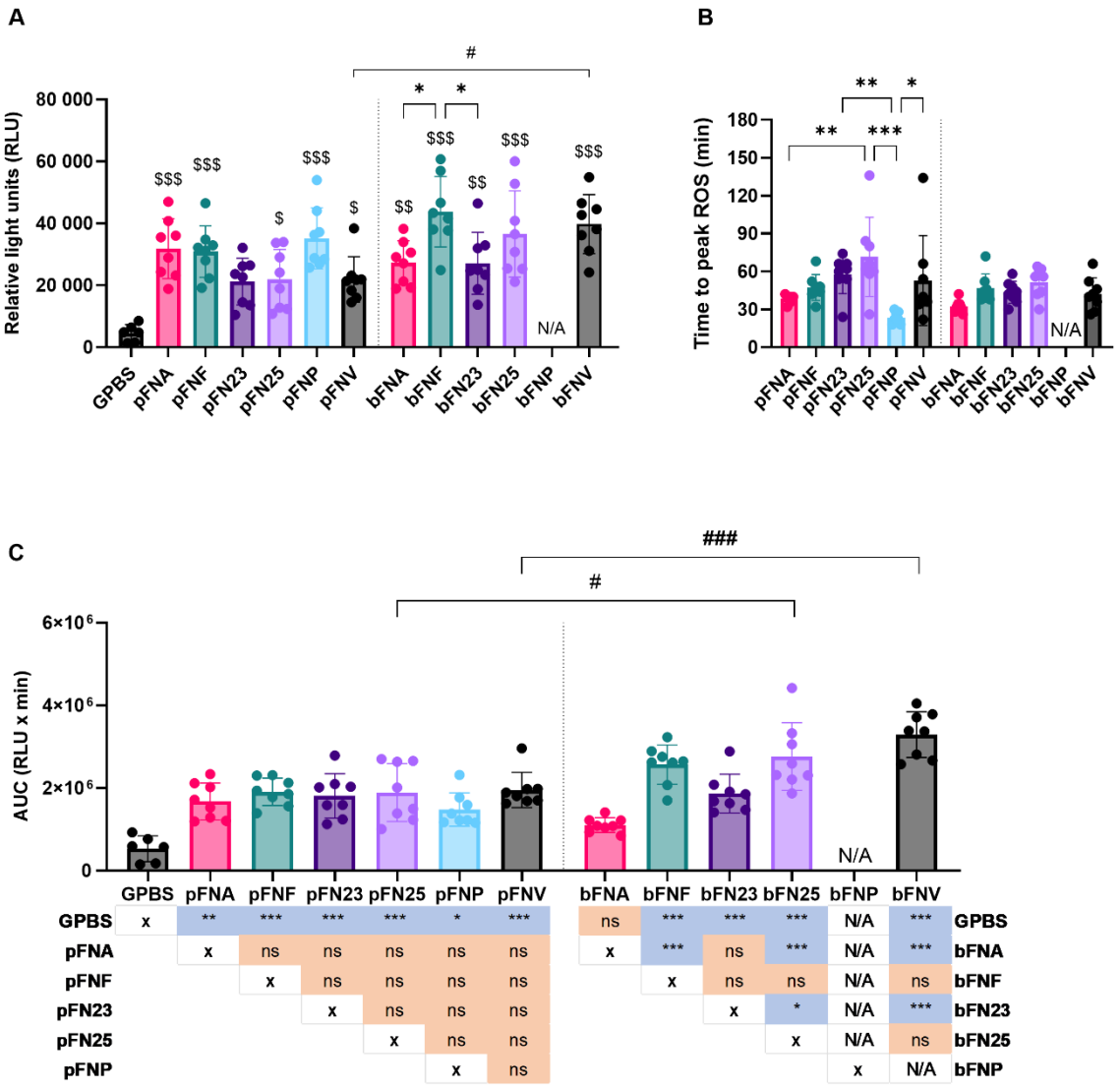

Figure 5.14. Analysis of intracellular ROS release by neutrophils stimulated with *F. nucleatum* subspecies. Biofilm-grown FNP (bFNP) was unavailable due to the absence of biofilm formation. **A –** Quantification of peak intracellular ROS release. All subspecies except pFN23 are significantly higher than the negative control (GPBS), differences are shown by "$" symbols. **B –** Time to peak intracellular ROS release. No differences between planktonic and biofilm subspecies were identified. No peak occurred in the negative control (GPBS), therefore it was excluded from the analysis. **C –** Overall intracellular ROS release. Statistical significance detailed in a p-value matrix. Significant differences between planktonic and biofilm-grown subspecies are indicated by "#" symbol. Asterisks indicate differences within each group (planktonic or biofilm). All data are shown as mean values ±SD. Datasets were analysed using one-way ANOVA with Tukey's post hoc test. ns – not significant; */#/$ - $p<0.05$; **/$$ - $p<0.01$; ***/###/$$$ - $p<0.001$. N=8 healthy adult volunteers. MOI = 100.

5.5.1.3. Extracellular ROS

As detailed in section 5.4.1.4, extracellular ROS values were not obtained by a direct measurement but were calculated mathematically by subtracting intracellular ROS values from total ROS values. Negative luminescence values were replaced with 0.

The highest amount of extracellular ROS was released in response to pFNP (mean RLU 11,700, 4; SD=7,044 RLU), which was significantly higher than the negative control GPBS (mean RLU 49.17; SD=120.4) and pFNV (mean RLU 1,468; SD=2,465). The second highest extracellular ROS response was stimulated by bFN25, which was, similarly to pFNP, significantly higher than the negative control (GPBS).

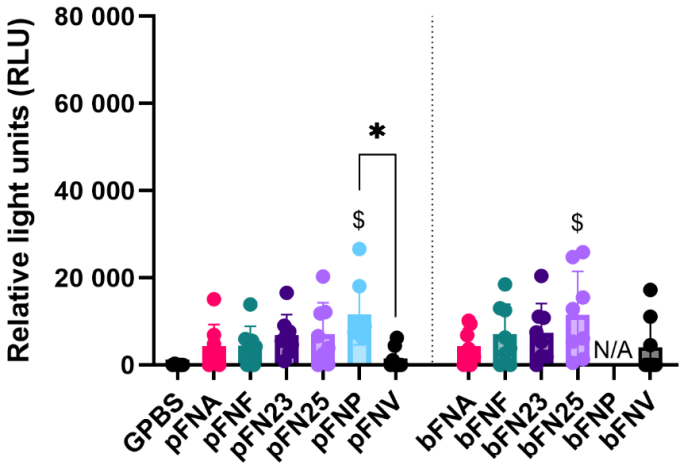

Figure 5.15. Release of extracellular peak ROS. Biofilm-grown FNP (bFNP) was unavailable due to the absence of biofilm formation. Planktonic FNP and biofilm-grown FN25 led to significantly higher extracellular ROS than the negative control (GPBS), significant differences compared to the GPBS control are shown by "$" symbols, asterisk shows a difference between the subspecies. */$ - $p<0.05$. N=8 healthy volunteers. MOI = 100.

5.5.1.4. Superoxide

Differences of a higher magnitude were found in superoxide generation. Planktonic subspecies pFNA and pFNP as well as bFNA elicited significantly higher superoxide generation when compared to the remaining subspecies, while planktonic and biofilm FNV resulted in the lowest

superoxide generation (Figure 5.16A). These subspecies also followed the same pattern for overall superoxide release expressed as areas under the curve (AUC; Figure 5.16C). The most rapid response was again stimulated by pFNP, whilst the slowest response was induced by pFNV, which also was significantly slower compared to bFNV (Figure 5.16B; Appendix 1).

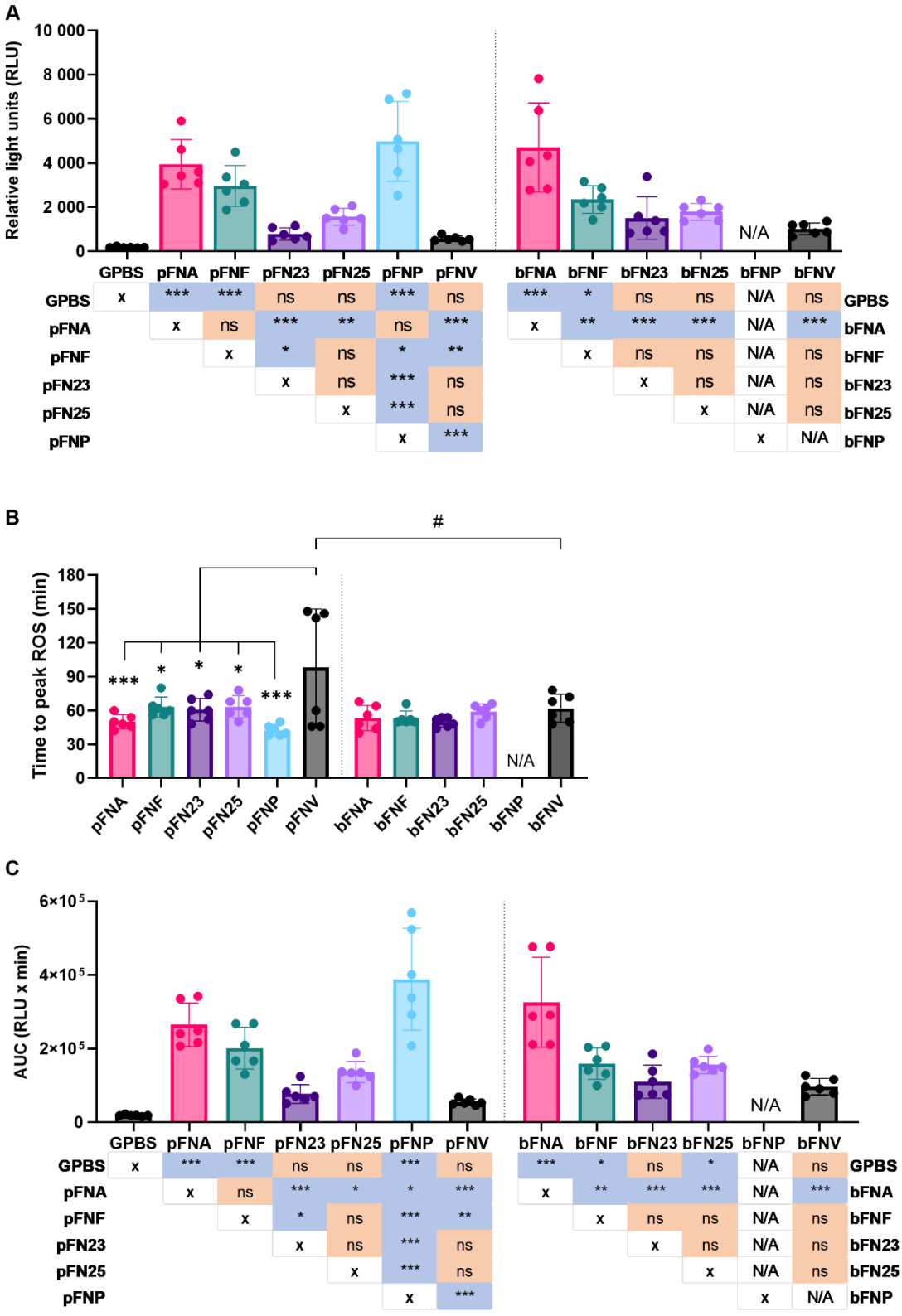

Figure 5.16. Analysis of superoxide release by neutrophils stimulated with *F. nucleatum* subspecies. Biofilm-grown FNP (bFNP) was unavailable due to the absence of biofilm formation. **A –** Quantification of peak superoxide release. **B –** Time to peak superoxide release.

Significant difference between planktonic and biofilm-grown FNV is indicated by "#" symbol. **C –** Quantification of overall superoxide release. Statistical significance detailed in p-value matrices. All data are shown as mean values ±SD. Datasets were analysed using a one-way ANOVA with Tukey's post hoc test. ns – not significant; */#- $p<0.05$; ** - $p<0.01$; *** - $p<0.001$. N=6 healthy adult volunteers. MOI = 100.

5.5.1.5. Quantification of ROS release stimulated by FadA and Fap2 adhesin mutans

Due to the differences observed among the subspecies, especially in superoxide generation, we hypothesised that adhesion proteins on the surface of *F. nucleatum*, namely FadA and Fap2, which are important for adhesion to the host cells as well as other bacteria, may play a role in stimulation of ROS generation by neutrophils.

To test the hypothesis, planktonic mutant ΔFadA and ΔFap2 strains (chromosomal gene deletions) were used as stimuli in the enhanced chemiluminescent ROS assay and neutrophil responses to the mutant strains were compared to a planktonic wild-type (WT) strain FN23 (pFN23), which is the parental strain.

The ΔFadA strain stimulated the highest amount of ROS release in all types of ROS studied (Figure 5.17A-D), however the differences were statistically significant only in the case of superoxide release (Figure 5.17C). The same pattern was observed also in overall ROS released (Figure 5.17H-J), with the highest values measured in ΔFadA and significant differences found in superoxide release (Figure 5.17J). The ΔFadA strain stimulated the fastest peak ROS release, which was significantly lower than ΔFap2 but not significant when compared to the WT (Figure 5.17E-G).

The opposite was observed in the case of ΔFap2, which stimulated the slowest peak ROS release (Figure 5.17E-G) and stimulated the lowest amount of peak total and intracellular ROS as well as peak superoxide (Figure 5.17A-C) and overall ROS released (Figure 5.17H-J).

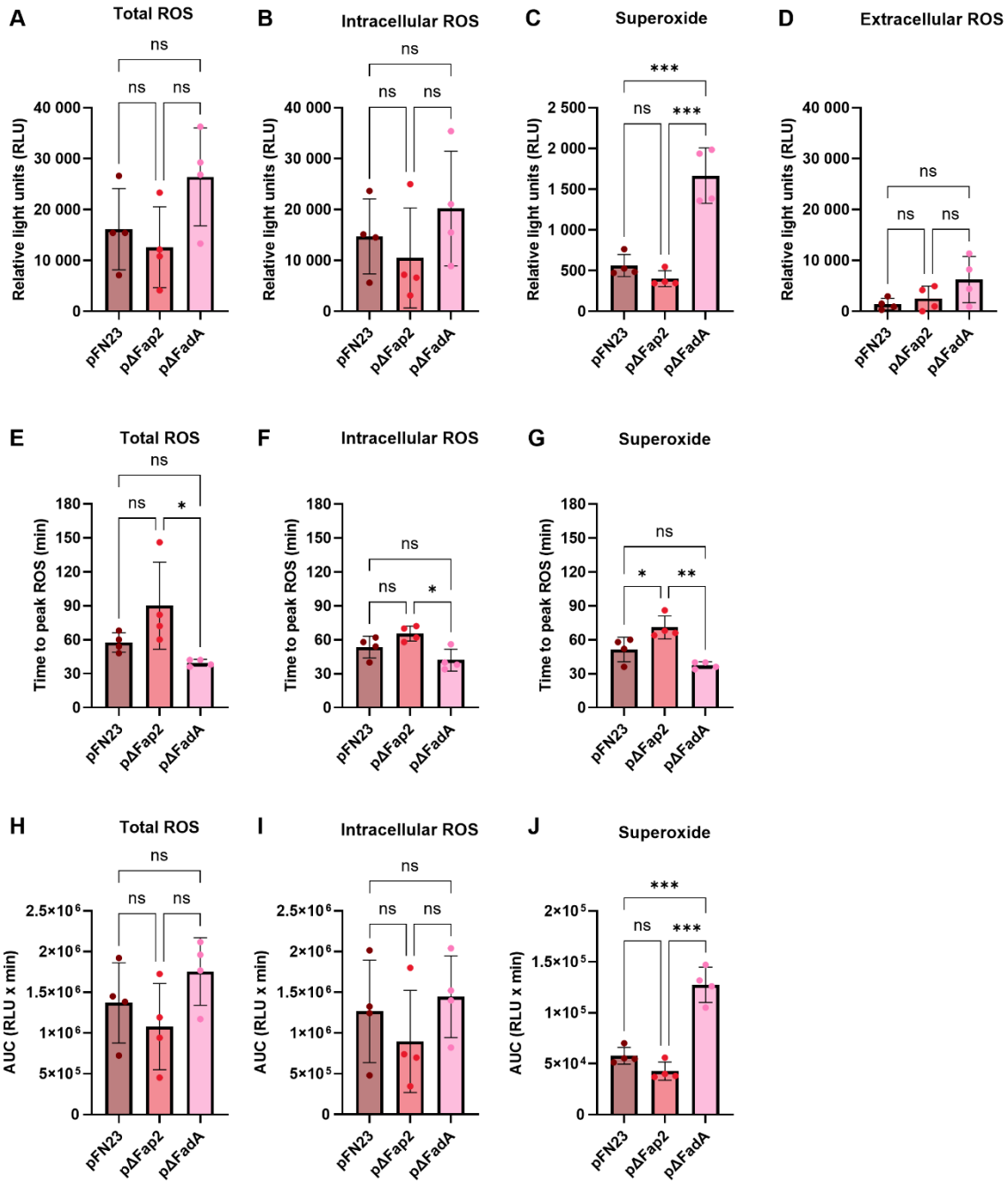

Figure 5.17. Quantification of ROS release stimulated by wild type pFN23 and Fap2 and FadA adhesin mutants. A - D – Quantification of total peak ROS release. Note the different y axis scale in C. **E – G -** Time to peak ROS release. **H – J –** Quantification of overall ROS released expressed as area under the curve (AUC). Note the difference in values shown on the y axis in J. All data are shown as mean values ±SD. Datasets were analysed using one-way ANOVA with Tukey's post hoc test. ns – not significant; * - $p<0.05$; ** - $p=0.0011$; *** - $p<0.001$. N=4 healthy adult volunteers. MOI = 100.

Considering that most significant differences were observed in superoxide release stimulated by the mutant strains, we next compared the mutants with pFNA, pFNP and pFNV, subspecies.

The analysis showed that the mutant strains stimulated significantly lower amount of peak and overall superoxide release when compared to pFNA and pFNP, while no difference was observed in time to peak superoxide release (Figure 5.18). No differences were found between the mutant strains and pFNV in total and overall superoxide release. Surprisingly, none of the mutant strains was significantly different from the WT strain in this analysis. Despite this lack of significance, some trends were observed: pΔFadA stimulated two times more mean superoxide in terms of peak (Figure 5.18A) as well as overall superoxide release (Figure 5.18C) and a significantly shorter response when compared to pFNV (Figure 5.18B). By contrast, pΔFap2 stimulated a relatively low level of mean peak (Figure 5.18A) and overall superoxide (Figure 5.18C), which was similar to the levels stimulated by pFNV.

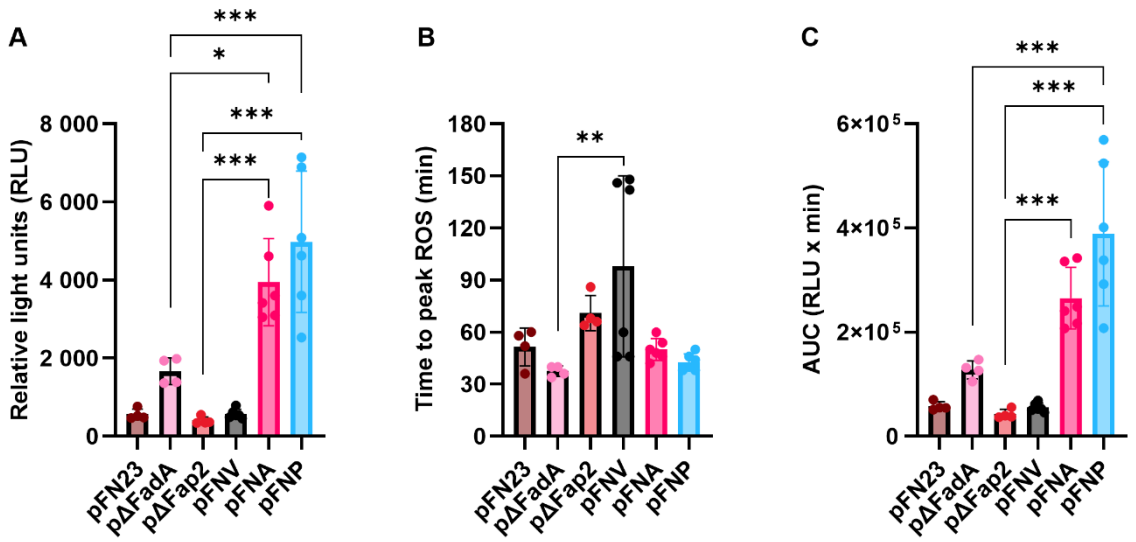

Figure 5.18. Comparison of superoxide generation in response to adhesin mutant FN23 strains pΔFadA and pΔFap2 and pFNA, pFNP and pFNV. A – Quantification of total peak superoxide. **B –** Time measured to peak superoxide. **C –** Quantification of overall superoxide release expressed as area under the curve (AUC). All data are shown as mean values ±SD. Datasets were analysed using one-way ANOVA with Tukey's post hoc test. Only significant differences between the mutant strains and the test samples are shown. * - p=0.02; ** - p=0.01;

*** - p<0.001. N(pFN23/ΔFap2/ΔFadA)=4 healthy adult volunteers, N(FNA, FNP, FNV)=6 healthy adult volunteers. MOI = 100.

5.5.2. Quantification of NET release

In addition to quantification of ROS, NET release was quantified. Overall, pFNP stimulated the highest mean amount of DNA (Figure 5.19), however, this was significantly higher compared to pFNA only. A high degree of variation was observed across the subspecies and none of the test samples were significantly different from the negative control (RPMI).

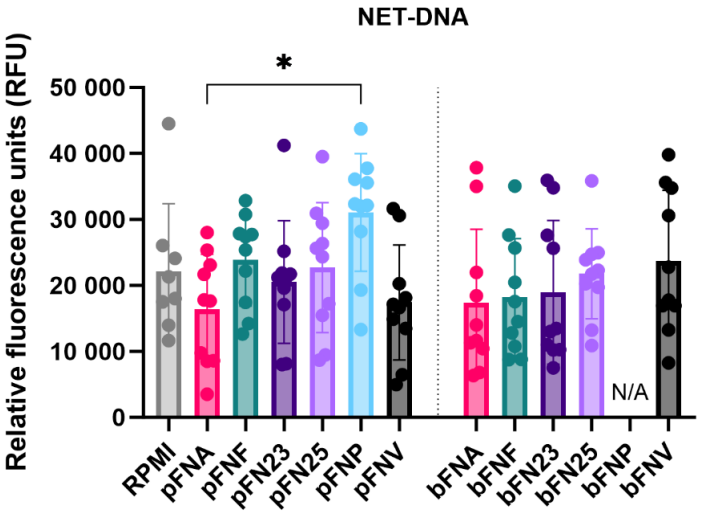

Figure 5.19. Quantification of extracellular NET-DNA. Data were analysed using one-way ANOVA followed by Tukey's post hoc test. Data are shown as mean values ±SD. N=8 for RPMI, N=10 for test samples. * p=0.03. MOI = 100.

5.5.3. Microscopic visualisation of NETs

In addition to fluorometric quantification of NET-DNA, NETs were also visualised microscopically to confirm whether the DNA being measured was due to NETosis. Neutrophils were stimulated as described in 2.26 and stained with fluorescent dyes: cell permeant DNA stain Hoechst 33342 (HCT), and live cell impermeant dye SYTOX Green, which stains extracellular DNA, and can therefore help visualise NETs.

Characteristic multilobed nuclei were observed in unstimulated neutrophils when stained with HCT (Figure 5.20A). However, unstimulated cells also displayed staining with SYTOX Green (Figure 5.20B). In cells stimulated with planktonic and biofilm-grown *F. nucleatum* subspecies, long SYTOX Green-stained structures characteristic of NETs were seen (Figure 5.20C).

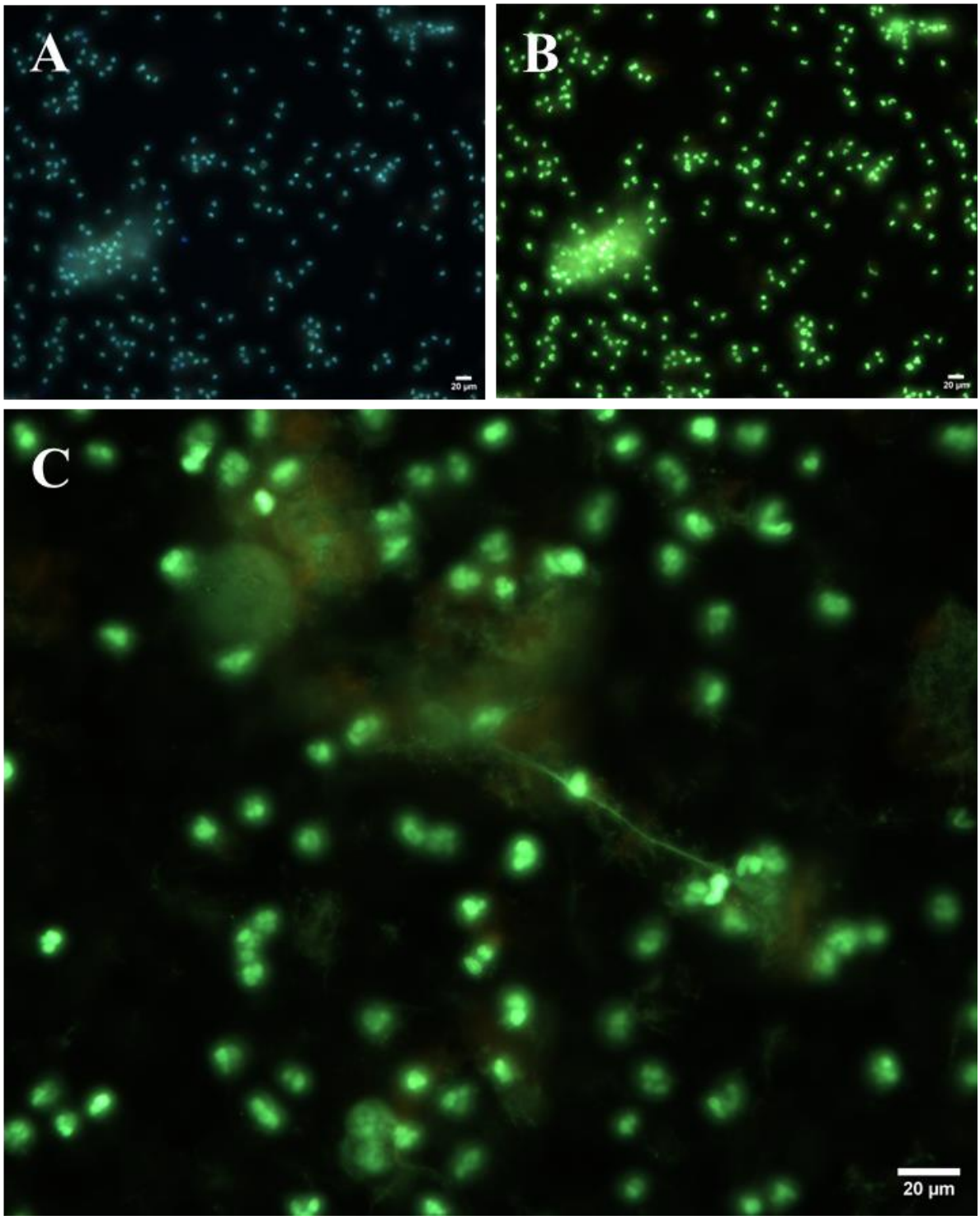

Figure 5.20. Microscopic visualisation of NETs. A – Unstimulated HCT-positive neutrophils. 20X objective lens was used. **B** - Unstimulated SYTOX-positive neutrophils. 20X objective lens was used. **C** – SYTOX-positive neutrophils stimulated with pFNA forming a NET structure. 40X objective lens was used. Scale bar – 20 µm.

5.5.4. Quantification of neutrophilic cytokine and enzyme release by ELISA

Next, neutrophils were incubated with *F. nucleatum* subspecies and the release of selected pro-inflammatory cytokines and neutrophil enzymes after 18 hours of incubation was quantified.

5.5.4.1. Quantification of cytokines

In order to describe quantification sensitivity of the ELISA assay as defined by the manufacturer, the lowest concentration of each standard was chosen as the lower limit of quantitation (LLOQ). If values were measured below the LLOQ, they were replaced with the value equal to LLOQ/2 as previously published (Doucet et al., 2013). The used LLOQ/2 values were as follows: 1.95 pg/ml for IL-1β, 4.69 pg/ml for IL-6 and 7.8 pg/ml for TNF-α.

Subspecies pFNA, pFNP and bFNA most frequently elicited the lowest cytokine release, which was most prominent in case of IL-8 (Figure 5.21D). Additionally, bFNF and bFN23 stimulated very low cytokine release. In most cases the cytokine levels released in response to these low-stimulating subspecies was below the LLOQ (Figure 5.21A-C). On the other hand, subspecies pFNV and bFNV triggered the highest mean cytokine release. Differences between planktonic and biofilm-grown stimuli were found in IL-1β in subspecies FNV (Figure 5.21A), and in TNF-α (Figure 5.21C) and IL-8 (Figure 5.21D) in subspecies FN23.

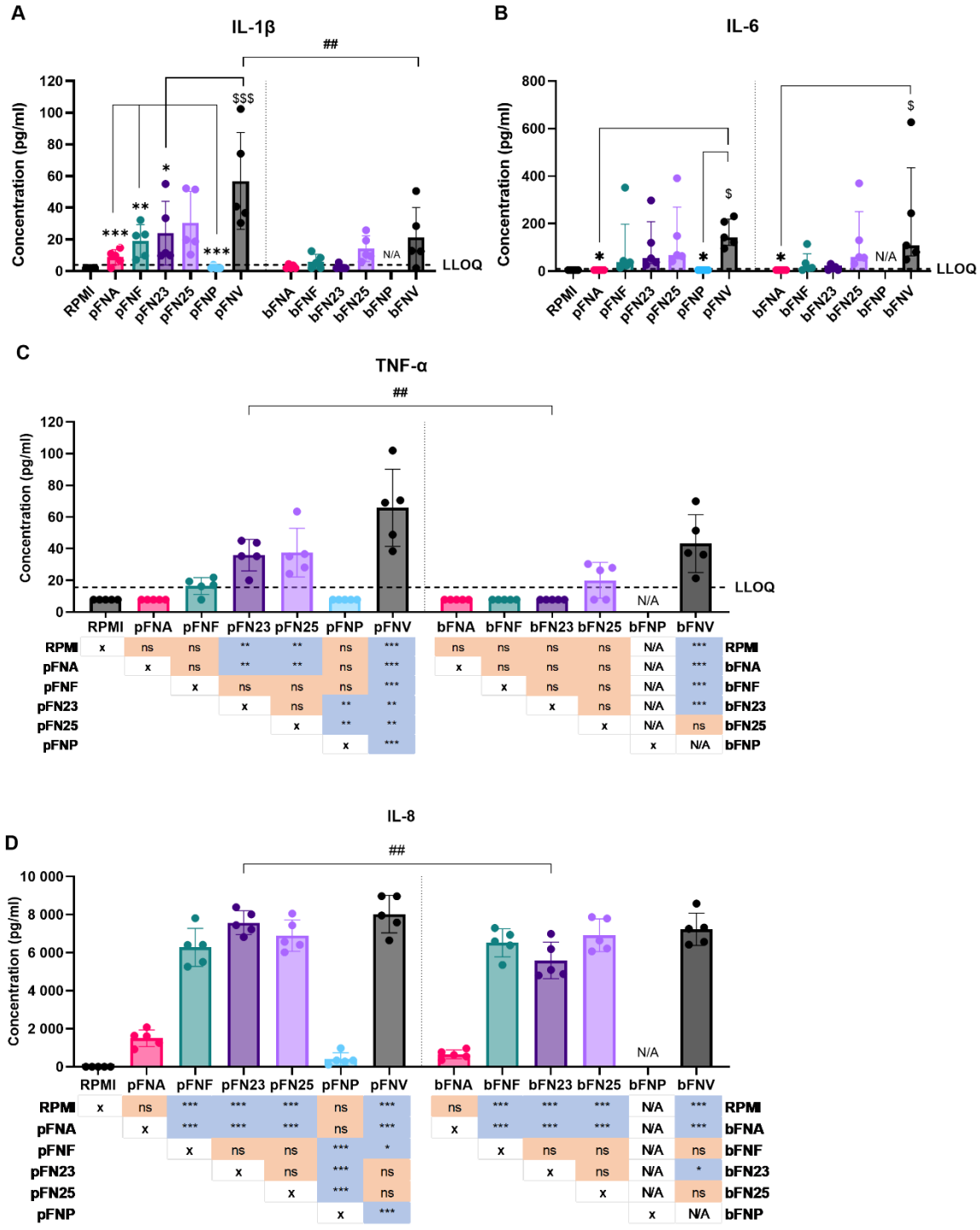

Figure 5.21. Quantification of cytokine release by neutrophils stimulated by *F. nucleatum* subspecies. A – Quantification of IL-1β; LLOQ=3.9 pg/ml. Values below the LLOQ were replaced with LLOQ/2. **B** – Quantification of IL-6. Data were not normally distributed and are therefore shown as medians and ranges. LLOQ=9.38 pg/ml. Values below the LLOQ were replaced with LLOQ/2. **C** – Quantification of TNF-α. Statistical significance is detailed in a p-value matrix. LLOQ=15.6 pg/ml. Values below the LLOQ were replaced with LLOQ/2. **D** – Quantification of IL-8. Statistical significance is detailed in a p-value matrix. Subspecies

indicated with "$" symbols in A and B are significantly higher compared to the negative control (RPMI). Significant differences between planktonic and biofilm-grown subspecies are indicated by "#" symbols. Normally distributed data were analysed using one-way ANOVA followed by Tukey's post hoc test. Non-normally distributed data were analysed using Kruskal-Wallis test followed by Dunn's post hoc test. Assays were performed in technical duplicate, N=5 healthy adult volunteers. Data in A, C and are shown as mean values ±SD. LOQ – limit of quantitation. */$ - p<0.05; **/## - p<0.01; ***/$$$ - p<0.001. MOI = 100.

5.5.4.2. Quantification of neutrophil enzyme release

With respect to neutrophil enzymes MMP-9 and HNE, the release was not stimulated in a subspecies-specific fashion. No significant differences were found among the subspecies and between planktonic and biofilm-grown subspecies (Figure 5.22). In the case of MMP-9 (Figure 5.22A), all subspecies led to significantly higher releases than the negative control RPMI. With regards to HNE release (Figure 5.22B), only pFNA, pFN25, pFNV, bFNF and bFN25 differed significantly from RPMI.

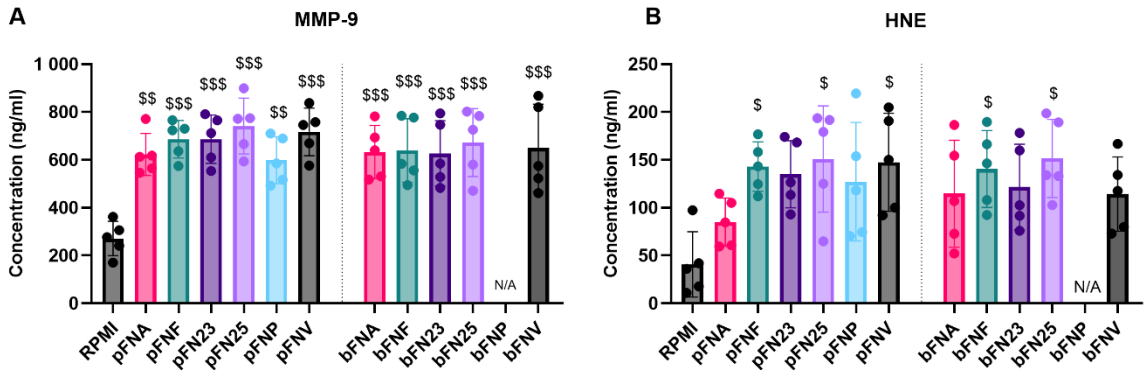

Figure 5.22. Quantification of antimicrobial enzyme release by neutrophils stimulated by *F. nucleatum* subspecies. A - Quantification of MMP-9 with no statistical difference among the tested subspecies. **B** – Quantification of HNE with no statistical difference among the tested subspecies. Subspecies indicated with "$" symbols are significantly higher compared to the negative control (RPMI). Data were normally distributed and analysed using one-way ANOVA followed by Tukey's post hoc test. Assays were performed in technical duplicate, N=5 healthy adult volunteers. Data are shown as mean values ±SD. $ - p<0.05; $$ - p<0.01; $$$ - p<0.001. MOI = 100.

Due to the nature of the results obtained, degradation of cytokines by subspecies FNA and FNP was hypothesised. Additionally, due to the high concentrations of neutrophil enzymes quantified, the assessment of the kinetics of their release was deemed necessary. Therefore, a time course release assay of neutrophil cytokines and enzymes was undertaken.

5.6. Time-course cytokine and enzyme release

The time-course release assay was carried out using pFNA, pFNP and pFNV as stimuli. Values measured below the LLOQ were deliberately kept as the original measured values in order to preserve the pattern of cytokine release over time, however no statistical analysis was performed if datapoints were below the LLOQ. Intriguingly, subspecies FNA and FNP did not appear to degrade the cytokines as their levels remained stable and significantly lower over the incubation period when compared to pFNV (Figure 5.23A-D) in all cytokines analysed. A high amount of both neutrophil enzymes MMP-9 and HNE (Figure 5.23E, F) was released as soon as 1 hour after stimulation and remained overall constant for the duration of the incubation (up to 18 hours). No differences in enzyme release were found among subspecies at any time point.

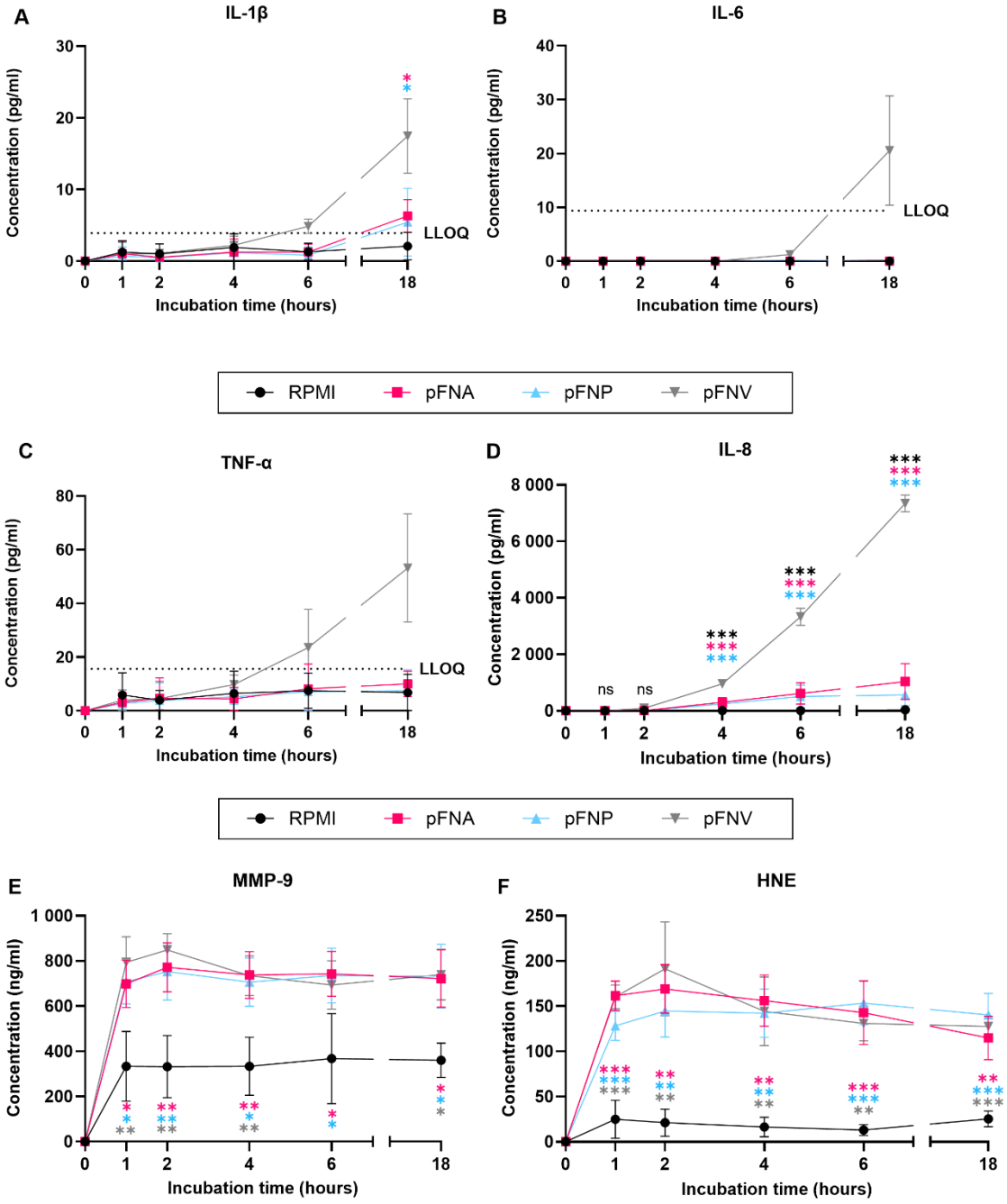

Figure 5.23. Time-course release of neutrophil cytokines and enzymes over 18 hours stimulated by selected *F. nucleatum* subspecies. A – Release of IL-1β. Only pFNA, pFNP and pFNV after 18 hours of incubation were statistically compared. LLOQ=3.9 pg/ml. **B** - Release of IL-6. No statistical analysis was performed as the majority of datapoints was below the LLOQ. LLOQ=9.38 pg/ml. **C** - Release of TNF-α. No statistical analysis was performed as the majority of datapoints was below the LLOQ. LLOQ=15.6 pg/ml. **D –** Release of IL-8. **E –** Release of MMP-9. **F –** Release of HNE. All data are shown as mean values ±SD. Statistical significance was calculated at individual time points using one-way ANOVA followed by Tukey's post hoc test. LLOQ – lower limit of quantitation. * - $p<0.05$; ** - $p<0.01$; *** -

$p<0.001$. Significant differences are in comparison to subspecies indicated by colour-coding for each time point. N=3 healthy adult volunteers. MOI = 100.

5.7. Quantification of neutrophil apoptosis and necrosis

Since the cytokines were not confirmed to be degraded by *F. nucleatum* subspecies, it was hypothesised that FNA and FNP cause premature death of neutrophils and therefore prevent the production of cytokines.

Both apoptosis (programmed anti-inflammatory cell death) and necrosis (uncontrolled pro-inflammatory cell death) were investigated to determine the mode of cell death triggered by the subspecies FNA and FNP. Utilising a commercially available kit, apoptosis was measured by quantifying luminescence emitted by Annexin V protein binding to phosphatidylserine exposed on the apoptotic cell membrane. Necrosis was quantified by fluorescence signal of DNA-specific dye, which only enters the cell and binds the DNA when the cell membrane loses its integrity. Apoptosis and necrosis were measured for 18 hours after stimulation with positive controls (100 ng/ml Fas ligand for apoptosis, 50 μg/ml LL-37 for necrosis), or with planktonic and biofilm-grown *F. nucleatum* subspecies (MOI 100).

From the measured apoptosis and necrosis data, the start and rate of apoptosis and necrosis were calculated in order to determine whether FNA and FNP cause earlier onset of cell death as well as more rapid cell death. Start of apoptosis and necrosis was defined as a time point in the assay at which the highest peak occurred in the second derivative of the cell death curve. The rate of apoptosis and necrosis was determined from the highest peak of the first derivative of the cell death curve.

5.7.1. Bacterial fluorescence and luminescence

In the selected apoptosis/necrosis assay, apoptosis was detected by quantifying luminescence and necrosis by fluorescence, therefore luminescence and fluorescence of *F. nucleatum* stimuli in the presence of assay reagents and in the absence of neutrophils was assessed in order to correct for possible non-specific bacterial signals measured during the assay.

Both luminescence and fluorescence were emitted by the bacteria. Interestingly, in the case of pFNA and bFNA, considerably sharp peaks in luminescence were measured (Figure 5.24A), while the amount of luminescence of the remaining subspecies was relatively constant for the duration of the assay. Markedly high levels of fluorescence, in some cases increasing during the assays (pFNA, pFNF, pFNP), were also quantified (Figure 5.24B).

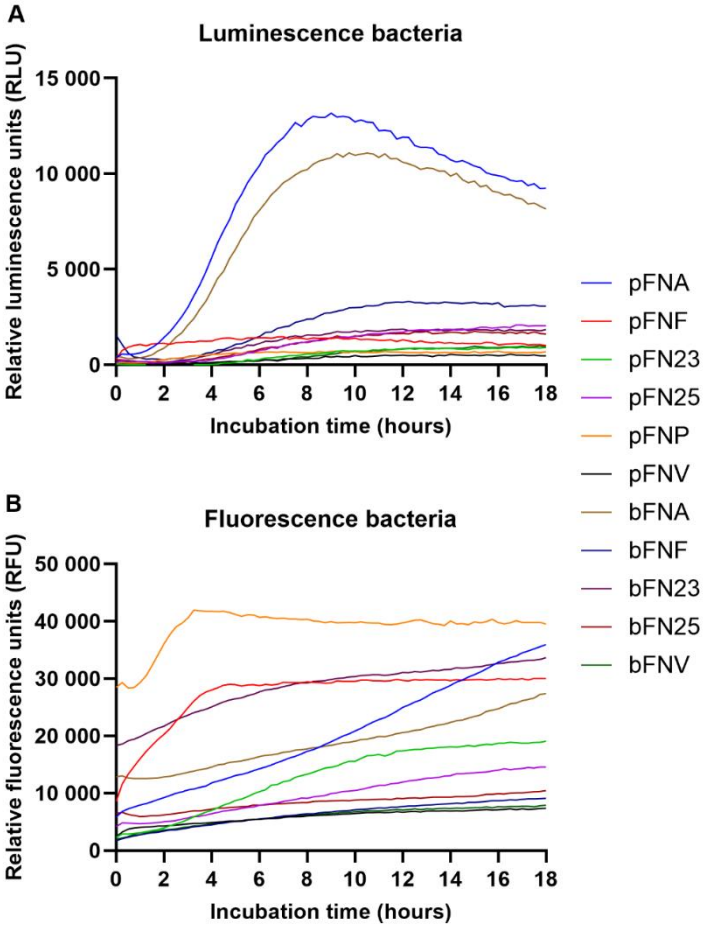

Figure 5.24. Quantification of luminescence (A) and fluorescence (B) of *F. nucleatum* planktonic (p) and biofilm (b) stimuli used in apoptosis and necrosis assays. Bacterial stimuli were incubated in the absence of neutrophils. The assay was performed once in technical duplicate.

5.7.2. Neutrophil apoptosis

To evaluate neutrophil apoptosis, luminescence values obtained from wells containing bacteria-stimulated neutrophils were first corrected for bacterial luminescence presented above (section 5.7.1).

The start of apoptosis was in most cases observed after at least 3 hours of incubation (Figure 5.25A; Appendix 2). The only subspecies among the 3 subspecies of interest that stimulated

apoptosis significantly earlier was pFNP (mean: 0.875 hour). Planktonic FN23 stimulated apoptosis significantly earlier when compared to its biofilm-grown counterpart.

Secondly, when the rate of apoptosis was evaluated, no statistically significant differences were identified among the subspecies and in comparison with the positive and negative controls (Figure 5.25B; Appendix 2). Moreover, a large spread of data was observed in this dataset.

It is important to highlight that the positive control (Fas ligand), however, did not stimulate a significantly higher rate or earlier onset of apoptosis when compared to unstimulated cells. Therefore, although comparison with unstimulated control samples enables the assessment of increases in apoptosis, the lack of a positive control does not allow for conclusions regarding the full extent of apoptosis.

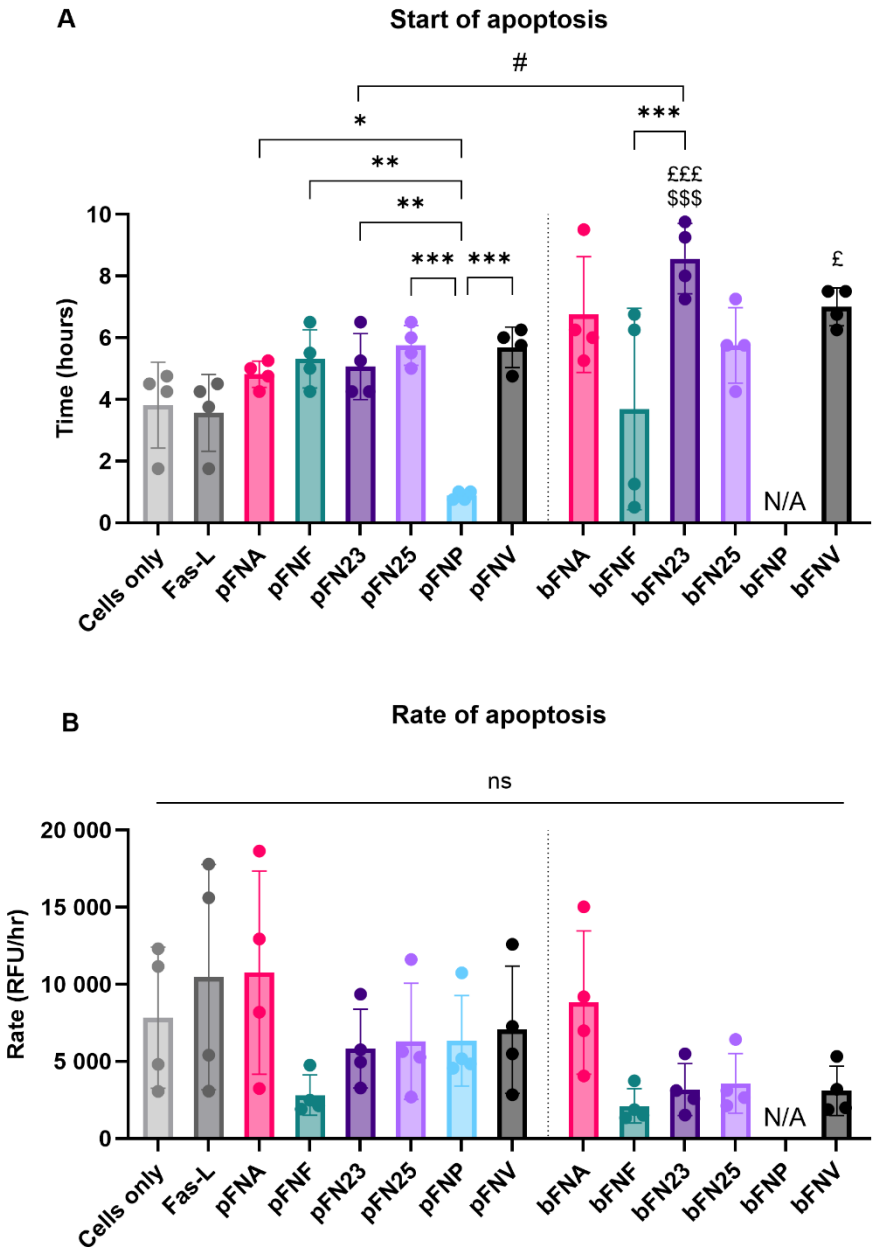

Figure 5.25. Analysis of neutrophil apoptosis upon stimulation with *F. nucleatum* subspecies. A – Start of apoptosis determined from second derivative of apoptosis curves. bFN23 indicated with "$" symbols was significantly higher compared to the negative control (cells only). Subspecies indicated with "£" were significantly higher compared to the positive control (Fas-L). **B** - Rate of apoptosis determined from the first derivative of apoptosis curves. All data are shown as mean values ±SD. Statistical significance was calculated using one-way ANOVA followed by Tukey's post hoc test. N=4 healthy adult volunteers. ns – not significant; */# - $p<0.05$; ** - $p<0.01$; ***/$$$ - $p<0.001$. MOI = 100.

5.7.3. Neutrophil necrosis

Next, in order to analyse neutrophil necrosis, fluorescence values obtained from wells containing bacteria-stimulated neutrophils were first corrected for bacterial fluorescence reported in section 5.7.1.

Planktonic FNA, FNP and biofilm-grown FNA stimulated the onset of necrosis significantly earlier (1.06, 1.75 and 1.44 hours post stimulation, respectively; Figure 5.26A; Appendix 3) compared to the necrosis positive control LL-37 (7.25 hours post stimulation). However, these subspecies were not significantly different from the remaining subspecies, except for pFNA when compared to pFNF (Figure 5.26A). Regarding rate of necrosis, pFNA, pFNP and bFNA were significantly lower only when compared to the positive necrosis control LL-37, however no differences were found among the subspecies (Figure 5.26B; Appendix 3).

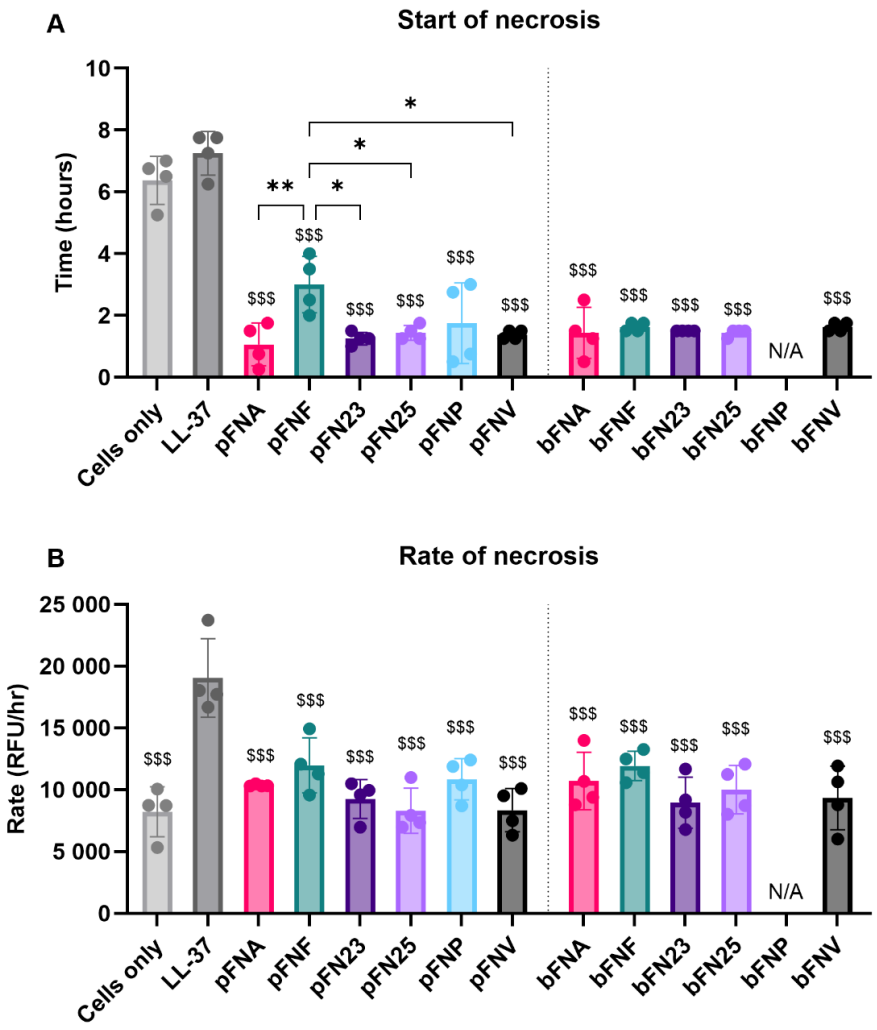

Figure 5.26. Analysis of neutrophil necrosis upon stimulation with *F. nucleatum* subspecies. A – Start of necrosis determined from the second derivative of necrosis curves. Test samples were significantly different from the negative control (cells only) and the positive control (LL-37). The level of significance was identical compared to both the negative and the positive control, therefore only one set of symbols is shown using "$" symbols. **B** – Rate of necrosis determined from the first derivative of necrosis curves. Negative control as well as test samples were significantly different from the positive control LL-37, as indicated by "$" symbols. Assays were performed in technical duplicate, N=4 healthy adult volunteers. All data are shown as mean values ±SD. One-way ANOVA was performed followed by Tukey's post hoc test. * - $p<0.05$; ** - $p=0.01$; $$$ - $p\leq0.001$. RFU – relative fluorescence units. MOI = 100.

5.8. Chapter discussion

The work presented in this chapter revealed that bacteria grown in biofilms can be successfully quantified by viable colony counting if more advanced quantification approaches, such as qPCR, prove to be challenging. High quality extracted DNA is necessary for accurate bacterial

quantification by qPCR, however, an efficient extraction of DNA from *F. nucleatum* was not possible with the DNA extraction methods used in this study. Work by de Bruin and Birnboim (2016) confirmed our observations that different lysis methods significantly affect DNA release and extraction efficiency from various bacteria, therefore DNA extraction needs further optimisation in *F. nucleatum,* which is considerably more difficult to lyse compared to *E. coli*. A recent study by Krieger et al. (2024) evaluating presence of *F. nucleatum* subspecies in healthy and diseased conditions utilised a significantly longer chemical lysis step for gDNA extraction (3 hours) compared to a much shorter chemical lysis in this study (maximum 30 minutes), which further supports the necessity to optimise the DNA extraction protocol. Regarding the quantification of live and dead bacteria in the biofilm, fluorescent quantification could be performed in the future to assess the proportion of dead bacteria in the biofilm.

While the viable colony counting utilised in this work allowed quantification of viable *F. nucleatum* subspecies, this approach has its limitations. It works on the premise that one colony on the plate comes from one bacterium from the bacterial suspension. However, potential autoaggregation of bacteria could provide inaccurate results as one colony on the agar may come from a bacterial aggregate rather than a single bacterium. Future work using phase contrast microscopy should confirm whether *F. nucleatum* subspecies form these aggregates and thus confirm the accuracy of the results presented here.

Viability testing of live planktonic and biofilm-grown *F. nucleatum* subspecies stored at -20°C and -80°C revealed that the optimal storage period length of live stimuli is up to 2 weeks at -20°C and up to 4 weeks at -80°C, however longer storage periods at -80C did not seem to negatively affect bacterial viability. Regular thawing and freezing of live bacterial stimuli should be avoided as this significantly reduces viability, as observed in our viability study and

supported by Sleight et al. (2006) who demonstrated decreased viability of *E. coli* after numerous freeze-thaw cycles.

Comparison of immunogenicity of planktonic and biofilm stimuli demonstrated that the biofilm state may be a factor influencing pro-inflammatory neutrophil responses. Biofilm-grown bacteria stimulated higher and faster total ROS release and higher intracellular ROS release. This could be explained by the expression of biofilm-specific levels of virulence factors, as shown in the case of outer membrane proteins and adhesins quantified by Ali Mohammed et al. (2021). Conversely, biofilm stimuli triggered lower IL-1β release. This could potentially be caused by the biofilm extracellular polymeric substances (EPS) masking recognition sites on the bacterial cells, as previously observed for *Pseudomonas aeruginosa* (Granton et al., 2024). Alternatively, the decreased response could be the result of receptor internalisation due to the presence of multiple stimuli (De Alessandris et al., 2019).

When more detailed neutrophil responses to individual subspecies were analysed, the results indicated that specific differences exist among the subspecies. In terms of ROS generation by neutrophils, some differences were observed in total and intracellular ROS, however the most pronounced differences were identified in superoxide generation, with FNA and FNP stimulating the highest, while FNV stimulated the lowest amount of superoxide. This finding is in agreement with subspecies-specific differences observed by Kurgan et al. (2017) in HL-60 neutrophil-like cells. Interestingly, the superoxide levels were inversely correlated with the levels of cytokines stimulated.

Quantification of ROS stimulated by mutant strains lacking adhesins FadA and Fap2 showed that the pΔFadA strain constantly stimulated the highest levels of ROS compared to the WT and pΔFap2 as well as the fastest response, and the differences were significant in the case of

superoxide generation. When the mutant strains were compared with FNA, FNP and FNV to find out possible similarities in immunogenicity, the WT was no longer different from the mutant strains. Therefore there is no evidence from our results that FadA and Fap2 are involved in neutrophil stimulation.

While literature focusing on the involvement of *F. nucleatum* adhesins in innate immune response stimulation is absent, a study performed using *Helicobacter pylori* showed that one of *H. pylori* adhesins, SabA , is essential for activation of neutrophils as well as phagocytosis and generation of ROS (Unemo et al., 2005). Further work is needed to understand whether adhesin mutant strains stimulate other neutrophil responses such as phagocytosis and degranulation in the same way as FNA, FNP or FNV and whether these and other adhesins play an important immunostimulatory role.

Analysis of NETosis showed that pFNP stimulated the highest mean NET release, however this was not different from the negative control. Fluorescent microscopy of NETs revealed that all neutrophils were SYTOX-positive, which could suggest that all neutrophils were damaged and thus dead, as this stain is non-permeable in intact cells. Nevertheless, it was also shown that neutrophil cell death occurs after much longer incubation with bacteria than used in the NETosis and microscopy assays. Another possibility is neutrophil autofluorescence, which has been observed previously (Monici et al., 1995) and was also utilised as an advantage in quantification of neutrophils in diseases using a label-free approach using 488 nm excitation/525 nm emission (Yakimov et al., 2019). Autofluorescence could also explain a high variation in the NETosis dataset and a high signal in the negative control, as not only NET-DNA signal but also neutrophil fluorescent signals could have been detected. Autofluorescence was, however, not checked without the SYTOX dye and therefore future experiments will need to confirm this hypothesis.

Suspected degradation of cytokines, which was confirmed in *P. gingivalis* (Stathopoulou et al., 2009), was in this study disproved by the time-course cytokine release assay. Further analysis of apoptosis and necrosis showed that none of the subspecies caused premature apoptosis apart from pFNP. However, taking into account that the positive control did not function as intended, data from this assay with respect to the extent of apoptosis must be interpreted with caution. In future experiments, increasing the number of donors may also lead to clearer results, as large interindividual differences were observed between donors. Additionally, more effective positive controls need to be identified for future apoptosis analyses, as finding a reliable apoptosis-inducer in the literature has been challenging. Staurosporine, even though used as inducer of apoptosis, stimulated an unconventional, delayed apoptosis (Franz et al., 2015). Gliotoxin, another apoptosis inducer (Taylor et al., 2007), stimulated apoptosis only in a fraction of a studied neutrophil population (Coméra et al., 2007).

In terms of necrosis, a type of cell death with the highest destructive potential in tissues caused by the uncontrolled release of cytotoxic neutrophil contents, all subspecies caused this form of cell death significantly earlier compared to the positive control. Thus, these results indicate that *F. nucleatum* subspecies trigger an early necrosis in neutrophils, however they do not seem to trigger necrosis in a subspecies-specific manner. Additionally, considering that primary and secondary necrosis have been described (Roth et al., 2015), neutrophils in this study may be undergoing primary necrosis, since secondary necrosis follows apoptosis and the necrotic signals in our assay were detected before apoptosis.

In conclusion, differences in immunogenicity between planktonic and biofilm-grown *F. nucleatum* were identified. *F. nucleatum* subspecies stimulated differential ROS responses, with the most pronounced differences in superoxide generation, which in turn was found to be inversely proportional to cytokine release by neutrophils. Subspecies stimulating the lowest

cytokine release were not found to degrade neutrophil cytokines. Moreover, none of the subspecies was found to conclusively stimulate significantly earlier neutrophil apoptosis or necrosis.

CHAPTER 6: FINAL DISCUSSION AND FUTURE WORK

In this doctoral thesis, functional and molecular responses of primary human neutrophils, an essential group of innate immune cells, towards the key structural oral bacterium and opportunistic pathogen *F. nucleatum*, were investigated. Immunogenicity of planktonic and biofilm modes of growth of individual *F. nucleatum* subspecies were evaluated together with a systematic characterisation of single-subspecies *F. nucleatum* biofilms formed by commercially available ATCC type strains.

Excessive neutrophil responses triggered by *F. nucleatum* have been reported in periodontitis (Matthews et al., 2007a, Ling et al., 2015, Chapple et al., 2023) as well as in CRC (Kong et al., 2023). In these disorders, *F. nucleatum* resides in biofilms (Chen et al., 2022a, Choi et al., 2023), likely expressing biofilm-specific levels of virulence factors (Ali Mohammed et al., 2021). Consequently, it is necessary to utilise biofilm-grown rather than planktonic *F. nucleatum* stimuli in *in vitro* assays to better simulate studied pathologies and obtain more clinically relevant results. Before utilising biofilm-grown *F. nucleatum* subspecies in immunogenicity experiments in the current study, systematic characterisation of single-subspecies biofilm formation was performed using inexpensive and widely available surfaces and surface modifications.

Biofilm analysis showed that *F. nucleatum* subspecies significantly differ in the ability to form biofilms, with FNP not being able to form biofilms in the tested conditions. It is important to highlight that this study utilised the ATCC type strain, which was originally isolated from inflamed gingiva (Dzink et al., 1990). However, previous studies were performed using clinical FNP isolates not only from the oral cavity but also from the gut (Nie et al., 2015, Queen et al., 2022, Ma et al., 2023) and the clinical isolates differed from the type strain in terms of virulence

genes and antimicrobial resistance genes (Ma et al., 2023). While literature studying biofilm formation of clinical FNP isolates is scarce, Queen et al. (2022) studied colonisation of mouse intestine employing two FNP isolates from CRC patients and they reported that the isolates differed in their autoaggregation abilities: the non-aggregating FNP successfully colonised the mice, whereas the strongly autoaggregating isolate failed to colonise the mice. Although this does not directly answer the question of the ability to form biofilms, it clearly shows a high level of heterogeneity in FNP isolates and their behaviours. Future work should compare biofilm formation of FNP isolates from various body sites and if indeed differences are found, their genomes as well as transcriptomes should be compared to identify the presence and expression of genes which could be targeted in biofilm formers in order to prevent biofilm formation.

Following biofilm characterisation, *F. nucleatum* subspecies were studied in the context of immune stimulation in primary human neutrophils as well as a neutrophil-like HL-60 cell line. The initial evaluation of neutrophil responses using formalin-fixed subspecies did not confirm the hypothesis proposing a difference among the *F. nucleatum* subspecies in terms of ROS generation and NET formation. Results obtained from assays using HL-60 cells suggested insufficient differentiation into neutrophil-like cells and thus this cell line was not deemed a reliable model. However, further and more detailed analysis using physiologically more relevant live bacteria in combination with primary neutrophils revealed clear differences in the subspecies' immunogenicity.

Comparison of planktonic and biofilm-grown *F. nucleatum* subspecies showed that biofilm-grown *F. nucleatum* stimulates significantly higher peak and overall ROS release in the case of total (combining intra- and extracellular ROS) and intracellular ROS. Time to peak total ROS was significantly shorter in response to biofilm-grown stimuli. As described in the thesis

introduction, intracellular ROS is crucial for clearance of phagocytosed microorganisms as it is released into the phagolysosome (Nguyen et al., 2017). Extracellular ROS is generated to eliminate extracellular pathogens that cannot be phagocytosed due to their size or high numbers (Dupré-Crochet et al., 2013), however this can lead to tissue damage.

Similarly to our study, Hahn and Gunn (2020) measured differential levels of ROS production by neutrophils when comparing planktonic and biofilm-grown *Salmonella enterica* serovars Typhi and Typhimurium. Interestingly, this was serovar-specific, as *S.* Typhi stimulated a higher ROS response in the biofilm state, while *S.* Typhimurium led to higher ROS release in the planktonic state. In addition, the authors systematically tested EPS produced by biofilm forming *Salmonella* and revealed that specific EPS can modulate neutrophil and macrophage responses. Future studies should assess the immunogenicity of EPS components of *F. nucleatum* biofilms in order to distinguish between bacterial cell-mediated and EPS-mediated virulence.

Stimulation of neutrophil ROS generation by individual subspecies demonstrated that this process is likely subspecies-specific, with most pronounced differences observed in superoxide generation. As mentioned earlier in this thesis, Kurgan et al. (2017) also observed subspecies-specificity in a neutrophil-like cell line, however, they reported opposing results: *F. nucleatum* ssp. *polymorphum* blocked superoxide generation and ssp. *vincentii* triggered the highest amount of superoxide. This difference could be explained by differences in methodology, as this group used a neutrophil-like cell line, while our study analysed the responses of primary human neutrophils, noting that the HL-60 cell line was reported to differ in antimicrobial responses when compared to primary neutrophils (Yaseen et al., 2017). In spite of this discrepancy with our findings, the results show that *F. nucleatum* subspecies significantly differ in their ability to stimulate superoxide generation by neutrophils.

The importance of superoxide stems from the fact that this specific ROS is the primary radical produced in neutrophils both within the cell and extracellularly. Superoxide radicals can react further in a chain reaction, producing other downstream radical species (Nguyen et al., 2017, Fujii et al., 2022). This is especially critical in the extracellular milieu, where excess of superoxide together with other ROS can cause significant oxidative stress and damage proteins, lipids and other crucial biomolecules (Fujii et al., 2022), leading to cell death and tissue damage. Considering that our study demonstrated subspecies-specific production of extracellular superoxide, it can be speculated that individual subspecies have distinct tissue-destructive potential when interacting with neutrophils.

In addition to wild-type *F. nucleatum* subspecies, adhesin FadA- and Fap2-deficient strains were used to identify possible involvement of selected adhesins in *F. nucleatum* virulence. The ΔFap2 strain stimulated levels of superoxide similar to FNV, the subspecies stimulating the lowest superoxide release, yet this was not statistically different from the parental strain. The ΔFadA strain stimulated higher and faster superoxide response in comparison with the parental strain and the ΔFap2 strain, however this was not statistically significant and it most cases the response was significantly lower compared to the subspecies of interest pFNA and pFNP. While stimulation of ROS release has not been studied to date, Ellett et al. (2023) showed that a Fap2 mutant successfully survives in human neutrophils and increases neutrophil velocity during chemotaxis. To the best of the author's knowledge, FadA mutant strain has not been studied in the context of neutrophil responses to date. Even if the adhesin mutants in the present study did not provide possible mechanistic answers explaining differences among the subspecies, future work should explore immunogenicity of mutant strains deficient of the remaining adhesins, such as FomA, RadD or CmpA or combinations of these.

Quantification of NETs revealed that neutrophils released the highest mean amount of NETs upon stimulation with FNP. This finding is in agreement with the results of Hirschfeld and colleagues (2017): the amount of NET-DNA released from neutrophils was higher when stimulated with ssp. *polymorphum* compared to ssp. *nucleatum*, but the difference was not statistically significant, similarly to the current study. Lack of statistical significance in our study was due to considerable inter-donor variation of neutrophil responses. This interindividual variability even in healthy and younger individuals has frequently been reported elsewhere (Yang et al., 2003, Hirschfeld et al., 2015, Hoffmann et al., 2016), and could be overcome by recruiting more neutrophil donors in future studies. Additionally, due to the fact that NET-DNA was quantified spectrofluorometrically, autofluorescence of neutrophils should be considered and potentially a different approach targeting NET-bound proteins should be used in future experiments.

The release of pro-inflammatory cytokines in our study was highly subspecies-specific, with subspecies *vincentii* consistently stimulating the highest levels of cytokine release and subspecies *animalis* and *polymorphum* the lowest, which was inversely correlated to superoxide release. Similar results were obtained by Ling et al. (2015), who measured cytokine release in neutrophils from healthy volunteers and in patients with periodontitis stimulated with FNP, and the concentrations of IL-6, TNF-α and IL-1β measured in their study, despite statistically significant differences, were markedly low. In combination, these results demonstrate the importance of either careful choice of the *F. nucleatum* subspecies used for experimentation, or of inclusion of more than one *F. nucleatum* subspecies in order to obtain clinically relevant results.

Secretion of neutrophil enzymes in this study was not shown to be subspecies-specific. HNE and MMP-9 are stored in the neutrophil granules, ready to be released rapidly upon bacterial

stimulation (Chakrabarti et al., 2006, Zeng et al., 2023). A rapid response was confirmed in this study, as both enzymes were detected in high concentrations as soon as 1 hour post stimulation. Both of these enzymes play a role in the resolution of infection, however, their activities have been reported to negatively affect a number of *F. nucleatum*-related diseases. Hiyoshi et al. (2022) demonstrated that HNE exacerbates periodontitis by breaking the gingival epithelial barrier and contributing to periodontal bone loss. In the context of CRC, HNE from NETs was found to significantly increase the migratory activity of CRC cells *in vitro* and inhibition of HNE activity in mice decreased migration of tumour cells to liver tissue, suggesting that HNE plays a role in the formation of liver metastases in CRC (Okamoto et al., 2023).

MMP-9, which can cause pathological connective tissue destruction, is detected in higher amounts in chronic periodontitis (Bildt et al., 2008, Luchian et al., 2022). Higher levels of MMP-9 were quantified in the saliva of patients with earlier stages of periodontitis (localised periodontitis), compared to later stages (generalised periodontitis) (Gursoy et al., 2013). Additionally, increased levels were also measured in gingival crevicular fluid in the early stages of periodontitis (Luchian et al., 2022). Considering that all *F. nucleatum* subspecies stimulated a considerably higher release of MMP-9 from neutrophils and that MMP-9 seems to be highly expressed early in periodontitis, future studies could focus on correlations between MMP-9 level and number of *F. nucleatum* ssp. present in periodontal lesions, shedding more light on the role of *F. nucleatum* subspecies in periodontitis onset.

Analysis of CRC tumour tissues showed that the expression of MMP-9 is significantly higher compared to the adjacent healthy tissue. Moreover, there was a strong correlation between high MMP-9 expression and pathological parameters such as lymph node and distant metastasis as well as poorer patient survival (Wang et al., 2019). MMP-9 produced by tumours was reported to promote breast cancer progression, metastasis and angiogenesis (Mehner et al., 2014, Guo et

al., 2024). Considering that tumour-associated neutrophils were found to be major producers of MMP-9 in tumour tissues (Deryugina et al., 2014) and *F. nucleatum* translocates to breast tissues, colonises them and plays a role in breast cancer metastasis (Guo et al., 2024), the influence of *F. nucleatum*-stimulated MMP-9 release by neutrophils should not be overlooked in future cancer studies.

This study also investigated the potential ability of ssp. *animalis* and *polymorphum* to degrade pro-inflammatory cytokines. Analysis of time-course cytokine release indicated that the selected subspecies did not seem to degrade cytokines released by neutrophils as was initially hypothesised based on the end-point cytokine quantification. This could be explained by the fact that *F. nucleatum* does not produce gingipains (Farrugia et al., 2022), proteases used by *P. gingivalis* to degrade cytokines (Stathopoulou et al., 2009). Taking together the low cytokine release stimulation with concurrent high superoxide generation in response to ssp. *animalis* and *polymorphum*, it was hypothesised that these subspecies trigger premature disorderly death (necrosis) of neutrophils. This hypothesis was supported by the fact that extracellularly produced superoxide can be pumped back inside the cell, where it can cause oxidative cell damage and potentially cell death if produced excessively (Fujii et al., 2022).

Subsequent analysis of the start of necrosis, however, did not show significant differences in the selected subspecies, except ssp. *animalis*, which stimulated necrosis significantly earlier than ssp. *fusiforme*. Analysis of the rate of necrosis also indicated no differences among the subspecies. Analysis of apoptosis, a controlled cell death, was performed as a comparison with necrosis. FNP was found to stimulate apoptosis significantly earlier compared to the remaining subspecies, while there were no differences in the rate of apoptosis. Nevertheless, a different type of cell death cannot be excluded as in addition to apoptosis and necrosis, neutrophils were reported to undergo necroptosis and pyroptosis (Pérez-Figueroa et al., 2021). Necroptosis is

also a programmed cell death, however the cells do not undergo apoptosis-specific morphological changes and DNA is not fragmented in the process. Stimulation of TLRs has been reported as one of the necroptosis pathway activators (Pérez-Figueroa et al., 2021). Costigan et al. (2023) described a protocol utilising phase-contrast microscopy to distinguish between necrosis and necroptosis using specific necroptosis inhibitors called necrostatins, however there is no commercial quantification kit available. Pyroptosis relies on caspase-1, a protease not utilised in apoptosis, and a complex of proteins called inflammasome. During pyroptosis, pores in the plasma membrane are formed via the activity of caspase-1, DNA is fragmented and the cell is osmotically lysed, releasing pro-inflammatory contents (Pérez-Figueroa et al., 2021). Annexin V, also used in this study to quantify apoptosis, does not discriminate between apoptosis and pyroptosis (Yu et al., 2021), therefore this kind of cell death cannot be ruled out in our study.

Apart from considering cell death, based on the patterns observed, it can be further speculated that these subspecies may modulate cytokine production, potentially at the transcriptional level. Wright et al. (2011) studied transcriptional regulation by ssp. *polymorphum* in human neutrophils and revealed that neutrophils stimulated with this subspecies upregulated genes for cytokines CXCL-1, CXCL-2 and CXCL-3. However, a comparison with the remaining subspecies was not performed, therefore future work should include comparisons of individual *F. nucleatum* subspecies and their ability to modulate neutrophil pro-inflammatory gene expression.

In an excessive response, release of ROS from neutrophils into the surrounding tissue creates oxidative stress, which leads to tissue damage. Products of host tissue damage serve as nutrients for pathogens resident in this niche, exemplified by the thriving pathogenic community in periodontal pockets (Gasmi Benahmed et al., 2022). Multiple pathogens have developed

protective mechanisms, such as antioxidant generation, in response to ROS attack (Li et al., 2021). Based on our results and current literature, it is possible that *F. nucleatum* ssp. *animalis* and *polymorphum* act as more pathogenic subspecies, stimulating higher superoxide release in order to liberate more nutrients during oxidative tissue damage whilst resisting ROS-related killing by neutrophils. Survival of *F. nucleatum* ssp. *nucleatum* and *polymorphum* in human neutrophils was shown by Ellett et al. (2023), which may support this hypothesis.

Interestingly, a recent study by Krieger et al. (2024) focusing on the presence of *F. nucleatum* subspecies in healthy dental plaque and disease-related odontogenic abscesses showed distinct subspecies patterns. Ssp. *animalis* was more abundant in the abscess specimens while ssp. *polymorphum* was more abundant in dental plaque, suggesting that they differ in virulence and thus not support our hypothesis. However, the samples analysed were obtained from paediatric dental patients, collecting supragingival plaque and abscess samples during tooth extraction, which may not be comparable to the inflammatory environment in periodontal pockets and responses of an adult immune system.

Considering subspecies *animalis* and *polymorphum* stimulated very low levels of pro-inflammatory cytokines, they may be able to evade immune clearance by downregulating the expression of neutrophil cytokines, which are important in activating and recruiting additional leukocytes (Fernando et al., 2014, Tecchio et al., 2014, Wajant and Siegmund, 2019). It is conceivable that ssp. *vincentii*, which stimulates very low superoxide and high cytokine production, might be much less virulent, not stimulating excessive oxidative stress and facilitating immune clearance by attracting leukocytes to the site of infection via increased pro-inflammatory cytokine release. In future studies of *F. nucleatum* pathogenicity, it would be interesting to explore whether ssp. *vincentii* and the remaining subspecies survive neutrophil

phagocytosis or whether they can be cleared successfully, which can further support the hypothesis of subspecies-specific virulence.

In conclusion, the findings of this doctoral project contributed to understanding of *F. nucleatum* single-subspecies biofilm formation, which has not been previously evaluated comparing all subspecies. While it is clinically relevant to study *F. nucleatum* in multi-species biofilms, information obtained from single-subspecies *F. nucleatum* biofilms without the presence of additional binding partners is necessary for better understanding of biofilm-related immunogenic and pathogenic properties of *F. nucleatum* subspecies and virulence factor expression. Moreover, significant differences in neutrophil antimicrobial responses towards individual subspecies were identified. More detailed understanding of *F. nucleatum* subspecies-specific immunogenicity, virulence properties and interaction with neutrophils can help identify both bacterial and neutrophil therapeutic targets not only in periodontal disease, but also in *F. nucleatum*-related systemic diseases.

REFERENCES

Abed, J., Emgård, Johanna E. M., Zamir, G., Faroja, M., Almogy, G., Grenov, A., Sol, A., Naor, R., Pikarsky, E., Atlan, Karine A., Mellul, A., Chaushu, S., Manson, Abigail L., Earl, Ashlee M., Ou, N., Brennan, Caitlin A., Garrett, Wendy S. and Bachrach, G. (2016) 'Fap2 Mediates *Fusobacterium nucleatum* Colorectal Adenocarcinoma Enrichment by Binding to Tumor-Expressed Gal-GalNAc', *Cell Host & Microbe,* 20(2), pp. 215-225. DOI: 10.1016/j.chom.2016.07.006.

Alemán, O. R., Mora, N., Cortes-Vieyra, R., Uribe-Querol, E. and Rosales, C. (2016) 'Differential Use of Human Neutrophil Fcγ Receptors for Inducing Neutrophil Extracellular Trap Formation', *Journal of Immunology Research,* 2016, pp. 2908034-2908034. DOI: 10.1155/2016/2908034.

Ali Mohammed, M. M., Pettersen, V. K., Nerland, A. H., Wiker, H. G. and Bakken, V. (2021) 'Label-free quantitative proteomic analysis of the oral bacteria *Fusobacterium nucleatum* and *Porphyromonas gingivalis* to identify protein features relevant in biofilm formation', *Anaerobe,* 72, pp. 102449. DOI: 10.1016/j.anaerobe.2021.102449.

Amulic, B., Cazalet, C., Hayes, G. L., Metzler, K. D. and Zychlinsky, A. (2012) 'Neutrophil Function: From Mechanisms to Disease', *Annual Review of Immunology,* 30(1), pp. 459-489. DOI: 10.1146/annurev-immunol-020711-074942.

Babatunde, K. A., Wang, X., Hopke, A., Lannes, N., Mantel, P.-Y. and Irimia, D. (2021) 'Chemotaxis and swarming in differentiated HL-60 neutrophil-like cells', *Scientific Reports,* 11(1), pp. 778. DOI: 10.1038/s41598-020-78854-6.

Babu, J. P., Dean, J. W. and Pabst, M. J. (1995) 'Attachment of *Fusobacterium nucleatum* to fibronectin immobilized on gingival epithelial cells or glass coverslips', *Journal of Periodontology,* 66(4), pp. 285-90. DOI: 10.1902/jop.1995.66.4.285.

Basic, A., Blomqvist, M., Dahlén, G. and Svensäter, G. (2017) 'The proteins of *Fusobacterium* spp. involved in hydrogen sulfide production from L-cysteine', *BMC Microbiology,* 17(1), pp. 61. DOI: 10.1186/s12866-017-0967-9.

Basu, J., Madhulika, S., Murmu, K. C., Mohanty, S., Samal, P., Das, A., Mahapatra, S., Saha, S., Sinha, I. and Prasad, P. (2023) 'Molecular and epigenetic alterations in normal and malignant myelopoiesis in human leukemia 60 (HL60) promyelocytic cell line model', *Frontiers in Cell and Developmental Biology,* 11. DOI: 10.3389/fcell.2023.1060537.

Batot, G., Martel, C., Capdeville, N., Wientjes, F. and Morel, F. (1995) 'Characterization of Neutrophil NADPH Oxidase Activity Reconstituted in a Cell-Free Assay Using Specific Monoclonal Antibodies Raised Against Cytochrome b558', *European Journal of Biochemistry,* 234(1), pp. 208-215. DOI: 10.1111/j.1432-1033.1995.208_c.x.

Baxter, S. S., Carlson, L. A., Mayer, A. M. S., Hall, M. L. and Fay, M. J. (2009) 'Granulocytic differentiation of HL-60 promyelocytic leukemia cells is associated with increased expression of Cul5', *In Vitro Cellular & Developmental Biology - Animal,* 45(5), pp. 264-274. DOI: 10.1007/s11626-008-9163-4.

Becker, P., Hufnagle, W., Peters, G. and Herrmann, M. (2001) 'Detection of differential gene expression in biofilm-forming versus planktonic populations of *Staphylococcus aureus* using micro-representational-difference analysis', *Applied and Environmental Microbiology,* 67(7), pp. 2958-65. DOI: 10.1128/aem.67.7.2958-2965.2001.

Bedouhène, S., Moulti-Mati, F., Hurtado-Nedelec, M., Dang, P. M.-C. and El-Benna, J. (2017) 'Luminol-amplified chemiluminescence detects mainly superoxide anion produced by human neutrophils', *American Journal of Blood Research,* 7(4), pp. 41-48.

Bello, A. B., Kim, D., Kim, D., Park, H. and Lee, S.-H. (2020) 'Engineering and Functionalization of Gelatin Biomaterials: From Cell Culture to Medical Applications', *Tissue Engineering Part B: Reviews,* 26(2), pp. 164-180. DOI: 10.1089/ten.teb.2019.0256.

Benn, G., Pyne, A. L. B., Ryadnov, M. G. and Hoogenboom, B. W. (2019) 'Imaging live bacteria at the nanoscale: comparison of immobilisation strategies', *Analyst,* 144(23), pp. 6944-6952. DOI: 10.1039/C9AN01185D.

Bert, S., Ward, E. J. and Nadkarni, S. (2021) 'Neutrophils in pregnancy: New insights into innate and adaptive immune regulation', *Immunology,* 164(4), pp. 665-676. DOI: 10.1111/imm.13392.

Bhakta, S. B., Lundgren, S. M., Sesti, B. N., Flores, B. A., Akdogan, E., Collins, S. R. and Mercer, F. (2024) 'Neutrophil-like cells derived from the HL-60 cell-line as a genetically-tractable model for neutrophil degranulation', *PloS One,* 19(2), pp. e0297758. DOI: 10.1371/journal.pone.0297758.

Bildt, M. M., Bloemen, M., Kuijpers-Jagtman, A. M. and Von den Hoff, J. W. (2008) 'Collagenolytic Fragments and Active Gelatinase Complexes in Periodontitis', *Journal of Periodontology,* 79(9), pp. 1704-1711. DOI: 10.1902/jop.2008.080021.

Birnie, G. D. (1988) 'The HL60 cell line: a model system for studying human myeloid cell differentiation', *British Journal of Cancer. Supplement,* 9, pp. 41-5.

Blanter, M., Gouwy, M. and Struyf, S. (2021) 'Studying Neutrophil Function *in vitro*: Cell Models and Environmental Factors', *Journal of Inflammation Research,* 14, pp. 141-162. DOI: 10.2147/JIR.S284941.

Blum, M., Chang, H. Y., Chuguransky, S., Grego, T., Kandasaamy, S., Mitchell, A., Nuka, G., Paysan-Lafosse, T., Qureshi, M., Raj, S., Richardson, L., Salazar, G. A., Williams, L., Bork, P., Bridge, A., Gough, J., Haft, D. H., Letunic, I., Marchler-Bauer, A., Mi, H., Natale, D. A., Necci, M., Orengo, C. A., Pandurangan, A. P., Rivoire, C., Sigrist, C. J. A., Sillitoe, I., Thanki, N., Thomas, P. D., Tosatto, S. C. E., Wu, C. H., Bateman, A. and Finn, R. D. (2021) 'The InterPro protein families and domains database: 20 years on', *Nucleic Acids Research,* 49(D1), pp. D344-d354. DOI: 10.1093/nar/gkaa977.

Boero, E., Brinkman, I., Juliet, T., van Yperen, E., van Strijp, J. A. G., Rooijakkers, S. H. M. and van Kessel, K. P. M. (2021) 'Use of Flow Cytometry to Evaluate Phagocytosis of

Staphylococcus aureus by Human Neutrophils', *Frontiers in Immunology,* 12. DOI: 10.3389/fimmu.2021.635825.

Bonacorsi, S., Visseaux, B., Bouzid, D., Pareja, J., Rao, S. N., Manissero, D., Hansen, G. and Vila, J. (2021) 'Systematic Review on the Correlation of Quantitative PCR Cycle Threshold Values of Gastrointestinal Pathogens With Patient Clinical Presentation and Outcomes', *Frontiers in Medicine (Lausanne),* 8, pp. 711809. DOI: 10.3389/fmed.2021.711809.

Bouchery, T. and Harris, N. (2019) 'Neutrophil–macrophage cooperation and its impact on tissue repair', *Immunology and Cell Biology,* 97(3), pp. 289-298. DOI: 10.1111/imcb.12241.

Branger, J., Knapp, S., Weijer, S., Leemans, J. C., Pater, J. M., Speelman, P., Florquin, S. and van der Poll, T. (2004) 'Role of Toll-like receptor 4 in gram-positive and gram-negative pneumonia in mice', *Infection and Immunity,* 72(2), pp. 788-794. DOI: 10.1128/iai.72.2.788-794.2004.

Branzk, N., Lubojemska, A., Hardison, S. E., Wang, Q., Gutierrez, M. G., Brown, G. D. and Papayannopoulos, V. (2014) 'Neutrophils sense microbe size and selectively release neutrophil extracellular traps in response to large pathogens', *Nature Immunology,* 15(11), pp. 1017-25. DOI: 10.1038/ni.2987.

Breitman, T. R., Selonick, S. E. and Collins, S. J. (1980) 'Induction of differentiation of the human promyelocytic leukemia cell line (HL-60) by retinoic acid', 77(5), pp. 2936-2940. DOI: doi:10.1073/pnas.77.5.2936.

Brennan, C. A. and Garrett, W. S. (2019) '*Fusobacterium nucleatum* - symbiont, opportunist and oncobacterium', *Nature Reviews: Microbiology,* 17(3), pp. 156-166. DOI: 10.1038/s41579-018-0129-6.

Bridier, A., Dubois-Brissonnet, F., Boubetra, A., Thomas, V. and Briandet, R. (2010) 'The biofilm architecture of sixty opportunistic pathogens deciphered using a high throughput CLSM method', *Journal of Microbiological Methods,* 82(1), pp. 64-70. DOI: 10.1016/j.mimet.2010.04.006.

Brinkmann, V., Reichard, U., Goosmann, C., Fauler, B., Uhlemann, Y., Weiss, D. S., Weinrauch, Y. and Zychlinsky, A. (2004) 'Neutrophil extracellular traps kill bacteria', *Science,* 303(5663), pp. 1532-5. DOI: 10.1126/science.1092385.

Bujold, A. R., Labrie, J., Jacques, M. and MacInnes, J. I. (2016) 'Differential expression of putative adhesin genes of *Actinobacillus suis* grown in *in vivo*-like conditions', *Veterinary Microbiology,* 195, pp. 60-69. DOI: 10.1016/j.vetmic.2016.09.005.

Carvalho, É. B. S., Romandini, M., Sadilina, S., Sant'Ana, A. C. P. and Sanz, M. (2023) 'Microbiota associated with peri-implantitis—A systematic review with meta-analyses', *Clinical Oral Implants Research,* 34(11), pp. 1176-1187. DOI: 10.1111/clr.14153.

Cassatella, M. A. (1995) 'The production of cytokines by polymorphonuclear neutrophils', *Immunology Today,* 16(1), pp. 21-26. DOI: 10.1016/0167-5699(95)80066-2.

Cassatella, M. A., Östberg, N. K., Tamassia, N. and Soehnlein, O. (2019) 'Biological Roles of Neutrophil-Derived Granule Proteins and Cytokines', *Trends in Immunology,* 40(7), pp. 648-664. DOI: 10.1016/j.it.2019.05.003.

Chakrabarti, S., Zee, J. M. and Patel, K. D. (2006) 'Regulation of matrix metalloproteinase-9 (MMP-9) in TNF-stimulated neutrophils: novel pathways for tertiary granule release', *Journal of Leukocyte Biology,* 79(1), pp. 214-222. DOI: 10.1189/jlb.0605353.

Chapple, I. L. C., Hirschfeld, J., Kantarci, A., Wilensky, A. and Shapira, L. (2023) 'The role of the host—Neutrophil biology', *Periodontology 2000,* 00, pp. 1-47. DOI: 10.1111/prd.12490.

Chapple, I. L. C., Mealey, B. L., Van Dyke, T. E., Bartold, P. M., Dommisch, H., Eickholz, P., Geisinger, M. L., Genco, R. J., Glogauer, M., Goldstein, M., Griffin, T. J., Holmstrup, P., Johnson, G. K., Kapila, Y., Lang, N. P., Meyle, J., Murakami, S., Plemons, J., Romito, G. A., Shapira, L., Tatakis, D. N., Teughels, W., Trombelli, L., Walter, C., Wimmer, G., Xenoudi, P. and Yoshie, H. (2018) 'Periodontal health and gingival diseases and conditions on an intact and a reduced periodontium: Consensus report of workgroup 1 of the 2017 World Workshop on the Classification of Periodontal and Peri-Implant Diseases and Conditions', *Journal of Periodontology,* 89(S1), pp. S74-S84. DOI: 10.1002/JPER.17-0719.

Chen, X., Sun, Y., Zhang, T., Shu, L., Roepstorff, P. and Yang, F. (2021) 'Quantitative Proteomics Using Isobaric Labeling: A Practical Guide', *Genomics, Proteomics & Bioinformatics,* 19(5), pp. 689-706. DOI: 10.1016/j.gpb.2021.08.012.

Chen, Y., Huang, Z., Tang, Z., Huang, Y., Huang, M., Liu, H., Ziebolz, D., Schmalz, G., Jia, B. and Zhao, J. (2022a) 'More Than Just a Periodontal Pathogen –the Research Progress on *Fusobacterium nucleatum*', *Frontiers in Cellular and Infection Microbiology,* 12. DOI: 10.3389/fcimb.2022.815318.

Chen, Y., Shi, T., Li, Y., Huang, L. and Yin, D. (2022b) '*Fusobacterium nucleatum*: The Opportunistic Pathogen of Periodontal and Peri-Implant Diseases', *Frontiers in Microbiology,* 13. DOI: 10.3389/fmicb.2022.860149.

Chew, J., Zilm, P. S., Fuss, J. M. and Gully, N. J. (2012) 'A proteomic investigation of *Fusobacterium nucleatum* alkaline-induced biofilms', *BMC Microbiology,* 12(1), pp. 189. DOI: 10.1186/1471-2180-12-189.

Choi, E., Murray, B. and Choi, S. (2023) 'Biofilm and Cancer: Interactions and Future Directions for Cancer Therapy', *International Journal of Molecular Sciences,* 24(16), pp. 12836. DOI: 10.3390/ijms241612836.

Collins, S. J., Gallo, R. C. and Gallagher, R. E. (1977) 'Continuous growth and differentiation of human myeloid leukaemic cells in suspension culture', *Nature,* 270(5635), pp. 347-9. DOI: 10.1038/270347a0.

Coméra, C., André, K., Laffitte, J., Collet, X., Galtier, P. and Maridonneau-Parini, I. (2007) 'Gliotoxin from *Aspergillus fumigatus* affects phagocytosis and the organization of the

actin cytoskeleton by distinct signalling pathways in human neutrophils', *Microbes and Infection,* 9(1), pp. 47-54. DOI: 10.1016/j.micinf.2006.10.009.

Coppenhagen-Glazer, S., Sol, A., Abed, J., Naor, R., Zhang, X., Han, Y. W. and Bachrach, G. (2015) 'Fap2 of *Fusobacterium nucleatum* is a galactose-inhibitable adhesin involved in coaggregation, cell adhesion, and preterm birth', *Infection and Immunity,* 83(3), pp. 1104-13. DOI: 10.1128/IAI.02838-14.

Cortés-Vieyra, R., Rosales, C. and Uribe-Querol, E. (2016) 'Neutrophil Functions in Periodontal Homeostasis', *Journal of Immunology Research,* 2016, pp. 1396106. DOI: 10.1155/2016/1396106.

Costigan, A., Hollville, E. and Martin, S. J. (2023) 'Discriminating Between Apoptosis, Necrosis, Necroptosis, and Ferroptosis by Microscopy and Flow Cytometry', *Current Protocols,* 3(12), pp. e951. DOI: 10.1002/cpz1.951.

Cowan, S. E., Liepmann, D. and Keasling, J. D. (2001) 'Development of engineered biofilms on poly- L-lysine patterned surfaces', *Biotechnology Letters,* 23(15), pp. 1235-1241. DOI: 10.1023/A:1010581503842.

Dassanayake, R. P., Falkenberg, S. M., Stasko, J. A., Shircliff, A. L., Lippolis, J. D. and Briggs, R. E. (2020) 'Identification of a reliable fixative solution to preserve the complex architecture of bacterial biofilms for scanning electron microscopy evaluation', *PloS One,* 15(5), pp. e0233973. DOI: 10.1371/journal.pone.0233973.

De Alessandris, S., Ferguson, G. J., Dodd, A. J., Juss, J. K., Devaprasad, A., Piper, S., Wyatt, O., Killick, H., Corkill, D. J., Cohen, E. S., Pandit, A., Radstake, T., Simmonds, R., Condliffe, A. M., Sleeman, M. A., Cowburn, A. S., Finch, D. K. and Chilvers, E. R. (2019) 'Neutrophil GM-CSF receptor dynamics in acute lung injury', *Journal of Leukocyte Biology,* 105(6), pp. 1183-1194. DOI: 10.1002/jlb.3ma0918-347r.

de Andrade, K. Q., Almeida-da-Silva, C. L. C. and Coutinho-Silva, R. (2019) 'Immunological Pathways Triggered by *Porphyromonas gingivalis* and *Fusobacterium nucleatum*: Therapeutic Possibilities?', *Mediators of Inflammation,* 2019, pp. 7241312. DOI: 10.1155/2019/7241312.

de Bruin, O. M. and Birnboim, H. C. (2016) 'A method for assessing efficiency of bacterial cell disruption and DNA release', *BMC Microbiology,* 16(1), pp. 197. DOI: 10.1186/s12866-016-0815-3.

de Buhr, N. and von Köckritz-Blickwede, M. (2016) 'How Neutrophil Extracellular Traps Become Visible', *Journal of Immunology Research,* 2016, pp. 4604713. DOI: 10.1155/2016/4604713.

De Paoli, P. (2005) 'Bio-banking in microbiology: from sample collection to epidemiology, diagnosis and research', *FEMS Microbiology Reviews,* 29(5), pp. 897-910. DOI: 10.1016/j.femsre.2005.01.005.

Deryugina, E. I., Zajac, E., Juncker-Jensen, A., Kupriyanova, T. A., Welter, L. and Quigley, J. P. (2014) 'Tissue-Infiltrating Neutrophils Constitute the Major In Vivo Source of

Angiogenesis-Inducing MMP-9 in the Tumor Microenvironment', *Neoplasia,* 16(10), pp. 771-788. DOI: 10.1016/j.neo.2014.08.013.

Diaz, P. I. and Valm, A. M. (2020) 'Microbial Interactions in Oral Communities Mediate Emergent Biofilm Properties', *Journal of Dental Research,* 99(1), pp. 18-25. DOI: 10.1177/0022034519880157.

Dorman, M. J. and Thomson, N. R. (2020) "Community evolution' - laboratory strains and pedigrees in the age of genomics', *Microbiology (Reading, England),* 166(3), pp. 233-238. DOI: 10.1099/mic.0.000869.

Doucet, J., Zhao, A., Fu, J. and Avrameas, A. (2013) 'Development and Validation of an ELISA at Acidic pH for the Quantitative Determination of IL-13 in Human Plasma and Serum', *Disease Markers,* 35(5), pp. 290670. DOI: 10.1155/2013/290670.

Dupré-Crochet, S., Erard, M. and Nüβe, O. (2013) 'ROS production in phagocytes: why, when, and where?', *Journal of Leukocyte Biology,* 94(4), pp. 657-670. DOI: 10.1189/jlb.1012544.

Dzink, J. L., Sheenan, M. T. and Socransky, S. S. (1990) 'Proposal of three subspecies of *Fusobacterium nucleatum* Knorr 1922: *Fusobacterium nucleatum* subsp. *nucleatum* subsp. nov., comb. nov.; *Fusobacterium nucleatum* subsp. *polymorphum* subsp. nov., nom. rev., comb. nov.; and *Fusobacterium nucleatum* subsp. *vincentii* subsp. nov., nom. rev., comb. nov', *International Journal of Systematic Bacteriology,* 40(1), pp. 74-8. DOI: 10.1099/00207713-40-1-74.

Eichelberger, K. R. and Goldman, W. E. (2020) 'Manipulating neutrophil degranulation as a bacterial virulence strategy', *PLoS Pathogens,* 16(12), pp. e1009054. DOI: 10.1371/journal.ppat.1009054.

Ellett, F., Kacamak, N. I., Alvarez, C. R., Oliveira, E. H. S., Hasturk, H., Paster, B. J., Kantarci, A. and Irimia, D. (2023) '*Fusobacterium nucleatum* dissemination by neutrophils', *Journal of Oral Microbiology,* 15(1), pp. 2217067. DOI: 10.1080/20002297.2023.2217067.

Erchick, D. J., Rai, B., Agrawal, N. K., Khatry, S. K., Katz, J., LeClerq, S. C., Reynolds, M. A. and Mullany, L. C. (2019) 'Oral hygiene, prevalence of gingivitis, and associated risk factors among pregnant women in Sarlahi District, Nepal', *BMC Oral Health,* 19(1), pp. 2. DOI: 10.1186/s12903-018-0681-5.

Fan, Z., Tang, P., Li, C., Yang, Q., Xu, Y., Su, C. and Li, L. (2023) '*Fusobacterium nucleatum* and its associated systemic diseases: epidemiologic studies and possible mechanisms', *Journal of Oral Microbiology,* 15(1), pp. 2145729. DOI: 10.1080/20002297.2022.2145729.

Farrugia, C., Stafford, G. P., Gains, A. F., Cutts, A. R. and Murdoch, C. (2022) '*Fusobacterium nucleatum* mediates endothelial damage and increased permeability following single species and polymicrobial infection', *Journal of Periodontology,* 93(9), pp. 1421-1433. DOI: 10.1002/jper.21-0671.

Fernando, M. R., Reyes, J. L., Iannuzzi, J., Leung, G. and McKay, D. M. (2014) 'The pro-inflammatory cytokine, interleukin-6, enhances the polarization of alternatively activated macrophages', *PloS One,* 9(4), pp. e94188. DOI: 10.1371/journal.pone.0094188.

Filep, J. G. (2022) 'Targeting Neutrophils for Promoting the Resolution of Inflammation', *Frontiers in Immunology,* 13. DOI: 10.3389/fimmu.2022.866747.

Franz, S., Muñoz, L. E., Heyder, P., Herrmann, M. and Schiller, M. (2015) 'Unconventional apoptosis of polymorphonuclear neutrophils (PMN): staurosporine delays exposure of phosphatidylserine and prevents phagocytosis by MΦ-2 macrophages of PMN', *Clinical and Experimental Immunology,* 179(1), pp. 75-84. DOI: 10.1111/cei.12412.

Fu, X., Liu, H., Huang, G. and Dai, S. S. (2021) 'The emerging role of neutrophils in autoimmune-associated disorders: effector, predictor, and therapeutic targets', *MedComm (2020),* 2(3), pp. 402-413. DOI: 10.1002/mco2.69.

Fuchs, T. A., Abed, U., Goosmann, C., Hurwitz, R., Schulze, I., Wahn, V., Weinrauch, Y., Brinkmann, V. and Zychlinsky, A. (2007) 'Novel cell death program leads to neutrophil extracellular traps', *Journal of Cell Biology,* 176(2), pp. 231-41. DOI: 10.1083/jcb.200606027.

Fujii, J., Homma, T. and Osaki, T. (2022) 'Superoxide Radicals in the Execution of Cell Death', *Antioxidants (Basel),* 11(3), pp. 501. DOI: 10.3390/antiox11030501.

Futosi, K., Fodor, S. and Mócsai, A. (2013) 'Neutrophil cell surface receptors and their intracellular signal transduction pathways', *International Immunopharmacology,* 17(3), pp. 638-50. DOI: 10.1016/j.intimp.2013.06.034.

Gasmi Benahmed, A., Kumar Mujawdiya, P., Noor, S. and Gasmi, A. (2022) '*Porphyromonas gingivalis* in the Development of Periodontitis: Impact on Dysbiosis and Inflammation', *Archives of Razi Institute,* 77(5), pp. 1539-1551. DOI: 10.22092/ari.2021.356596.1875.

Gharbia, S. E. and Shah, H. N. (1990) 'Heterogeneity within *Fusobacterium nucleatum*, proposal of four subspecies', *Letters in Applied Microbiology,* 10(2), pp. 105-108. DOI: 10.1111/j.1472-765X.1990.tb00276.x.

Gharbia, S. E. and Shah, H. N. (1992) '*Fusobacterium nucleatum* subsp. *fusiforme* subsp. *nov*. and *Fusobacterium nucleatum* subsp. *animalis* subsp. *nov*. as additional subspecies within *Fusobacterium nucleatum*', *International Journal of Systematic Bacteriology,* 42(2), pp. 296-8. DOI: 10.1099/00207713-42-2-296.

Gharbia, S. E., Shah, H. N., Lawson, P. A. and Haapasalo, M. (1990) 'The distribution and frequency of *Fusobacterium nucleatum* subspecies in the human oral cavity', *Oral Microbiology and Immunology,* 5(6), pp. 324-327. DOI: 10.1111/j.1399-302X.1990.tb00434.x.

Golenberg, E. M., Bickel, A. and Weihs, P. (1996) 'Effect of Highly Fragmented DNA on PCR', *Nucleic Acids Research,* 24(24), pp. 5026-5033. DOI: 10.1093/nar/24.24.5026 %J Nucleic Acids Research.

Granton, E., Brown, L., Defaye, M., Moazen, P., Almblad, H., Randall, T. E., Rich, J. D., Geppert, A., Abdullah, N. S., Hassanabad, M. F., Hiroki, C. H., Farias, R., Nguyen, A. P., Schubert, C., Lou, Y., Andonegui, G., Iftinca, M., Raju, D., Vargas, M. A., Howell, P. L., Füzesi, T., Bains, J., Kurrasch, D., Harrison, J. J., Altier, C. and Yipp, B. G. (2024) 'Biofilm exopolysaccharides alter sensory-neuron-mediated sickness during lung infection', *Cell,* 187(8), pp. 1874-1888.e14. DOI: 10.1016/j.cell.2024.03.001.

Gray, R. D., Lucas, C. D., MacKellar, A., Li, F., Hiersemenzel, K., Haslett, C., Davidson, D. J. and Rossi, A. G. (2013) 'Activation of conventional protein kinase C (PKC) is critical in the generation of human neutrophil extracellular traps', *Journal of Inflammation,* 10(1), pp. 12. DOI: 10.1186/1476-9255-10-12.

Guo, L., Shokeen, B., He, X., Shi, W. and Lux, R. (2017) '*Streptococcus mutans* SpaP binds to RadD of *Fusobacterium nucleatum* ssp. *polymorphum*', *Molecular Oral Microbiology,* 32(5), pp. 355-364. DOI: 10.1111/omi.12177.

Guo, X., Yu, K. and Huang, R. (2024) 'The ways *Fusobacterium nucleatum* translocate to breast tissue and contribute to breast cancer development', *Molecular Oral Microbiology,* 39(1), pp. 1-11. DOI: 10.1111/omi.12446.

Guo, Y., Gao, F., Wang, Q., Wang, K., Pan, S., Pan, Z., Xu, S., Li, L. and Zhao, D. (2021) 'Differentiation of HL-60 cells in serum-free hematopoietic cell media enhances the production of neutrophil extracellular traps', *Experimental and Therapeutic Medicine,* 21(4), pp. 353. DOI: 10.3892/etm.2021.9784.

Gur, C., Ibrahim, Y., Isaacson, B., Yamin, R., Abed, J., Gamliel, M., Enk, J., Bar-On, Y., Stanietsky-Kaynan, N., Coppenhagen-Glazer, S., Shussman, N., Almogy, G., Cuapio, A., Hofer, E., Mevorach, D., Tabib, A., Ortenberg, R., Markel, G., Miklic, K., Jonjic, S., Brennan, C. A., Garrett, W. S., Bachrach, G. and Mandelboim, O. (2015) 'Binding of the Fap2 protein of *Fusobacterium nucleatum* to human inhibitory receptor TIGIT protects tumors from immune cell attack', *Immunity,* 42(2), pp. 344-355. DOI: 10.1016/j.immuni.2015.01.010.

Gursoy, U. K., Könönen, E., Huumonen, S., Tervahartiala, T., Pussinen, P. J., Suominen, A. L. and Sorsa, T. (2013) 'Salivary type I collagen degradation end-products and related matrix metalloproteinases in periodontitis', *Journal of Clinical Periodontology,* 40(1), pp. 18-25. DOI: 10.1111/jcpe.12020.

Hahn, M. M. and Gunn, J. S. (2020) '*Salmonella* Extracellular Polymeric Substances Modulate Innate Phagocyte Activity and Enhance Tolerance of Biofilm-Associated Bacteria to Oxidative Stress', *Microorganisms,* 8(2), pp. 253. DOI: 10.3390/microorganisms8020253.

Han, Y. W. (2015) '*Fusobacterium nucleatum*: a commensal-turned pathogen', *Current Opinion in Microbiology,* 23, pp. 141-147. DOI: 10.1016/j.mib.2014.11.013.

Han, Y. W., Fardini, Y., Chen, C., Iacampo, K. G., Peraino, V. A., Shamonki, J. M. and Redline, R. W. (2010) 'Term stillbirth caused by oral *Fusobacterium nucleatum*', *Obstetrics & Gynecology,* 115(2 Pt 2), pp. 442-445. DOI: 10.1097/AOG.0b013e3181cb9955.

Han, Y. W., Ikegami, A., Rajanna, C., Kawsar, H. I., Zhou, Y., Li, M., Sojar, H. T., Genco, R. J., Kuramitsu, H. K. and Deng, C. X. (2005) 'Identification and characterization of a novel adhesin unique to oral fusobacteria', *Journal of Bacteriology,* 187(15), pp. 5330-40. DOI: 10.1128/jb.187.15.5330-5340.2005.

Han, Y. W., Shi, W., Huang, G. T., Kinder Haake, S., Park, N. H., Kuramitsu, H. and Genco, R. J. (2000) 'Interactions between periodontal bacteria and human oral epithelial cells: *Fusobacterium nucleatum* adheres to and invades epithelial cells', *Infection and Immunity,* 68(6), pp. 3140-3146. DOI: 10.1128/iai.68.6.3140-3146.2000.

Hashimoto, Y., Okada, S., Yasuda, K., Kawagoe, M., Kajiya, M. and Tsuga, K. (2022) 'Microbial differences between active and remission peri-implantitis', *Scientific Reports,* 12(1), pp. 5284. DOI: 10.1038/s41598-022-09192-y.

Hirschfeld, J., Chicca, I. J., Moonen, C. G. J., White, P. C., Ling, M. R., Wright, H. J., Cooper, P. R., Milward, M. R. and Chapple, I. L. C. (2023) 'Characterization, Quantification, and Visualization of Neutrophil Extracellular Traps', in Seymour, G.J., Cullinan, M.P., Heng, N.C.K. & Cooper, P.R. (eds.) *Oral Biology: Molecular Techniques and Applications*. New York, NY: Springer US, pp. 451-472.

Hirschfeld, J., Dommisch, H., Skora, P., Horvath, G., Latz, E., Hoerauf, A., Waller, T., Kawai, T., Jepsen, S., Deschner, J. and Bekeredjian-Ding, I. (2015) 'Neutrophil extracellular trap formation in supragingival biofilms', *International Journal of Medical Microbiology,* 305(4-5), pp. 453-63. DOI: 10.1016/j.ijmm.2015.04.002.

Hirschfeld, J., White, P. C., Milward, M. R., Cooper, P. R. and Chapple, I. L. C. (2017) 'Modulation of Neutrophil Extracellular Trap and Reactive Oxygen Species Release by Periodontal Bacteria', *Infection and Immunity,* 85(12). DOI: 10.1128/IAI.00297-17.

Hiyoshi, T., Domon, H., Maekawa, T., Tamura, H., Isono, T., Hirayama, S., Sasagawa, K., Takizawa, F., Tabeta, K. and Terao, Y. (2022) 'Neutrophil elastase aggravates periodontitis by disrupting gingival epithelial barrier via cleaving cell adhesion molecules', *Scientific Reports,* 12(1), pp. 8159. DOI: 10.1038/s41598-022-12358-3.

Hoffmann, J. H. O., Schaekel, K., Gaiser, M. R., Enk, A. H. and Hadaschik, E. N. (2016) 'Interindividual variation of NETosis in healthy donors: introduction and application of a refined method for extracellular trap quantification', *Experimental Dermatology,* 25(11), pp. 895-900. DOI: 10.1111/exd.13125.

How, K. Y., Song, K. P. and Chan, K. G. (2016) '*Porphyromonas gingivalis*: An Overview of Periodontopathic Pathogen below the Gum Line', *Frontiers in Microbiology,* 7, pp. 53-53. DOI: 10.3389/fmicb.2016.00053.

Howe, K. L., Achuthan, P., Allen, J., Allen, J., Alvarez-Jarreta, J., Amode, M. R., Armean, I. M., Azov, A. G., Bennett, R., Bhai, J., Billis, K., Boddu, S., Charkhchi, M., Cummins, C., Da Rin Fioretto, L., Davidson, C., Dodiya, K., El Houdaigui, B., Fatima, R., Gall, A., Garcia Giron, C., Grego, T., Guijarro-Clarke, C., Haggerty, L., Hemrom, A., Hourlier, T., Izuogu, O. G., Juettemann, T., Kaikala, V., Kay, M., Lavidas, I., Le, T., Lemos, D., Gonzalez Martinez, J., Marugán, J. C., Maurel, T., McMahon, A. C.,

Mohanan, S., Moore, B., Muffato, M., Oheh, D. N., Paraschas, D., Parker, A., Parton, A., Prosovetskaia, I., Sakthivel, M. P., Salam, Ahamed I A., Schmitt, B. M., Schuilenburg, H., Sheppard, D., Steed, E., Szpak, M., Szuba, M., Taylor, K., Thormann, A., Threadgold, G., Walts, B., Winterbottom, A., Chakiachvili, M., Chaubal, A., De Silva, N., Flint, B., Frankish, A., Hunt, S. E., IIsley, G. R., Langridge, N., Loveland, J. E., Martin, F. J., Mudge, J. M., Morales, J., Perry, E., Ruffier, M., Tate, J., Thybert, D., Trevanion, S. J., Cunningham, F., Yates, A. D., Zerbino, D. R. and Flicek, P. (2020) 'Ensembl 2021', *Nucleic Acids Research,* 49(D1), pp. D884-D891. DOI: 10.1093/nar/gkaa942 %J Nucleic Acids Research.

Huang, L., Tian, W., Chen, X., Xu, H., Dai, W., Zhang, Y., Wu, X., Yu, W., Tian, J. and Su, D. (2022) 'Peripheral Neutrophils-Derived Matrix Metallopeptidase-9 Induces Postoperative Cognitive Dysfunction in Aged Mice', *Frontiers in Aging Neuroscience,* 14, pp. 683295. DOI: 10.3389/fnagi.2022.683295.

Huang, R., Li, M. and Gregory, R. L. (2011) 'Bacterial interactions in dental biofilm', *Virulence,* 2(5), pp. 435-44. DOI: 10.4161/viru.2.5.16140.

Idrissi Janati, A., Karp, I., Latulippe, J.-F., Charlebois, P. and Emami, E. (2022) 'Periodontal disease as a risk factor for sporadic colorectal cancer: results from COLDENT study', *Cancer Causes & Control,* 33(3), pp. 463-472. DOI: 10.1007/s10552-021-01541-y.

Ikegami, A., Chung, P. and Han, Y. W. (2009) 'Complementation of the fadA mutation in *Fusobacterium nucleatum* demonstrates that the surface-exposed adhesin promotes cellular invasion and placental colonization', *Infection and Immunity,* 77(7), pp. 3075-9. DOI: 10.1128/iai.00209-09.

Ismail, H. S., Ali, A. I., Abo El-Ella, M. A. and Mahmoud, S. H. (2020) 'Effect of different polishing techniques on surface roughness and bacterial adhesion of three glass ionomer-based restorative materials: *In vitro* study', *Journal of Clinical and Experimental Dentistry,* 12(7), pp. e620-e625. DOI: 10.4317/jced.56616.

Jancinová, V., Drábiková, K., Nosál, R., Racková, L., Májeková, M. and Holománová, D. (2006) 'The combined luminol/isoluminol chemiluminescence method for differentiating between extracellular and intracellular oxidant production by neutrophils', *Redox Report,* 11(3), pp. 110-116. DOI: 10.1179/135100006X116592.

Ji, S., Shin, J. E., Kim, Y. C. and Choi, Y. (2010) 'Intracellular degradation of *Fusobacterium nucleatum* in human gingival epithelial cells', *Molecules and Cells,* 30(6), pp. 519-26. DOI: 10.1007/s10059-010-0142-8.

Kai, A., Cooke, F., Antoun, N., Siddharthan, C. and Sule, O. (2008) 'A rare presentation of ventriculitis and brain abscess caused by *Fusobacterium nucleatum*', *Journal of Medical Microbiology,* 57(5), pp. 668-671. DOI: 10.1099/jmm.0.47710-0.

Kalaskar, D. M., Downes, J. E., Murray, P., Edgar, D. H. and Williams, R. L. (2013) 'Characterization of the interface between adsorbed fibronectin and human embryonic stem cells', *Journal of the Royal Society Interface,* 10(83), pp. 20130139. DOI: 10.1098/rsif.2013.0139.

Kaplan, C. W., Lux, R., Haake, S. K. and Shi, W. (2009) 'The *Fusobacterium nucleatum* outer membrane protein RadD is an arginine-inhibitable adhesin required for inter-species adherence and the structured architecture of multispecies biofilm', *Molecular Microbiology,* 71(1), pp. 35-47. DOI: 10.1111/j.1365-2958.2008.06503.x.

Kaplan, C. W., Ma, X., Paranjpe, A., Jewett, A., Lux, R., Kinder-Haake, S. and Shi, W. (2010) '*Fusobacterium nucleatum* outer membrane proteins Fap2 and RadD induce cell death in human lymphocytes', *Infection and Immunity,* 78(11), pp. 4773-8. DOI: 10.1128/iai.00567-10.

Karched, M., Bhardwaj, R. G. and Asikainen, S. E. (2015) 'Coaggregation and biofilm growth of *Granulicatella* spp. with *Fusobacterium nucleatum* and *Aggregatibacter actinomycetemcomitans*', *BMC Microbiology,* 15, pp. 114. DOI: 10.1186/s12866-015-0439-z.

Katoh, K., Rozewicki, J. and Yamada, K. D. (2019) 'MAFFT online service: multiple sequence alignment, interactive sequence choice and visualization', *Briefings in Bioinformatics,* 20(4), pp. 1160-1166. DOI: 10.1093/bib/bbx108.

Klebanoff, S. J., Kettle, A. J., Rosen, H., Winterbourn, C. C. and Nauseef, W. M. (2013) 'Myeloperoxidase: a front-line defender against phagocytosed microorganisms', *Journal of Leukocyte Biology,* 93(2), pp. 185-98. DOI: 10.1189/jlb.0712349.

Kong, X., Zhang, Y., Xiang, L., You, Y., Duan, Y., Zhao, Y., Li, S., Wu, R., Zhang, J., Zhou, L. and Duan, L. (2023) '*Fusobacterium nucleatum*-triggered neutrophil extracellular traps facilitate colorectal carcinoma progression', *Journal of Experimental and Clinical Cancer Research,* 42(1), pp. 236. DOI: 10.1186/s13046-023-02817-8.

Krieger, M., AbdelRahman, Y. M., Choi, D., Palmer, E. A., Yoo, A., McGuire, S., Kreth, J. and Merritt, J. (2024) 'Stratification of *Fusobacterium nucleatum* by local health status in the oral cavity defines its subspecies disease association', *Cell Host & Microbe,* 32(4), pp. 479-488.e4. DOI: 10.1016/j.chom.2024.02.010.

Kurgan, S., Kansal, S., Nguyen, D., Stephens, D., Koroneos, Y., Hasturk, H., Van Dyke, T. E. and Kantarci, A. (2017) 'Strain-Specific Impact of *Fusobacterium nucleatum* on Neutrophil Function', *Journal of Periodontology,* 88(4), pp. 380-389. DOI: 10.1902/jop.2016.160212.

Lacy, P. (2006) 'Mechanisms of Degranulation in Neutrophils', *Allergy, Asthma & Clinical Immunology,* 2(3), pp. 98. DOI: 10.1186/1710-1492-2-3-98.

Lee, E. J., Zheng, M., Craft, C. M. and Jeong, S. (2021) 'Matrix metalloproteinase-9 (MMP-9) and tissue inhibitor of metalloproteinases 1 (TIMP-1) are localized in the nucleus of retinal Müller glial cells and modulated by cytokines and oxidative stress', *PloS One,* 16(7), pp. e0253915. DOI: 10.1371/journal.pone.0253915.

Lee, W. L., Harrison, R. E. and Grinstein, S. (2003) 'Phagocytosis by neutrophils', *Microbes and Infection,* 5(14), pp. 1299-1306. DOI: 10.1016/j.micinf.2003.09.014.

Li, H., Zhou, X., Huang, Y., Liao, B., Cheng, L. and Ren, B. (2021) 'Reactive Oxygen Species in Pathogen Clearance: The Killing Mechanisms, the Adaption Response, and the Side Effects', *Frontiers in Microbiology,* 11. DOI: 10.3389/fmicb.2020.622534.

Li, Y., Wang, W., Yang, F., Xu, Y., Feng, C. and Zhao, Y. (2019) 'The regulatory roles of neutrophils in adaptive immunity', *Cell Communication and Signaling,* 17(1), pp. 147. DOI: 10.1186/s12964-019-0471-y.

Lima, B. P., Shi, W. and Lux, R. (2017) 'Identification and characterization of a novel *Fusobacterium nucleatum* adhesin involved in physical interaction and biofilm formation with *Streptococcus gordonii*', *MicrobiologyOpen,* 6(3). DOI: 10.1002/mbo3.444.

Ling, M. R., Chapple, I. L. and Matthews, J. B. (2015) 'Peripheral blood neutrophil cytokine hyper-reactivity in chronic periodontitis', *Innate Immunity,* 21(7), pp. 714-25. DOI: 10.1177/1753425915589387.

Lipke, P. N. and Ragonis-Bachar, P. (2023) 'Sticking to the Subject: Multifunctionality in Microbial Adhesins', *Journal of Fungi (Basel),* 9(4). DOI: 10.3390/jof9040419.

Liu, J., Hsieh, C.-L., Gelincik, O., Devolder, B., Sei, S., Zhang, S., Lipkin, S. M. and Chang, Y.-F. (2019a) 'Proteomic characterization of outer membrane vesicles from gut mucosa-derived *Fusobacterium nucleatum*', *Journal of Proteomics,* 195, pp. 125-137. DOI: 10.1016/j.jprot.2018.12.029.

Liu, L., Liang, L., Liang, H., Wang, M., Lu, B., Xue, M., Deng, J. and Chen, Y. (2019b) '*Fusobacterium nucleatum* Aggravates the Progression of Colitis by Regulating M1 Macrophage Polarization via AKT2 Pathway', *Frontiers in Immunology,* 10(1324). DOI: 10.3389/fimmu.2019.01324.

Liu, M., Lin, P., Qu, M., Zhai, R., Zhang, L., Zhang, L., Zhu, L., Liu, C., Shu, H., Feng, X., Su, C., Yu, T., Wang, F. and Man, D. (2022) 'Neutrophil count is a useful marker to predict the severity of preeclampsia', *Clinical and Experimental Hypertension,* 44(4), pp. 334-340. DOI: 10.1080/10641963.2022.2043891.

Liu, P.-F., Shi, W., Zhu, W., Smith, J. W., Hsieh, S.-L., Gallo, R. L. and Huang, C.-M. (2010) 'Vaccination targeting surface FomA of *Fusobacterium nucleatum* against bacterial co-aggregation: Implication for treatment of periodontal infection and halitosis', *Vaccine,* 28(19), pp. 3496-3505. DOI: 10.1016/j.vaccine.2010.02.047.

Lucena-Aguilar, G., Sánchez-López, A. M., Barberán-Aceituno, C., Carrillo-Ávila, J. A., López-Guerrero, J. A. and Aguilar-Quesada, R. (2016) 'DNA Source Selection for Downstream Applications Based on DNA Quality Indicators Analysis', *Biopreservation and Biobanking,* 14(4), pp. 264-70. DOI: 10.1089/bio.2015.0064.

Luchian, I., Goriuc, A., Sandu, D. and Covasa, M. (2022) 'The Role of Matrix Metalloproteinases (MMP-8, MMP-9, MMP-13) in Periodontal and Peri-Implant Pathological Processes', *International Journal of Molecular Sciences,* 23(3), pp. 1806. DOI: 10.3390/ijms23031806.

Ma, X., Sun, T., Zhou, J., Zhi, M., Shen, S., Wang, Y., Gu, X., Li, Z., Gao, H., Wang, P. and Feng, Q. (2023) 'Pangenomic Study of *Fusobacterium nucleatum* Reveals the Distribution of Pathogenic Genes and Functional Clusters at the Subspecies and Strain Levels', *Microbiol Spectr,* 11(3), pp. e0518422. DOI: 10.1128/spectrum.05184-22.

Manley, H. R., Keightley, M. C. and Lieschke, G. J. (2018) 'The Neutrophil Nucleus: An Important Influence on Neutrophil Migration and Function', *Frontiers in Immunology,* 9(2867). DOI: 10.3389/fimmu.2018.02867.

Manson McGuire, A., Cochrane, K., Griggs, A. D., Haas, B. J., Abeel, T., Zeng, Q., Nice, J. B., MacDonald, H., Birren, B. W., Berger, B. W., Allen-Vercoe, E. and Earl, A. M. (2014) 'Evolution of Invasion in a Diverse Set of *Fusobacterium* Species', *mBio,* 5(6), pp. e01864-14. DOI: 10.1128/mBio.01864-14.

Matta, B., Battaglia, J. and Barnes, B. J. (2022) 'Detection of neutrophil extracellular traps in patient plasma: method development and validation in systemic lupus erythematosus and healthy donors that carry IRF5 genetic risk', *Frontiers in Immunology,* 13. DOI: 10.3389/fimmu.2022.951254.

Matthews, J. B., Wright, H. J., Roberts, A., Cooper, P. R. and Chapple, I. L. (2007a) 'Hyperactivity and reactivity of peripheral blood neutrophils in chronic periodontitis', *Clinical and Experimental Immunology,* 147(2), pp. 255-64. DOI: 10.1111/j.1365-2249.2006.03276.x.

Matthews, J. B., Wright, H. J., Roberts, A., Ling-Mountford, N., Cooper, P. R. and Chapple, I. L. (2007b) 'Neutrophil hyper-responsiveness in periodontitis', *Journal of Dental Research,* 86(8), pp. 718-22. DOI: 10.1177/154405910708600806.

Mayadas, T. N., Cullere, X. and Lowell, C. A. (2014) 'The multifaceted functions of neutrophils', *Annual Review of Pathology,* 9, pp. 181-218. DOI: 10.1146/annurev-pathol-020712-164023.

McKinnon, K. M. (2018) 'Flow Cytometry: An Overview', *Current Protocols in Immunology,* 120, pp. 5.1.1-5.1.11. DOI: 10.1002/cpim.40.

Mehner, C., Hockla, A., Miller, E., Ran, S., Radisky, D. C. and Radisky, E. S. (2014) 'Tumor cell-produced matrix metalloproteinase 9 (MMP-9) drives malignant progression and metastasis of basal-like triple negative breast cancer', *Oncotarget,* 5(9), pp. 2736-2749. DOI: 10.18632/oncotarget.1932.

Meng, Q., Gao, Q., Mehrazarin, S., Tangwanichgapong, K., Wang, Y., Huang, Y., Pan, Y., Robinson, S., Liu, Z., Zangiabadi, A., Lux, R., Papapanou, P. N., Guo, X. E., Wang, H., Berchowitz, L. E. and Han, Y. W. (2021) '*Fusobacterium nucleatum* secretes amyloid-like FadA to enhance pathogenicity', *EMBO reports,* 22(7), pp. e52891. DOI: 10.15252/embr.202152891.

Miles, A. A., Misra, S. S. and Irwin, J. O. (1938) 'The estimation of the bactericidal power of the blood', *Journal of Hygiene,* 38(6), pp. 732-49. DOI: 10.1017/s002217240001158x.

Millhouse, E. (2015) *Microbial biofilm composition influences the host immune response.* PhD Thesis, University of Glasgow.

Millhouse, E., Jose, A., Sherry, L., Lappin, D. F., Patel, N., Middleton, A. M., Pratten, J., Culshaw, S. and Ramage, G. (2014) 'Development of an *in vitro* periodontal biofilm model for assessing antimicrobial and host modulatory effects of bioactive molecules', *BMC Oral Health,* 14(1), pp. 80. DOI: 10.1186/1472-6831-14-80.

Mira, P., Yeh, P. and Hall, B. G. (2022) 'Estimating microbial population data from optical density', *PloS One,* 17(10), pp. e0276040. DOI: 10.1371/journal.pone.0276040.

Molloy, M. P. (2008) 'Isolation of Bacterial Cell Membranes Proteins Using Carbonate Extraction', in Posch, A. (ed.) *2D PAGE: Sample Preparation and Fractionation*. Totowa, NJ: Humana Press, pp. 397-401.

Monici, M., Pratesi, R., Bernabei, P. A., Caporale, R., Ferrini, P. R., Croce, A. C., Balzarini, P. and Bottiroli, G. (1995) 'Natural fluorescence of white blood cells: spectroscopic and imaging study', *Journal of Photochemistry and Photobiology B: Biology,* 30(1), pp. 29-37. DOI: 10.1016/1011-1344(95)07149-V.

Moonen, C. G. J., Hirschfeld, J., Cheng, L., Chapple, I. L. C., Loos, B. G. and Nicu, E. A. (2019) 'Oral Neutrophils Characterized: Chemotactic, Phagocytic, and Neutrophil Extracellular Trap (NET) Formation Properties', *Frontiers in Immunology,* 10(635). DOI: 10.3389/fimmu.2019.00635.

Muchova, M. (2020) *Characterisation of Fusobacterium nucleatum biofilms and cyclic di-nucleotide production.* Master's Thesis, University of Birmingham.

Muraoka, A., Suzuki, M., Hamaguchi, T., Watanabe, S., Iijima, K., Murofushi, Y., Shinjo, K., Osuka, S., Hariyama, Y., Ito, M., Ohno, K., Kiyono, T., Kyo, S., Iwase, A., Kikkawa, F., Kajiyama, H. and Kondo, Y. (2023) '*Fusobacterium* infection facilitates the development of endometriosis through the phenotypic transition of endometrial fibroblasts', *Science Translational Medicine,* 15(700), pp. eadd1531. DOI: 10.1126/scitranslmed.add1531.

Nguyen, G. T., Green, E. R. and Mecsas, J. (2017) 'Neutrophils to the ROScue: Mechanisms of NADPH Oxidase Activation and Bacterial Resistance', *Frontiers in Cellular and Infection Microbiology,* 7(373). DOI: 10.3389/fcimb.2017.00373.

Nie, S., Tian, B., Wang, X., Pincus, D. H., Welker, M., Gilhuley, K., Lu, X., Han, Y. W. and Tang, Y. W. (2015) '*Fusobacterium nucleatum* subspecies identification by matrix-assisted laser desorption ionization-time of flight mass spectrometry', *Journal of Clinical Microbiology,* 53(4), pp. 1399-402. DOI: 10.1128/JCM.00239-15.

Okamoto, M., Mizuno, R., Kawada, K., Itatani, Y., Kiyasu, Y., Hanada, K., Hirata, W., Nishikawa, Y., Masui, H., Sugimoto, N., Tamura, T., Inamoto, S., Sakai, Y. and Obama, K. (2023) 'Neutrophil Extracellular Traps Promote Metastases of Colorectal Cancers through Activation of ERK Signaling by Releasing Neutrophil Elastase', *International Journal of Molecular Sciences,* 24(2), pp. 1118. DOI: 10.3390/ijms24021118.

Olsen, I. and Hajishengallis, G. (2016) 'Major neutrophil functions subverted by *Porphyromonas gingivalis*', *Journal of Oral Microbiology,* 8, pp. 30936-30936. DOI: 10.3402/jom.v8.30936.

Özçaka, Ö., Bıçakcı, N., Pussinen, P., Sorsa, T., Köse, T. and Buduneli, N. (2011) 'Smoking and matrix metalloproteinases, neutrophil elastase and myeloperoxidase in chronic periodontitis', *Oral Diseases,* 17(1), pp. 68-76. DOI: 10.1111/j.1601-0825.2010.01705.x.

Palmer, L. J. (2010) *Neutrophil extracellular traps in periodontitis.* PhD Thesis, University of Birmingham.

Palmer, L. J., Cooper, P. R., Ling, M. R., Wright, H. J., Huissoon, A. and Chapple, I. L. C. (2012) 'Hypochlorous acid regulates neutrophil extracellular trap release in humans', *Clinical and Experimental Immunology,* 167(2), pp. 261-268. DOI: 10.1111/j.1365-2249.2011.04518.x.

Park, A., Jeong, H.-H., Lee, J., Kim, K. P. and Lee, C.-S. (2011) 'Effect of shear stress on the formation of bacterial biofilm in a microfluidic channel', *BioChip Journal,* 5(3), pp. 236-241. DOI: 10.1007/s13206-011-5307-9.

Park, J., Shokeen, B., Haake, S. K. and Lux, R. (2016) 'Characterization of *Fusobacterium nucleatum* ATCC 23726 adhesins involved in strain-specific attachment to *Porphyromonas gingivalis*', *International Journal of Oral Science,* 8(3), pp. 138-144. DOI: 10.1038/ijos.2016.27.

Park, K.-S., Ahn, J., Kim, J. Y., Park, H., Kim, H. O. and Lee, S.-H. (2014) 'Poly-L-Lysine Increases the *Ex Vivo* Expansion and Erythroid Differentiation of Human Hematopoietic Stem Cells, as Well as Erythroid Enucleation Efficacy', *Tissue Engineering Part A,* 20(5-6), pp. 1072-1080. DOI: 10.1089/ten.tea.2013.0193.

Pérez-Figueroa, E., Álvarez-Carrasco, P., Ortega, E. and Maldonado-Bernal, C. (2021) 'Neutrophils: Many Ways to Die', *Frontiers in Immunology,* 12. DOI: 10.3389/fimmu.2021.631821.

Periasamy, S., Chalmers, N. I., Du-Thumm, L. and Kolenbrander, P. E. (2009) '*Fusobacterium nucleatum* ATCC 10953 requires *Actinomyces naeslundii* ATCC 43146 for growth on saliva in a three-species community that includes *Streptococcus oralis* 34', *Applied and Environmental Microbiology,* 75(10), pp. 3250-3257. DOI: 10.1128/AEM.02901-08.

Pilsczek, F. H., Salina, D., Poon, K. K., Fahey, C., Yipp, B. G., Sibley, C. D., Robbins, S. M., Green, F. H., Surette, M. G., Sugai, M., Bowden, M. G., Hussain, M., Zhang, K. and Kubes, P. (2010) 'A novel mechanism of rapid nuclear neutrophil extracellular trap formation in response to *Staphylococcus aureus*', *Journal of Immunology,* 185(12), pp. 7413-25. DOI: 10.4049/jimmunol.1000675.

Prince, L. R., Whyte, M. K., Sabroe, I. and Parker, L. C. (2011) 'The role of TLRs in neutrophil activation', *Current Opinion in Pharmacology,* 11(4), pp. 397-403. DOI: 10.1016/j.coph.2011.06.007.

Queen, J., Domingue, J. C., White, J. R., Stevens, C., Udayasuryan, B., Nguyen, T. T. D., Wu, S., Ding, H., Fan, H., McMann, M., Corona, A., Larman, T. C., Verbridge, S. S., Housseau, F., Slade, D. J., Drewes, J. L. and Sears, C. L. (2022) 'Comparative Analysis of Colon Cancer-Derived *Fusobacterium nucleatum* Subspecies: Inflammation and Colon Tumorigenesis in Murine Models', *mBio,* 13(1), pp. e02991-21. DOI: doi:10.1128/mbio.02991-21.

Ramage, G., Lappin, D. F., Millhouse, E., Malcolm, J., Jose, A., Yang, J., Bradshaw, D. J., Pratten, J. R. and Culshaw, S. (2017) 'The epithelial cell response to health and disease associated oral biofilm models', *Journal of Periodontal Research,* 52(3), pp. 325-333. DOI: 10.1111/jre.12395.

Renvert, S., Persson, G. R., Pirih, F. Q. and Camargo, P. M. (2018) 'Peri-implant health, peri-implant mucositis, and peri-implantitis: Case definitions and diagnostic considerations', *Journal of Periodontology,* 89(S1), pp. S304-S312. DOI: 10.1002/JPER.17-0588.

Resch, A., Rosenstein, R., Nerz, C. and Götz, F. (2005) 'Differential gene expression profiling of *Staphylococcus aureus* cultivated under biofilm and planktonic conditions', *Applied and Environmental Microbiology,* 71(5), pp. 2663-2676. DOI: 10.1128/AEM.71.5.2663-2676.2005.

Roberts, H. M., Ling, M. R., Insall, R., Kalna, G., Spengler, J., Grant, M. M. and Chapple, I. L. (2015) 'Impaired neutrophil directional chemotactic accuracy in chronic periodontitis patients', *Journal of Clinical Periodontology,* 42(1), pp. 1-11. DOI: 10.1111/jcpe.12326.

Rosales, C. (2018) 'Neutrophil: A Cell with Many Roles in Inflammation or Several Cell Types?', *Frontiers in Physiology,* 9, pp. 113. DOI: 10.3389/fphys.2018.00113.

Rostami, A., Lambie, M., Yu, C. W., Stambolic, V., Waldron, J. N. and Bratman, S. V. (2020) 'Senescence, Necrosis, and Apoptosis Govern Circulating Cell-free DNA Release Kinetics', *Cell Reports,* 31(13), pp. 107830. DOI: 10.1016/j.celrep.2020.107830.

Roth, S., Agthe, M., Eickhoff, S., Möller, S., Karsten, C. M., Borregaard, N., Solbach, W. and Laskay, T. (2015) 'Secondary necrotic neutrophils release interleukin-16C and macrophage migration inhibitory factor from stores in the cytosol', *Cell Death Discovery,* 1(1), pp. 15056. DOI: 10.1038/cddiscovery.2015.56.

Rubinstein, M. R., Baik, J. E., Lagana, S. M., Han, R. P., Raab, W. J., Sahoo, D., Dalerba, P., Wang, T. C. and Han, Y. W. (2019) '*Fusobacterium nucleatum* promotes colorectal cancer by inducing Wnt/β catenin modulator Annexin A1', *EMBO reports,* 20(4), pp. e47638. DOI: 10.15252/embr.201847638.

Saitou, N. and Nei, M. (1987) 'The neighbor-joining method: a new method for reconstructing phylogenetic trees', *Molecular Biology and Evolution,* 4(4), pp. 406-25. DOI: 10.1093/oxfordjournals.molbev.a040454.

Scott, D. A. and Krauss, J. (2012) 'Neutrophils in periodontal inflammation', *Frontiers of Oral Biology,* 15, pp. 56-83. DOI: 10.1159/000329672.

Shammas, N. W., Murphy, G. W., Eichelberger, J., Klee, D., Schwartz, R. and Bachman, W. (1993) 'Infective endocarditis due to *Fusobacterium nucleatum:* case report and review of the literature', *Clinical Cardiology,* 16(1), pp. 72-5. DOI: 10.1002/clc.4960160116.

Sharma, R., Panner Selvam, M. K. and Agarwal, A. (2019) 'Chapter 3.1 - Reactive Oxygen Species Methodology Using Chemiluminescence Assay', in Henkel, R., Samanta, L. & Agarwal, A. (eds.) *Oxidants, Antioxidants and Impact of the Oxidative Status in Male Reproduction*: Academic Press, pp. 183-193.

Sheshachalam, A., Srivastava, N., Mitchell, T., Lacy, P. and Eitzen, G. (2014) 'Granule Protein Processing and Regulated Secretion in Neutrophils', *Frontiers in Immunology,* 5(448). DOI: 10.3389/fimmu.2014.00448.

Singh, R. R., Randhawa, D. and Valera, I. (2016) 'Human neutrophil extracellular trap formation is modulated upon stimulation with Toll-like-receptor ligands', *The Journal of Immunology,* 196(1 Supplement), pp. 60.7. DOI: 10.4049/jimmunol.196.Supp.60.7.

Sleight, S. C., Wigginton, N. S. and Lenski, R. E. (2006) 'Increased susceptibility to repeated freeze-thaw cycles in *Escherichia coli* following long-term evolution in a benign environment', *BMC Evolutionary Biology,* 6, pp. 104. DOI: 10.1186/1471-2148-6-104.

Sng, J. J., Prazakova, S., Thomas, P. S. and Herbert, C. (2017) 'MMP-8, MMP-9 and Neutrophil Elastase in Peripheral Blood and Exhaled Breath Condensate in COPD', *COPD: Journal of Chronic Obstructive Pulmonary Disease,* 14(2), pp. 238-244. DOI: 10.1080/15412555.2016.1249790.

Socransky, S. S., Haffajee, A. D., Cugini, M. A., Smith, C. and Kent Jr., R. L. (1998) 'Microbial complexes in subgingival plaque', *Journal of Clinical Periodontology,* 25(2), pp. 134-144. DOI: 10.1111/j.1600-051X.1998.tb02419.x.

Stapels, D. A., Geisbrecht, B. V. and Rooijakkers, S. H. (2015) 'Neutrophil serine proteases in antibacterial defense', *Current Opinion in Microbiology,* 23, pp. 42-8. DOI: 10.1016/j.mib.2014.11.002.

States, D. J. and Gish, W. (1994) 'Combined use of sequence similarity and codon bias for coding region identification', *Journal of Computational Biology,* 1(1), pp. 39-50. DOI: 10.1089/cmb.1994.1.39.

Stathopoulou, P. G., Benakanakere, M. R., Galicia, J. C. and Kinane, D. F. (2009) 'The host cytokine response to *Porphyromonas gingivalis* is modified by gingipains', *Oral Microbiology and Immunology,* 24(1), pp. 11-7. DOI: 10.1111/j.1399-302X.2008.00467.x.

Strunk, T., Richmond, P., Prosser, A., Simmer, K., Levy, O., Burgner, D. and Currie, A. (2011) 'Method of bacterial killing differentially affects the human innate immune response to *Staphylococcus epidermidis*', *Innate Immunity,* 17(6), pp. 508-16. DOI: 10.1177/1753425910379840.

Sun, L., Liu, Y., Lehnert, T., Gijs, M. A. M. and Li, S. (2022) 'The enhancement of DNA fragmentation in a bench top ultrasonic water bath with needle-induced air bubbles:

Simulation and experimental investigation', *Biomicrofluidics,* 16(4), pp. 044103. DOI: 10.1063/5.0101740.

Tamassia, N., Bianchetto-Aguilera, F., Arruda-Silva, F., Gardiman, E., Gasperini, S., Calzetti, F. and Cassatella, M. A. (2018) 'Cytokine production by human neutrophils: Revisiting the "dark side of the moon"', *European Journal of Clinical Investigation,* 48(S2), pp. e12952. DOI: 10.1111/eci.12952.

Tavares, L. J., Klein, M. I., Panariello, B. H. D., Dorigatti de Avila, E. and Pavarina, A. C. (2018) 'An in vitro model of *Fusobacterium nucleatum* and *Porphyromonas gingivalis* in single- and dual-species biofilms', *Journal of Periodontal & Implant Science,* 48(1), pp. 12-21. DOI: 10.5051/jpis.2018.48.1.12.

Taylor, E. L., Rossi, A. G., Dransfield, I. and Hart, S. P. (2007) 'Analysis of Neutrophil Apoptosis', in Quinn, M.T., DeLeo, F.R. & Bokoch, G.M. (eds.) *Neutrophil Methods and Protocols*. Totowa, NJ: Humana Press, pp. 177-200.

Tecchio, C., Micheletti, A. and Cassatella, M. A. (2014) 'Neutrophil-derived cytokines: facts beyond expression', *Frontiers in Immunology,* 5, pp. 508-508. DOI: 10.3389/fimmu.2014.00508.

Thålin, C., Aguilera, K., Hall, N. W., Marunde, M. R., Burg, J. M., Rosell, A., Daleskog, M., Månsson, M., Hisada, Y., Meiners, M. J., Sun, Z. W., Whelihan, M. F., Cheek, M. A., Howard, S. A., Saxena-Beem, S., Noubouossie, D. F., Key, N. S., Sheikh, S. Z., Keogh, M. C., Cowles, M. W., Lundström, S., Mackman, N., Wallén, H. and Johnstone, A. L. (2020) 'Quantification of citrullinated histones: Development of an improved assay to reliably quantify nucleosomal H3Cit in human plasma', *Journal of Thrombosis and Haemostasis,* 18(10), pp. 2732-2743. DOI: 10.1111/jth.15003.

Thurnheer, T., Karygianni, L., Flury, M. and Belibasakis, G. N. (2019) '*Fusobacterium* Species and Subspecies Differentially Affect the Composition and Architecture of Supra- and Subgingival Biofilms Models', *Frontiers in Microbiology,* 10, pp. 1716. DOI: 10.3389/fmicb.2019.01716.

Tonetti, M. S., Jepsen, S., Jin, L. and Otomo-Corgel, J. (2017) 'Impact of the global burden of periodontal diseases on health, nutrition and wellbeing of mankind: A call for global action', *Journal of Clinical Periodontology,* 44(5), pp. 456-462. DOI: 10.1111/jcpe.12732.

Toussi, D. N., Liu, X. and Massari, P. (2012) 'The FomA Porin from *Fusobacterium nucleatum* Is a Toll-Like Receptor 2 Agonist with Immune Adjuvant Activity', *Clinical and Vaccine Immunology,* 19(7), pp. 1093-1101. DOI: 10.1128/CVI.00236-12.

Umaña, A., Sanders, B. E., Yoo, C. C., Casasanta, M. A., Udayasuryan, B., Verbridge, S. S., Slade, D. J. and DiRita, V. J. (2019) 'Utilizing Whole *Fusobacterium* Genomes To Identify, Correct, and Characterize Potential Virulence Protein Families', *Journal of Bacteriology,* 201(23), pp. e00273-19. DOI: 10.1128/JB.00273-19.

Unemo, M., Aspholm-Hurtig, M., Ilver, D., Bergström, J., Borén, T., Danielsson, D. and Teneberg, S. (2005) 'The Sialic Acid Binding SabA Adhesin of *Helicobacter pylori* Is Essential for Nonopsonic Activation of Human Neutrophils', *Journal of Biological Chemistry,* 280(15), pp. 15390-15397. DOI: 10.1074/jbc.M412725200.

Urban, C. F., Reichard, U., Brinkmann, V. and Zychlinsky, A. (2006) 'Neutrophil extracellular traps capture and kill *Candida albicans* yeast and hyphal forms', *Cellular Microbiology,* 8(4), pp. 668-76. DOI: 10.1111/j.1462-5822.2005.00659.x.

Uriarte, S. M., Edmisson, J. S. and Jimenez-Flores, E. (2016) 'Human neutrophils and oral microbiota: a constant tug-of-war between a harmonious and a discordant coexistence', *Immunological Reviews,* 273(1), pp. 282-98. DOI: 10.1111/imr.12451.

Uribe-Querol, E. and Rosales, C. (2020) 'Phagocytosis: Our Current Understanding of a Universal Biological Process', *Frontiers in Immunology,* 11(1066). DOI: 10.3389/fimmu.2020.01066.

van Kessel, K. P. M., Bestebroer, J. and van Strijp, J. A. G. (2014) 'Neutrophil-Mediated Phagocytosis of *Staphylococcus aureus*', *Frontiers in Immunology,* 5(467). DOI: 10.3389/fimmu.2014.00467.

Vander Haar, E. L., So, J., Gyamfi-Bannerman, C. and Han, Y. W. (2018) '*Fusobacterium nucleatum* and adverse pregnancy outcomes: Epidemiological and mechanistic evidence', *Anaerobe,* 50, pp. 55-59. DOI: 10.1016/j.anaerobe.2018.01.008.

Velasquez, M., O'Sullivan, C., Brockett, R., Mikels-Vigdal, A., Mikaelian, I., Smith, V. and Greenstein, A. E. (2023) 'Characterization of Active MMP9 in Chronic Inflammatory Diseases Using a Novel Anti-MMP9 Antibody', *Antibodies,* 12(1), pp. 9. DOI: 10.3390/antib12010009.

Vieira Colombo, A. P., Magalhães, C. B., Hartenbach, F. A. R. R., Martins do Souto, R. and Maciel da Silva-Boghossian, C. (2016) 'Periodontal-disease-associated biofilm: A reservoir for pathogens of medical importance', *Microbial Pathogenesis,* 94, pp. 27-34. DOI: 10.1016/j.micpath.2015.09.009.

Vyas, N., Wang, Q. X., Manmi, K. A., Sammons, R. L., Kuehne, S. A. and Walmsley, A. D. (2020) 'How does ultrasonic cavitation remove dental bacterial biofilm?', *Ultrasonics Sonochemistry,* 67, pp. 105112. DOI: 10.1016/j.ultsonch.2020.105112.

Wajant, H. and Siegmund, D. (2019) 'TNFR1 and TNFR2 in the Control of the Life and Death Balance of Macrophages', *Frontiers in Cell and Developmental Biology,* 7. DOI: 10.3389/fcell.2019.00091.

Wang, C. H., Putri, D. U., Lee, J. C., Liao, C. C., Tsao, S. T., Hsiao, A. L., Wu, J. H., Chen, X. W., Lee, C. H. and Tsai, I. L. (2021) 'Biosafety and Proteome Profiles of Different Heat Inactivation Methods for *Mycobacterium tuberculosis*', *Microbiol Spectr,* 9(3), pp. e0071621. DOI: 10.1128/spectrum.00716-21.

Wang, J. (2018) 'Neutrophils in tissue injury and repair', *Cell and Tissue Research,* 371(3), pp. 531-539. DOI: 10.1007/s00441-017-2785-7.

Wang, W., Li, D., Xiang, L., Lv, M., Tao, L., Ni, T., Deng, J., Gu, X., Masatara, S., Liu, Y. and Zhou, Y. (2019) 'TIMP-2 inhibits metastasis and predicts prognosis of colorectal cancer via regulating MMP-9', *Cell Adhesion & Migration,* 13(1), pp. 272-283. DOI: 10.1080/19336918.2019.1639303.

Wang, Y., Sun, L., Hu, L., Wang, Z., Wang, X. and Dong, Q. (2022) 'Adhesion and kinetics of biofilm formation and related gene expression of *Listeria monocytogenes* in response to nutritional stress', *Food Research International,* 156, pp. 111143. DOI: doi.org/10.1016/j.foodres.2022.111143.

Waskom, M. L. (2021) 'seaborn: statistical data visualization', *The Journal of Open Source Software,* 6(60), pp. 3021. DOI: 10.21105/joss.03021.

White-Owen, C., Alexander, J. W., Sramkoski, R. M. and Babcock, G. F. (1992) 'Rapid whole-blood microassay using flow cytometry for measuring neutrophil phagocytosis', *Journal of Clinical Microbiology,* 30(8), pp. 2071-6. DOI: 10.1128/jcm.30.8.2071-2076.1992.

White, P., Sakellari, D., Roberts, H., Risafi, I., Ling, M., Cooper, P., Milward, M. and Chapple, I. (2016) 'Peripheral blood neutrophil extracellular trap production and degradation in chronic periodontitis', *Journal of Clinical Periodontology,* 43(12), pp. 1041-1049. DOI: 10.1111/jcpe.12628.

Winterbourn, C. C., Kettle, A. J. and Hampton, M. B. (2016) 'Reactive Oxygen Species and Neutrophil Function', *Annual Review of Biochemistry,* 85, pp. 765-92. DOI: 10.1146/annurev-biochem-060815-014442.

Wright, H. J., Chapple, I. L., Matthews, J. B. and Cooper, P. R. (2011) '*Fusobacterium nucleatum* regulation of neutrophil transcription', *Journal of Periodontal Research,* 46(1), pp. 1-12. DOI: 10.1111/j.1600-0765.2010.01299.x.

Wu, J., Li, Q. and Fu, X. (2019) '*Fusobacterium nucleatum* Contributes to the Carcinogenesis of Colorectal Cancer by Inducing Inflammation and Suppressing Host Immunity', *Translational Oncology,* 12(6), pp. 846-851. DOI: 10.1016/j.tranon.2019.03.003.

Wu, L., Zhang, S.-Q., Zhao, L., Ren, Z.-H. and Hu, C.-Y. (2022) 'Global, regional, and national burden of periodontitis from 1990 to 2019: Results from the Global Burden of Disease study 2019', *Journal of Periodontology,* 93(10), pp. 1445-1454. DOI: 10.1002/JPER.21-0469.

Xu, H., Zhao, J., Lu, J. and Sun, X. (2020) 'Ovarian endometrioma infiltrating neutrophils orchestrate immunosuppressive microenvironment', *Journal of Ovarian Research,* 13(1), pp. 44. DOI: 10.1186/s13048-020-00642-7.

Yakimov, B., Gogoleva, M., Semenov, A., Rodionov, S., Novoselova, M., Gaier, A., Kovalev, A., Bernakevich, A., Fadeev, V., Armaganov, A., Drachev, V., Gorin, D., Darvin, M., Shcheslavskiy, V., Budylin, G., Priezzhev, A. and Shirshin, E. (2019) 'Label-free characterization of white blood cells using fluorescence lifetime imaging and flow-cytometry: molecular heterogeneity and erythrophagocytosis', *Biomedical Optics Express,* 10, pp. 4220. DOI: 10.1364/BOE.10.004220.

Yang, K., Azoulay, É., Attalah, L., Zahar, J.-R., Van de Louw, A., Cerf, C., Soussy, C.-J., Duvaldestin, P., Brochard, L., Brun-Buisson, C., Harf, A. and Delclaux, C. (2003) 'Bactericidal activity response of blood neutrophils from critically ill patients to *in vitro* granulocyte colony-stimulating factor stimulation', *Intensive Care Medicine,* 29(3), pp. 396-402. DOI: 10.1007/s00134-002-1623-9.

Yaseen, R., Blodkamp, S., Lüthje, P., Reuner, F., Völlger, L., Naim, H. Y. and von Köckritz-Blickwede, M. (2017) 'Antimicrobial activity of HL-60 cells compared to primary blood-derived neutrophils against *Staphylococcus aureus*', *Journal of Negative Results in Biomedicine,* 16(1), pp. 2. DOI: 10.1186/s12952-017-0067-2.

Yasuda, H., Takishita, Y., Morita, A., Tsutsumi, T., Tsuchiya, M. and Sato, E. F. (2020) 'DNA demethylation increases NETosis', *Archives of Biochemistry and Biophysics,* 689, pp. 108465. DOI: 10.1016/j.abb.2020.108465.

Yousefi, S., Mihalache, C., Kozlowski, E., Schmid, I. and Simon, H. U. (2009) 'Viable neutrophils release mitochondrial DNA to form neutrophil extracellular traps', *Cell Death and Differentiation,* 16(11), pp. 1438-44. DOI: 10.1038/cdd.2009.96.

Yu, P., Zhang, X., Liu, N., Tang, L., Peng, C. and Chen, X. (2021) 'Pyroptosis: mechanisms and diseases', *Signal Transduction and Targeted Therapy,* 6(1), pp. 128. DOI: 10.1038/s41392-021-00507-5.

Zeng, W., Song, Y., Wang, R., He, R. and Wang, T. (2023) 'Neutrophil elastase: From mechanisms to therapeutic potential', *Journal of Pharmaceutical Analysis,* 13(4), pp. 355-366. DOI: 10.1016/j.jpha.2022.12.003.

Zepeda-Rivera, M., Minot, S. S., Bouzek, H., Wu, H., Blanco-Míguez, A., Manghi, P., Jones, D. S., LaCourse, K. D., Wu, Y., McMahon, E. F., Park, S.-N., Lim, Y. K., Kempchinsky, A. G., Willis, A. D., Cotton, S. L., Yost, S. C., Sicinska, E., Kook, J.-K., Dewhirst, F. E., Segata, N., Bullman, S. and Johnston, C. D. (2024) 'A distinct *Fusobacterium nucleatum* clade dominates the colorectal cancer niche', *Nature,* 628(8007), pp. 424-432. DOI: 10.1038/s41586-024-07182-w.

Zhan, X., Li, B., Zhan, X., Schlüter, H., Jungblut, P. R. and Coorssen, J. R. (2019) 'Innovating the Concept and Practice of Two-Dimensional Gel Electrophoresis in the Analysis of Proteomes at the Proteoform Level', *Proteomes,* 7(4). DOI: 10.3390/proteomes7040036.

Zhang, J. H. and Xu, M. (2000) 'DNA fragmentation in apoptosis', *Cell Research,* 10(3), pp. 205-211. DOI: 10.1038/sj.cr.7290049.

Zheng, S., Bawazir, M., Dhall, A., Kim, H.-E., He, L., Heo, J. and Hwang, G. (2021) 'Implication of Surface Properties, Bacterial Motility, and Hydrodynamic Conditions on Bacterial Surface Sensing and Their Initial Adhesion', *Frontiers in Bioengineering and Biotechnology,* 9(82). DOI: 10.3389/fbioe.2021.643722.

Zilm, P. S. and Rogers, A. H. (2007) 'Co-adhesion and biofilm formation by *Fusobacterium nucleatum* in response to growth pH', *Anaerobe,* 13(3), pp. 146-152. DOI: 10.1016/j.anaerobe.2007.04.005.

APPENDIX 1: TIME-COURSE CURVES OF TOTAL AND INTRACELLULAR ROS AND SUPEROXIDE USED TO CALCULATE TIME TO PEAK

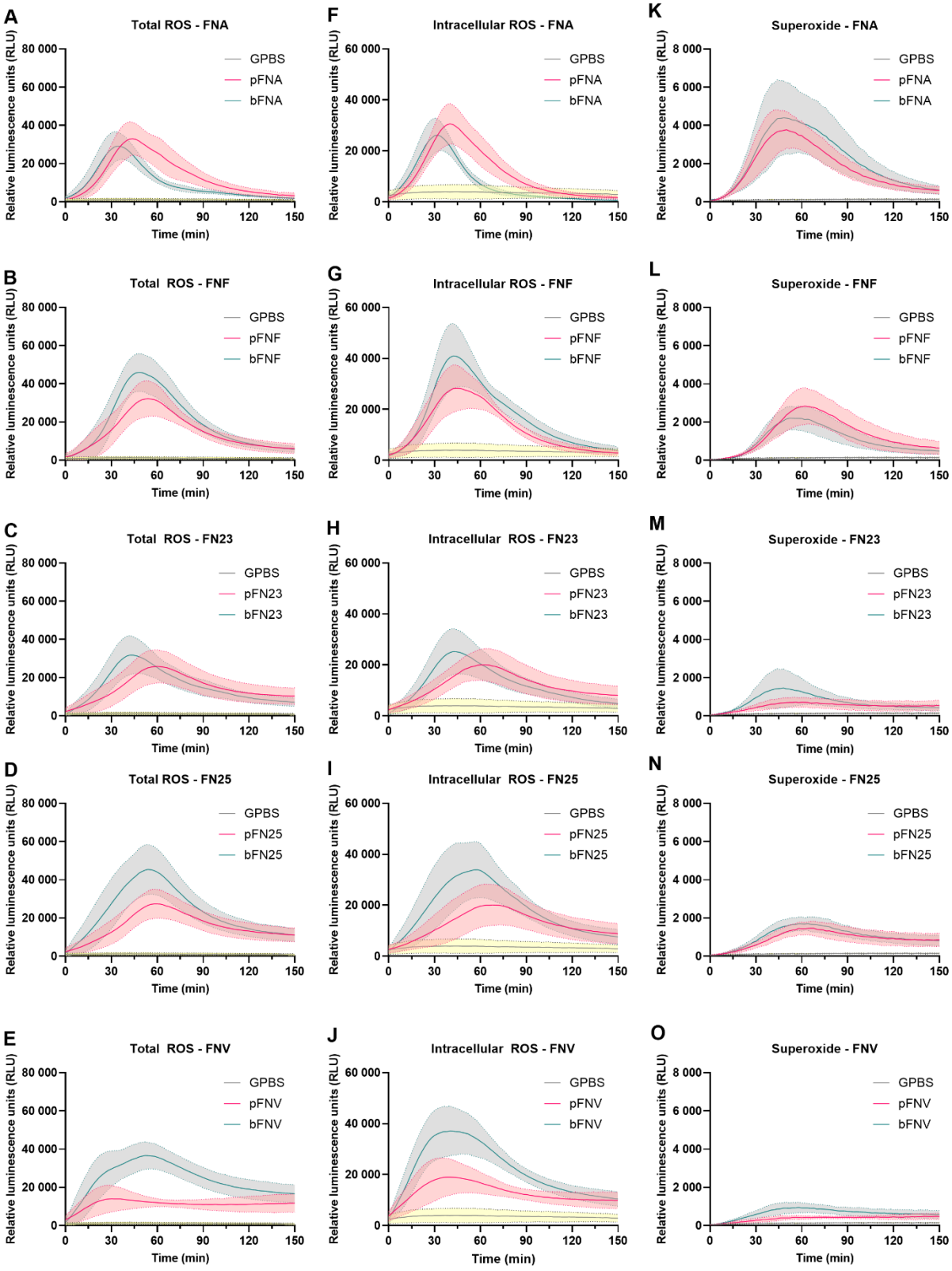

Appendix 1. Time-course of total and intracellular ROS and superoxide detected by the enhanced chemiluminescent assay. Graphs show chemiluminescence detected over the course of the assay (150 minutes) in response to planktonic (p) and biofilm-grown (b) *F. nucleatum* subspecies. **A – E:** Total ROS measured over time. **F – J:** Intracellular ROS measured over

time. **K – O:** Superoxide measured over time. Solid lines indicate mean ROS values, shaded areas above and below the solid line represent 95% confidence intervals. Yellow-shaded curves show baseline chemiluminescence of the negative control (GPBS). Experiments were performed in technical duplicates, N=8 healthy adult donors for total and intracellular ROS, N=6 healthy adult donors for superoxide.

APPENDIX 2: APOPTOSIS TIME-COURSE CURVES USED TO CALCULATE THE START AND RATE OF APOPTOSIS

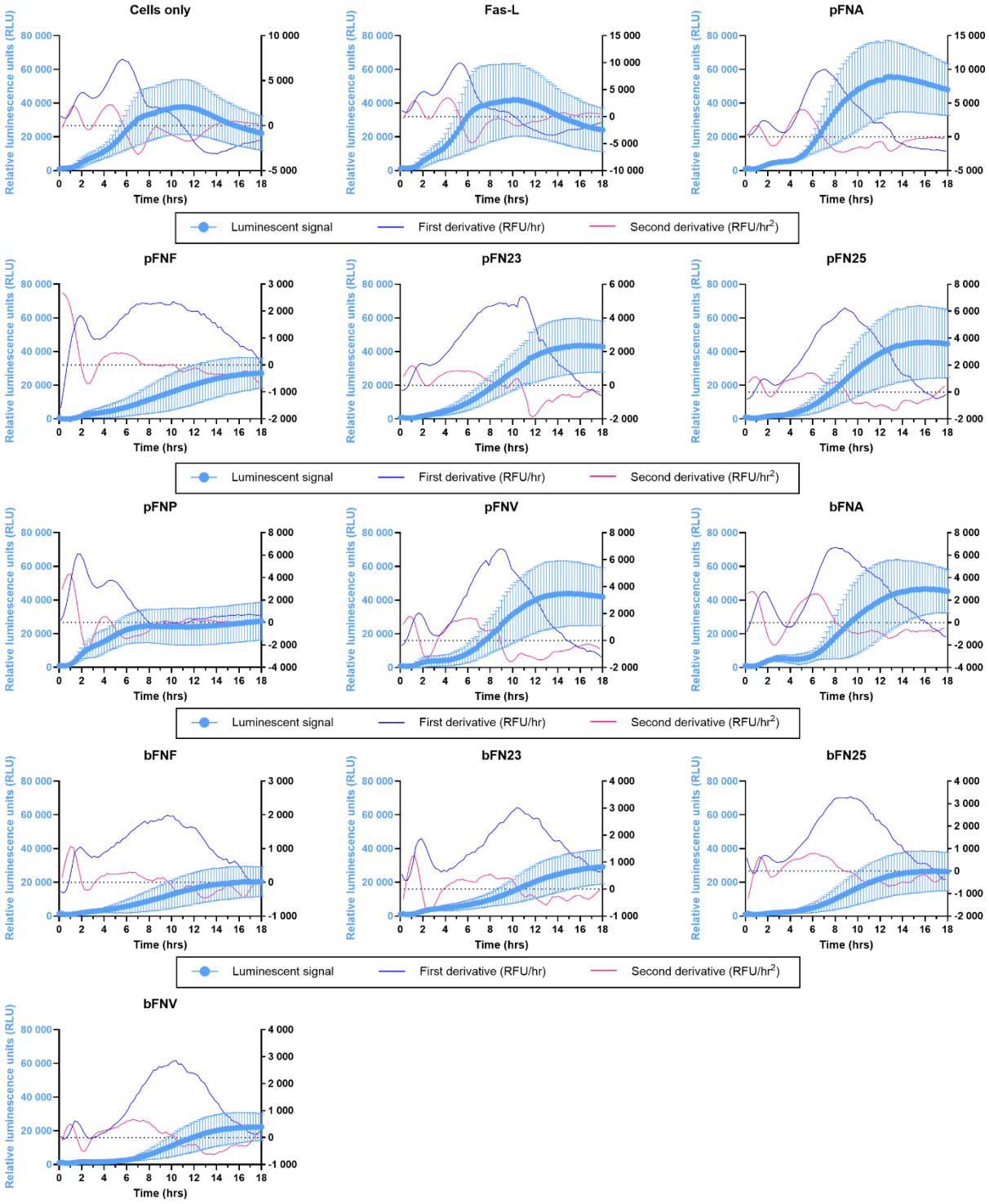

Appendix 2. Apoptosis curves with their respective first and second derivative curves. Left y-axis shows the relative luminescence units (RLU). The right y-axis shows the first and second derivative of the apoptosis curves. The highest peak in the first derivative (blue line) indicates the maximum rate of apoptosis while the highest peak in the second derivative (pink line) shows the start of apoptosis. Please note differences in the ranges of values on the right y-axes in order to clearly show first and second derivative peaks. Experiments were performed in technical

duplicate, N=4 healthy adult donors. Values shown as means with standard deviations at each time point.

APPENDIX 3: NECROSIS TIME-COURSE CURVES USED TO CALCULATE THE START AND RATE OF NECROSIS

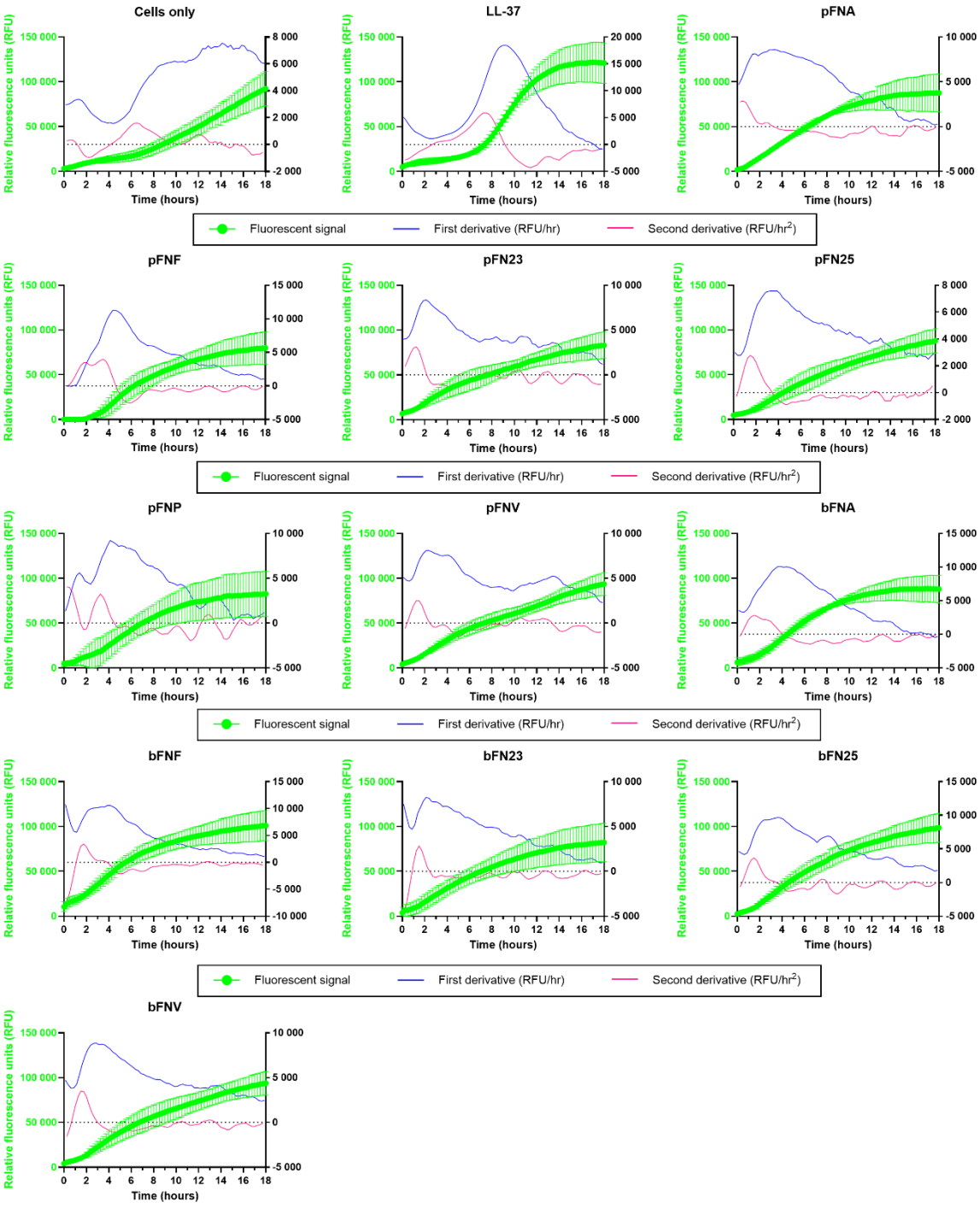

Appendix 3. Necrosis curves with their respective first and second derivative curves. Left y-axis shows the relative fluorescence units (RFU). The right y-axis shows the first and second derivative of the necrosis curves. The highest peak in the first derivative (blue line) indicates the maximum rate of necrosis while the highest peak in the second derivative (pink line) shows the start of necrosis. Please note differences in the ranges of values on the right y-axes in order to clearly show first and second derivative peaks. Experiments were performed in technical duplicate, N=4 healthy adult donors. Values shown as means with standard deviations at each time point.

APPENDIX 4: CONFERENCE ABSTRACTS

- **Functional responses of neutrophils to *Fusobacterium nucleatum* subspecies**
    - Maria Muchova, Ajoy Bardhan, Sarah A. Kuehne, Melissa M. Grant, Iain L. C. Chapple, Josefine Hirschfeld
    - Microbiology Society Annual Conference Online 2021
    - *Virtual poster presentation*

- ***Fusobacterium nucleatum* subspecies differ in biofilm forming ability *in vitro***
    - Maria Muchova, Sarah A. Kuehne, Melissa M. Grant, Iain L.C. Chapple, Josefine Hirschfeld
    - British Society for Oral and Dental Research, Annual Meeting 2021, University of Birmingham, Birmingham, UK
    - *Poster presentation*

- ***Fusobacterium nucleatum* subspecies differ in biofilm forming ability *in vitro***
    - Maria Muchova, Dario L. Balacco, Melissa M. Grant, Iain L.C. Chapple, Sarah A. Kuehne, Josefine Hirschfeld
    - PGR and ECR meeting of the Oral Microbiolgoy and Immunology Group, British Society for Dental Research, Birmingham, 2022
    - *Oral presentation*

- ***Fusobacterium nucleatum* subspecies differ in biofilm forming ability *in vitro***
    - Maria Muchova, Dario L. Balacco, Melissa M. Grant, Iain L.C. Chapple, Sarah A. Kuehne, Josefine Hirschfeld

- Anaerobe 2022, The 16th Biennial Congress of the Anaerobe Society of the Americas, Seattle, WA USA 2022
- *Oral presentation*

- **Responses of human neutrophils to *Fusobacterium nucleatum* subspecies grown planktonically and in biofilm**
  - Maria Muchova, Sarah A. Kuehne, Melissa M. Grant, Iain L.C. Chapple, Josefine Hirschfeld
  - Microbiology Society Annual Conference 2023, Birmingham, UK
  - *Poster presentation*

- **Immunogenicity of *Fusobacterium nucleatum* subspecies towards human neutrophils**
  - Maria Muchova, Sarah A. Kuehne, Melissa M. Grant, Iain L.C. Chapple, Josefine Hirschfeld
  - Anaerobe 2023, Focused Meeting of the Microbiology Society, Cardiff, UK
  - *Oral presentation*

APPENDIX 5: AWARDS, GRANTS AND PRIZES

- **Microbiology Society Travel Grant, 2022**
    - £750 awarded by the Microbiology Society to support travel to attend the Anaerobe 2022, The 16th Biennial Congress of the Anaerobe Society of the Americas, Seattle, WA USA 2022

- **Workstation Travel Grant, Don Whitley Scientific, 2022**
    - £250 awarded by the Don Whitley Scientific to support travel to attend the Anaerobe 2022, The 16th Biennial Congress of the Anaerobe Society of the Americas, Seattle, WA USA 2022

- **Oral Microbiology and Immunology Group Bursary, 2022**
    - £150 awarded by the Oral Microbiology and Immunology Group (part of British Society for Oral and Dental Research, UK) to support the attendance at the Anaerobe 2022, The 16th Biennial Congress of the Anaerobe Society of the Americas, Seattle, WA USA 2022

- **Oral and Dental Research Trust - GSK Award 2022**
    - £7 500 awarded to support the project, the aim of which was "*To investigate and understand the ability of Fusobacterium nucleatum subspecies to modulate neutrophil-mediated immune responses, and to identify disease-associated subspecies with their possible pathogenic mechanisms.*"

- **Workstation Travel Grant, Don Whitley Scientific, 2023**

- £250 awarded by Don Whitley Scientific to support the attendance of the Anaerobe 2023, Focused Meeting of the Microbiology Society, Cardiff, UK

- **Oral Microbiology and Immunology Group Bursary, 2023**
  - £135 awarded by the Oral Microbiology and Immunology Group Group (part of British Society for Oral and Dental Research, UK) to support the attendance of the Anaerobe 2023, Focused Meeting of the Microbiology Society, Cardiff, UK

APPENDIX 6: LIST OF PUBLICATIONS

First-author

- Maria Muchova, Dario L. Balacco, Melissa M. Grant, Iain L. C. Chapple, Sarah A Kuehne, Josefine Hirschfeld (2022). ***Fusobacterium nucleatum*** **Subspecies Differ in Biofilm Forming Ability** ***in vitro*****.** Frontiers in Oral Health 3:853618. doi: 10.3389/froh.2022.853618
- Maria Muchova, Sarah A. Kuehne, Melissa M. Grant, Iain L.C. Chapple, Josefine Hirschfeld (2023). ***Fusobacterium nucleatum*** **elicits subspecies-specific responses in human neutrophils**. Frontiers in Cellular and Infection Microbiology. *Manuscript submitted.*

Contributing-author

- Peter P. Smith; Ilaria J. Chicca; Jennifer L. J. Heaney; Maria Muchova; Farhat L. Khanim; Adrian M. Shields; Mark T. Drayson; Iain L. C. Chapple; Josefine Hirschfeld (2023) **Paracetamol suppresses neutrophilic oxygen radicals through competitive inhibition and scavenging.** Cell Reports. *Manuscript submitted.*

APPENDIX 7: FIRST-AUTHOR PUBLICATIONS

frontiers in Oral Health

ORIGINAL RESEARCH
published: 15 March 2022
doi: 10.3389/froh.2022.853618

Fusobacterium nucleatum Subspecies Differ in Biofilm Forming Ability *in vitro*

*Maria Muchova, Dario L. Balacco, Melissa M. Grant, Iain L. C. Chapple, Sarah A. Kuehne and Josefine Hirschfeld**

Periodontal Research Group, School of Dentistry, Institute of Clinical Sciences, University of Birmingham, Birmingham, United Kingdom

Development of dysbiosis in complex multispecies bacterial biofilms forming on teeth, known as dental plaque, is one of the factors causing periodontitis. *Fusobacterium nucleatum* (*F. nucleatum*) is recognised as a key microorganism in subgingival dental plaque, and is linked to periodontitis as well as colorectal cancer and systemic diseases. Five subspecies of *F. nucleatum* have been identified: *animalis*, *fusiforme*, *nucleatum*, *polymorphum*, and *vincentii*. Differential integration of subspecies into multispecies biofilm models has been reported, however, biofilm forming ability of individual *F. nucleatum* subspecies is largely unknown. The aim of this study was to determine the single-subspecies biofilm forming abilities of *F. nucleatum* ATCC type strains. Static single subspecies *F. nucleatum* biofilms were grown anaerobically for 3 days on untreated or surface-modified (sandblasting, artificial saliva, fibronectin, gelatin, or poly-L-lysine coating) plastic and glass coverslips. Biofilm mass was quantified using crystal violet (CV) staining. Biofilm architecture and thickness were analysed by scanning electron microscopy and confocal laser scanning microscopy. Bioinformatic analysis was performed to identify orthologues of known adhesion proteins in *F. nucleatum* subspecies. Surface type and treatment significantly influenced single-subspecies biofilm formation. Biofilm formation was overall highest on poly-L-lysine coated surfaces and sandblasted glass surfaces. Biofilm thickness and stability, as well as architecture, varied amongst the subspecies. Interestingly, *F. nucleatum* ssp. *polymorphum* did not form a detectable, continuous layer of biofilm on any of the tested substrates. Consistent with limited biofilm forming ability *in vitro*, *F. nucleatum* ssp. *polymorphum* showed the least conservation of the adhesion proteins CmpA and Fap2 *in silico*. Here, we show that biofilm formation by *F. nucleatum in vitro* is subspecies- and substrate-specific. Additionally, *F. nucleatum* ssp. *polymorphum* does not appear to form stable single-subspecies continuous layers of biofilm *in vitro*. Understanding the differences in *F. nucleatum* single-subspecies biofilm formation may shed light on multi-species biofilm formation mechanisms and may reveal new virulence factors as novel therapeutic targets for prevention and treatment of *F. nucleatum*-mediated infections and diseases.

Keywords: biofilm, *Fusobacterium nucleatum*, periodontitis, subspecies, pathogen, fusobacteria, adhesin

OPEN ACCESS

Edited by:
Georgios N. Belibasakis, Karolinska Institutet (KI), Sweden

Reviewed by:
Sebastian Aguayo, Pontificia Universidad Católica de Chile, Chile
Thomas Thurnheer, University of Zurich, Switzerland

****Correspondence:***
Josefine Hirschfeld
j.hirschfeld@bham.ac.uk

Specialty section:
This article was submitted to Oral Infections and Microbes, a section of the journal Frontiers in Oral Health

Received: *12 January 2022*
Accepted: *18 February 2022*
Published: *15 March 2022*

Citation:
Muchova M, Balacco DL, Grant MM, Chapple ILC, Kuehne SA and Hirschfeld J (2022) Fusobacterium nucleatum Subspecies Differ in Biofilm Forming Ability in vitro. Front. Oral. Health 3:853618. doi: 10.3389/froh.2022.853618

INTRODUCTION

The oral environment consists of a multitude of bacterial species living on both soft and hard tissues in complex multispecies communities known as biofilms [1]. Dental plaque, a type of biofilm which forms on the surface of teeth, has been extensively studied for decades due to its association with periodontitis, a chronic inflammatory disease of the tooth-supporting tissues [2]. Periodontitis causes connective tissue attachment loss, inflammation and, if left untreated, tooth loss [2, 3]. One of the factors leading to periodontitis is the accumulation of dental plaque and emergence of dysbiosis therein [2, 3].

Health-related supra- and sub-gingival bacterial communities are often composed of Gramme-positive and Gram-negative early colonisers including *Streptococcus, Neisseria, Prevotella, Haemophilus*, and *Rothia* genera, among other less abundant genera, creating a distinct signature of a healthy, symbiotic state [4–7]. However, studies analysing diseased periodontal sites exhibited a shift toward communities containing anaerobic, Gram-negative periodontal pathogens belonging to Socransky's "red complex" and leading to dysbiosis with an associated destructive immune-inflammatory response resulting in tissue damage [8–12].

Fusobacterium nucleatum, an anaerobic commensal member of dental biofilms [13], is present in low numbers in healthy subgingival dental biofilm [4] but is enriched in periodontal pockets [14]. It has been identified as a key bridging organism between the early colonisers and periodontal pathogens [15]. It is also considered an opportunistic pathogen due to its association with systemic diseases, such as cardiovascular disease, ulcerative colitis and colorectal cancer [13, 16], as well as with extra-oral infections which can lead to adverse pregnancy outcomes [13]. Five subspecies of *F. nucleatum* have been identified to date: *animalis*, *fusiforme*, *nucleatum*, *polymorphum*, and *vincentii* [13]. Some authors only recognise four subspecies, classifying *fusiforme* and *vincentii* as one subspecies *vincentii* [17].

Despite the close genomic relatedness of all subspecies, differences in pathogenicity have been recognised, such as host immune response modulation: subspecies *nucleatum* (ATCC 25586), *polymorphum* (ATCC 10953) and *vincentii* (ATCC 49256) were shown to prevent superoxide generation induced by N-formylmethionyl-leucyl-phenylalanine in neutrophil-like HL-60 cells. Additionally, subspecies *polymorphum* increased the rate of apoptosis in HL-60 cells when compared to the other subspecies [18]. *F. nucleatum* subspecies were also studied in *in vitro* multi-species biofilm models. Differences in the incorporation of subspecies into the biofilm were described, where bacterial numbers of *F. nucleatum* ssp. *vincentii* and ssp. *polymorphum* were significantly lower in comparison with ssp. *nucleatum* [19].

F. nucleatum adhesion proteins have been identified, which mediate coaggregation and biofilm formation with various oral microbes as well as salivary proteins: outer membrane protein RadD with a putative accessory protein Aid1 [20], autotransporter Fap2 [20], porin FomA [20], outer membrane protein CmpA [20], and adhesin FadA [21]. Homologues of adhesins from other bacterial species have also been identified in *F. nucleatum in silico*, such as YadA-like adhesin originally found in *Yersinia* species [22].

Surprisingly, despite its structural importance in dental plaque and its role in pathogenic biofilms in colorectal cancer and other diseases, biofilm formation by single *F. nucleatum* subspecies is poorly understood. Moreover, few authors have used type strains as reference strains to the clinical isolates in studies of *F. nucleatum*, and many have not reported the subspecies used, making a comparison of these results difficult. While it is clinically relevant to study *F. nucleatum* in multi-species biofilms, information obtained from single-subspecies *F. nucleatum* biofilms without the presence of additional binding partners is necessary for better understanding of biofilm-related immunogenic and pathogenic properties of *F. nucleatum* subspecies and virulence factor expression.

Therefore, this study aimed to investigate single-subspecies biofilm formation abilities by *F. nucleatum* subspecies along with analysis of differences in adhesins known to mediate biofilm formation and aggregation. A further aim was to utilise a simplified *in vitro* single-subspecies biofilm model which could be repeated by other researchers, using widely available substrates and substrate coatings, to better understand biological properties of each subspecies. We hypothesised that there is no difference in biofilm formation and architecture among *F. nucleatum* subspecies.

MATERIALS AND METHODS

Bacterial Strains and Growth Conditions

The following type strains of *F. nucleatum* were obtained from the Periodontal Research Group culture collection (School of Dentistry, University of Birmingham, UK) and were originally purchased from the American Tissue Culture Collection (ATCC): *F. nucleatum* ssp. *animalis* ATCC 51191 (FNA), *F. nucleatum* ssp. *fusiforme* ATCC 51190 (FNF), *F. nucleatum* ssp. *nucleatum* ATCC 25586 (FNN25), *F. nucleatum* ssp. *polymorphum* ATCC 10593 (FNP), and *F. nucleatum* ssp. *vincentii* ATCC 49256 (FNV). Additionally, a genetically tractable strain *F. nucleatum* ssp. *nucleatum* ATCC 23726 (FNN23) was kindly provided by Dr. Daniel Slade (Virginia Polytechnic Institute and State University, Blacksburg VA, USA). The identity of all subspecies was confirmed by 16S rRNA sequencing.

All subspecies were grown at 37°C in an anaerobic chamber (80% N_2, 10% CO_2, and 10% H_2; Don Whitley DG250 Anaerobic Workstation, Don Whitley Scientific, Bingley, UK) on Schaedler anaerobe agar plates (SAA; Sigma-Aldrich/Merck, Darmstadt, Germany). Liquid cultures were grown in Schaedler anaerobe broth (SAB; Oxoid, Basingstoke, UK).

Surface Coating and Biofilm Growth

In order to evaluate biofilm formation of *F. nucleatum* subspecies, substrates commonly used for *in vitro* biofilm studies were used: glass (12 mm diameter; Marienfeld Superior, Lauda-Königshofen, Germany) and plastic (13 mm diameter; Thermo Scientific™ Nunc™ Thermanox™, Thermo Fisher Scientific, Loughborough, UK; referred to as "Thermanox" hereafter) coverslips placed in a 24-well-plate. Artificial saliva (AS) was used as a coating agent to mimic human saliva and formation

of salivary pellicle to promote bacterial adhesion [23]. AS was prepared according to Millhouse et al. [24] by using the following reagents: porcine stomach mucins 0.25% w/v, potassium chloride 0.02% w/v, calcium chloride dihydrate 0.02% w/v, yeast extract 0.2% w/v, proteose peptone 0.5% w/v (all obtained from Sigma-Aldrich/Merck, Darmstadt, Germany), sodium chloride 0.35% w/v (Thermo Fisher Scientific, Loughborough, UK), and Lab-Lemco powder 0.1% w/v (Oxoid, Basingstoke, UK) in ultrapure water (Milli-Q, Merck Millipore, Burlington, MA, USA); urea was added after autoclaving to a final concentration of 0.05% v/v (Sigma-Aldrich). Additionally, substrates were coated using agents promoting cell attachment to culture surfaces: fibronectin (from human plasma, Merck Millipore) [25], gelatin (from porcine skin) [26], and poly-L-lysine (both from Sigma-Aldrich/Merck) [27].

Substrate coating was performed as follows: AS was added to coverslips and incubated at 37°C for 1 h [28]. Next, AS was removed and bacterial cultures were added immediately without substrate washing or drying to simulate *in vivo* conditions. Fibronectin diluted in PBS (5 $\mu g/cm^2$) was applied and incubated for 45 min at room temperature. Gelatin solution (0.1% in PBS) was incubated for 20 min at 37°C. Poly-L-lysine coating was performed for 10 min at room temperature. These surface coatings were left to dry in a laminar flow hood as per the manufacturers' instructions without washing. Additionally, a set of glass coverslips was sandblasted to create a roughened surface. Sandblasting was completed using a Basic quattro sandblasting unit (Renfert, Hilzingen, Germany), in which each coverslip was treated for 5 s with aluminium oxide (25 μm grit size, 1.2 mm nozzle).

To initiate biofilm growth, planktonic *F. nucleatum* cultures were washed once with PBS and the optical density of each culture was adjusted to $OD_{600} = 1$ in SAB, corresponding to 1.62×10^9 CFU/ml for each subspecies. For each single-subspecies biofilm, 400 µl of bacterial suspension was added to each well containing studied substrates and biofilms were incubated static for 72 h, under anaerobic conditions. SAB was replaced after 24 and 48 h and biofilms were monitored for contamination daily.

Biomass Quantification Using Crystal Violet

Biofilm biomass was quantified by crystal violet (CV) staining. After 72 h of incubation, biofilms were carefully washed once with 100 µl PBS and air-dried for 2 h at 37°C, then stained with a CV solution (200 µl, 0.05 % w/v) at room temperature for 30 min. After staining, biofilms were gently washed with 200 µl PBS and air dried at 37°C for 2 h. Ethanol (100%, 200 µl) was used to destain the biofilms for 1 h on a plate shaker. Ethanol solution from each well was diluted in Milli-Q water 1:10 in a 96-well plate and the absorbance was measured at 600 nm (Microplate reader Spark®, Tecan; software SparkControl, v. 2.3, Tecan). To account for differences between glass and plastic coverslip surface area, absorbance readings per cm^2 were calculated using the formula below. The surface area of a glass coverslip was 113.04 mm^2, the area of a Thermanox coverslip was 132.67 mm^2.

$$average\ CV\ absorbance\ corrected\ for\ blank\ \times \frac{100\ mm^2}{area\ of\ the\ coverslip\ (mm^2)}$$

Fluorescent Biofilm Staining and Confocal Laser Scanning Microscopy (CLSM)

Biofilms for CLSM analysis were grown in 24-well black plates with clear base (polystyrene, thickness 190 µm, Vision Plate™, 4titude, Surrey, UK) either with no surface treatment, or coated with fibronectin, gelatin or poly-L-lysine as stated above. In order to avoid excessive detachment, biofilms were first fixed with 4% paraformaldehyde for 10 min, then washed in PBS and stained using green fluorescent, cell permeant nucleic acid stain SYTO™ 9 (FilmTracer™ LIVE/DEAD® Biofilm Viability Kit, Invitrogen, Renfrew, UK) according to the manufacturer's instructions. Briefly, 3 µl of SYTO™ 9 were added to 1 ml of sterile PBS and biofilms were stained with 200 µl of the diluted stain for 20 min at room temperature in the dark.

Samples were imaged immediately after staining using CLSM (LSM 700, Zeiss, Germany), with a 40X oil immersion objective at 488/500 nm. Maximum thickness of the biofilms was estimated by obtaining z-stack horizontal images at 1.3 µm intervals. Biofilms were grown in triplicate in one experiment and images were acquired in the centre of each well using Zeiss Zen 2011 software.

Preparation of Biofilms and Scanning Electron Microscopy (SEM)

In order to examine single-subspecies biofilm architecture using SEM, biofilms were grown on poly-L-lysine coated plastic (Thermanox™) coverslips in 24-well plates. Biofilms were fixed using 2.5% glutaraldehyde (Agar Scientific, Stansted, United Kingdom) in 0.1 M sodium cacodylate buffer (pH 7.4, BioWorld, Dublin, Ireland) for 10 min at room temperature. Following fixation, biofilms were dehydrated with increasing ethanol concentrations (20–100%) and incubated for 10 min at each step.

Finally, drying agent hexamethyldisilizane (Sigma-Aldrich/Merck, Darmstadt, Germany) was applied and left to evaporate overnight. Coverslips with biofilms were mounted onto aluminium specimen stubs (Agar Scientific, Stansted, United Kingdom), sputter coated with two layers of gold and visualised using a scanning electron microscope (Zeiss EVO MA10). A visible layer of biofilm was chosen after visual evaluation of each specimen under low magnification (50X) and recorded at 1000X and 5000X magnification.

Bioinformatics and Phylogenetic Analyses

Bacterial genomes of *F. nucleatum* ssp. *animalis* ATCC 51191 (GCA_000220825), *F. nucleatum* ssp. *nucleatum* ATCC 23726 (GCA_000178895), *F. nucleatum* ssp. *nucleatum* ATCC 25586 (GCA_000007325), *F. nucleatum* ssp. *polymorphum* ATCC 10953 (GCA_000153625), *F. nucleatum* ssp. *vincentii* ATCC 49256 (GCA_000182945) were retrieved from EnsemblBacteria (Release 52) [29]. *F. nucleatum* ssp. *fusiforme* data were not available on this portal, possibly due to their close genetic relatedness with *F. nucleatum* ssp. *vincentii*.

Orthologues were identified using blastp (v. 2.12.0) [30] with default parameters and *F. nucleatum*, ssp. *nucleatum* ATCC 25586 proteins as queries, with a cutoff e-value of 1e-10. Protein domains were annotated using InterPro [31] with a cutoff e-value of 1e-5. Multisequence alignment of CmpA and Fap2 proteins was performed using MAFFT (v. 6) [32] with the "–auto" option. The phylogenetic tree was constructed using the Neighbour-Joining method [33], JTT substitution model and bootstrap 1000.

Statistical Analysis

Statistical analysis was performed using GraphPad Prism (version 9.3.0 for Windows, GraphPad Software, San Diego, California, USA). Biomass quantification data were analysed using Shapiro-Wilk normality test and shown to conform to normal distribution. Samples were compared within subspecies and either untreated Thermanox™ surface or untreated glass surface were considered as controls. Values were analysed by one-way ANOVA, followed by Dunnett's *post-hoc* test. Results were considered statistically significant if $p < 0.05$. Graphs were created using GraphPad Prism, version 9.3.0.

RESULTS

Biofilm Thickness and Stability Varies Among *F. nucleatum* Subspecies and on Different Surfaces

All subspecies formed biofilms detectable with CV, with the exception of FNP, which did not form a continuous biofilm on any of the tested surfaces. When examined visually during the incubation period, this subspecies was found to remain planktonic in the biofilm supernatant.

Differences in biofilm mass were seen amongst the subspecies and on the different surfaces (**Figures 1A,B**): Generally, sandblasted glass surfaces supported biofilm formation best with significantly higher biofilm mass in most subspecies compared to untreated glass. Second best surface coating was AS, supporting significantly higher biofilm formation by FNN25 and FNP on glass surfaces, and FNN25, FNP, and FNV on plastic surfaces. However, even though absorbance values of FNP biofilms were significantly higher on both glass and plastic coated with AS compared to untreated surfaces ($p = 0.04$ and $p = 0.02$, respectively), the amount of biofilm quantified was consistently low (mean absorbance values of 0.017 and 0.029, respectively). FNF adhered significantly better to uncoated Thermanox coverslips when compared to uncoated glass ($p = 0.002$), however the other subspecies showed no difference in biofilm formation between glass and plastic surfaces. FNA and FNF were the best biofilm formers on plastic surfaces.

Biofilm thickness was also examined using CLSM and mean values estimated from three-dimensional biofilm images (**Figure 2**). Similar to the results obtained by CV staining, all subspecies except FNP formed a continuous layer of biofilm. Only single bacterial cells of FNP were observed on untreated and coated surfaces (**Supplementary Figure 1**). A small area of biofilm formation by FNP was detected in the centre of poly-L-lysine coated wells, for which the thickness was determined (**Figure 2B**; 9.1 ±1.3 μm, mean ± SD).

Large standard deviations were associated with some subspecies-surface combinations (FNA, FNF) and were seen in both CV and CLSM experiments. These reflect a high degree of visually observed biofilm detachment during handling, indicating low adhesive strength of these biofilms.

Biofilm Architecture Differs Among *F. nucleatum* Subspecies

Thermanox coverslips coated with poly-L-lysine were chosen as the surface for biofilm analysis by SEM based on CLSM results, which showed higher biofilm thickness on this type of surface. Overall, high magnification (1000X, **Figure 3A**) revealed uneven layers of biofilm with raised areas and water channels. FNA, FNF, and FNN25 formed continuous, multi-layered biofilms with visible aggregates, whilst FNN23 formed thinner biofilms, mostly observed as mono-layers with smaller aggregates. Biofilms formed by FNV appeared as flat, continuous mono-layers. Again, FNP did not form a continuous layer of biofilm, but individual bacteria and small pre-biofilm aggregates were observed.

Cell-to-cell cohesion was observed in more detail under 5000X magnification (**Figure 3B**). In all biofilms, bacterial cells were found to cohere with neighbouring cells either in a parallel fashion, or cells were intertwined. Interestingly, all analysed biofilms seemed to be lacking extracellular matrix (ECM). Taken together, biofilm architecture visibly differed among *F. nucleatum* subspecies with regard to thickness and formation of aggregates and water channels. Cell-to-cell cohesion did not seem to differ among subspecies.

Conservation of Adhesion Protein Orthologues Varies Among *F. nucleatum* Subspecies

To investigate possible differences in adhesion proteins amongst the subspecies, which might explain the observed lack of biofilm formation in FNP, analysis of the bacterial genomes was carried out. Sequence alignments of Aid1, CmpA, FadA, Fap2, FomA, RadD, and YadA from FNN25 identified orthologous proteins in the *F. nucleatum* ATCC subspecies genomes publicly available on EnsemblBacteria (Release 52) [29]. As expected, FNN23 orthologues were highly conserved (identity >90%). In contrast, our approach did not identify any Aid1, FomA, and RadD orthologues in FNV and any FadA and YadA orthologues in FNA. The genome of FNF was not available on this database.

Orthologues of all the considered proteins were found in FNP. Interestingly, CmpA and Fap2 orthologues were identified in all subspecies; however, FNP orthologues were less conserved with the lowest identity percentage among the four analysed subspecies (**Figure 4A**). Annotation of the protein domains highlighted variability in protein domains and length of proteins. Interestingly, both CmpA and Fap2 presented an Autotransporter domain in FNN25 (**Figure 4A**). Phylogenetic

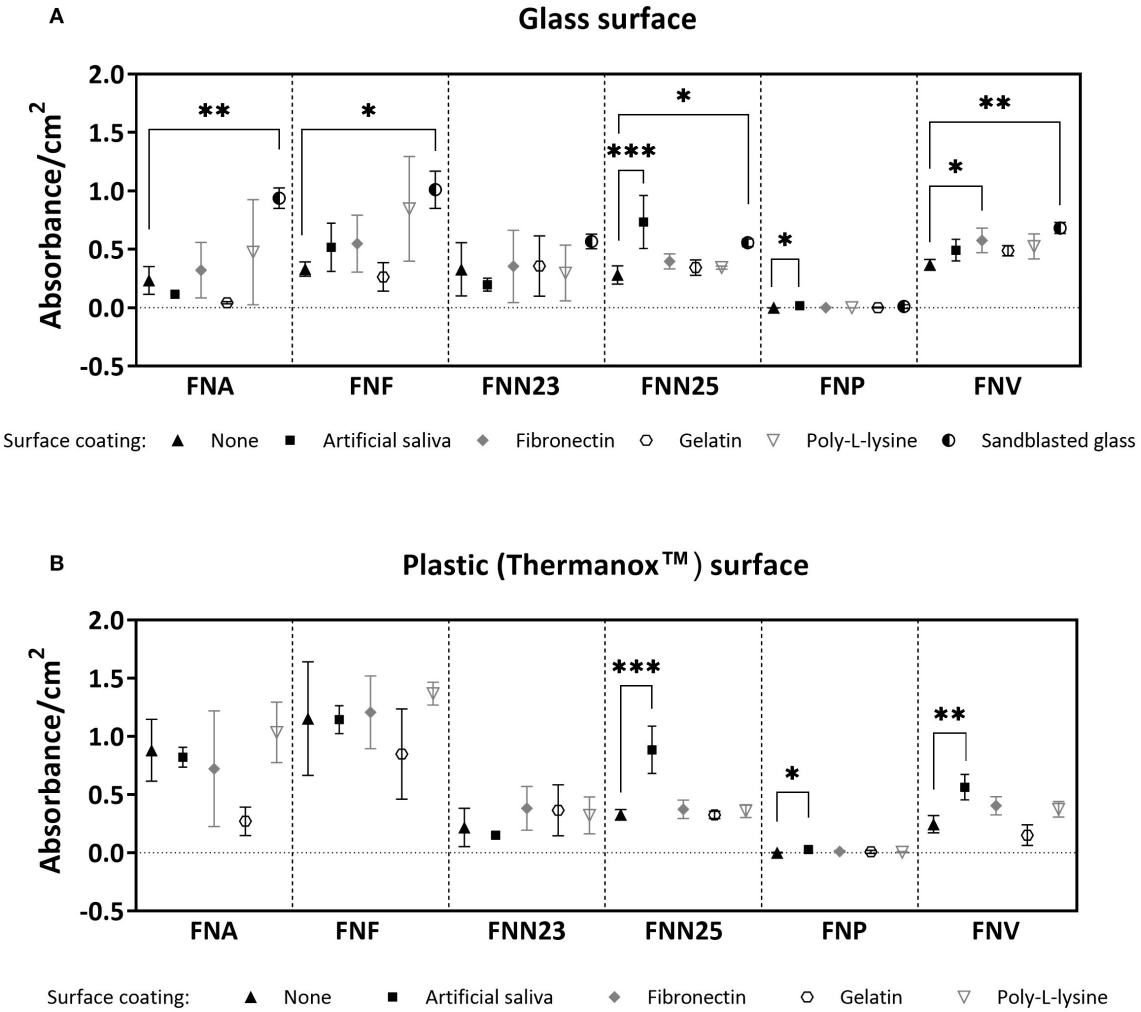

FIGURE 1 | Crystal violet biomass quantification results. **(A)** Quantification on glass coverslips with or without (control) surface coatings. No significant differences were found for FNN23. **(B)** Quantification on Thermanox coverslips with or without (control) surface coatings. No significant differences were found for FNA, FNF, and FNN23. Assays were carried out as three independent experiments in triplicate. Mean values with standard deviations are shown. One-way ANOVA was performed followed by Dunnett's *post-hoc* test for within subspecies differences between control (uncoated glass/uncoated Thermanox) and test samples (*$p < 0.05$; **$p < 0.01$; ***$p < 0.001$).

analysis of CmpA and Fap2 shows that the respective orthologues in all the subspecies are highly conserved, except for the FNP proteins, which are more distantly related (**Figure 4B**).

DISCUSSION

F. nucleatum as a commensal microorganism, opportunistic pathogen, and emerging oncobacterium in the oral cavity and at extraoral sites has received considerable attention in recent years [16]. Individual subspecies have been differentially related to oral health and disease: FNN and FNA have been associated with disease [34–36]; while FNF and FNV have been identified in healthy sites [13, 34]; interestingly, FNP is found in both healthy [34] and diseased periodontal tissues [35].

Differential involvement of subspecies in health and disease might suggest differences in their virulence properties. It is increasingly evident from *in vitro* studies that differences in pathogenicity among *F. nucleatum* subspecies exist, such as differences in coaggregation with other oral bacteria and biofilm formation in multispecies biofilm models [19]. To the authors' knowledge, formation of single-subspecies biofilms by *F. nucleatum* ATCC type strains has not been addressed in the literature to date, and data presented in this study showed for the first time that not all *F. nucleatum* subspecies have the ability to form stable single-subspecies biofilms. In our study, FNP did not form biofilms but only small bacterial aggregates. In support of this finding, similar results were obtained by Karched et al., who showed poor single-subspecies biofilm formation by FNP, whilst a strong autoaggregating ability was shown in this subspecies [37].

Biofilm stability of *F. nucleatum* subspecies has not been addressed in the literature to date. The present study showed

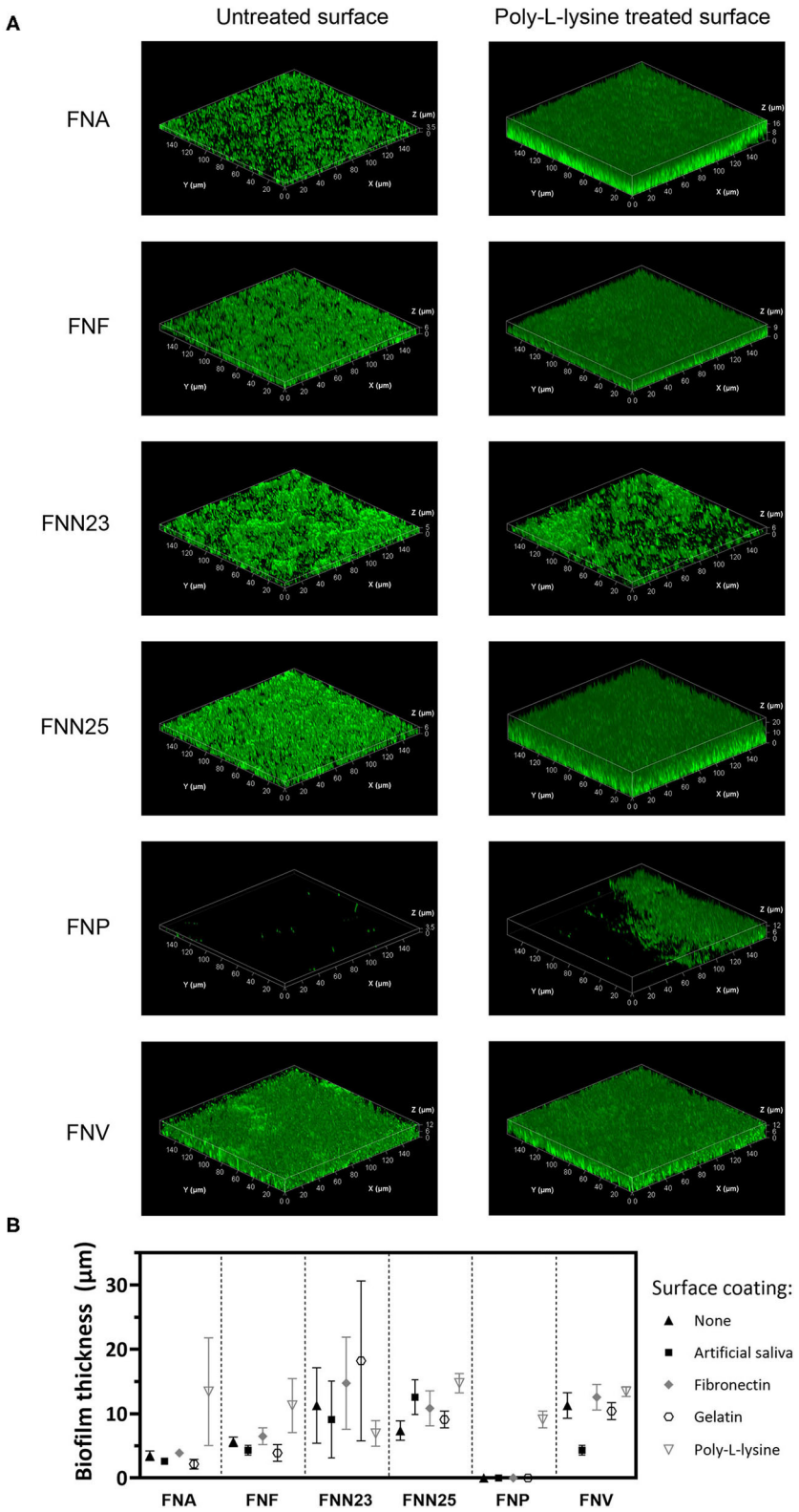

FIGURE 2 | Biofilm thickness of *F. nucleatum* subspecies determined by CLSM. **(A)** Representative Z-stack 3D images of single-subspecies biofilms grown on poly-L-lysine coated plastic surface. Biofilms are enclosed in a bounding box with scaled coordinates; x, y, and z axes show the dimensions indicated in µm. Differences in biofilm thickness can be observed. **(B)** Biofilm thickness estimated from z-stacks. Experiment was performed once with biofilms grown in triplicates. Mean values with standard deviations are shown.

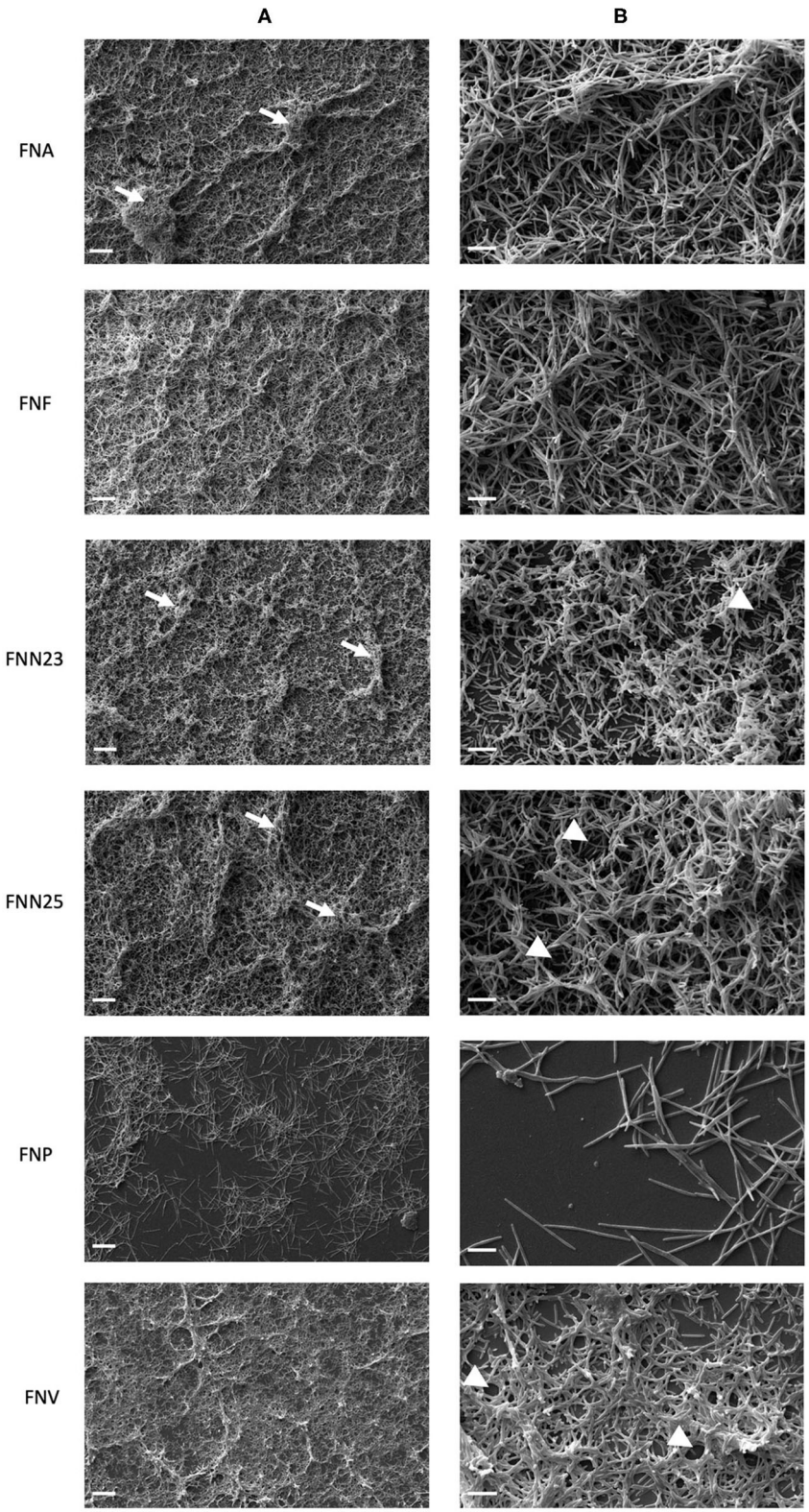

FIGURE 3 | Micrographs of single-subspecies *F. nucleatum* biofilms grown on poly-L-lysine coated Thermanox coverslips. **(A)** Micrographs showing differences in biofilm architecture. White arrows indicate bacterial aggregates within the biofilm. 1000X magnification, scale bar 20 μm. **(B)** Micrographs showing cell-to-cell cohesion. White arrow heads indicate presumed water channels. 5000X magnification, scale bar 5 μm. Biofilms from two independent experiments grown in duplicates were imaged and representative micrographs are shown.

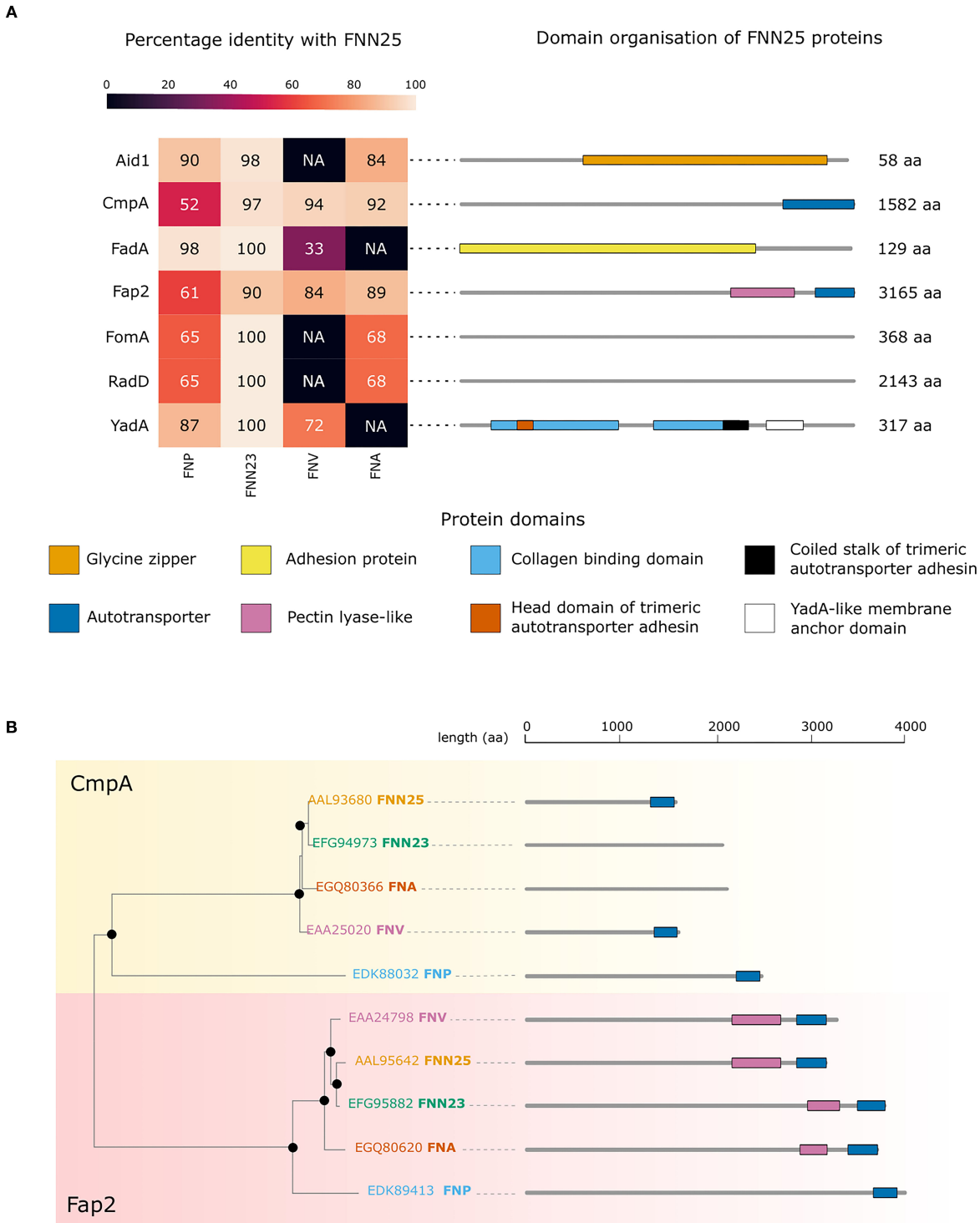

FIGURE 4 | Bioinformatic analysis of adhesion proteins in *F. nucleatum* subspecies. **(A)** Conservation of adhesion proteins in ATCC strains of *F. nucleatum*. The heatmap shows the percentage of identity with the FNN25 adhesion proteins Aid1, CmpA, FadA, Fap2, FomA, RadD, YadA. Protein length and domain organisation are indicated on the right for each of FNN25 proteins. The domains are indicated and coloured differently: glycine zipper (orange); autotransporter (dark blue); adhesion protein (yellow); pectin lyase-like (pink); collagen binding domain (light blue); head domain of trimeric autotransporter adhesin (dark orange); coiled stalk of trimeric autotransporter adhesin (black); YadA-like membrane anchor domain (white). **(B)** CmpA and Fap2 phylogenetic tree. The CmpA branch is highlighted in yellow, the Fap2 branch is highlighted in pink. Black circles represent bootstrap values > 95. FNN25 proteins are coloured in orange; FNN23 proteins in green; FNA proteins in dark orange; FNV in pink; FNP in light blue. Protein structures and lengths are outlined on the right of the tree. Autotransporter domains are coloured in blue, pectin lyase-like domains in pink. Figures were drawn with seaborn (version 0.11.2) and R (version 4.1.2).

considerable biomass variation likely caused by unstable biofilm formation. Under physiological conditions in the oral cavity, *F. nucleatum* grows as a component of complex multi-species biofilms in the presence of multiple binding partners, especially early colonisers [38]. Periasamy et al. showed that subspecies *polymorphum* formed stable biofilms with the early coloniser *Actinomyces naeslundii*, however, it did not form single-subspecies biofilms in saliva [39]. This further supports our observation that FNP does not form stable biofilms on its own. Another factor, which was not considered in the present study, is pH: its manipulation and increase to 8.2 was found to induce biofilm growth in subspecies *polymorphum* [40, 41]. Investigating the impact of pH on biofilm formation by all subspecies may be an important parameter to include in future experiments.

In our study, formation of stable biofilms was also substrate-specific. First, surfaces were coated with AS, which is used to mimic *in vivo* conditions and improve adhesion of bacteria to substrates [23]. The advantage of using AS is the elimination of potentially confounding effects of human salivary components and their natural fluctuations, such as antimicrobial peptides, presence of other bacterial species and their products, and extrinsic or systemic factors [42]. AS significantly supported biofilm formation only in case of FNN25 grown on glass and plastic and FNV grown on plastic surfaces. To the best of the authors' knowledge, *F. nucleatum* single-species biofilm formation on AS coated surfaces has not been reported in the literature to date, however Tavares et al. showed stable single-species biofilm formation by FNF on plastic surfaces coated with human saliva [43]. Using human saliva in future studies of *F. nucleatum* single-species can help to understand whether and how specific salivary properties may influence the selection and growth of certain subspecies in the oral cavity.

Secondly, surfaces coated with fibronectin, a glycoprotein present in physiological fluids such as plasma and saliva [44], were covered with an intermediate amount of biofilm biomass by all subspecies but FNP. In a previous study, *F. nucleatum* was shown to adhere to fibronectin [45] and more specifically, subspecies *polymorphum* ATCC 10953 was found to adhere to fibronectin-coated gingival epithelial cells and fibronectin-coated coverslips as single cells, whilst biofilm formation was not investigated. This supports our finding that single FNP cells adhere to fibronectin coated surfaces, however, studies analysing FNP biofilm formation on fibronectin coated surfaces are missing.

Thirdly, gelatin, a derivative of collagen found in the extracellular matrix of tissues, is a commonly used polymer for coating tissue culture vessels [26]. Benn et al. reported that adhesion of *Escherichia coli* (*E. coli*) was improved by gelatin, but was dependent on specific buffering conditions and bacterial strains [46]. In our study, however, gelatin supported only a low amount of biofilm formation and may therefore not be a recommendable coating agent for *F. nucleatum* biofilms. Additionally, surfaces coated with poly-L-lysine, a cationic coating agent promoting bacterial adhesion by electrostatic interactions as mostly shown in *E. coli* studies [46, 47], led to higher amounts of biofilm in the present study seen microscopically (**Figures 2**, **3**), but this was not statistically significant in CV assays (**Figure 1**). Nevertheless, we recommend poly-L-lysine as a biofilm-supporting coating agent for *F. nucleatum*.

Apart from surface coatings, surface roughness was also found to promote biofilm formation on multiple types of surfaces by providing a larger surface area for adhesion of bacteria and also protecting adherent bacteria from detachment by shear forces [48]. In this study, the highest mean amount of biomass on glass surfaces was measured on sandblasted glass coverslips. Sandblasting, however, makes glass opaque, rendering biofilm analysis by conventional CLSM challenging if an inverted CLSM is not available. Another material frequently used for oral biofilm assays is hydroxyapatite (HA) [49], mimicking dental enamel surfaces. *In vivo*, periodontal biofilms predominantly adhere to enamel, dentine [50] and cementum [51]. In future studies, utilising dental tissue substrates such as dentine slices or other relevant surfaces such as titanium used in dental implant manufacturing, in combination with inverted CLSM [52] or atomic force microscopy [53, 54] could provide more detailed information on bacterial adhesion and biofilm architecture.

Assessment of the architecture of single-subspecies biofilms showed observable differences among subspecies. Similar observations were made in a previous study investigating *Staphylococcus aureus* and *Pseudomonas aeruginosa*, showing strain-specific differences such as large mushroom-like structures, aggregates and differences in thickness [55]. Possible underlying reasons for differences in architecture might be differences in utilisation of available nutrients by subspecies affecting biofilm maturation or subspecies-specific combination of outer membrane proteins influencing coaggregation.

Of note, biofilm structure also differed between microscopy techniques in our study. For example, FNA biofilms analysed with CLSM appeared as mono-layered structures, while FNA biofilms imaged with SEM were shown to be multi-layered. This may have been due to the fixation procedures affecting the degree of biofilm detachment. Fixation preserves cell morphology and the native structure of biofilms [56], however the degree of paraformaldehyde fixation might have been insufficient in our study due to a short fixation period. Longer incubation in paraformaldehyde [52, 56] and comparison with other types of fixatives in future studies may resolve this issue.

In general, biofilm sample preparation for imaging is often a destructive process, involving multiple washing steps, which may affect biofilm structure and introduce artefacts [57]. Presumed water channels, which were observed in the studied biofilms, could also be considered as such artefacts. Additionally, ECM was not observed in any of the samples assessed in this study. Lack of ECM is likely attributed to the preparation technique for microscopy, as it was demonstrated that biofilm fixation and dehydration for SEM can damage ECM [58]. Presence of ECM in *F. nucleatum* biofilms has been observed in a number of studies, suggesting that *F. nucleatum* forms biofilms according to the definition by Costerton et al. [59]. Ali Mohammed et al. characterised overall composition of ECM in single-species biofilms formed by *F. nucleatum* ssp. *nucleatum* (ATCC 25586) [60]. Subsequently, ECM proteins of the same subspecies were further analysed [61]. Tavares et al. reported ECM surrounding

F. nucleatum ssp. *fusiforme* cells in single-species biofilms [43]. However, the ECM of the remaining *F. nucleatum* subspecies has not been studied in a single-species biofilm context.

In order to address the limited ability of FNP to form stable biofilms, bioinformatic analysis of known adhesion proteins was performed and showed that a number of orthologues found in this subspecies have very low identity when compared to FNN25, a biofilm forming strain often used as a control in biofilm models [19]. The analysed adhesion proteins RadD, Aid1 [20, 62], Fap2 [63], FadA [21], and CmpA [64] were mainly reported to adhere to other oral pathogens, however they have not been studied in relation to autoaggregation and biofilm formation within the same *F. nucleatum* subspecies. FomA binds to human protein statherin found in saliva [65]. The YadA-like protein, which was originally reported as an adhesin and virulence factor in *Yersinia* species and was identified in *F. nucleatum* [66], adheres to fibronectin and collagen present in the salivary pellicle and extracellular matrix of human cells [22].

Based on our analysis, all proteins were found in the FNP genome, however four of these (CmpA, Fap2, FomA, and RadD) were not well-conserved. Only two proteins, CmpA and Fap2 were detected in all subspecies and were found to share a common autotransporter domain in FNN25. In addition, our *in silico* analysis found the autotransporter domain in Fap2 in all subspecies. Hence, one may speculate that these adhesion proteins and perhaps the autotransporter domain are important for cell-cell adhesion in single-subspecies biofilms. CmpA and Fap2 had a very low identity in FNP, and this subspecies was the most distant in the phylogenetic tree. This might indicate an inability to form stable single-subspecies biofilms. It is, however, important to note that these bioinformatic results have to be considered with caution and no final conclusions can be drawn due to the small scale of the analysis. Only a selected set of adhesion proteins reported in the literature was analysed and it is likely that other putative adhesion proteins involved in biofilm formation remain to be discovered.

With the method employed here, no autotransporter domains for CmpA were detected in subspecies FNA and FNN23. Additionally, despite a high identity of the YadA-like protein in FNP, a general lack of enhanced adhesion of FNP to fibronectin and gelatin in our study might suggest that YadA in FNP does not play a key role in adhesion to these proteins. Mutagenesis studies could be performed in the genetically modifiable strain FNN23 in order to validate these findings. Mutants lacking each of the above-mentioned adhesion proteins could be studied regarding their adhesion, autoaggregation and biofilm forming ability.

Many authors have utilised planktonic cultures in pathogenicity studies of *F. nucleatum*, however this might not reflect true virulence of this anaerobic microorganism, as virulence genes have been shown to be upregulated in biofilms [67, 68]. Availability of *F. nucleatum* single-subspecies biofilm characterisation data might help researchers to perform more biologically relevant *F. nucleatum* pathogenicity studies using single-subspecies biofilms. Our experiments showed that in general both glass and plastic surfaces supported biofilm growth and thus can be utilised for studies of *F. nucleatum* subspecies biofilms when transparent substrates are required. Additionally, surface coatings do not seem to be necessary when quantity of the biofilm is not a priority.

Whilst we appreciate that behaviour of laboratory type strains might differ significantly from clinical isolates obtained from patients, we believe that it is important to first characterise virulence properties of subspecies of *F. nucleatum*, represented by widely available ATCC type strains, to build a knowledge base, which can later be utilised to study virulence of specific clinical isolates. As biofilm formation is one of the virulence properties of bacteria, understanding the differences in pathogenicity of individual *F. nucleatum* subspecies may reveal new virulence factors as novel therapeutic targets for prevention and treatment of *F. nucleatum*-mediated infections and diseases.

DATA AVAILABILITY STATEMENT

The original contributions presented in the study are included in the article/**Supplementary Material**, further inquiries can be directed to the corresponding author/s.

AUTHOR CONTRIBUTIONS

MM carried out experiments and data analysis and wrote the manuscript. DB performed bioinformatic analysis and wrote the corresponding parts of the manuscript. MG, SK, IC, and JH were involved in planning experiments, supervised the project, and contributed to the interpretation of the results. JH provided support with statistical analysis and figure preparation. All authors provided critical feedback on the manuscript. All authors contributed to the article and approved the submitted version.

FUNDING

This study was funded by a grant provided by Birmingham Community Healthcare NHS Foundation Trust. Publication of this study was possible thanks to funds provided by the University of Birmingham, Birmingham, UK.

ACKNOWLEDGMENTS

We would like to thank Dr. Lauter E. Pelepenko (Endodontics Division, Piracicaba Dental School FOP-Unicamp, Piracicaba, SP, Brazil) for his assistance during the figure formatting process. We are grateful to Dr. Nicholas Jakubovics (School of Dental Sciences, Newcastle University, Newcastle upon Tyne, UK) for his valuable advice on CLSM imaging of *F. nucleatum* biofilms. We would also like to acknowledge the kind gift of FNN23 from Dr. Daniel Slade (Virginia Polytechnic Institute and State University, Blacksburg VA, USA).

SUPPLEMENTARY MATERIAL

The Supplementary Material for this article can be found online at: https://www.frontiersin.org/articles/10.3389/froh.2022.853618/full#supplementary-material

REFERENCES

1. Kilian M, Chapple ILC, Hannig M, Marsh PD, Meuric V, Pedersen AML, et al. The oral microbiome – an update for oral healthcare professionals. *Br Dent J.* (2016) 221:657–66. doi: 10.1038/sj.bdj.2016.865
2. Papapanou PN, Sanz M, Buduneli N, Dietrich T, Feres M, Fine DH, et al. Periodontitis: consensus report of workgroup 2 of the 2017. world workshop on the classification of periodontal and peri-implant diseases and conditions. *J Clin Periodontol.* (2018) 45:S162–S70. doi: 10.1111/jcpe.12946
3. Kwon T, Lamster IB, Levin L. Current concepts in the management of periodontitis. *Int Dent J.* (2021) 71:462–76. doi: 10.1111/idj.12630
4. Caselli E, Fabbri C, D'Accolti M, Soffritti I, Bassi C, Mazzacane S, et al. Defining the oral microbiome by whole-genome sequencing and resistome analysis: the complexity of the healthy picture. *BMC Microbiol.* (2020) 20:120. doi: 10.1186/s12866-020-01801-y
5. Marsh PD. Role of the oral microflora in health. *Microb Ecol Health Dis.* (2000) 12:130–7. doi: 10.1080/089106000750051800
6. Deo PN, Deshmukh R. Oral microbiome: unveiling the fundamentals. *J Oral Maxillofac Pathol.* (2019) 23:122–8. doi: 10.4103/jomfp.JOMFP_152_19
7. Chen C, Hemme C, Beleno J, Shi ZJ, Ning D, Qin Y, et al. Oral microbiota of periodontal health and disease and their changes after nonsurgical periodontal therapy. *ISME J.* (2018) 12:1210–24. doi: 10.1038/s41396-017-0037-1
8. Socransky SS, Haffajee AD, Cugini MA, Smith C, Kent RL Jr. Microbial complexes in subgingival plaque. *J Clin Periodontol.* (1998) 25:134–44. doi: 10.1111/j.1600-051X.1998.tb02419.x
9. Socransky SS, Haffajee AD. Periodontal microbial ecology. *Periodontol.* (2005) 38:135–87. doi: 10.1111/j.1600-0757.2005.00107.x
10. Sharma A. Virulence mechanisms of *Tannerella forsythia*. *Periodontol.* (2010) 54:106–16. doi: 10.1111/j.1600-0757.2009.00332.x
11. Dashper SG, Seers CA, Tan KH, Reynolds EC. Virulence factors of the oral spirochete *Treponema denticola*. *J Dent Res.* (2011) 90:691–703. doi: 10.1177/0022034510385242
12. Singhrao SK, Harding A, Poole S, Kesavalu L, Crean S. *Porphyromonas gingivalis* periodontal infection and its putative links with Alzheimer's disease. *Mediators Inflamm.* (2015) 2015:137357. doi: 10.1155/2015/137357
13. Han YW. *Fusobacterium nucleatum*: a commensal-turned pathogen. *Curr Opin Microbiol.* (2015) 23:141–7. doi: 10.1016/j.mib.2014.11.013
14. Lourenço TGB, Heller D, Silva-Boghossian CM, Cotton SL, Paster BJ, Colombo APV. Microbial signature profiles of periodontally healthy and diseased patients. *J Clin Periodontol.* (2014) 41:1027–36. doi: 10.1111/jcpe.12302
15. Jung Y-J, Jun H-K, Choi B-K. *Porphyromonas gingivalis* suppresses invasion of *Fusobacterium nucleatum* into gingival epithelial cells. *J Oral Microbiol.* (2017) 9:1320193. doi: 10.1080/20002297.2017.1320193
16. Brennan CA, Garrett WS. *Fusobacterium nucleatum* - symbiont, opportunist and oncobacterium. *Nat Rev Microbiol.* (2019) 17:156–66. doi: 10.1038/s41579-018-0129-6
17. Kook JK, Park SN, Lim YK, Choi MH, Cho E, Kong SW, et al. *Fusobacterium nucleatum* subsp. fusiforme Gharbia and Shah 1992 is a later synonym of *Fusobacterium nucleatum* subsp. vincentii Dzink et al. 1990. *Curr Microbiol.* (2013) 66:414–7. doi: 10.1007/s00284-012-0289-y
18. Kurgan S, Kansal S, Nguyen D, Stephens D, Koroneos Y, Hasturk H, et al. Strain-specific impact of *Fusobacterium nucleatum* on neutrophil function. *J Periodontol.* (2017) 88:380–9. doi: 10.1902/jop.2016.160212
19. Thurnheer T, Karygianni L, Flury M, Belibasakis GN. *Fusobacterium* species and subspecies differentially affect the composition and architecture of supra- and subgingival biofilms models. *Front Microbiol.* (2019) 10:1716. doi: 10.3389/fmicb.2019.01716
20. Diaz PI, Valm AM. Microbial interactions in oral communities mediate emergent biofilm properties. *J Dent Res.* (2020) 99:18–25. doi: 10.1177/0022034519880157
21. Meng Q, Gao Q, Mehrazarin S, Tangwanichgapong K, Wang Y, Huang Y, et al. *Fusobacterium nucleatum* secretes amyloid-like FadA to enhance pathogenicity. *EMBO Rep.* (2021) 22:e52891. doi: 10.15252/embr.202152891
22. Umaña A, Sanders BE, Yoo CC, Casasanta MA, Udayasuryan B, Verbridge SS, et al. Utilizing whole *fusobacterium* genomes to identify, correct, and characterize potential virulence protein families. *J Bacteriol.* (2019) 201:e00273–19. doi: 10.1128/JB.00273-19
23. Vyas N, Wang QX, Manmi KA, Sammons RL, Kuehne SA, Walmsley AD. How does ultrasonic cavitation remove dental bacterial biofilm? *Ultrason Sonochem.* (2020) 67:105112. doi: 10.1016/j.ultsonch.2020.105112
24. Millhouse E, Jose A, Sherry L, Lappin DF, Patel N, Middleton AM, et al. Development of an in vitro periodontal biofilm model for assessing antimicrobial and host modulatory effects of bioactive molecules. *BMC Oral Health.* (2014) 14:80. doi: 10.1186/1472-6831-14-80
25. Kalaskar DM, Downes JE, Murray P, Edgar DH, Williams RL. Characterization of the interface between adsorbed fibronectin and human embryonic stem cells. *J R Soc Interface.* (2013) 10:20130139. doi: 10.1098/rsif.2013.0139
26. Bello AB, Kim D, Kim D, Park H, Lee S-H. Engineering and functionalization of gelatin biomaterials: from cell culture to medical applications. *Tissue Eng B Rev.* (2020) 26:164–80. doi: 10.1089/ten.teb.2019.0256
27. Park K-S, Ahn J, Kim JY, Park H, Kim HO, Lee S-H. Poly-L-Lysine increases the *ex vivo* expansion and erythroid differentiation of human hematopoietic stem cells, as well as erythroid enucleation efficacy. *Tissue Eng A.* (2014) 20:1072–80. doi: 10.1089/ten.tea.2013.0193
28. Ismail HS, Ali AI, Abo El-Ella MA, Mahmoud SH. Effect of different polishing techniques on surface roughness and bacterial adhesion of three glass ionomer-based restorative materials: *in vitro* study. *J Clin Exp Dent.* (2020) 12:e620–5. doi: 10.4317/jced.56616
29. Howe KL, Achuthan P, Allen J, Allen J, Alvarez-Jarreta J, Amode MR, et al. Ensembl 2021. *Nucleic Acids Res.* (2020) 49:D884–91. doi: 10.1093/nar/gkaa942
30. States DJ, Gish W. Combined use of sequence similarity and codon bias for coding region identification. *J Comput Biol.* (1994) 1:39–50. doi: 10.1089/cmb.1994.1.39
31. Blum M, Chang HY, Chuguransky S, Grego T, Kandasaamy S, Mitchell A, et al. The InterPro protein families and domains database: 20 years on. *Nucleic Acids Res.* (2021) 49:D344–54. doi: 10.1093/nar/gkaa977
32. Katoh K, Rozewicki J, Yamada KD. MAFFT online service: multiple sequence alignment, interactive sequence choice and visualization. *Brief Bioinform.* (2019) 20:1160–6. doi: 10.1093/bib/bbx108
33. Saitou N, Nei M. The neighbor-joining method: a new method for reconstructing phylogenetic trees. *Mol Biol Evol.* (1987) 4:406–25.
34. Gharbia SE, Shah HN, Lawson PA, Haapasalo M. The distribution and frequency of *Fusobacterium nucleatum* subspecies in the human oral cavity. *Oral Microbiol Immunol.* (1990) 5:324–7. doi: 10.1111/j.1399-302X.1990.tb00434.x
35. Feres M, Louzoun Y, Haber S, Faveri M, Figueiredo LC, Levin L. Support vector machine-based differentiation between aggressive and chronic periodontitis using microbial profiles. *Int Dent J.* (2018) 68:39–46. doi: 10.1111/idj.12326
36. Gmür R, Munson MA, Wade WG. Genotypic and phenotypic characterization of fusobacteria from Chinese and European patients with inflammatory periodontal diseases. *Syst Appl Microbiol.* (2006) 29:120–30. doi: 10.1016/j.syapm.2005.07.011
37. Karched M, Bhardwaj RG, Asikainen SE. Coaggregation and biofilm growth of *Granulicatella* spp. with *Fusobacterium nucleatum* and *Aggregatibacter actinomycetemcomitans*. *BMC Microbiol.* (2015) 15:114. doi: 10.1186/s12866-015-0439-z
38. Park J, Shokeen B, Haake SK, Lux R. Characterization of *Fusobacterium nucleatum* ATCC 23726 adhesins involved in strain-specific attachment to *Porphyromonas gingivalis*. *Int J Oral Sci.* (2016) 8:138–44. doi: 10.1038/ijos.2016.27
39. Periasamy S, Chalmers NI, Du-Thumm L, Kolenbrander PE. *Fusobacterium nucleatum* ATCC 10953 requires *Actinomyces naeslundii* ATCC 43146 for growth on saliva in a three-species community that includes *Streptococcus oralis* 34. *Appl Environ Microbiol.* (2009) 75:3250–7. doi: 10.1128/AEM.02901-08
40. Chew J, Zilm PS, Fuss JM, Gully NJ. A proteomic investigation of *Fusobacterium nucleatum* alkaline-induced biofilms. *BMC Microbiol.* (2012) 12:189. doi: 10.1186/1471-2180-12-189
41. Zilm PS, Rogers AH. Co-adhesion and biofilm formation by *Fusobacterium nucleatum* in response to growth pH. *Anaerobe.* (2007) 13:146–52. doi: 10.1016/j.anaerobe.2007.04.005
42. Grant M, Kilsgård O, Åkerman S, Klinge B, Demmer RT, Malmström J, et al. The human salivary antimicrobial peptide profile according to the oral

microbiota in health, periodontitis and smoking. *J Innate Immun.* (2019) 11:432–44. doi: 10.1159/000494146
43. Tavares LJ, Klein MI, Panariello BHD, Dorigatti de Avila E, Pavarina AC. An in vitro model of *Fusobacterium nucleatum* and *Porphyromonas gingivalis* in single- and dual-species biofilms. *J Periodontal Implant Sci.* (2018) 48:12–21. doi: 10.5051/jpis.2018.48.1.12
44. Babu JP, Dean JW, Pabst MJ. Attachment of *Fusobacterium nucleatum* to fibronectin immobilized on gingival epithelial cells or glass coverslips. *J Periodontol.* (1995) 66:285–90. doi: 10.1902/jop.1995.66.4.285
45. Winkler JR, John SR, Kramer RH, Hoover CI, Murray PA. Attachment of oral bacteria to a basement-membrane-like matrix and to purified matrix proteins. *Infect Immun.* (1987) 55:2721–6. doi: 10.1128/iai.55.11.2721-2726.1987
46. Benn G, Pyne ALB, Ryadnov MG, Hoogenboom BW. Imaging live bacteria at the nanoscale: comparison of immobilisation strategies. *Analyst.* (2019) 144:6944–52. doi: 10.1039/C9AN01185D
47. Cowan SE, Liepmann D, Keasling JD. Development of engineered biofilms on poly- L-lysine patterned surfaces. *Biotechnol Lett.* (2001) 23:1235–41. doi: 10.1023/A:1010581503842
48. Zheng S, Bawazir M, Dhall A, Kim H-E, He L, Heo J, et al. Implication of surface properties, bacterial motility, and hydrodynamic conditions on bacterial surface sensing and their initial adhesion. *Front Bioeng Biotechnol.* (2021) 9:643722. doi: 10.3389/fbioe.2021.643722
49. Jaffar N, Miyazaki T, Maeda T. Biofilm formation of periodontal pathogens on hydroxyapatite surfaces: implications for periodontium damage. *J Biomed Mater Res A.* (2016) 104:2873–80. doi: 10.1002/jbm.a.35827
50. Sterzenbach T, Helbig R, Hannig C, Hannig M. Bioadhesion in the oral cavity and approaches for biofilm management by surface modifications. *Clin Oral Investig.* (2020) 24:4237–60. doi: 10.1007/s00784-020-03646-1
51. Bozbay E, Dominici F, Gokbuget A, Cintan S, Guida L, Aydin M, et al. Preservation of root cementum: a comparative evaluation of power-driven versus hand instruments. *Int J Dental Hygiene*. (2018) 16:202–9. doi: 10.1111/idh.12249
52. Rezende G, Arthur RA, Lamers ML, Hashizume LN. Structural organization of dental biofilm formed in situ in the presence of sucrose associated to maltodextrin. *Braz Dent J.* (2019) 30:36–42. doi: 10.1590/0103-6440201902183
53. Salavadhi SS, Chintalapani S, Ramachandran R, Nagubandi K, Ramisetti A, Boyapati R. Atomic force microscopy: a three-dimensional reconstructive tool of oral microbiota in gingivitis and periodontitis. *J Indian Soc Periodontol.* (2017) 21:264–9. doi: 10.4103/jisp.jisp_209_17
54. Germano F, Bramanti E, Arcuri C, Cecchetti F, Cicciù M. Atomic force microscopy of bacteria from periodontal subgingival biofilm: preliminary study results. *Eur J Dent.* (2013) 7:152–8. doi: 10.4103/1305-7456.110155
55. Bridier A, Dubois-Brissonnet F, Boubetra A, Thomas V, Briandet R. The biofilm architecture of sixty opportunistic pathogens deciphered using a high throughput CLSM method. *J Microbiol Methods.* (2010) 82:64–70. doi: 10.1016/j.mimet.2010.04.006
56. Chao Y, Zhang T. Optimization of fixation methods for observation of bacterial cell morphology and surface ultrastructures by atomic force microscopy. *Appl Microbiol Biotechnol.* (2011) 92:381–92. doi: 10.1007/s00253-011-3551-5
57. Azeredo J, Azevedo NF, Briandet R, Cerca N, Coenye T, Costa AR, et al. Critical review on biofilm methods. *Crit Rev Microbiol.* (2017) 43:313–51. doi: 10.1080/1040841X.2016.1208146
58. Barreto M, Meyer JJM. The preservation of biofilms on macroalgae by osmium vapour. *S Afr J Bot.* (2007) 73:64–9. doi: 10.1016/j.sajb.2006.08.004
59. Costerton JW, Cheng KJ, Geesey GG, Ladd TI, Nickel JC, Dasgupta M, et al. Bacterial biofilms in nature and disease. *Annu Rev Microbiol.* (1987) 41:435–64. doi: 10.1146/annurev.mi.41.100187.002251
60. Ali Mohammed MM, Nerland AH, Al-Haroni M, Bakken V. Characterization of extracellular polymeric matrix, and treatment of *Fusobacterium nucleatum* and *Porphyromonas gingivalis* biofilms with DNase I and proteinase K. *J Oral Microbiol.* (2013) 5:10.3402/jom.v5i0.20015. doi: 10.3402/jom.v5i0.20015
61. Ali Mohammed MM, Pettersen VK, Nerland AH, Wiker HG, Bakken V. Quantitative proteomic analysis of extracellular matrix extracted from mono- and dual-species biofilms of *Fusobacterium nucleatum* and *Porphyromonas gingivalis*. *Anaerobe.* (2017) 44:133–42. doi: 10.1016/j.anaerobe.2017.03.002
62. Kaplan CW, Lux R, Haake SK, Shi W. The *Fusobacterium nucleatum* outer membrane protein RadD is an arginine-inhibitable adhesin required for inter-species adherence and the structured architecture of multispecies biofilm. *Mol Microbiol.* (2009) 71:35–47. doi: 10.1111/j.1365-2958.2008.06503.x
63. Coppenhagen-Glazer S, Sol A, Abed J, Naor R, Zhang X, Han YW, et al. Fap2 of *Fusobacterium nucleatum* is a galactose-inhibitable adhesin involved in coaggregation, cell adhesion, and preterm birth. *Infect Immun.* (2015) 83:1104–13. doi: 10.1128/IAI.02838-14
64. Lima BP, Shi W, Lux R. Identification and characterization of a novel *Fusobacterium nucleatum* adhesin involved in physical interaction and biofilm formation with *Streptococcus gordonii*. *MicrobiologyOpen.* (2017) 6:e00444. doi: 10.1002/mbo3.444
65. Nakagaki H, Sekine S, Terao Y, Toe M, Tanaka M, Ito HO, et al. *Fusobacterium nucleatum* envelope protein FomA is immunogenic and binds to the salivary statherin-derived peptide. *Infect Immun.* (2010) 78:1185–92. doi: 10.1128/IAI.01224-09
66. Liu J, Hsieh C-L, Gelincik O, Devolder B, Sei S, Zhang S, et al. Proteomic characterization of outer membrane vesicles from gut mucosa-derived fusobacterium nucleatum. *J Proteomics.* (2019) 195:125–37. doi: 10.1016/j.jprot.2018.12.029
67. Becker P, Hufnagle W, Peters G, Herrmann M. Detection of differential gene expression in biofilm-forming versus planktonic populations of *Staphylococcus aureus* using micro-representational-difference analysis. *Appl Environ Microbiol.* (2001) 67:2958–65. doi: 10.1128/AEM.67.7.2958-2965.2001
68. Resch A, Rosenstein R, Nerz C, Götz F. Differential gene expression profiling of *Staphylococcus aureus* cultivated under biofilm and planktonic conditions. *Appl Environ Microbiol.* (2005) 71:2663–76. doi: 10.1128/AEM.71.5.2663-2676.2005

Conflict of Interest: The authors declare that the research was conducted in the absence of any commercial or financial relationships that could be construed as a potential conflict of interest.

Publisher's Note: All claims expressed in this article are solely those of the authors and do not necessarily represent those of their affiliated organizations, or those of the publisher, the editors and the reviewers. Any product that may be evaluated in this article, or claim that may be made by its manufacturer, is not guaranteed or endorsed by the publisher.

Copyright © 2022 Muchova, Balacco, Grant, Chapple, Kuehne and Hirschfeld. This is an open-access article distributed under the terms of the Creative Commons Attribution License (CC BY). The use, distribution or reproduction in other forums is permitted, provided the original author(s) and the copyright owner(s) are credited and that the original publication in this journal is cited, in accordance with accepted academic practice. No use, distribution or reproduction is permitted which does not comply with these terms.